1986

Transient critical heat flux

Kemal O. Pasamehmetoglu
University of Central Florida

TRANSIENT CRITICAL HEAT FLUX

by

KEMAL O. PASAMEHMETOGLU

A dissertation submitted in partial fulfillment of the requirements
for the degree of Doctor of Philosophy in
the Department of Mechanical Engineering at
the University of Central Florida
Orlando, Florida

August 1986

Major Professor: Fred S. Gunnerson

ABSTRACT

The term Critical Heat Flux (CHF) is used in boiling heat transfer to describe the local value of the heat flux at which a characteristic reduction in heat transfer coefficient first occurs. In today's technology, the CHF is a phenomenon related to the design and safety of various important devices.

A major limitation on the thermal design of a light-water reactor (LWR) is the necessity to maintain an adequate safety margin between the CHF and the local heat flux. Extended operations at local power levels in excess of the CHF can lead to high temperature oxidation and embrittlement or melting of the zircaloy cladding, thus jeopardizing the fuel rod's integrity. In the nuclear industry, there have been many empirical CHF correlations developed over the years. These correlations are mostly based on steady-state (or quasi-steady) data obtained from various experiments covering different ranges of CHF parameters. Therefore, the application of such correlations is not only restricted by their parametric ranges, but is also limited to steady (or quasi-steady) operating conditions. In nuclear reactors, however, the CHF level is more likely to be reached during abnormal (transient) operating conditions, rather than during normal (steady) operations. Depending upon the type of accident, a wide range of thermal-hydraulic conditions may arise. For accurate nuclear reactor modeling, the accurate prediction of CHF as a function of time-

dependent, thermal-hydraulic conditions is essential. This was the motivation of the subject study.

This research was a two-fold study. In the first part, the quasi-steady approach in predicting the CHF is defined and analyzed. In this part, data from blowdown experiments are compared to commonly used steady-state correlations on a local-instantaneous basis. This is done as a continuation of the previous studies conducted at Argonne National Laboratory. In all these studies, including the present study, a simple computer program, Coolant Dynamic Analysis (CODA), is used. The results are discussed in terms of the limitations of the quasi-steady approach.

In the second part of this study, faster transients, where the quasi-steady approach is unable to predict the CHF, are considered. A new theory is developed to predict the CHF in power transients, which are typical of Reactivity Initiated Accidents (RIA) in LWRs. The proposed theory is purely analytical. It incorporates the effect of the hydrodynamic instability on the surface dryout in addition to evaporation, which was studied as the unique mechanism by previous researchers. The presented theory compares quite favorably with the available data from electrical heaters.

Two other types of transients which are of interest to the nuclear industry are rapid depressurization and rapid flow reduction. These are typical of Loss-of-Coolant Accidents (LOCA) and Loss-of-Flow Accidents (LOFA). The effects of these transients on CHF are also discussed from first principles. Finally, the important parameters of a generalized transient CHF correlation are identified and are grouped into dimensionless numbers. The physical significance of each group

is discussed. Based on experimental and theoretical observations, a general mathematical model is developed to correlate transient CHF.

TO MY WIFE, YASEMIN

ACKNOWLEDGEMENT

The author would like to express his deepest gratitute to Dr. Fred Gunnerson who has been an excellent advisor during the dissertation and throughout the entire Ph.D. program. His outstanding help and guidance made this dissertation possible.

The author's gratitute is also extended to Dr. Burton Eno. His ever-lasting guidance, support and encouragements are deeply appreciated.

The author would also like to express his appreciations for the technical guidance of Dr. Ralph Nelson at Los Alamos National Laboratory. Without his expert suggestions and long-lasting interest it would be very difficult to finish the subject study.

The efforts of Dr. Ramon Hosler, Dr. Larry Andrews, and Dr. Roy Walters, in serving in the author's Ph.D. committee, are also deeply appreciated.

The author is also indepted to the Department of Mechanical Engineering and the College of Engineering for the financial support provided during his graduate studies.

Thanks are also extended to U. S. Nuclear Regulatory Commission which funded the initial phases of the subject study.

The author would also like to thank the chairman, faculty, staff, and graduate students of the Mechanical Engineering Depart-

ment for creating an enjoyable and efficient work environment.

The author wishes to extend a special thanks to his parents, Ilhan and Suna Pasamehmetoglu, and his wife, Yasemin Pasamehmetoglu, for their inspiration and ever-lasting support during the various phases of the author's education.

TABLE OF CONTENTS

LIST OF TABLES

LIST OF FIGURES

NOMENCLATURE

A : Area (m^2)

A^* : Minimum area for area averaging (m^2)

A_f : Heater area covered by liquid (m^2)

A_v : Heater area covered by vapor (m^2)

A_w : Total heater area, $A_w = A_v + A_f$ (m^2)

B : Empirical Constant in Equation 67 (dimensionless)

b : Empirical Constant in Equation 70

C : Concentration of liquid droplets (kg/m^3)

C_{eq}: Concentration of liquid droplets at hydrodynamic equilibrium state (kg/m^3)

C_p : Specific heat (J/kg-°K)

c : Sonic velocity (m/s)

D : Deposition rate of liquid droplets (kg/m^2-s)

d : Diameter (m)

d_{HE}: Heated equivalent diameter (m)

d_{HY}: Hydraulic equivalent diameter (m)

E : Entrainment rate of liquid droplets (kg/m^2-s)

E_t : Volumetric total energy (J/m^3)

E_v : Rate of liquid layer evaporation (kg/s)

$E(v)$: Expected value of radial velocity (m/s)

e : Internal energy (J/kg)

F : Correction factor for non-uniform axial heat flux distribution (dimensionless)

$f_1(P)$: Prescribed function of pressure (W^2/m)

$f_2(P)$: Prescribed function of pressure (J/m^3)

$f_2'(P)$: Prescribed function of pressure (J/m^3)

$f_3(P,\Delta T_{SUB})$: Prescribed function of pressure and subcooling (dimensionless)

G : Mass velocity (kg/m^2-s)

G_f: Mass velocity of liquid film (kg/m^2-s)

G_3: Average radial mass velocity from core to bubbly layer (kg/m^2-s)

g : Gravitational acceleration (m/s^2)

$g_1(\ )$, $g_2(\ )$, $g_3(\ )$: Generalized CHF functions

H : Thickness of flat ribbon heater (m)

h : Enthalpy (J/kg)

h_c: Convective heat transfer coefficient (W/m^2-°K)

h_{fg}: Latent heat of vaporization (J/kg)

h_{ld}: Enthalpy at point of bubble detachment (J/kg)

i : Index in Taylor series expansion (dimensionless)

K : Empirical constant in Equation 70

k : Thermal conductivity (W/m-°K)

k_m: Mass transfer coefficient for deposition (m/s)

L : Heated channel length (m)

L_{SAT}: Heated length above saturation point (m)

L_o: Laplace coefficient (m)

m : Liquid film thickness in annular flow (m)

$\dot{m}_1$: Axial mass flow rate in core (kg/s)

$\dot{m}_2$: Axial mass flow rate in bubbly layer (kg/s)

$\dot{m}_3$: Radial mass flow rate from core to bubbly layer (kg/s)

$\dot{m}_4$: Radiant mass flow rate from bubbly layer to core (kg/s)

n : Empirical exponent for the effect of liquid supply on CHF (dimensionless)

n': Empirical exponent, n' = n + 2 (dimensionless)

n*: Minimum number of controlling phenomenon (dimensionless)

P : Pressure (Pa)

P_{cr}: Critical pressure (Pa)

P_H: Heated channel perimeter (m)

p(v): Probability density function of radial velocity fluctuations (dimensionless)

Q : Heat generation rate per unit volume (W/m^3)

Q_s: Heat generation rate per unit surface area (W/m^2)

Q_{SAT}: Total power input from the saturation point (W)

q : Heat flux (W/m^2)

q_B: Heat flux at the switch-over point between hydrodynamic instability and evaporation mechanisms (W/m^2)

q_b: Portion of the heat flux in generating vapor (W/m^2)

q_{CHF}: Critical heat flux (W/m^2)

$q_{CHF,0}$: Critical heat flux in subcooled pool boiling (W/m^2)

$q_{CHF,00}$: Critical heat flux in saturated pool boiling (W/m^2)

$q_{CHF,IP}$: Critical heat flux in saturated pool boiling over an infinite horizontal plate (W/m^2)

$q_{CHF,SS}$: Steady-state critical heat flux (W/m^2)

$q_{CHF,SS,0}$: Steady-state critical heat flux with zero flow (W/m^2)

$q_{CHF,SS,OO}$: Steady-state critical heat flux with zero flow and zero subcooling (W/m^2)

$q_{CHF,TR}$: Transient critical heat flux (W/m^2)

q_{SS}: Steady or quasi-steady surface heat flux (W/m^2)

$q^i_{\underset{\sim}{x}}$: Local-instantaneous heat flux (W/m^2)

$\bar{q}_{\underset{\sim}{x}}$: Time averaged local heat flux (W/m^2)

$<q^i>$: Space averaged instantaneous heat flux (W/m^2)

$<\bar{q}>$ Time and space averaged heat flux (W/m^2)

R : Radius (m)

r : Radial coordinate (m)

S : Total surface area of the heater (m^2)

s : Bubbly-layer thickness (m)

T : Temperature (°K)

T_c: Coolant temperature (°K)

T_{SAT}: Saturation temperature (°K)

T_W: Heater wall temperature

t : Time (s)

t_B: Switch-over time between the hydrodynamic instability and evaporation mechanisms (s)

t_{CHF}: Time-to-CHF (s)

$t_{CHF,SS}$: Time-to-steady-state CHF (s)

$t_{CHF,TR}$: Time-to-transient CHF (s)

t_t: Time transit parameter (s)

$t_{0.5}$: Time for 50% flow reduction (s)

U : Axial velocity (m/s)

V : Heater volume (m^3)

v : Radial velocity (m/s)

v_v: Vapor escape velocity (m/s)

v_1: Volumetric growth rate of a bubble (m^3/s)

W : Width of flat ribbon heater (m)

W_f: Rate of liquid supply (kg/s)

W_{fs}: Rate of liquid supply at steady-state CHF level (kg/s)

x : Quality (dimensionless)

x_{eq}: Quality at hydrodynamic equilibrium state (dimensionless)

x_1: Average quality in the core region (dimensionless)

x_2: Average quality in the bubbly layer (dimensionless)

$\underset{\sim}{x}$: Space vector (m)

z : Axial coordinate (m)

α : Transient parameter (P,G or Q) (Pa, kg/m^2-s or W/m^3)

β, β': Entrainment parameters (dimensionless)

β_v: Void Fraction

γ : Empirical constant in Equation 16 (dimensionless)

γ_1, γ_2: Empirical constants in Equation 87 (dimensionless)

ΔA: Incremental area (m^2)

ΔE_v: Net evaporation rate (kg/s)

Δh_{SUB}: Subcooling in terms of enthalpy difference (J/kg)

$\Delta \dot{m}_2$: Change in axial mass flow in bubbly layer (kg/s)

ΔT_{SAT}: Wall superheat, $\Delta T_{SAT} = T_W - T_{SAT}$ (°K)

ΔT_{SUB}: Subcooling, $\Delta T_{SUB} = T_c - T_{SAT}$ (°K)

Δt: Incremental time (s)

$\Delta t'$: Period of the controlling phenomenon (s)

Δt^*: Minimum time period for time averaging (s)

Δt_e: Time period for complete evaporation of liquid layer (s)

$\delta_{c,0}$: Critical liquid layer thickness in saturated pool boiling(m)*

$\delta_{c,s}$: Critical liquid layer thickness in subcooled pool boiling(m)

δ_c: Critical liquid layer thickness in forced convective boiling(m)

λ_c: Taylor instability wavelength (m)

λ_D: The most susceptible Taylor instability wavelength over a flat surface (m)

λ_D' The most susceptible Taylor instability wavelength over cylindrical heaters (m)

λ_H: Helmholtz instability wavelength (m)

μ : Dynamic viscosity (Pa-s)

ε : Volumetric ratio of the accompanying liquid to the moving bubble (dimensionless)

Ω : Empirical function in Equation 5 (m^{-1})

ρ : Density (kg/m^3)

σ : Surface tension (N/m)

τ : Exponential period (sec)

τ_c: Time period for complete evaporation of liquid layer in forced convective boiling (s)

τ_d: Hovering period of a bubble in saturated pool boiling (s)

τ_g: Growth period of a bubble in subcooled pool boiling (s)

τ_i: Shear stress at the vapor-liquid interface (Pa)

$\tau_{S,0}$: Shear stress before transient (Pa)

$\tau_{S,1}$: Shear stress after transient (Pa)

τ_W: Wall shear stress (Pa)

τ_1, τ_2: Specific values of exponential period τ (s)

Φ : Transient contribution to CHF (W/m^2)

ϕ : Transient contribution to CHF (dimensionless)

Ψ : Empirical coefficient of transient contribution to CHF

Dimensionless Groups:

B_s: Parameter to determine the switch-over point between the hydrodynamic instability and evaporation mechanisms.

m^+: Non-dimensionalized liquid layer thickness, $m^+ = m(\tau_W/\rho_f)^{\frac{1}{2}}(\rho_f/\mu_f)$

q': Dimensionless heat flux, $q' = q/Q_o R$

R': Dimensionless radius, $R' = R/L_o$

r': Dimensionless radial coordinate, $r' = r/R$

T': Dimensionless temperature, $T' = (T - T_W)k/(Q_o R^2)$

T'_w; Dimensionless wall temperature, $T'_w = (T_w - T_{SAT})h_c/(Q_o R)$

t': Dimensionless time, $t' = t/\tau$

η : Ratio of transient CHF to steady-state CHF, $\eta = q_{CHF,TR}/q_{CHF,SS}$

τ': Ratio of 50% reduction period to time transit parameter, $\tau' = t_{0.5}/t_t$

Ψ_{CHF}: CHF modeling parameter of Ahmad

Subscripts:

CHF: Critical heat flux

f : Saturated liquid

G : Mass flow rate transient

g : Saturated vapor

i :	Inlet
l :	Liquid
loc:	Local
o :	Initial value
P :	Pressure transient
Q :	Power transient
α :	α transient

LIST OF ACRONYMS AND ABBREVIATIONS

AEEW:	Atomic Energy Establishment, Winfrith (United Kingdom Atomic Energy Authority)
ANS:	American Nuclear Society
ANL:	Argonne National Laboratory
ASME:	American Society of Mechanical Engineers
ATWS:	Anticipated Transients Without Scram
B & W-2:	Babcock and Wilcox 2 Correlation
BWC:	Babcock and Wilcox Correlation
BWR:	Boiling Water Reactor
BOHL:	Beginning of Heated Length
CE:	Combustion Engineering
CHF:	Critical Heat Flux
CHFR:	Critical Heat Flux Ratio
CISE:	Centro Informazioni Studie d'Experience
CODA:	Coolant Dynamic Analysis Computer Program
DNB:	Departure From Nucleate Boiling
DNBR:	Departure From Nucleate Boiling Ratio
EOHL:	End of Heated Length
EPRI:	Electric Power Research Institute
GE:	General Electric
G-Z:	Griffith-Zuber Correlation
IBLOCA:	Intermediate Break Loss-of-Coolant Accident

INEL:	Idaho National Engineering Laboratory
JSME:	Japanese Society of Mechanical Engineers
LBLOCA:	Large Break Loss-of-Coolant Accident
LMFBR:	Liquid Metal Fast Breeder Reactor
LOCA:	Loss-of-Coolant Accident
LOFA:	Loss-of-Flow Accident
LOFT:	Foss-of-Fluid Test
LWR:	Light Water Reactor
MZ:	Modified Zuber Correlation
NUREG:	Nuclear Regulatory Commission Publication
ORNL:	Oak Ridge National Laboratory
PBF:	Power Burst Facility
PWR:	Pressurized Water Reactor
RIA:	Reactivity Initiated Accident
SBLOCA:	Small Break Loss-of-Coolant Accident
TFBP:	Thermal Fuel Behavior Program
THTF:	Thermal Hydraulic Test Facility
W-3:	Westinghouse 3 Correlation

CHAPTER I

INTRODUCTION

The term Critical Heat Flux (CHF) is used in boiling heat transfer to describe the local value of the heat flux at which a characteristic reduction in heat transfer coefficient first occurs. For heat-flux controlled surfaces, CHF is generally recognized by its physical effect as a sudden increase of the surface temperature. Figure 1 shows the CHF on a boiling curve, the complete characteristics of which were first established by Nukiyama (1934). The curve ABCDE corresponds to boiling over temperature-controlled surfaces at constant pressure. For heat-flux controlled surfaces the transition boiling and the lower portion of the film boiling do not exist, and the surface temperature jumps from C to F once the critical heat flux is reached. In the literature, the CHF is sometimes defined slightly towards the left of the peak heat flux, at the point where the slope of the nucleate boiling curve starts decreasing.

Burnout, dryout, departure from nucleate boiling (DNB), and boiling crisis are other terms commonly used in the literature in conjunction with CHF. They all describe the same characteristic reduction in the heat transfer coefficient during nucleate boiling. Macbeth (1963) suggested the term burnout for heat flux controlled surfaces, and the term CHF for temperature controlled surfaces. The departure from nucleate boiling (DNB) was defined by Tong (1968a) as

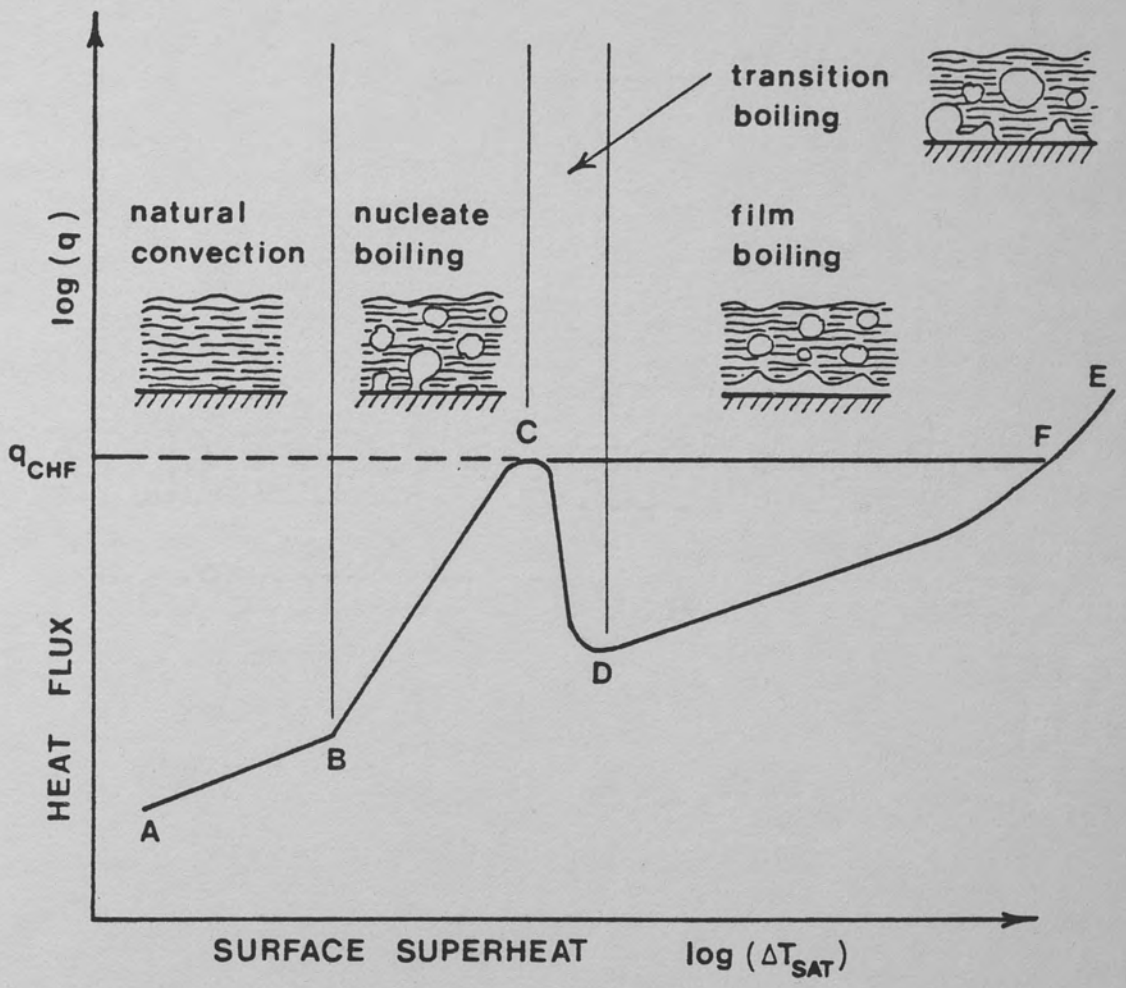

Figure 1. Boiling Curve

the CHF associated with low quality; whereas, the term dryout is reserved for CHF associated with high quality. Macbeth (1963) prefers to use the term fast burnout instead of DNB and slow burnout instead of dryout. This terminology is associated with the speed of the temperature rise following the burnout point. The term boiling crisis (Tong 1972) is also used by some authors as an encompassing term. Hereafter, in this study, the CHF is used as an encompassing term, since it is possibly the most common term in the international literature, and it does not suggest the mechanism by which CHF is reached. In conjunction with CHF, the terms DNB and dryout are also used in this study to specify low-quality and high-quality CHF, respectively.

Historically, Leidenfrost (1756) is credited as the author of the first publication in boiling heat transfer. This publication, however, is based mostly on observations and by no means is truly scientific, since even the latent heat of vaporization was not known until many years later. The first scientific CHF study was probably the establishment of the complete boiling curve by Nukiyama (1934). Since then, many CHF studies have been conducted at a rapidly-growing rate. The major portion of these studies, however, is of empirical nature with little analytical content. This situation has probably arisen due to the necessity of "quick answers" to the practical problems raised by the rapidly-growing technology, based on boiling heat transfer. Such "quick answers" provided by the empirical results are restricted to specific situations and usually mask the physics of the general CHF problem. Since, in many instances, the complexity of the CHF problem requiring an elaborate theory contradicts the idea of obtaining a quick, practical solution to the problem, the analytical

aspects are usually ignored. More recently, however, the detailed theoretical considerations of the CHF have started receiving more emphasis, possibly due to the growing complexity of the practical problems and to the restricted capacity of the empirical approach. As a result, despite the huge collection compiled over half a century, the CHF problem still offers a challenge to scientists. A complete understanding of CHF phenomenon must be preceded by a strong two-phase flow theory, which will possibly remain as a challenge for the rest of the century.

In today's technology, the CHF is a phenomenon related to the design and safety of various important devices, such as nuclear reactors, chemical-process plants, steam generators, liquid-fuel rocket engines, superconducting magnets, two-phase flow heat exchangers, laser mirror cooling, and water-cooling turbine blades. The present study, however, is mostly directed towards the requirements of the nuclear industry, although the general nature of the problem is also preserved.

A major limitation on the thermal design of a light-water reactor (LWR) is the necessity to maintain an adequate safety margin between the critical heat flux (CHF) and the local heat flux. The safety margin is generally quantified by the ratio of the CHF to the local-heat flux and is commonly termed as the departure from nucleate boiling ratio (DNBR), or the critical heat-flux ratio (CHFR). Since the CHFR is a measure of the safety margin to CHF, a value less than unity implies that the CHF has been exceeded. Extended operation at local power levels in excess of the CHF can lead to high-temperature oxidation and embrittlement of the zircaloy cladding, thus

jeopardizing the fuel-rod's integrity. The "time at temperature" criteria of Pawel (1974), in conjunction with the isothermal-kinetic correlation of Cathcart (1977), is often used to assess the post-CHF conditions leading to cladding failure. Figure 2 illustrates Pawel's (1974) "time at temperature" embrittlement criterion for post-CHF operation that may lead to cladding failure. Low-quality CHF (or DNB) is usually characterized by an inordinate thermal excursion and high cladding temperatures and may result in early cladding failure. Contrastingly, high-quality CHF (or dryout) is not heralded by a rapid increase in cladding temperature and may continue at post-CHF conditions for extended periods prior to jeopardizing the cladding. Therefore, an accurate prediction of the CHF is fundamentally important for nuclear plant safety. Although reaching the CHF level does not necessarily mean failure, it is the first threshold on the way to failure. Thus, the CHF is to be avoided; or, if it is accidentally reached, corrective measures must be taken.

For use in the nuclear industry, there have been many empirical CHF correlations developed over the years. These correlations are mostly based on steady-state (or quasi-steady) data obtained from different experiments covering different ranges of CHF parameters. Therefore, the application of such correlations is not only restricted by their parametric ranges, but is also limited to steady (or quasi-steady) operating conditions. In nuclear reactors, however, the CHF level is more likely to be reached during abnormal (transient) operating conditions, rather than during normal (steady) operations. Depending upon the type of accident, a wide range of thermal-hydraulic conditions may arise. For accurate nuclear reactor modeling, the

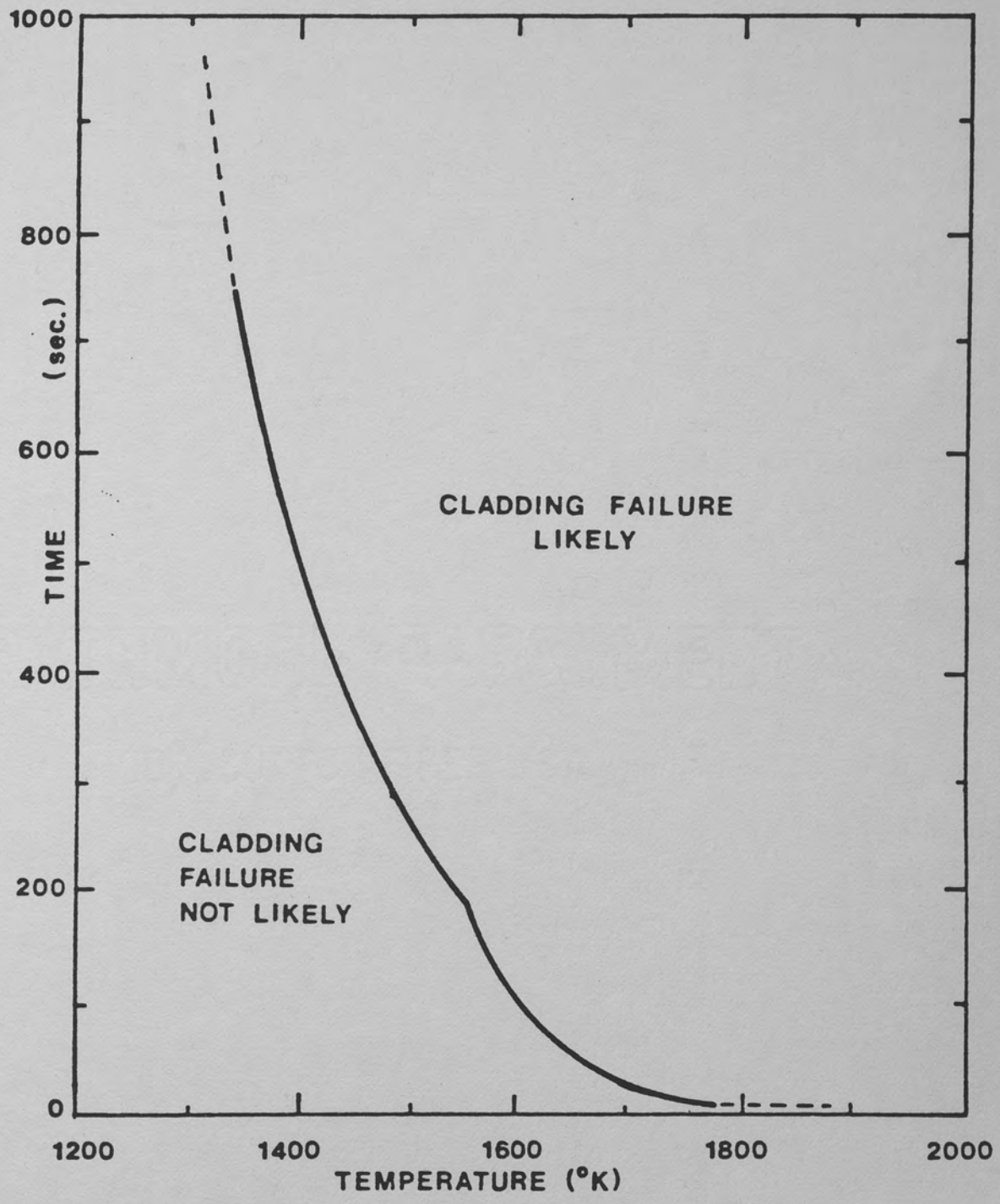

Figure 2. The "Time-at-Temperature Criterion" (Pawel 1974)

prediction of the CHF as a function of the time-dependent thermal-hydraulic conditions is essential.

This is the motivation of the present study. The author's intention is neither to develop a new steady-state CHF correlation, nor to improve the theory of steady-state CHF. The primary intent of the present study was to develop methods to predict the transient CHF, using previously developed knowledge of steady-state CHF. Chapter II briefly summarizes the basic concepts of steady-state CHF. In Chapter III, emphasis is placed upon analytical considerations of the CHF problem. Certain postulated thermal accidents in Light Water Reactors (LWR) are summarized in Chapter IV. The quasi-steady approach is defined in Chapter V, and the application of such an approach to transient CHF problem is discussed in Chapter VI. Examples from the literature, where the CHF cannot be determined through the quasi-steady approach, are cited in Chapter VII. In Chapter VIII, theoretical correlations to predict the CHF in power transients are developed and compared with experimental data. The pressure and mass flow-rate transients are theoretically analyzed, based on the first principles in Chapter IX. Based on the theoretical and experimental observations of previous chapters, a general mathematical model to correlate the transient CHF is obtained in Chapter X. The necessity for future research is discussed in Chapter XI. Chapter XI also concludes and summarizes the subject study.

CHAPTER II

BASIC CONCEPTS OF THE CRITICAL HEAT FLUX

Some basic concepts of the CHF are summarized within this chapter. The summary is restricted to the material which is necessary in the discussion of transient CHF. The CHF problems associated with external flow and with rotating liquid films (Mudawwar 1985) are not included in this summary. For a more detailed review of steady-state CHF, the readers are referred to Collier (1981), Gambill (1977), Bergles (1979), and Katto (1985). The concept of forced convective CHF in vertical circular cylinders with uniform heat flux is first considered.

CHF for Forced Convective Boiling in Vertical Circular Cylinders with Uniform Heat Flux

The geometry of this problem is shown in Figure 3. Before going into details, it is interesting to look at the upper and lower limits of the CHF, as observed by Collier (1981).

Boundaries of the CHF

For forced convective boiling in vertical circular cylinders with uniform heat flux, the minimum possible value of CHF can occur when the surface temperature at the exit reaches the saturation temperature.

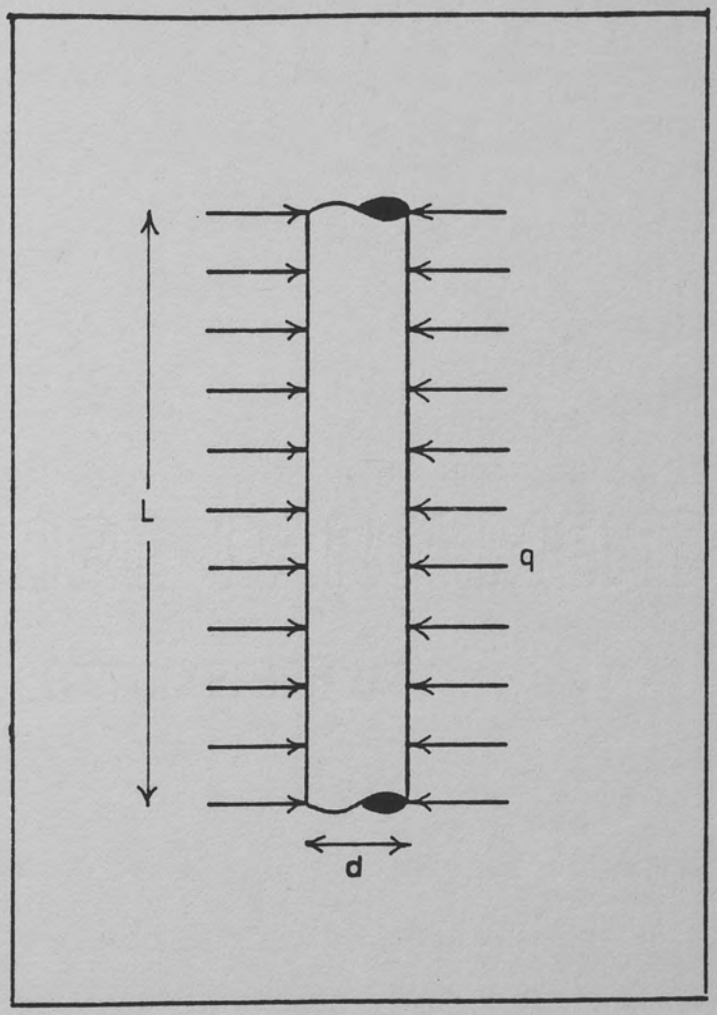

Figure 3. Vertical Circular Cylinders with Uniform Heat Flux

$$(q_{CHF})_{min} = (\Delta T_{SUB})_i / \left[\frac{4L}{GC_{pf}d} + \frac{1}{h_{c,f}} \right] \quad (1)$$

where $h_{c,f}$ is the convective heat transfer coefficient when the total flow is assumed to be liquid.

The maximum value of CHF can occur when the exit quality is equal to 1.

$$(q_{CHF})_{max} = \frac{G\, d\, h_{fg}}{4L} \left\{ 1 + \frac{C_{pf}(\Delta T_{SUB})_i}{h_{fg}} \right\} \quad (2)$$

For any system the value of CHF is within these limits, which cover a wide range. Equations 1 and 2 are also useful in identifying the independent parameters of CHF.

Independent Parameters of CHF

Equations 1 and 2 suggest a CHF correlation in the following form:

$$q_{CHF} = f[G, P, (\Delta T_{SUB})_i, L, d] \quad (3)$$

The CHF can also be expressed in terms of exit quality. The exit quality can be related to inlet subcooling via the energy-balance equation. In case of non-uniform heating, the CHF does not necessarily occur at the exit, as will be discussed in a later section. In this case, the total length L in equation 3 must be replaced by the axial coordinate z.

The effect of these parameters on the CHF are experimentally observed. Figures 4 through 9, obtained from Collier (1981),

illustrate these effects. Figure 4 shows that the CHF increases linearly with an increase in inlet subcooling. Although this is the general trend, a non-linear variation is also possible under certain conditions, as shown in Figure 8. Figure 5 shows that the CHF decreases linearly with the exit quality. An interesting result of Figure 5 is that the CHF increases as the mass velocity increases for low-quality and subcooled exit conditions, but an opposite trend is observed for high-exit quality. The tube length has a negative effect on the CHF, as seen in Figure 6; the CHF decreases as the tube length increases for fixed-inlet conditions. But for fixed-exit conditions, the tube length has no effect on the CHF, as shown in Figure 7. For fixed-inlet conditions, the CHF decreases rapidly for small tubes, and less rapidly for larger tubes, as shown in Figure 8. Figure 9 shows the effect of system pressure on the CHF. For a fixed-mass flux, diameter, length, and exit quality, the CHF increases with increasing pressure at low pressures and decreases with increasing pressure at higher pressures. If the inlet temperature is held constant, instead of exit quality, the rapid decrease in the CHF at high pressures is almost eliminated.

Besides these major parameters, there are additional minor influences on the CHF.

Minor Influences on the CHF

It has been experimentally observed that the following variables have some minor effects on the CHF, as cited by Collier (1981):

a. Method of heating the tube

b. Material of the tube wall

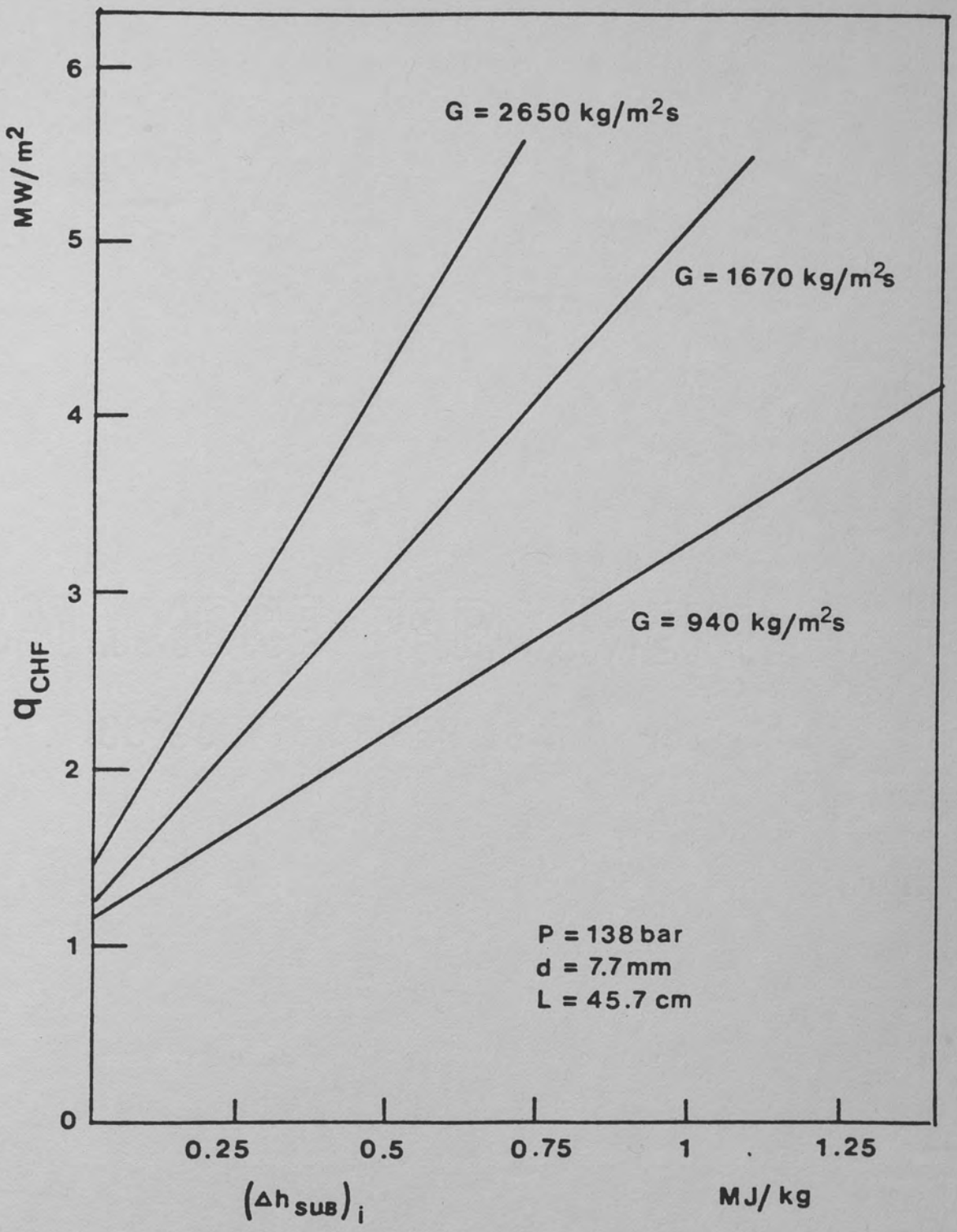

Figure 4. The Effect of Inlet Subcooling on CHF (Collier 1981)

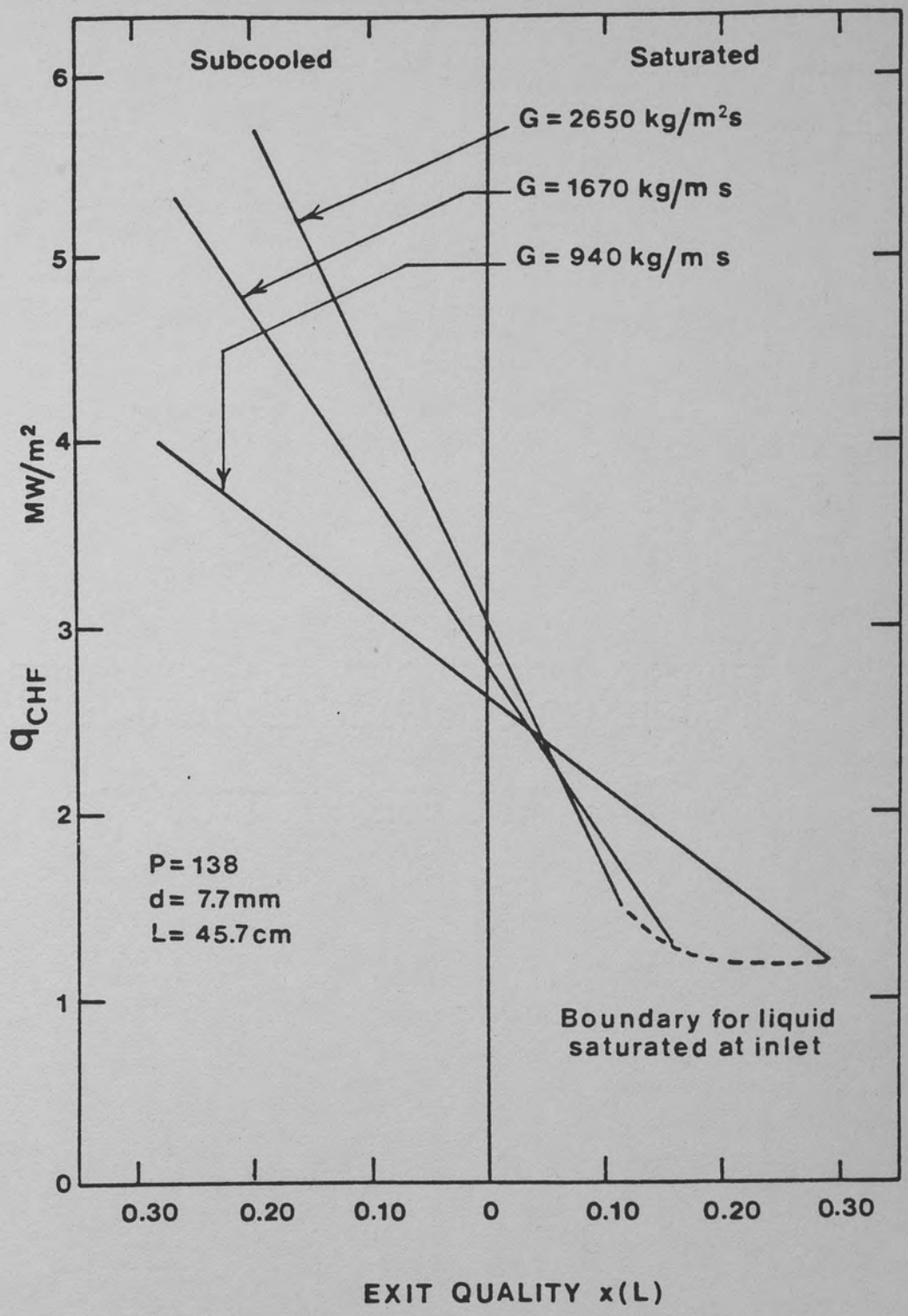

Figure 5. The Effect of Exit Quality on CHF (Collier 1981)

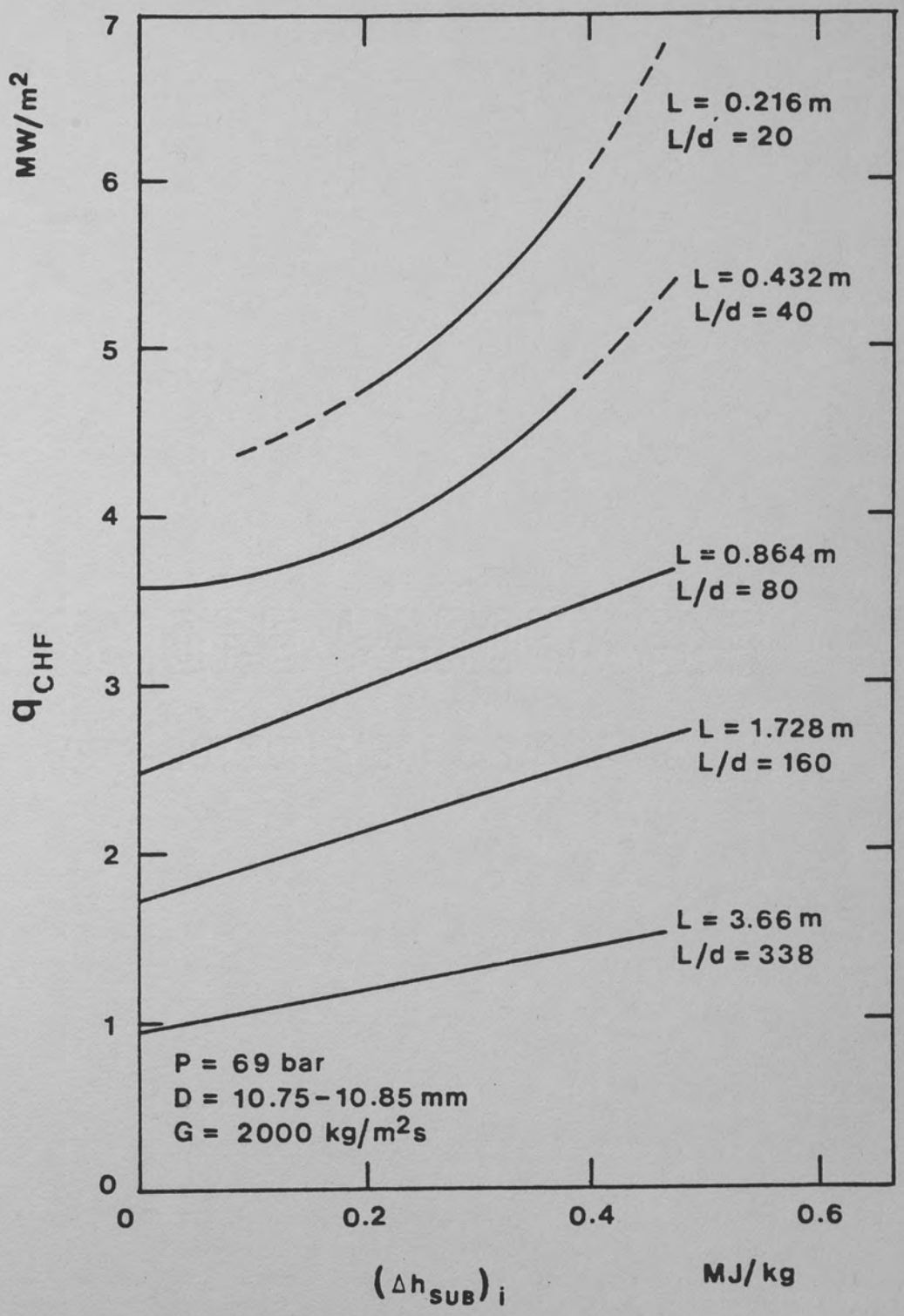

Figure 6. The Effect of Tube Length on CHF at Fixed Inlet Conditions (Collier 1981)

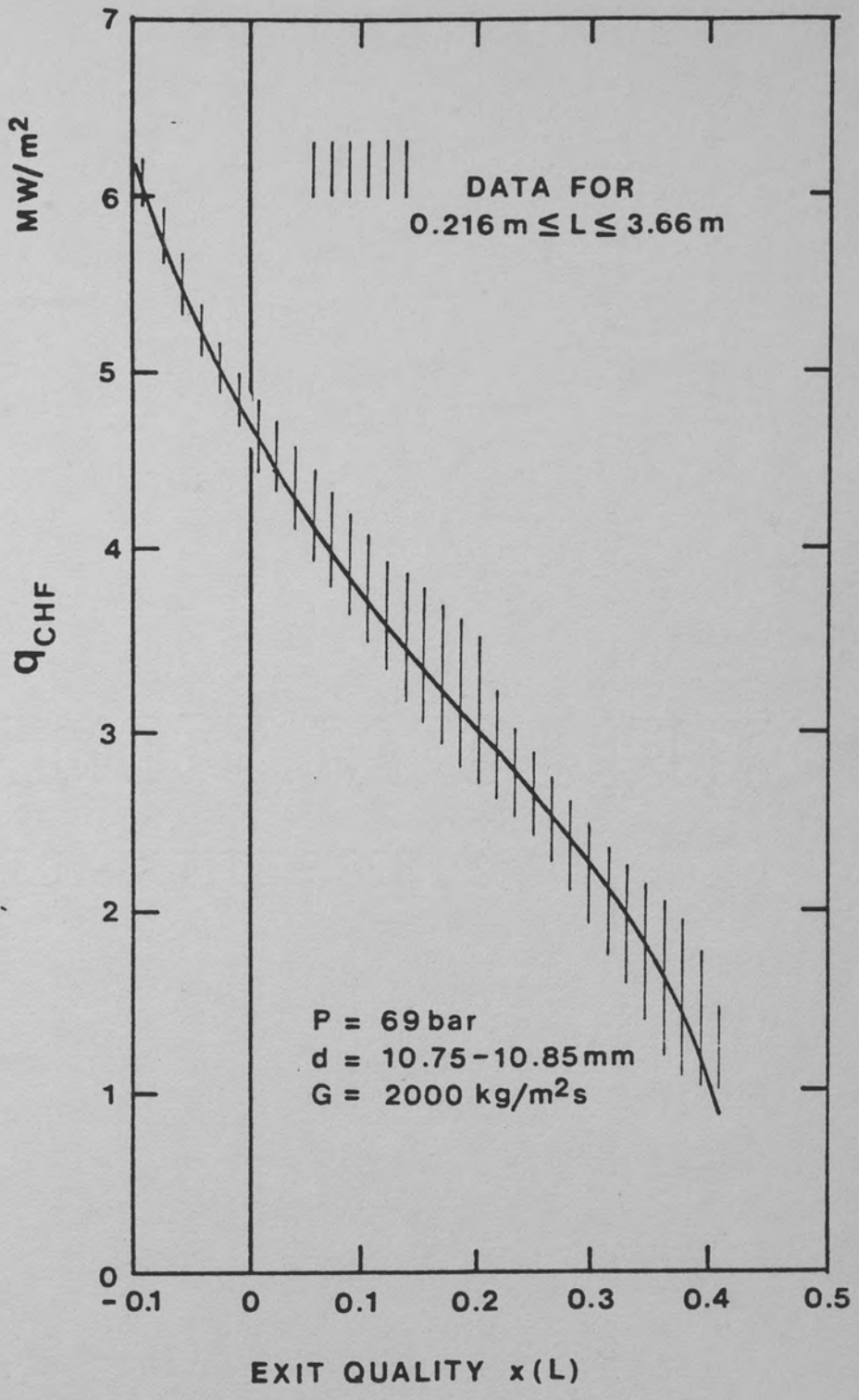

Figure 7. The Effect of Tube Length on CHF at Fixed Exit Conditions (Collier 1981)

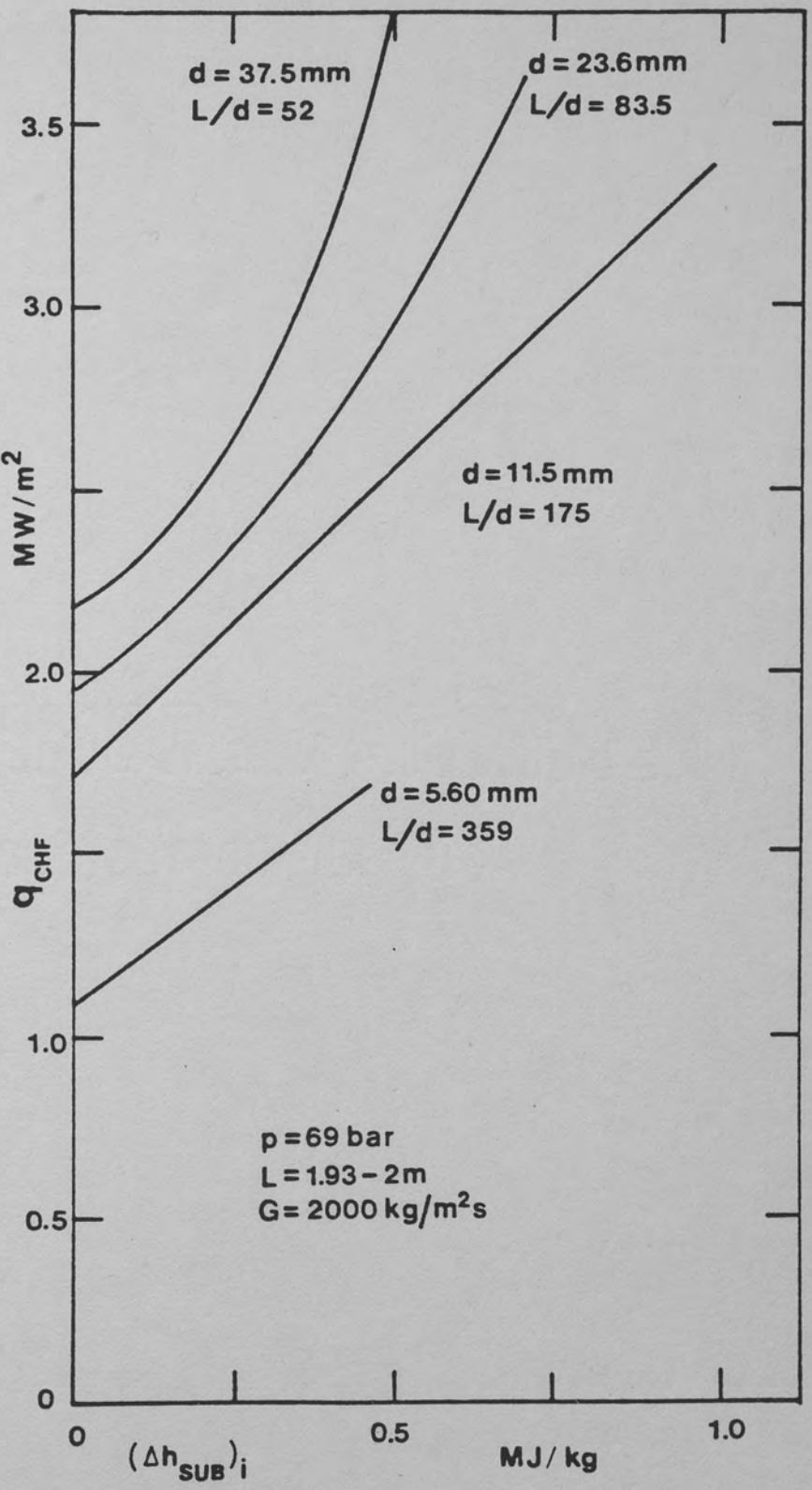

Figure 8. The Effect of Tube Diameter on CHF at Fixed Inlet Conditions (Collier 1981)

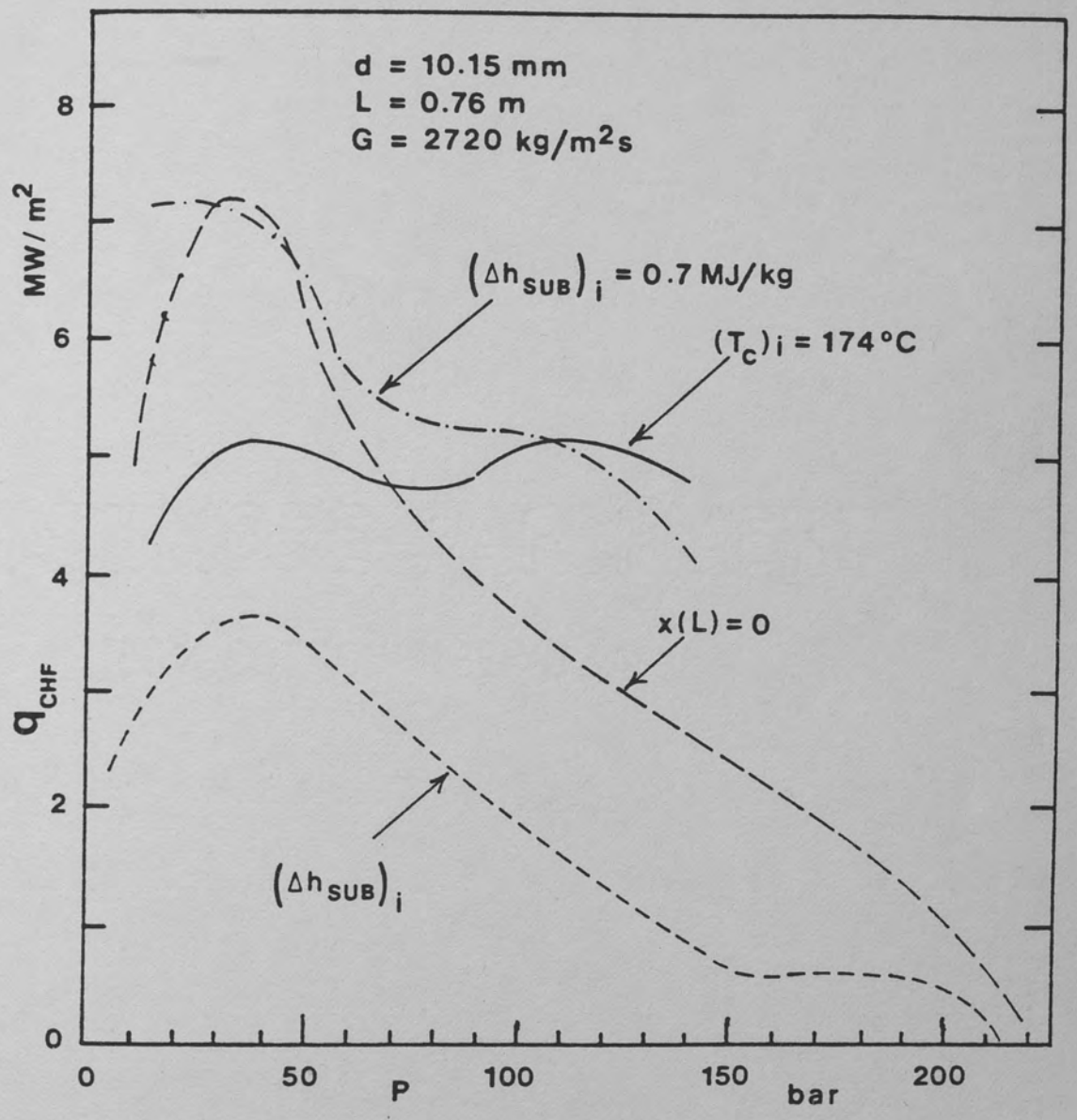

Figure 9. The Effect of System Pressure on CHF (Collier 1981)

c. Tube wall thickness

d. Internal bare surface finish: Surface roughness has no effect on film boiling but enhances nucleate boiling. The nucleate boiling portion of the boiling curve is shifted towards right by smoother surfaces, but the effect on the magnitude of CHF is very small. This is shown in Figure 10.

Although informative, the material of this section is not directly applicable to CHF problems associated with nuclear technology. These problems deal with a cosine-shaped axial heat-flux profile, rather than a uniform heat flux profile, as shown in Figure 11. The flow is also parallel to a rod bundle, rather than an internal flow inside a verticalcircular cylinder. These two characteristics are examined in the following sections.

CHF for Forced Convective Boiling in Vertical Circular Channel, with Non-Uniform Axial Heal Flux

At low-quality conditions, minimal integral effects are present. Therefore, the local conditions approach, which assumes only the local heat flux, pressure and quality control CHF, is valid even for non-uniform-axial heat flux. But, for high quality situations ($x \gtrsim 15\%$) an integral approach predicts the CHF best.

One approach to an integral correlation is to write a critical quality-boiling length correlation as was done in the CISE correlation. This concept is explained in a later section about CHF correlations.

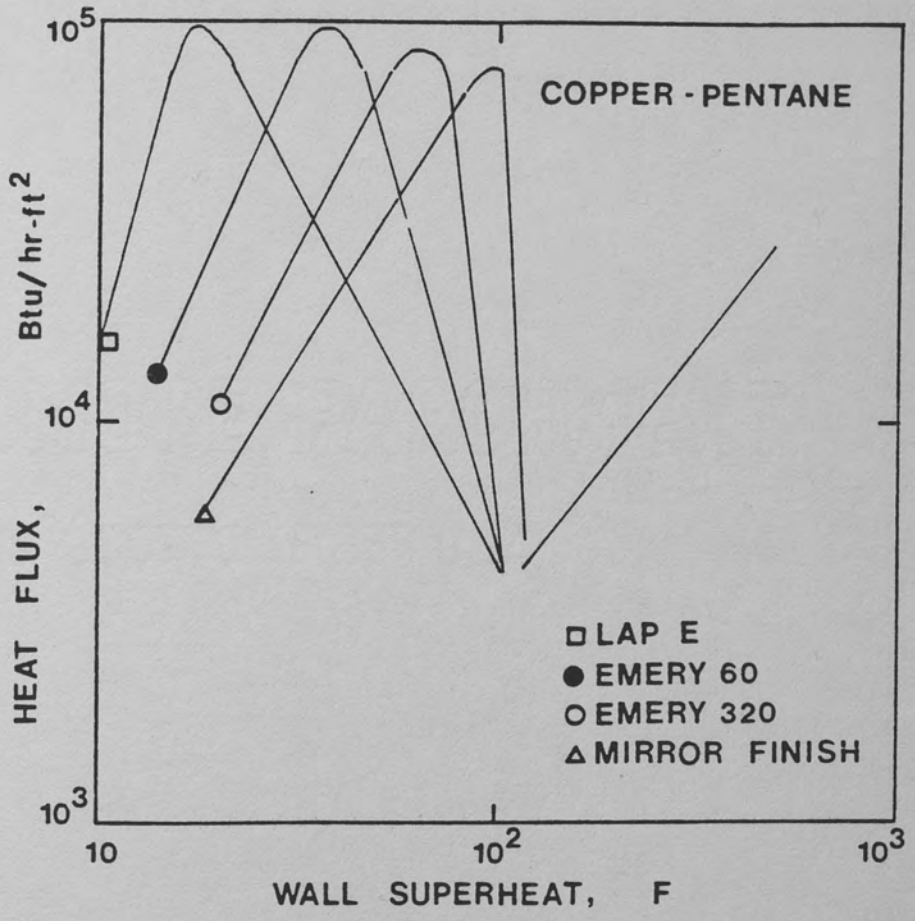

Figure 10. The Effect of Surface Finish on the Boiling Curve (Berenson 1962)

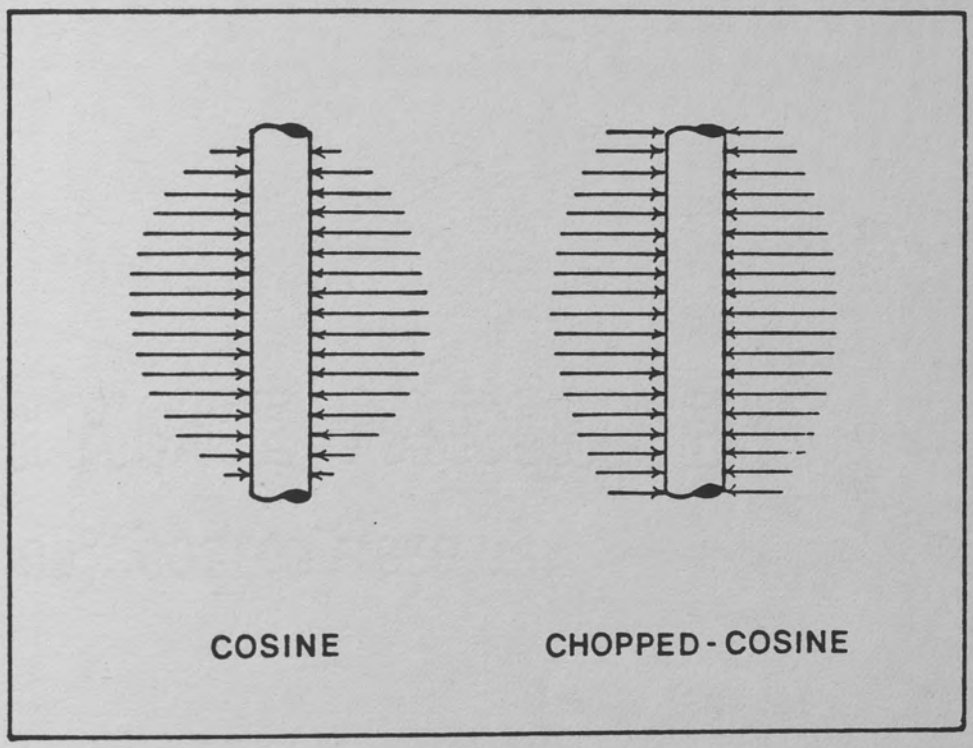

Figure 11. Cosine-Shaped Axial Heat Flux Distribution

Another approach is the F-factor method, which is proposed by Tong and his co-workers (Tong 1966), (Smith 1965), (Tong 1967). At the present time, this method as applied by Lee (1966) is recommended by Collier (1981) as the best empirical correlation for smooth non-uniform axial heat-flux profiles. In this method, a factor F is defined such that

$$F = \frac{[q_{CHF}(z)]_u}{[q_{CHF}(z)]_{nu}} \tag{4}$$

where $[q_{CHF}(z)]_u$ is the value of the CHF at any given local enthalpy for the uniform heat flux profile case and $[q_{CHF}(z)]_{nu}$ is the value of the CHF at the same given local enthalpy for the particular non-uniform heat flux profile case.

By considering an energy balance on the superheated boundary layer in the bubbly-flow region (Tong 1966) or a mass balance on a liquid film in the annular-flow region (Smith 1965), F is found to be

$$F = \frac{\Omega}{1 - \exp(-\Omega z_{CHF})} \int_0^{z_{CHF}} \frac{q(z)}{q(z_{CHF})} \exp[-\Omega(z_{CHF} - z)]dz \tag{5}$$

The value of Ω is found by comparing the method to experimental data. Tong et al. (Tong 1966) obtained the following relation for Ω:

$$\Omega = 0.44[1 - x(z_{CHF})]^{7.9}/(G/10^6)^{1.72} \ (in^{-1}) \tag{6}$$

where G is given in lb/hr-ft^2. In his application, Lee (1966) suggested a different correlation for Ω. A more detailed analysis of this method is beyond the scope of the present study. For further information, the individual papers as referenced above may be consulted.

The CHF problem in rod bundle geometry is discussed in the next section.

Rod Bundle Geometry

In the previous sections, the circular channel was considered. There are also CHF problems associated with other geometries, like annuli (Katto 1979 and 1981) and rectangular ducts (Katto 1981), discussed in the literature. But one major area of application for CHF is the nuclear-reactor core, where the flow is through a rod bundle rather than a circular channel. Therefore, the rod bundle geometry is of major importance for practical applications. The rod bundle prediction models can be classified in two categories:

a. Lumped parameter correlations, where average values of heat flux, mass flow, etc., are used and a correlation relating these values is derived.

b. For more accurate results, the subchannel analysis is performed. There are two different approaches for subchannel analysis. The difference between the classical subchannel and rod-centered subchannels is shown in Figure 12. With the classical subchannel models, it is usually necessary to develop independent CHF correlations, but with the rod-centered models, quite accurate predictions can be obtained

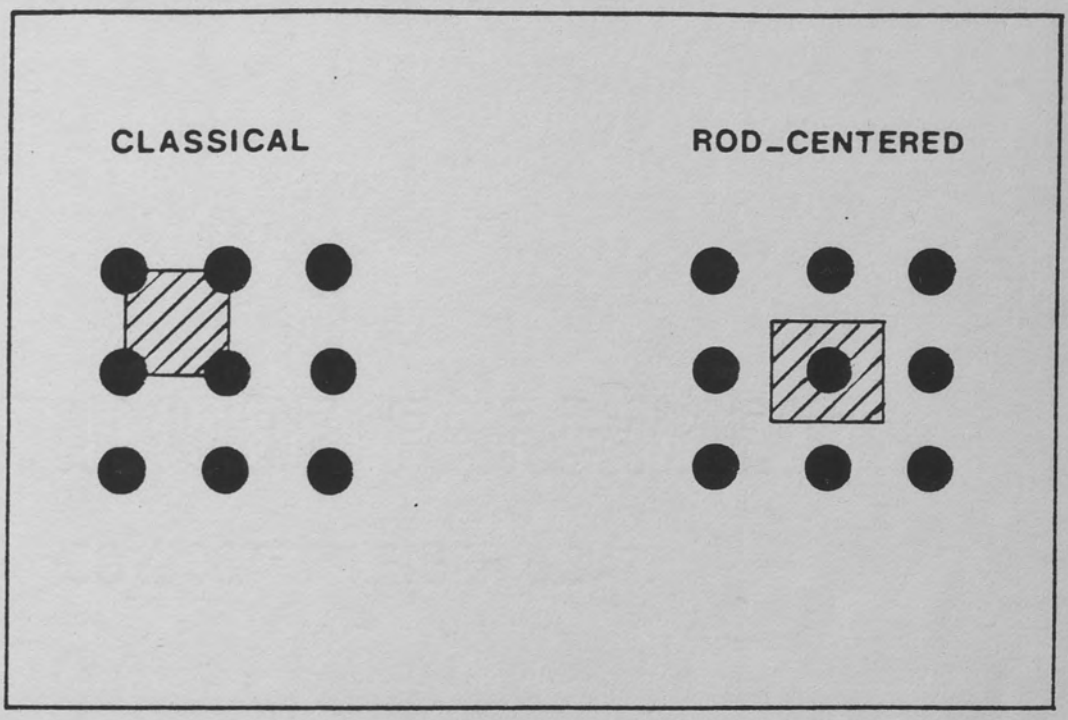

Figure 12. Subchannels in Rod Bundles

by using round tube or annulus correlations on an equivalent diameter basis (Hewitt 1979).

The different mechanisms which lead to CHF are reviewed in the next sections.

Mechanisms of CHF

Although there are a few postulates to explain the CHF phenomenon, there is not yet a complete understanding of all mechanisms involved. There are different explanations for CHF's occurring at low-quality (DNB) and at high-quality conditions (Dryout).

Subcooled and Low-Quality Regions

a. Near Wall Bubble Crowding and Vapor Blanketing: This condition is schematically shown in Figure 13. A boundary layer of bubbles grows to a point where it restricts the access of liquid to the heated surface. Kutateladze (1966) and Tong (1968b) suggest that the critical phenomenon is the separation of the hydrodynamic boundary layer. A successful analytical prediction of DNB for this mechanism is obtained by Weisman and Pei (Weisman 1983). This theoretical approach is summarized in Chapter III.

b. Dryout under a vapor clot: This is due to local overheating, following the bubble growth from a nucleation center. As shown in Figure 14, the temperature at the spot is too high, such that it cannot be rewetted when the bubble departs. It is generally assumed that, for this form of CHF, the CHF depends only on local enthalpy and there are no history effects.

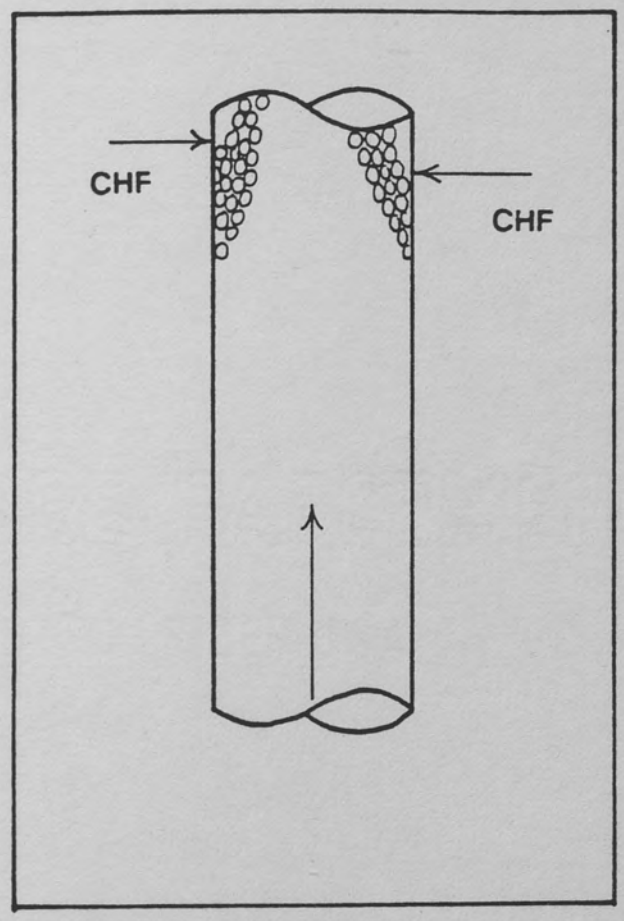

Figure 13. Near Wall Bubble Crowding and Vapor Blanketing (Collier 1981)

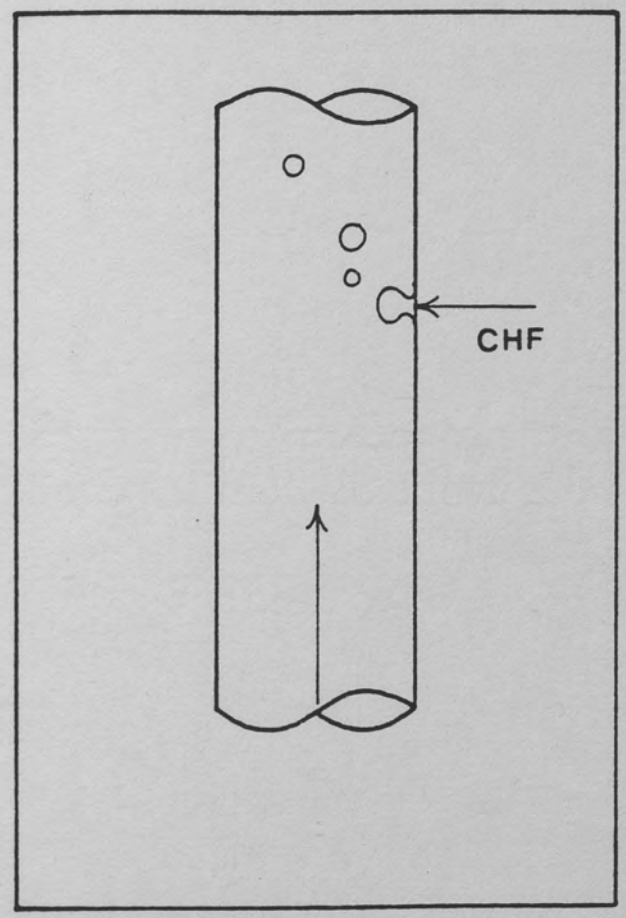

Figure 14. Dryout Under a Vapor Clot (Collier 1981)

c. Evaporation of liquid surrounding a slug-flow bubble: This phenomenon is illustrated in Figure 15, and it is likely to occur for slow flow in small diameter tubes. Bubbles form in the thin liquid film and cause local dryout. A runaway burnout condition could develop whenever the local temperature did not quite return to the original value after a liquid slug has passed by. Under this condition, the wall temperature would rise through a saw-toothed pattern and eventually become hotter than the Leidenfrost temperature, thus eliminating the possibility of liquid quenching and promoting a post-CHF condition. Since the slug frequency is hard to determine, there is no analytical criterion for the onset of this kind of CHF. Such a CHF phenomenon exists in the slug flow regime only, which is very difficult to obtain if the pipe diameter is larger than the critical wavelength, λ_c (Hsu 1976). The critical Taylor instability wavelength is given by:

$$\lambda_c = 2\pi\sqrt{3}[\sigma/g(\rho_f - \rho_g)]^{\frac{1}{2}} \qquad (7)$$

The slug flow is also very unlikely at elevated pressure. Therefore, this type of CHF is very unlikely, especially for pressurized water reactors (PWR).

High-Quality Region/Annular Flow

To a reasonable approximation, the CHF in annular flow occurs when the film-flow rate locally and smoothly goes to zero. Figure 16 illustrates the critical phenomenon associated with annular-flow regime. For CHF occurring at high quality under annular-flow

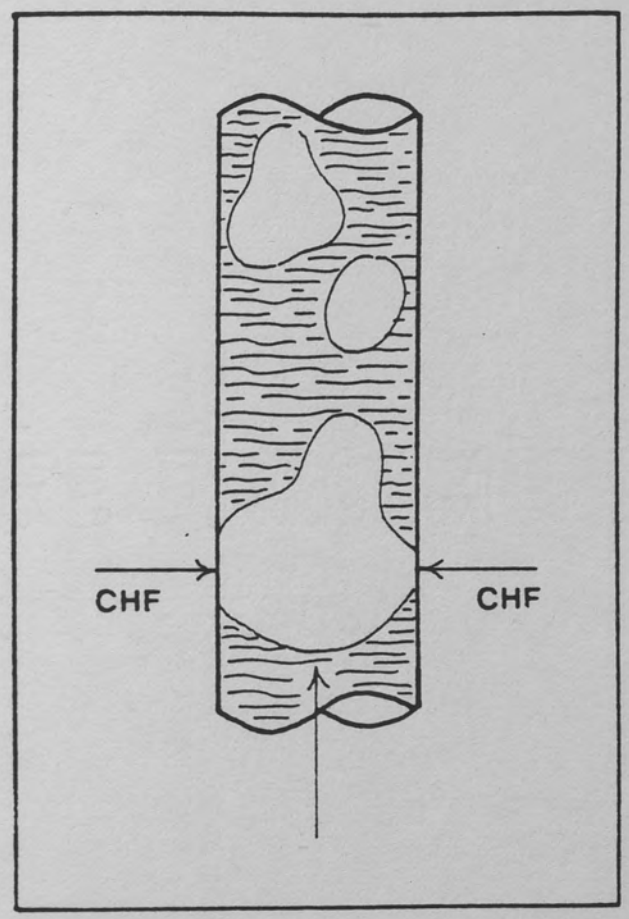

Figure 15. CHF Associated with Slug Flow (Collier 1981)

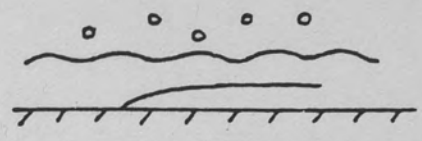

(a) Vapor film formation under liquid film

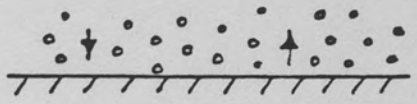

(b) Droplet mass transfer rate = rate of evaporation

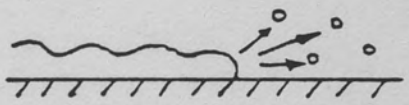

(c) Sudden disruption of film

(d) Dry patch formation

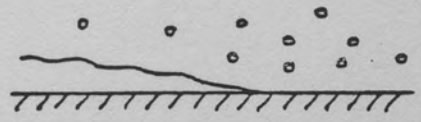

(e) Film dryout

Figure 16. CHF Mechanisms in Annular Flow (Hewitt 1979)

conditions, there are successful analytical approaches which compare reasonably with the experimental data. These approaches will also be summarized in Chapter III.

A tentative map of regions of operation of various CHF mechanisms is given in Figure 17.

Empirical CHF Correlations

There are hundreds of CHF correlations available in the literature. Some of these are relatively successful. But in using these correlations, one should be careful about the range of independent variables over which data were correlated. Some of the frequently used correlations are given in the Appendix A. A successful CHF correlation must manifest the following asymptotic trends, as observed by Groeneveld et al. (1981).

a. CHF approaches pool boiling CHF at low flows,

b. CHF approaches zero as x approaches unity,

c. CHF cannot become negative, even for negative flow (downflow),

d. CHF reaches a maximum within an approximate pressure range of 3-6 MPa for water,

e. CHF approaches zero when P approaches critical pressure.

There are different approaches in correlating the CHF data. The local condition hypothesis assumes CHF is only a function of the local fluid conditions. According to Hsu and Graham (Hsu 1976), the local condition CHF may be correlated in the form:

$$g_1 (x, q_{CHF}) = 0 \tag{8}$$

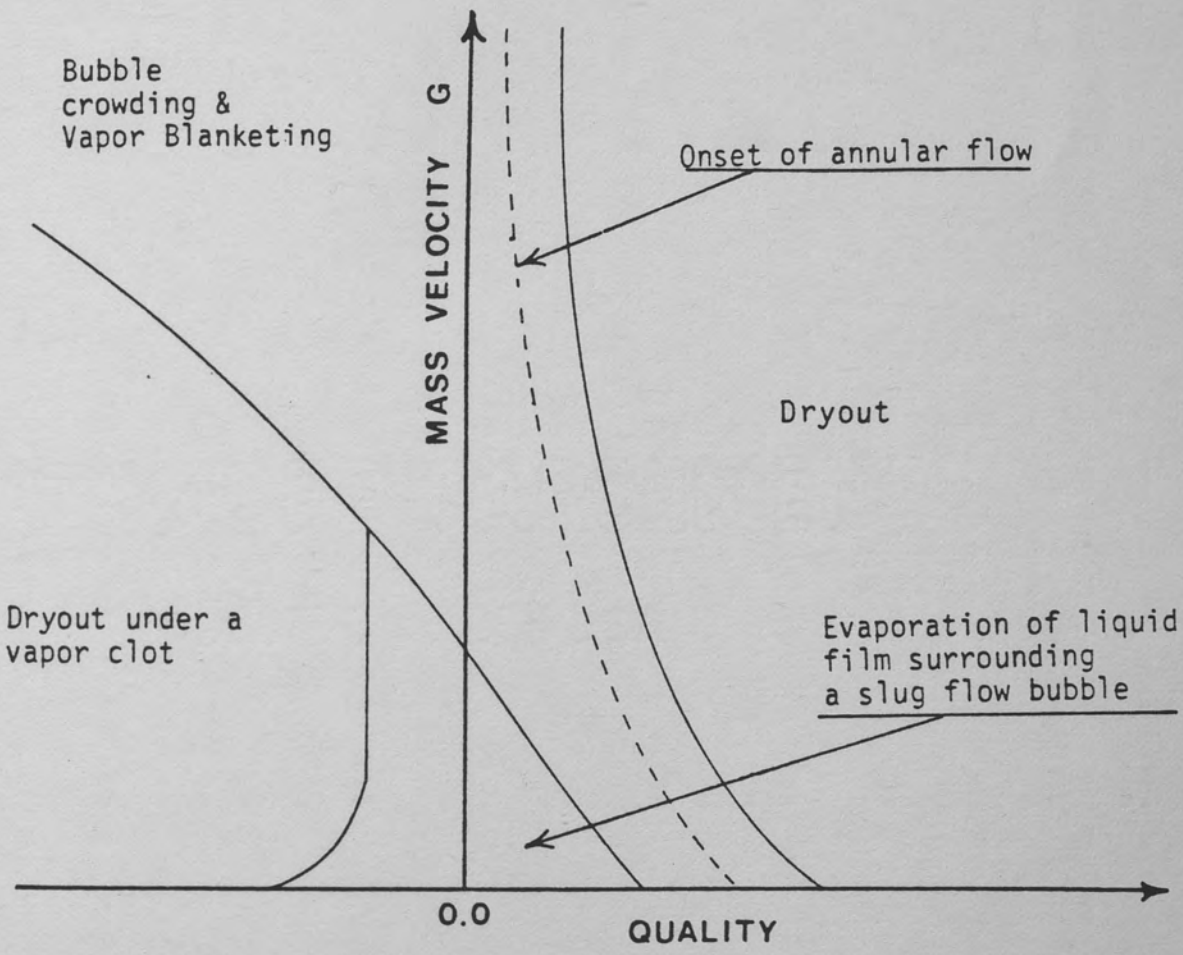

Figure 17. Map for Different CHF Mechanisms (Collier 1981)

If the CHF is assumed to be dependent on flow history or upstream effects, the correlation should be (Hsu 1976)

$$g_2(x, L_{SAT}) = 0 \tag{9}$$

where L_{SAT} is the saturation length.

Bertoletti et al. (1965) also considered the global effects on CHF, in which case the correlation takes the form

$$g_3 [Q_{SAT}(z), L_{SAT}(z)] = 0 \tag{10}$$

where Q_{SAT} (z) is the total power input from the saturation point.

The last two approaches state that an integral approach is required to determine CHF, as opposed to the first approach which states that CHF is only a function of the local parameters. Both approaches have successful applications in different problems. For CHF occurring under uniform heating, the local conditions approach is quite successful. For non-uniform heating, however, the local condition approach is still satisfactory to determine the DNB; but for dryout conditions, an integral approach is necessary.

In nuclear reactors, especially during accident situations, a wide range of thermal-hydraulic conditions are possible, and the CHF may not be predicted by a single correlation. The parametric ranges for the independent variables are restricted for individual correlations. In addition, each correlation is valid for a specific CHF mechanism, as discussed earlier. Therefore, to encompass all possible thermal-hydraulic conditions, many independently developed correla-

tions must be tied together in a CHF mapping as suggested by Dahlquist et al. (1985).

Another rather difficult method is to start from scratch and develop a set of consistent correlations for a wide thermal-hydraulic range, as accomplished by Katto (1978 through 1982). In four different regimes, which he named L, N, H, and HP regimes, Katto analyzed the data in terms of five dimensionless groups: $(q_{CHF,0}/Gh_{fg})$, $(G\rho_l/G^2L)$, (L/d), (ρ_v/ρ_l) and $(\Delta h_{SUB})_i/h_{fg}$. The term $q_{CHF,0}$ is the value of CHF for saturated inlet conditions. If the liquid is subcooled at the entrance, the CHF is found by using the following linear relation:

$$q_{CHF} = q_{CHF,0}\,[1 + K(\Delta h_{SUB})_i/h_{fg}] \tag{11}$$

For flow in a vertical-circular channel with uniform heat flux, Katto correlated the data for each regime. The correlations yield to each other at the regime boundaries. The empirical correlations for each regime, the proportionality constant K for each regime, and the equations for the regime boundaries are given in Appendix A. Here the characteristics of each regime are discussed.

The L-regime is characterized by annular flow which is closely allied to dispersed flow. Here the CHF mechanism is due to the deficiency of liquid (Dryout). The linear relation between q_{CHF} and $(\Delta h_{SUB})_i$ is observed.

The N-regime displays a bubbly flow. The exit quality is low. The CHF occurs by transition from nucleate boiling to film boiling

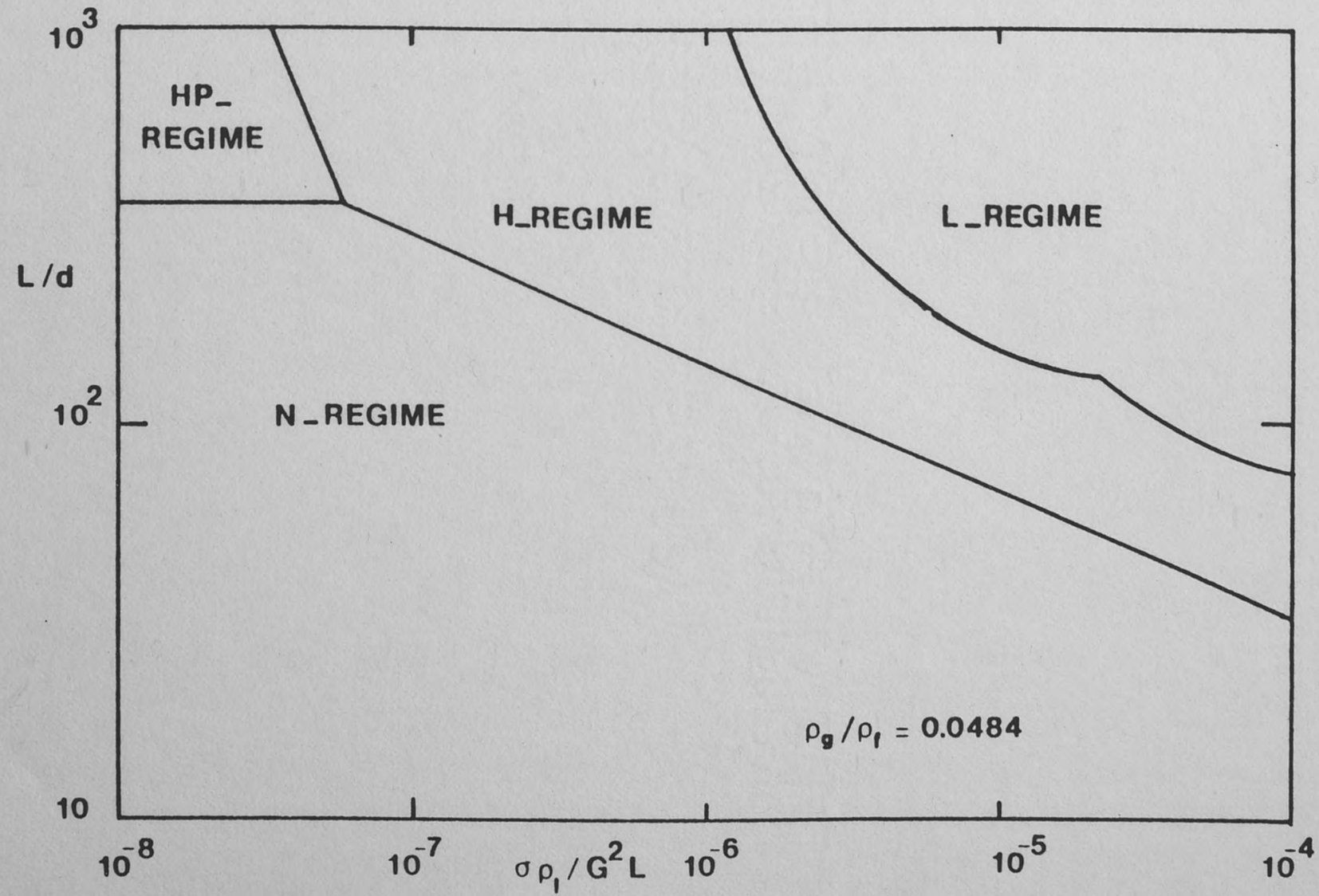

Figure 18. The Regime Map for Katto Correlations (Katto 1982)

(DNB). Katto noticed that the relation between q_{CHF} and $(\Delta h_{SUB})_i$ is not linear in this regime (1978).

The H-regime is characterized by annular flow. This is an intermediate regime between L and N regimes. Katto assumed that the hydrodynamic instability of the interface is responsible for the CHF (1979b). The linear relation between q_{CHF} and $(\Delta h_{SUB})_i$ is also observed in this regime.

Finally, the HP-regime is defined as the substitute for the N regime at high system pressures. The exit flow patterns in this regime could not be determined. The linear relation between q_{CHF} and $(\Delta h_{SUB})_i$ is also observed.

By using the empirical correlation for each regime and by neglecting the existence of any transition region, the boundaries for the regimes were obtained by Katto (1980b). This regime map is shown in Figure 18.

In his studies, Katto also analyzed the heating-length concept (Katto 1979b) and the limiting exit quality concept (Katto 1982). The empirical correlations for high-quality regimes are employed to predict the limiting exit quality, and the prediction compares satisfactorily with the existing data (Katto 1982).

CHF in Forced Convection of Fluids Other Than Water

Although most of the test data are for water, some data for different liquids also appear in the literature. The impetus for other fluid CHF modeling include:

a. In the chemical and process industries, a wide variety of liquids are used in boiling equipment; and there is a need to predict CHF for these cases.

b. Because of the high latent heat and high critical pressure of water, the CHF experiments with this liquid tend to be very expensive. To reduce the cost, there is a trend towards other liquids.

c. Having measured the CHF using the modeling fluid, then the problem is to establish a quantitative relationship to water. One of the more successful approaches to this problem of scaling is that of Ahmad (1973). By classical dimensional analysis, Ahmad (1973) combined three dimensionless groups into a modeling parameter Ψ_{CHF} as follows:

$$\Psi_{CHF} = \left(\frac{G\ d}{\mu_f}\right)\left(\frac{\mu_f}{\sigma\ d\ \rho_f}\right)^{2/3}\left(\frac{\mu_f}{\mu_g}\right)^{1/8} \qquad (12)$$

The success of this scaling model can be seen in Figure 19.

The other liquids which are of interest to the nuclear industry are the liquid metals which are used in Liquid Metal Fast Breeder Reactors (LMFBR). Unfortunately, boiling heat transfer in liquid metals is more of a challenge than water and other organic liquids. Even the problem of single-phase convection with liquid metals shows completely different characteristics than the liquids with higher Prandl number. For instance, a commonly-used Dittus-Boelter equation for single-phase convective heat transfer may not be used for liquid metals with very low Prandtl number (Bejan 1984). This different

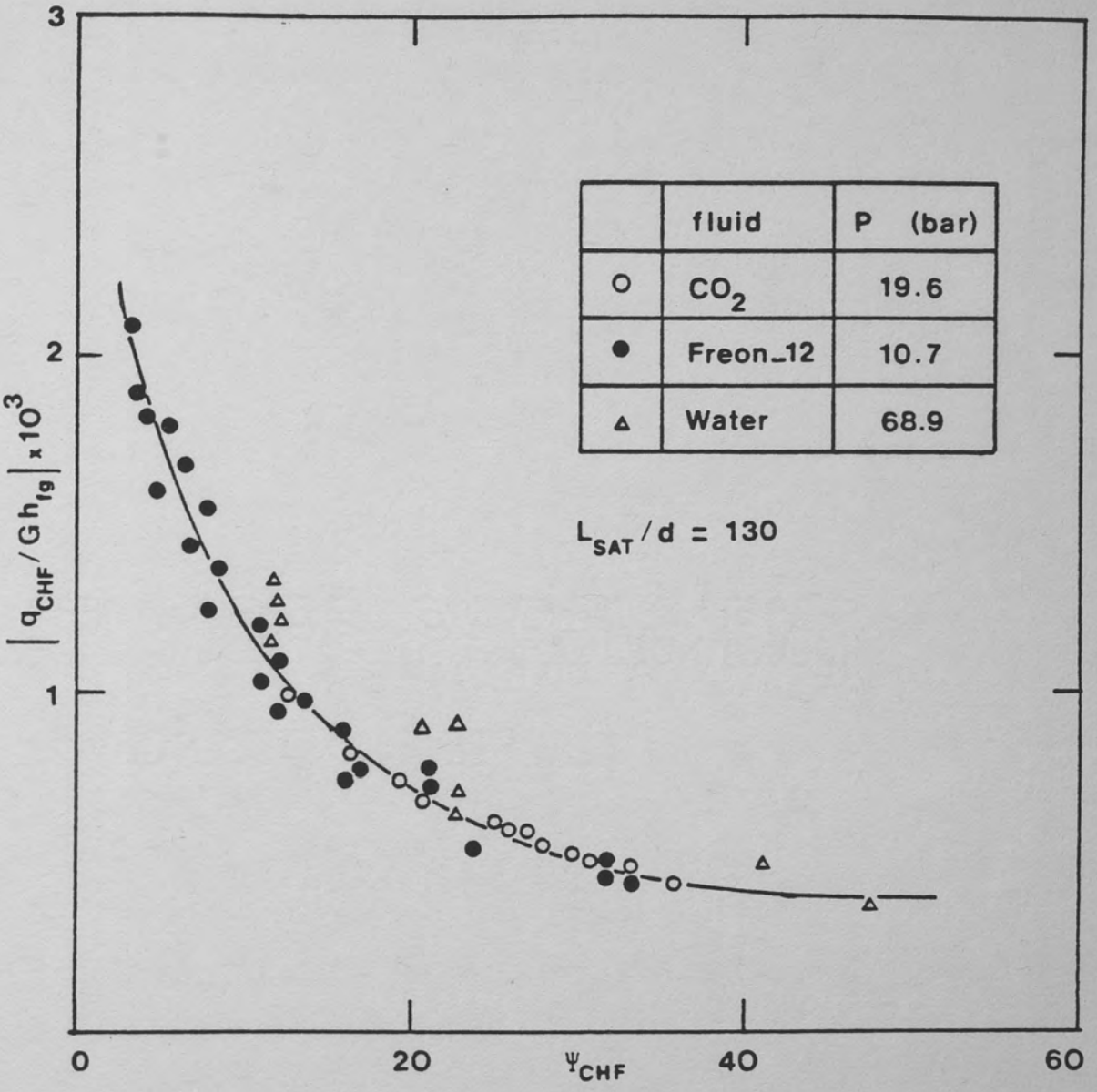

Figure 19. Application of Ahmad's Scaling Model (Ahmad 1973) for Water, Freon-12 and Carbon Dioxide (Collier 1981)

behavior of liquid metals is attributed to their high thermal conductivity, which results in a high radial and axial molecular conduction (Kays 1980). In general, single-phase convection of liquid metals does not lead to a simple analytical formulation, and there are many open questions concerning liquid-metal heat transfer (Holman 1981).

Considering the fact that the single-phase convection of liquid metals has many unanswered questions, one can appreciate the difficulties in the boiling heat transfer problem of liquid metals. Therefore, it is not surprising that the CHF in liquid metals may not be predicted by the empirical CHF correlations developed for water and other organic liquids. There are CHF correlations available for individual liquid metals, like potassium (Garlov 1975), sodium (Costa 1970), etc. But, in general, the boiling heat transfer in liquid metals is in its early stages, as compared to the boiling heat transfer in water and other organic liquids, as observed in the study of Kottowski and Savatteri (1984). Therefore, a general scaling criterion to correlate the CHF for all the liquid metals is not established yet. And due to the above explained reasons, it is doubtful that a general scaling model similar to Ahmad's (1973) may be established to include all possible liquids, like organic liquids, water, liquid metals, and oils.

CHAPTER III

THEORETICAL STUDIES OF CRITICAL HEAT FLUX

A detailed summary of theoretical CHF studies is given in this chapter. The first section contains the theoretical models for pool-boiling CHF. In the second section, forced convective CHF is considered and analytical CHF models for near-wall bubble crowding and annular flow dryout mechanisms are summarized.

Pool Boiling CHF

Empiricism generally prevails in determining the CHF. However, for saturated pool boiling, Zuber's (1958) analytical model, with a few modifications, is the most widely used CHF criterion. Zuber's model postulates that the vapor generated at the heater surface forms a continuous columnar escape flow with $\lambda_c/2$ diameter vapor jets at intervals of λ_c, where λ_c is the critical wavelength due to Taylor instability. According to the model, CHF occurs where the liquid-vapor interface becomes unstable due to the Helmholtz instability. Using this CHF model, and within a few approximations, Zuber obtained the following pool boiling CHF correlation:

$$q_{CHF,OO} = 0.131\, \rho_g h_{fg} [\sigma\, g\, (\rho_f - \rho_g)/\rho_g^2]^{\frac{1}{4}} \qquad (13)$$

The same form of the equation was also obtained by Kutatelatze (1963), who correlated the data through dimensional analysis; instead of the constant 0.131, Kutatelatze proposed the constant to be 0.16 ± 0.03. Later, Leinhard and co-workers (Leinhard 1981) reviewed Zuber's model in light of the experimental data. They proposed that the critical, unstable wavelength λ_c should be the most susceptible wavelength, due to a Taylor instability, given by

$$\lambda_D = 2\pi\sqrt{3}\,[\sigma/g(\rho_f - \rho_g)]^{\frac{1}{2}} \qquad (14)$$

They also assumed that at the onset of the CHF the Helmholtz instability wavelength is equal to the Taylor instability wavelength. With these assumptions, they suggested that the constant 0.131 be raised to 0.149. This pool boiling CHF model is illustrated in Figure 20. Leinhard and co-workers also extended Zuber's model originally postulated for infinite upward-facing horizontal flat plates, to heaters of finite geometry (Leinhard 1981). Later reports on nucleate boiling, however, contradict the assumptions of continuous vapor-escape columns. In actuality, vapor is observed (Moissis 1963) to escape in the form of vapor slugs with unsteady behavior.

Gaertner and Westwater (1960; 1965) observed the following in their experiments: (1) the heated surface is wetted by a liquid film which contains numerous columnar vapor stems, as shown in Figure 21.a, (2) the massive vapor bubbles on top of the liquid film departs when it reaches a certain size and is immediately replaced by a new bubble, (3) the total cross-sectional area of the vapor stems is independent of the heat flux, and (4) the thickness of the liquid film decreases

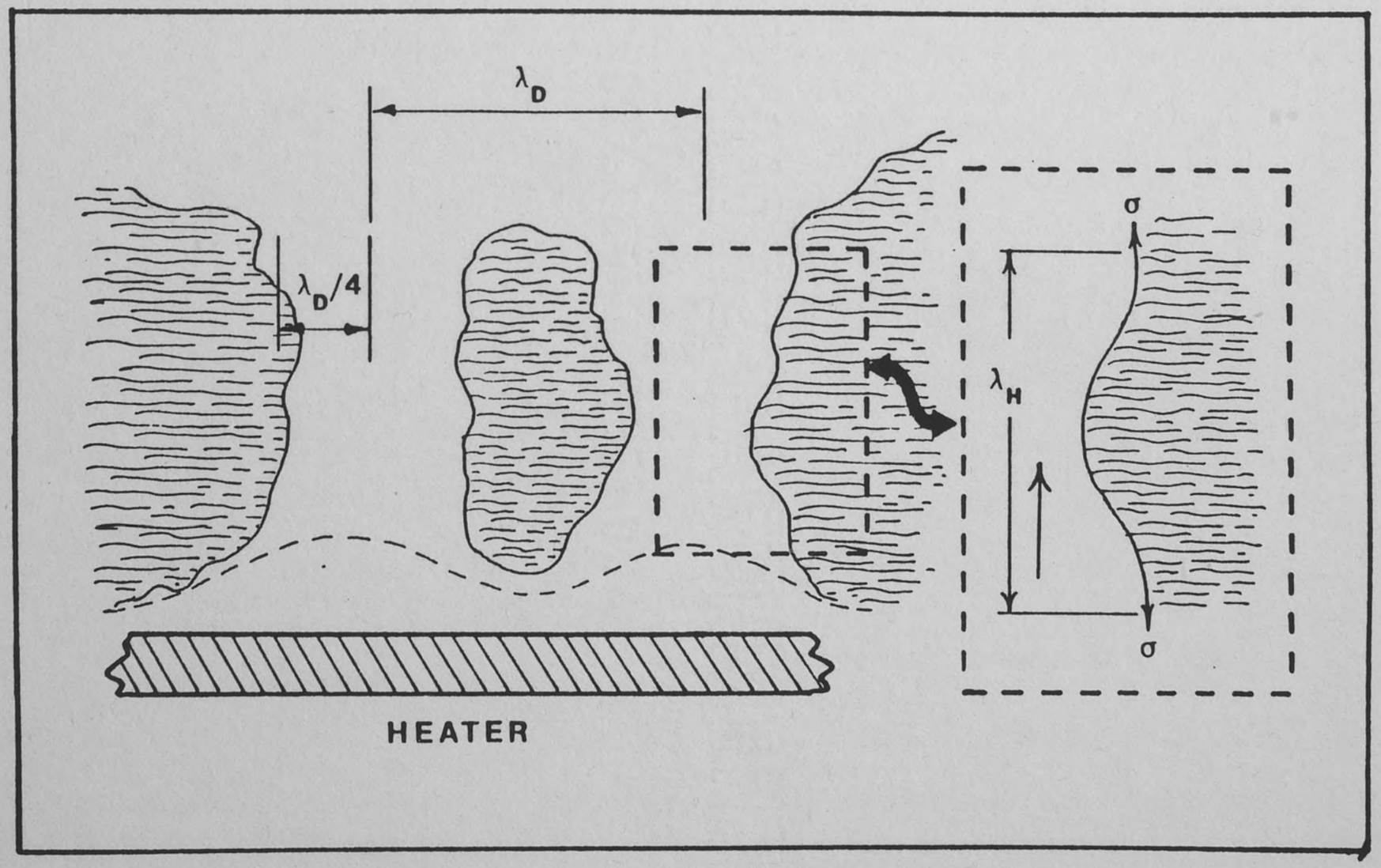

Figure 20. Zuber's (1958) CHF Model (Leinhard 1981)

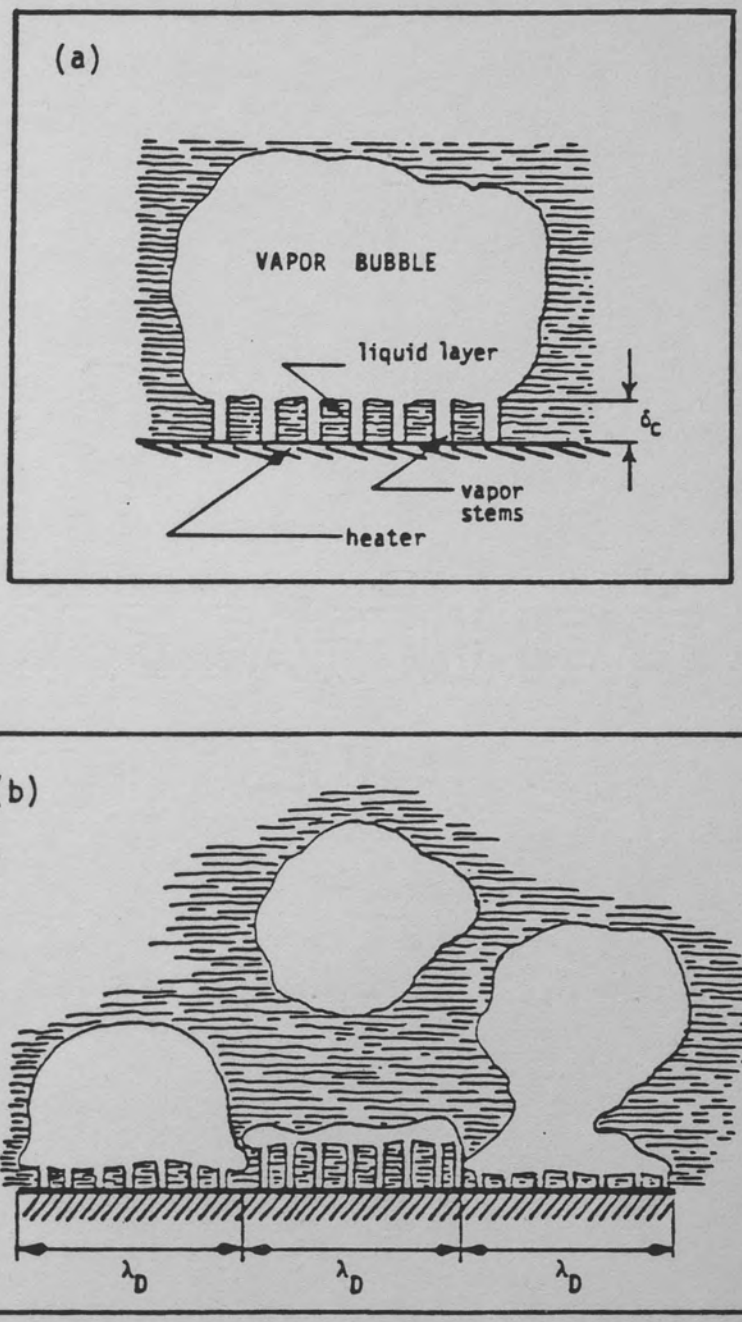

Figure 21. Boiling Configuration at High Heat Fluxes Over Flat Plates (Haramura 1983)

with increasing heat flux. Based on these experimental observations, the model of Zuber has been questioned (Katto 1970) and, recently, Haramura and Katto (1983) proposed a new hydrodynamic model for pool boiling CHF. Their physical model incorporates the observations reported by Gaertner and Westwater (1960; 1965) and is called (Katto 1985) the "multi-step" model, because it suggests that the CHF occurs as a result of various factors such as: (1) the appearance of an interference region in nucleate boiling, accompanying the critical liquid film thickness phenomenon due to the Helmholtz instability, (2) the vapor blanket overlying the liquid film on the heated surface, (3) the hydrodynamic mechanism feeding liquid from the bulk liquid to the heated surface, and (4) liquid depletion on the heated surface.

The model of Haramura and Katto (1983) is based on the experimental observation that the bubble is observed to hover over the liquid film, and the hovering period is formulated in the following form, as given by Haramura and Katto (1983):

$$\tau_d = (3/4\pi)^{0.2} \{[4(\xi \rho_f + \rho_g)]/[g(\rho_f - \rho_g)]\}^{0.6} v_1^{0.2} \qquad (15)$$

where v_1 is the volumetric growth rate of the bubble and ξ is the volumetric ratio of the accompanying liquid to the moving bubble. The term ξ is taken as 11/16 by Haramura and Katto.

Haramura and Katto (1983) assumed that the liquid layer thickness, δ_c, is a fraction between 0 and 0.5 of the critical wavelength, λ_H, for the Helmholtz instability in the vapor stems, and is given as:

$$\delta_c = \gamma\, 2\pi\, \sigma\, [(\rho_f + \rho_g)/(\rho_f\, \rho_g)](A_v/A_w)^2\, (\rho_g\, h_{fg}/q)^2 \qquad (16)$$

where $0 < \gamma < 0.5$

In their study Haramura and Katto used an average value for γ of 0.25.

Also based on the experimental results of Gaertner and Westwater (1960; 1965), the bubbles were assumed to be equally spaced and the interval between the bubbles, λ_D is the most susceptible wavelength, due to a Taylor instability as shown in Figure 21.b. λ_D is given by

$$\lambda_D = 2\pi\sqrt{3}[\sigma/g(\rho_f - \rho_g)]^{\frac{1}{2}} \qquad (17)$$

Since the heater area participating to the growth of one vapor bubble is assumed λ_D^2, the volumetric growth rate of a bubble is

$$v_1 = \lambda_D^2 q/(\rho_g h_{fg}) \qquad (18)$$

and the corresponding hovering time is given by equation 15.

At high heat fluxes, the liquid film at the heater surface is not fed with liquid from the bulk region during the hovering period of the bubble. Thus, Haramura and Katto (1983) postulated that the CHF will occur if the liquid film dries out at the end of the hovering time τ_d, in which case the heat balance equation is

$$\tau_d\, q_{CHF,00}\, A_w = \rho_1\, \delta_{c,o}\, (A_w - A_v) h_{fg} \qquad (19)$$

Thus, solving equations 15 through 19 simultaneously, the critical heat flux correlation may be determined in terms of A_v/A_w as

$$(q_{CHF,oo} / \rho_g h_{fg})/[\sigma g (\rho_f - \rho_g)/ \rho_g^2]^{\frac{1}{4}} =$$

$$0.721 (A_v/A_w)^{5/8} [1 - (A_v/A_w)]^{5/16}$$

$$x \{[(\rho_f/ \rho_g) + 1]/[(11 \rho_f/16 \rho_g) + 1]^{3/5}\}^{5/16} \qquad (20)$$

Finally setting the right-hand-side of Equation 20 equal to 0.131 (Zuber's constant), A_v/A_w is found. Haramura and Katto (1983) give an approximate form for A_v/A_w as

$$A_v/A_w = 0.0584 (\rho_g/ \rho_f)^{0.2} \qquad (21)$$

This result confirms Gaertner and Westwater's (1960; 1965) observations, as (i) A_v/A_w is much smaller than 1 even for elevated pressures, (ii) A_v/A_w is independent of the local heat flux.

For the case of pool boiling from an infinitely-long cylindrical heater, some modifications are suggested by Haramura and Katto (1983). At the CHF, the heat balance equation on the liquid film is given by

$$\tau_d \, q_{CHF,oo} \, A_w = \rho_f \, \delta_c \, (A_w - A_v + A_w \, \delta_{c,o}/d) \qquad (22)$$

rather than Equation 19. Instead of Equation 17, the following equation must be used to find the modified, unstable Taylor wavelength:

$$\lambda_D' = 2\pi\sqrt{3}\{[\sigma/g(\rho_f - \rho_g)]/[1 + 2\sigma/d^2 g(\rho_f - \rho_g)]\}^{\frac{1}{2}} \quad (23)$$

The form in Equation 23 is due to the additional effect of the surface tension along the curvature. Finally, since the heater area contributing to one vapor jet is $\pi d\lambda_D'$, the volumetric grow rate of the bubble is

$$v_1 = \pi d\lambda_D' q/(\rho_g h_{fg}) \quad (24)$$

Therefore, the steady-state CHF for horizontal cylinders is obtained by solving equations 15, 16, 21, 22, 23 and 24 simultaneously and is given as

$$q_{CHF,OO}/q_{CHF,IP} = (\sqrt{3}/R')^{1/16}[1 + (1/2R'^2)]^{1/32} \quad (25)$$

where $q_{CHF,IP}$ is the steady-state CHF for a horizontal infinite plate in saturated pool boiling, and is given by Equation 20 and R' is the dimensionless radius and is defined as

$$R' = (d/2)/[\sigma/g(\rho_f - \rho_g)]^{\frac{1}{2}} \quad (26)$$

The bubble configuration for infinitely-long cylinders is shown in Figure 22. Figure 23 shows the comparison of Equation 25 with the experimental data.

Haramura and Katto also considered pool boiling with infinitely-long horizontal thin and flat ribbon heaters, with the broad side oriented vertically and with both sides heated. If the vertical

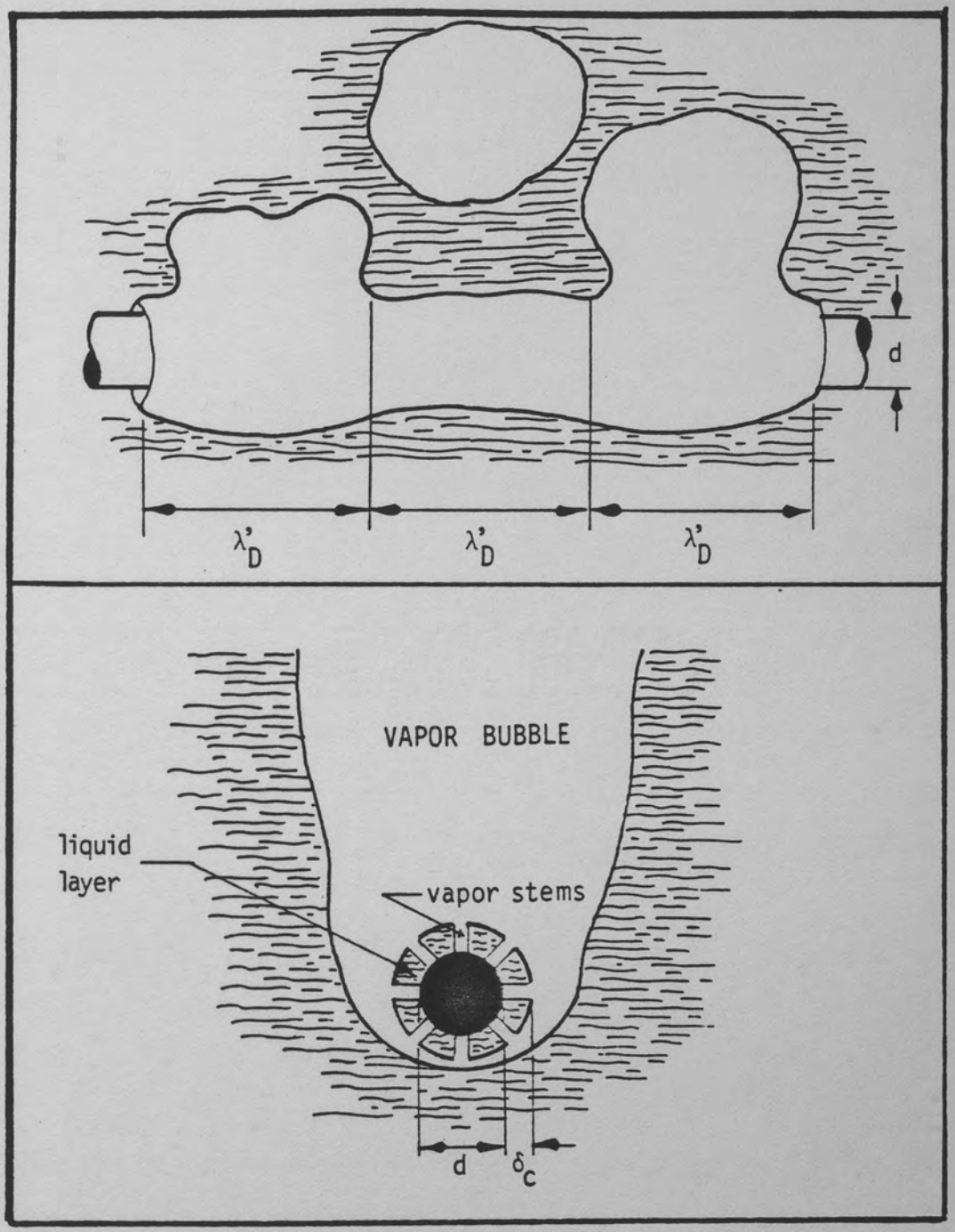

Figure 22. Boiling Configuration at High Heat Fluxes Over Horizontal Cylinders (Haramura 1983)

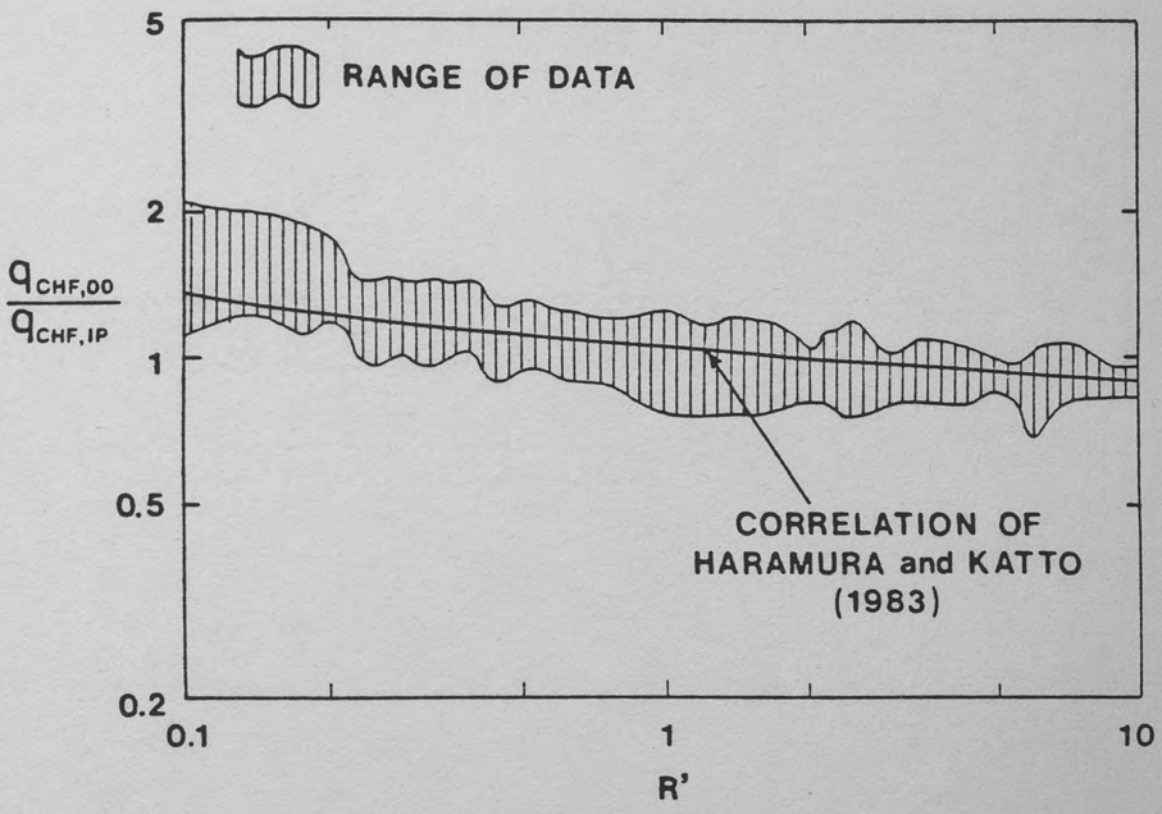

Figure 23. CHF in Saturated Pool Boiling for Horizontal Cylinders (Haramura 1983)

dimension (W) is small, they suggest to use the same set of equations as for a horizontal cylinder, using an equivalent diameter defined as

$$\pi d = 2W \tag{27}$$

However, since the various effects of the thickness are ignored and the exact value of the unstable Taylor wavelength is unknown for such a geometry, the solution can only be considered as a rough estimate. The "multi-step model" is also applied to CHF problems associated with external flow (Haramura and Katto 1983; Katto and Haramura 1983), but this problem is not included here, since the study is not specifically concerned with the external flow problems.

The original model of Zuber (1958), as well as the model of Haramura and Katto (1983), are both for saturated pool boiling. The effect of subcooling on the pool boiling CHF was first studied by Kutateladze (1963). Later, Kutateladze's equation was slightly modified by Ivey and Morris (Ivey 1962), so as to better agree with the experimental data, yielding

$$q_{CHF,O} = q_{CHF,OO} \left[1 + 0.102(\rho_l/\rho_v)^{0.75} C_p(\Delta T_{SUB})/h_{fg}\right] \tag{28}$$

There are further restrictions on the above models. They do not apply to very small geometries, characteristic length less than λ_c or λ_D, and they are restricted to water and most of the organic liquids. They do not predict the pool boiling CHF in liquid metals, as reported by Subbotin et al. (1969).

Forced Convective Boiling CHF

In this section, the analytical models for two commonly encountered CHF mechanisms will be summarized. First, the "near-wall bubble crowding" mechanism for low-quality CHF (or DNB), then the high-quality annular-flow dryout mechanisms will be considered.

Prediction of Low-Quality/Subcooled CHF in Vertical Pipes

For low-quality or subcooled CHF, commonly referred to as DNB, the most important CHF mechanism is "Near-Wall Bubble Crowding and Vapor Blanketing." For this mechanism, an analytical prediction was made by Thorgerson et al. (1974). Their model is based on the Reynold's analogy and relates the CHF to a critical friction factor. Although successful in correlating their own experimental data, the method cannot be recommended as widely usable, since the pressure drop must be measured in the same experiment as the CHF. The most successful approach to the problem of determining the DNB was published recently by Weisman and Pei (1983).

Weisman and Pei investigated the CHF problem associated with a bubble boundary layer adjacent to the wall in boiling at subcooled or low-quality conditions (1983). The characteristics of such a boundary layer were experimentally investigated earlier by Jiji and Clark (1964). Weisman and Pei (1983) based their method on the following postulates:

a. Under subcooled or low-quality conditions, the CHF is a local phenomenon.

b. There exists a bubble boundary layer which builds up in thickness along the channel and very close to the wall, where the turbulent eddy size is insufficient to transport the bubbles radially.

c. At the CHF location, the boundary layer is assumed to have its maximum thickness.

d. The CHF occurs when the void fraction of vapor in the bubbly layer exceeds the critical void fraction, which is defined at the value of the void fraction where an array of ellipsoidal bubbles can be maintained without significant contact between the bubbles.

e. The volume fraction of vapor in the boundary layer is determined by a balance between the outward flow of vapor and inward flow of liquid at the boundary layer interface, which implies that the liquid entering the boundary layer eventually reaches the wall.

Figure 24 shows the transport between the core and the bubbly layer. The mass balance in the bubbly layer may be written as

$$\dot{m}_3 = \Delta\dot{m}_2 + \dot{m}_4 \tag{29}$$

A mass balance on the liquid in the bubbly layer yields

$$\dot{m}_3(1-x_1) = q_b(2\pi R)\Delta z/h_{fg} - \dot{m}_2(\Delta x_2) + \Delta\dot{m}_2(1-x_2) + \dot{m}_4(1-x_2) \tag{30}$$

when second-order terms are ignored. In Equation 30, q_b represents the portion of the total heat flux effective in generating vapor.

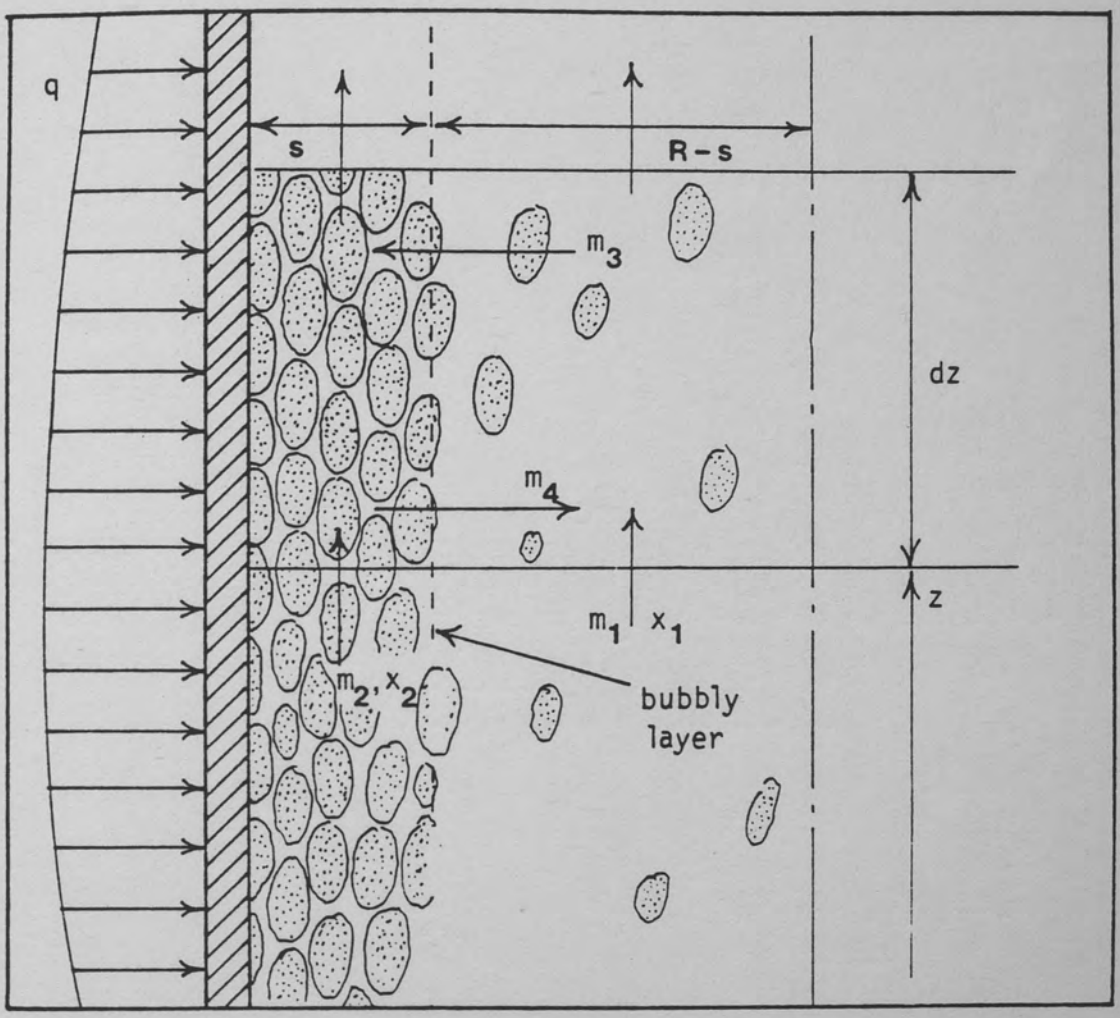

Figure 24. Schematic Diagram of Transport Between Core and Bubbly Layer (Weisman 1983)

Combining equations 29 and 30, replacing $\dot{m}_3$ by $G_3\ 2\pi(R-s)\Delta z$, and using the following assumptions:

(i) $R/(R-s)$ is close to unity,

(ii) at CHF location $[\dot{m}_2/2\pi(R-s)](\Delta x_2/\Delta z)$ is negligible (this assumption is justified in the study), the following equation is obtained:

$$G_3(x_2-x_1) = q_b/h_{fg} \tag{31}$$

The term q_b may be written as

$$q_b = q(h_1-h_{1d})/(h_f-h_{1d}) \tag{32}$$

where h_{1d} is the enthalpy at the point of detachment. For saturated boiling Equation 32 obviously reduces to

$$q_b = q \tag{33}$$

Therefore, the final correlation takes the following non-dimensional form:

$$\frac{q}{h_{fg}\ G_3} \cdot \frac{(h_1- h_{1d})}{(h_f- h_{1d})} = (x_2-x_1) \tag{34}$$

where q becomes the critical heat flux when x_2 corresponds to the critical quality. The value of the critical void fraction is calculated by estimating the maximum void fraction at which separate

ellipsoidal bubbles with the ratio of long-to-short ellipse axis being about 3:1, could be maintained in the bubbly layer. An infinite array of such bubbles is found to correspond to a void fraction of 0.82. The value of x_2 is the quality corresponding to this void fraction with no-slip conditions. For high mass fluxes, a negligible vapor slip may be a good assumption. The evaluation of G_3 is based on the estimation of the magnitude of fluctuating radial velocity components at the interface. The mathematics of this requires a certain degree of empiricism and is beyond the scope of the present study. Weisman and Pei (Weisman 1983) compared their theoretical correlation with the available data for uniformly and non-uniformly heated round tubes with various liquids used as coolant. The results are quite successful.

Prediction of Dryout in Vertical Pipes

The prediction of the CHF for annular flow in vertical pipes has been the subject of numerous investigations, the most comprehensive one being the method developed by Walley (1974, 1976, 1978a, 1978b), called the Harwell Model. Recently, Levy (1980) proposed a model which is based on the Harwell model with a few exceptions. This recent model is applied with relatively better success. Here the Harwell model with Levy's interpretation is summarized.

Figure 25 shows a section of a vertical pipe where there exists annular flow. The heat flux at any position z, the total-mass velocity, the inlet-fluid subcooling, and the system pressure are specified. The problem of interest is to determine whether the CHF will occur along the pipe, and, if it does, the location and the fluid properties at that location.

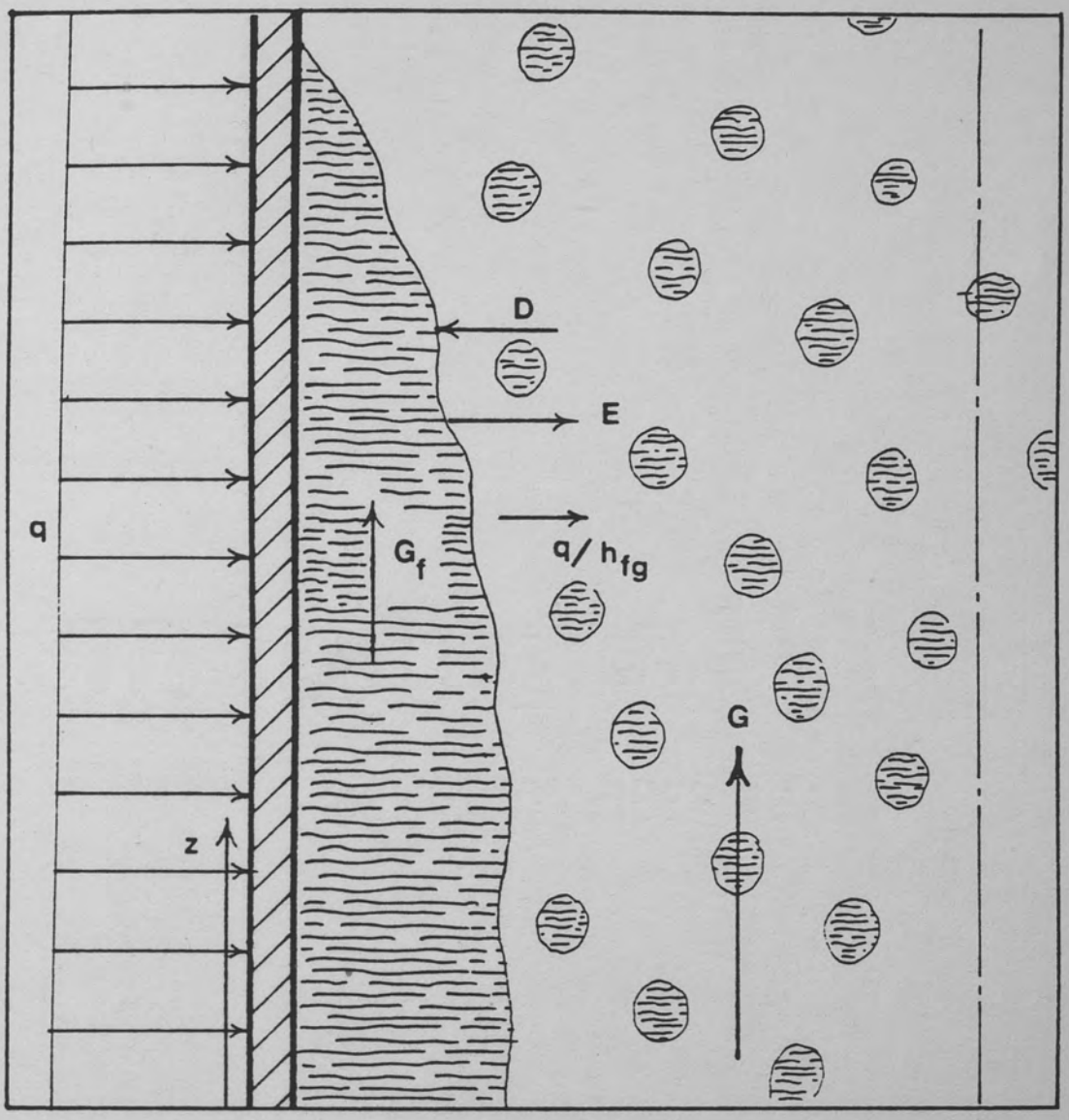

Figure 25. Schematic Diagram for Annular Flow Dryout (Levy 1980)

At a position z, the mass balance perpendicular to the flow direction may be written as follows:

$$\frac{dG_f}{dz} = \frac{2}{R} (D-E- q/h_{fg}) \tag{35}$$

where D is the deposition rate of the liquid upon the liquid film, and E is the entrainment rate of the liquid into the vapor core. D and E are defined in terms of the liquid concentration C away from the liquid film. C is given by

$$C = \frac{G(1-x) - G_f}{\frac{Gx}{\rho_g} + \frac{G(1-x) - G_f}{\rho_f}} \tag{36}$$

where x at any position z may be calculated from an energy balance equation

$$G[(\Delta h_{SUB})_i + h_{fg}x] = \frac{2}{R}\int_o^z q dz \tag{37}$$

The deposition rate, D, is given by

$$D = k_m C \tag{38}$$

where k_m is the mass transfer coefficient.

E is defined by Walley (1976) in terms of an equilibrium concentration C_{eq} as follows:

$$E = k_m C_{eq} \tag{39}$$

Figure 26 shows the variation of the equilibrium concentration with respect to τ_i m/σ. The empirical values of C_{eq} are correlated by Katto (1982b) as follows:

$$C_{eq} = 1.01 \times 10^3[(\tau_i m)/\sigma]^{2.50} \quad \text{for} \quad (\tau_i m)/\sigma < 0.0366$$

$$C_{eq} = 1.03 \times 10^2[(\tau_i m)/\sigma]^{1.81} \quad \text{for} \quad 0.0366 < (\tau_i m)/\sigma < 0.247 \qquad (40)$$

$$C_{eq} = 10^{(0.439 + 1.92\ \tau_i m/\sigma)} \quad \text{for} \quad 0.247 < (\tau_i m)/\sigma$$

where C_{eq} is given in kg/m^3.

Rather than using this approach, Levy (1980) expressed C_{eq} in terms of an equilibrium quality, x_{eq}, as

$$C_{eq} = \frac{G(1- x_{eq}) - G_f}{\frac{Gx_{eq}}{\rho_g} + \frac{G(1-x_{eq}) - G_f}{\rho_f}} \qquad (41)$$

In the same reference (Levy 1980), the following relation is given:

$$G(1-x_{eq}) - G_f = G(1-x_{eq})(1/\beta^{\frac{1}{2}}) \qquad (42)$$

where β, with the gravity effects neglected, is given by:

$$\beta = 1 + \{[(\rho_f-\rho_g)^{1/\beta} - 1]\frac{\sigma}{k_m R}\ \frac{\rho_f}{(Gx_{eq})^2}\}^{\frac{1}{2}} \qquad (43)$$

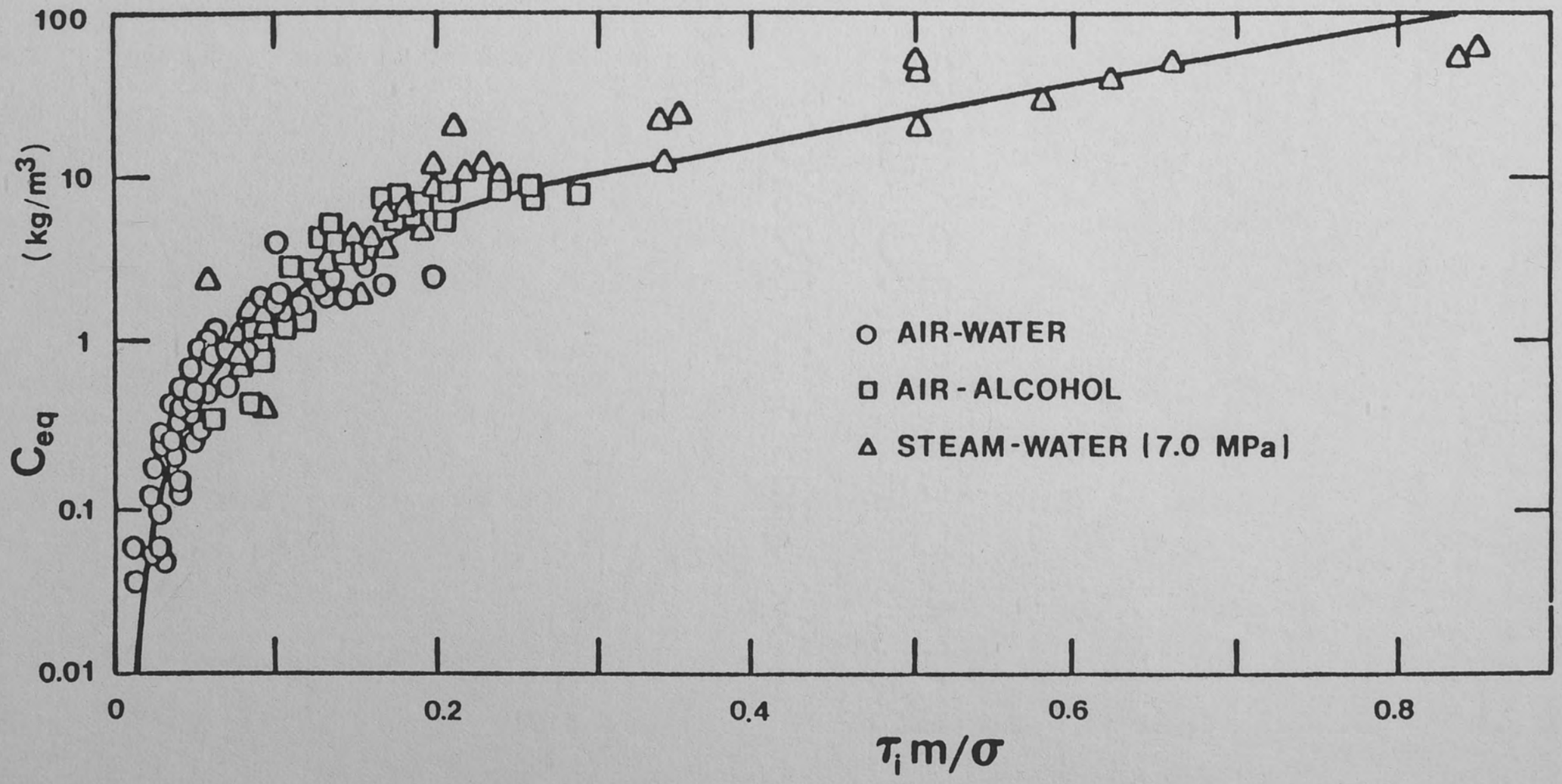

Figure 26. Harwell Equilibrium Entrainment Correlation

(Hutchinson 1973)

For given values of G and G_f, equations 42 and 43 may be solved to determine β and x_{eq}. If the liquid film becomes thin, β must be replaced by β' to account for the reduced mixing length. Levy (1980) reported that β is replaced by β' such that

$$\beta' = 1 + \sqrt{2}(\beta-1) \quad \text{for } m^+ < 30 \tag{44}$$

where m^+ is the nondimensional film thickness given by:

$$m^+ = m(\tau_w/\rho_f)^{\frac{1}{2}}(\rho_f/\mu_f) \tag{45}$$

Finally the value of the mass transfer coefficient, k_m, must be determined. Walley (1976) correlated the experimental data in terms of the surface tension. This relation is shown in Figure 27. The correlation is reported by Katto (1982b) as follows, in m/s:

$$\begin{aligned} k_m &= 0.405\ \sigma^{0.913} && \text{for } \sigma < 0.0383 \text{ N/m} \\ k_m &= 9.48 \times 10^4\ \sigma^{4.70} && \text{for } \sigma > 0.0383 \text{ N/m} \end{aligned} \tag{46}$$

In his study, Levy used the steam-water mixture tabulation developed by Wurtz. Table 1 shows the recommended values.

Now that all terms are defined, the calculation for the CHF may proceed, but a boundary condition is required. Levy (1980) used a value of 0.8 for the void fraction at the onset of annular flow. Later, however, he showed that the final result is not very sensitive to this quantity. Table 2 presents this result.

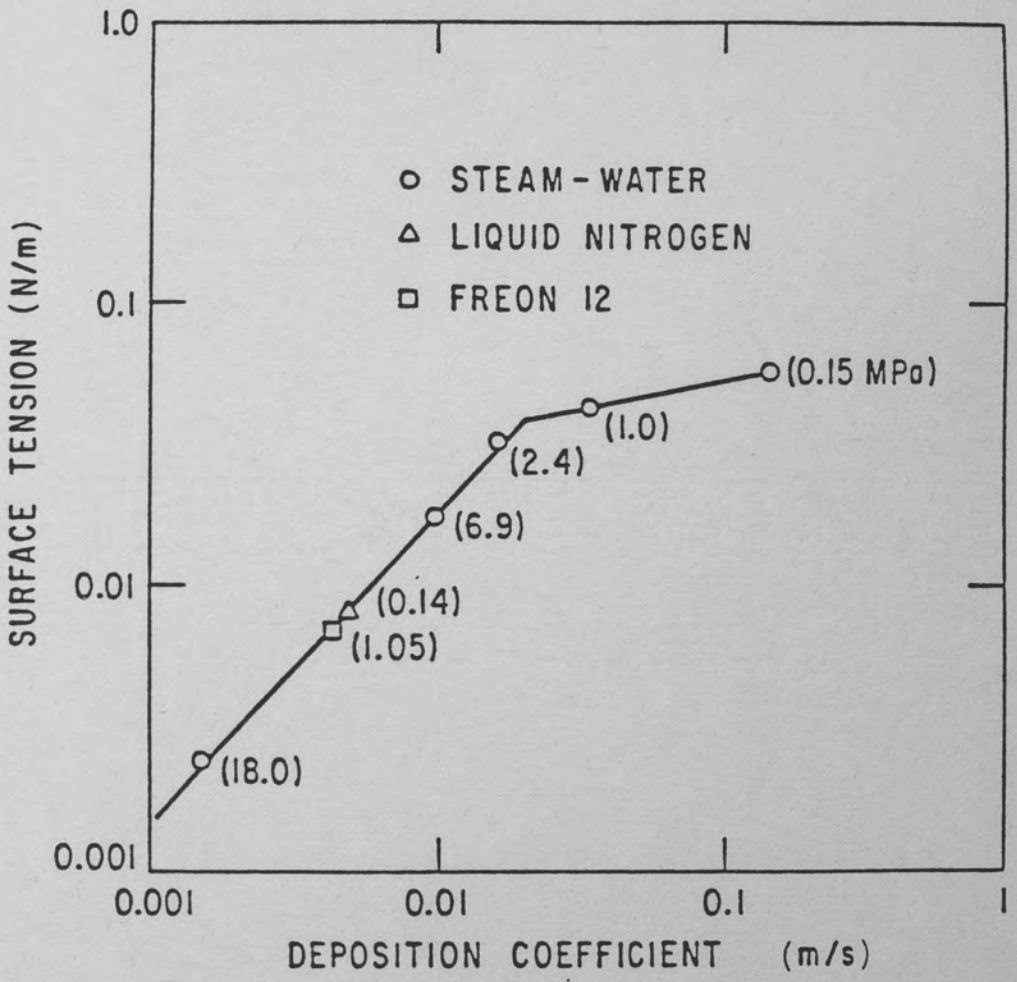

Figure 27. Harwell Droplet Deposition Correlation (Walley 1978a)

TABLE 1

MASS TRANSFER COEFFICIENTS FOR STEAM-WATER (Levy 1980)

Pressure P (bars)	30	50	70	90
Mass Transfer Coefficient k_m (m/sec)	0.021	0.013	0.010	0.006

TABLE 2

THE VALUES OF x_{CHF} FOR DIFFERENT VALUES OF G_{fi} AND x_i IN CASE WHERE G = 1000 $kg/m^2.hr$ AT 70 bars. (Levy 1980)

G_{fi} / x_i	$\frac{Gh_{fg}\ k_m}{q} = 10$	$\frac{Gh_{fg}\ k_m}{q} = 20$
341.5 / 0.08	$x_{CHF} = 0.471$	$x_{CHF} = 0.540$
314.5 / 0.102	$x_{CHF} = 0.471$	$x_{CHF} = 0.541$

The calculations are rather simplified in case of constant heat flux where the following equation lead to the solution:

$$G[(\Delta h_{SUB})_i + h_{fg}\, x] = \frac{2}{R}\, q_{CHF} z \tag{47}$$

For uniform heating, the CHF condition is at the pipe exit, thus,

$$G[(\Delta h_{SUB})_i + h_{fg}\, x_{CHF}] = \frac{2}{R}\, q_{CHF}\, L \cdot \tag{48}$$

and equation 47 yields

$$\frac{dz}{dx} = \frac{Gh_{fg}\, R}{2q_{CHF}} \tag{49}$$

Substituting Equation 49 into Equation 35 and integrating gives

$$G_f - G_{fi} = \frac{Gh_{fg}}{q_{CHF}} \left[\int_{x_i}^{x} (D-E)dx \right] - G(x-x_i) \tag{50}$$

and setting G_f equal to zero, the critical steam quality, x_{CHF}, may be found from the following equation:

$$G_{fi} = G(x_{CHF} - x_i) - \frac{Gh_{fg}}{q_{CHF}} \int_{x_i}^{x_{CHF}} (D-E)dx \tag{51}$$

The results show good agreement with the experimental data and with the widely used Biasi correlation. The results are not very sensitive to the starting value of the steam void fraction but extremely sensitive to the mass-transfer coefficient, k_m. The

solution shows that the mass transfer coefficient might be dependent upon the steam quality and the flow. The coefficient k_m increases with increasing steam quality and mass flow rates. The model reveals that the critical heat flux is vaporization controlled at low steam qualities and high heat flux and becomes deposition controlled at high steam qualities and low heat flux.

For very high heat flux as $q_{CHF} \rightarrow \infty$ Equation 51 reduces to

$$x_{CHF} = \frac{G_{fi}}{G} + x_i \tag{52}$$

This equation implies a pure vaporization without any deposition or entrainment.

In the case of nonuniform heat flux, the same solution technique is valid with more complicated mathematical steps. Equation 35 may be integrated to yield

$$G_f - G_{fi} = \frac{2}{R} \int_{z_i}^{z} (D-E)dz - \frac{2}{R} \int_{z_i}^{z} \frac{q}{h_{fg}} \, dz \tag{53}$$

The last term of the RHS of Equation 53 is equal to $G(x-x_i)$ and at any location z

$$\frac{dx}{dz} = \frac{2}{R} \frac{q}{Gh_{fg}} \tag{54}$$

At the critical location

$$G_{fi} = G(x-x_i) - Gh_{fg} \int_{x_i}^{x_{CHF}} \frac{1}{q} (D - E)dx \qquad (55)$$

where q is a function of x obtained by integrating Equation 54.

If the term Gh_{fq}/q in Equation 55 is small, the equation reduces to Equation 52, where the process is controlled by evaporation. Therefore, the local condition approach for critical steam quality becomes valid.

Recently, Katto (1984b) analyzed the CHF based on the annular-flow hydrodynamic model developed by Levy (1980). Katto studied the CHF problem in short tubes, where Levy's model exhibits a quite-different character from that of experimental data. By introducing the concept of critical liquid film thickness (Haramura and Katto 1983), Katto was able to predict the CHF for short tubes (Katto and Haramura 1983). The details of this study are not summarized here, since it is concerned with a very specific problem.

This summary of forced-convective CHF is restricted to channel flow. Both the Harwell model for dryout and the DNB model of Weisman and Pei (1983) are successfully applied to rod-bundle geometry, which is of interest to the nuclear industry. An excellent review of the application of these models to rod bundle geometry is presented by Weisman (1985).

CHAPTER IV

TRANSIENT CONDITIONS IN NUCLEAR REACTORS

Since the primary objective of the present study is to provide a better theoretical understanding of the CHF during transient conditions, certain accident situations which result in thermal-hydraulic transients in nuclear reactors are summarized in this chapter.

Accident Categories

The American National Standards Institute divided Nuclear Power Plant Conditions into four categories according to their anticipated frequency of occurrence and potential radiological consequences to the public. The four categories, as cited by Croucher and Charyulu (1979), are as follows:

a. Condition 1: Normal Operation

b. Condition 2: Incidents of Moderate Frequency

c. Condition 3: Infrequent Incidents

d. Condition 4: Limiting Faults

Condition 1 occurrences are expected frequently or regularly in the course of power operation, refueling maintenance, or maneuvering of the plant. Start up, power operation, shutdown, step-load changes up to 10 percent, and ramp-load changes up to 5 percent per minute are typical physical events in this category.

Condition 2 events are anticipated transients and may occur during a calendar year. Generator or turbine trip, loss of normal feedwater, loss of offsite power are examples for condition 2 events.

Condition 3 events are likely to occur during the lifetime of a particular reactor, and these are also classified as anticipated transients. A complete loss of forced reactor coolant flow and minor secondary pipe breaks are typical examples for this type of events.

Condition 4 faults are not expected to occur but are postulated because of their severe consequences. They can result in a release of significant amount of radioactive material. Loss of coolant accidents (LOCA), fuel-handling accidents, reactivity-initiated accidents (RIA) and other anticipated transients without scram are condition 4 type of faults.

The scram is defined as the most drastic form of automatic response of the protection system, by causing the control rods to move rapidly into the reactor core to shut down the nuclear reaction. Figure 28 shows the decay power following the reactor scram. As it is seen in about 0.1 sec into the accident, the local power drops to less than 10 percent of the initial value. Therefore, the decay heat has little effect during the first few seconds of most accidents, and the power that has to be absorbed by the coolant consists mainly of the stored energy in the fuel rods on the onset of the accident. In an ATWS event, however, in spite of all the scram signals generated during the event, the control rods are not allowed to move into the core to terminate the nuclear operation. Operator intervention is allowed to begin 10 minutes after the initiation of the ATWS events. Therefore, the ATWS-type of accidents, although not very likely, are

important and dangerous occurrences in terms of nuclear reactor safety; and corrective measures are necessary.

Table 3 and Table 4 show boiling water reactors (BWR) and pressurized water reactor (PWR) transient categories, respectively. Since all these transients can easily result in failure, necessary safety measures should be taken. Failure, as defined by Croucher and Loyd (1979), means that the fuel rod hermecity is lost and that the first fission product barrier (the cladding) has been breached. For LWR safety analyses, and in the licensing procedure, the fuel design limits require that:

a. DNB does not occur.
b. Oxidation of the total cladding thickness does not exceed 17 percent.
c. Cladding strain remains less than 1 percent.
d. Fuel centerline temperature remains below the melting point.
e. A coolable geometry is maintained.
f. Fuel rod internal pressure remains below the system pressure.
g. Internal moisture remains low.
h. The peak cladding temperature does not exceed 2200°F (1477°K) with no cladding collapse, and 1800° F (1255°K) with collapse.

The standard Review Plan (Croucher and Loyd 1979) states that the occurrence of DNB does not necessarily constitute failure; but it is sufficient to cause the initiation of overheating and is the limiting criterion for the purpose of the present study. Although hypothetical, there are certain accidents which are of major concern to the nuclear community. Therefore, the determination of the CHF during these hypothetical accidents is an important task for nuclear safety

TABLE 3

BWR TRANSIENT CATEGORIES (Croucher and Charyulu 1979)

EPRI Category	Event	Frequency (per year)
1.	Electric Load Rejection	1.04 ± 1.67
2.	Electric Load Rejection with Turbine Bypass Valve Failure	0*
3.	Turbine Trip	1.41 ± 1.89
4.	Turbine Trip with Turbine Bypass Valve Failure	0*
5.	Main Steam Isolation Valve Closure	0.67 ± 1.25
6.	Inadvertent Closure of One MSIV (Rest Open)	0.08 ± 0.28
7.	Partial MSIV Closure	0.04 ± 0.20
8.	Loss of Normal Condenser Vacuum	0.67 ± 1.45
9.	Pressure Regulator Fails Open	0.29 ± 0.71
10.	Pressure Regulator Fails Closed	0.14 ± 0.41
11.	Inadvertent Opening of a Safety/Relief Valve (Stuck)	0.20 ± 0.71
12.	Turbine Bypass Fails Open	0.40 ± 0.20
13.	Turbine Bypass or Control Valve Causes Increase Pressure (Closed)	0.51 ± 1.19
14.	Recirculation Control Failure-Increasing Flow	0.24 ± 0.75
15.	Recirculation Control Failure-Decreasing Flow	0.06 ± 0.24
16.	Trip of One Recirculation Pump	0.02 ± 0.14
17.	Trip of All Recirculation Pumps	0.06 ± 0.24
18.	Abnormal Startup of Idle Recirculation Pump	0*
19.	Recirculation Pump Seizure	0*
20.	Feedwater-Increasing Flow at Power	0.31 ± 0.68
21.	Loss of Feedwater Heater	0.02 ± 0.14
22.	Loss of All Feedwater Flow	0.27 ± 0.53
23.	Trip of One Feedwater Pump (or Condensate Pump)	0.20 ± 0.76
24.	Feedwater-Low Flow	0.43 ± 0.71
25.	Low Feedwater Flow During Startup or Shutdown	0.33 ± 0.72
26.	High Feedwater Flow During Startup or Shutdown	0.10 ± 0.37
27.	Rod Withdrawal at Power	0*
28.	High Flux Due to Rod Withdrawal at Startup	0.04 ± 0.20
29.	Inadvertent Insertion of Rod or Rods	0.10 ± 0.31
30.	Detected Fault in Reactor Protection System	0.02 ± 0.14
31.	Loss of Offsite Power	0.16 ± 0.37
32.	Loss of Auxiliary Power (Loss of Auxiliary Transformer)	0.04 ± 0.20
33.	Inadvertent Startup of HPCI/HPCS	0*
34.	SCRAM Due to Plant Occurrences	0.35 ± 0.78
35.	Spurious Trip Via Instrumentation, RPS Fault	1.16 ± 1.70
36.	Manual SCRAM-No Out-of-Tolerance Condition	0.27 ± 0.70
37.	Cause Unknown	0.02 ± 0.14

* This transient has not occurred to date in a BWR.

TABLE 4

PWR TRANSIENT CATEGORIES (Croucher and Charyulu 1979)

EPRI Category	Event	Frequency (per year)
1.	Loss of RCS Flow (1 Loop)	0.19 ± 0.55
2.	Uncontrolled Rod Withdrawal	0.01 ± 0.09
3.	CRDM Problems and/or Rod Drop	0.85 ± 2.68
4.	Leakage from Control Rods	0.04 ± 0.33
5.	Leakage in Primary System	0.08 ± 0.40
6.	High or Low Pressurizer Pressure	0.08 ± 0.31
7.	Pressurizer Leakage	0.04 ± 0.20
8.	Pressurizer Relief or Safety Valve Opening	0.02 ± 0.13
9.	Inadvertant Safety Injection Signal	0.03 ± 0.21
10.	Containment Pressure Problems	0.03 ± 0.21
11.	CVCS Malfunction-Boron Dilution	0.02 ± 0.13
12.	Pressure, Temperature, Power Imbalance	0.41 ± 1.16
13.	Startup of Inactive Coolant Pump	0*
14.	Total Loss of RCS Flow	0.03 ± 0.18
15.	Loss or Reduction in Feedwater Flow (1 Loop)	0.79 ± 1.80
16.	Total Loss of Feedwater Flow (All Loops)	0.07 ± 0.31
17.	Full or Partial Closure of MSIV (1 Loop)	0.26 ± 0.87
18.	Closure of All MSIVs	0.04 ± 0.30
19.	Increase in Feedwater Flow (1 Loop)	0.22 ± 0.73
20.	Increase in Feedwater Flow (All Loop)	0*
21.	Feedwater Flow Instability-Operator Error	0.57 ± 1.43
22.	Feedwater Flow Instability-Miscellaneous Mechanical Causes	0.42 ± 1.03
23.	Loss of Condensate Pumps (1 Loop)	0.04 ± 0.24
24.	Loss of Condensate Pumps (All Loops)	0*
25.	Loss of Condenser Vacuum	0.10 ± 0.33
26.	Steam Generator Leakage	0.06 ± 0.30
27.	Condenser Leakage	0.02 ± 0.13
28.	Miscellaneous Leakage in Secondary System	0.09 ± 0.45
29.	Sudden Opening of Steam Relief Valves	0.05 ± 0.29
30	Loss of Circulating Water	0.06 ± 0.27
31.	Loss of Component Cooling	0.01 ± 0.09
32.	Loss of Service Water System	0*
33.	Turbine Trip, Throttle Valve Closure, EHC Problems	1.19 ± 1.77
34.	Generator Trip or Generator Caused Faults	0.36 ± 0.71
35.	Loss of Station Power	0.27 ± 0.61
36.	Loss of Power to Necessary Plant Systems	0.18 ± 0.53
37.	Spurious Auto Trip-No Transient Condition	1.69 ± 2.44
38.	Auto/Manual Trip Due to Operator Error	0.25 ± 0.54
39.	Manual Trip Due to False Signals	0.04 ± 0.20
40.	Spurious Trips-Cause Unknown	0.09 ± 0.43
41.	Fire Within Plant	0.03 ± 0.21

* This transient has not occurred to date in a PWR.

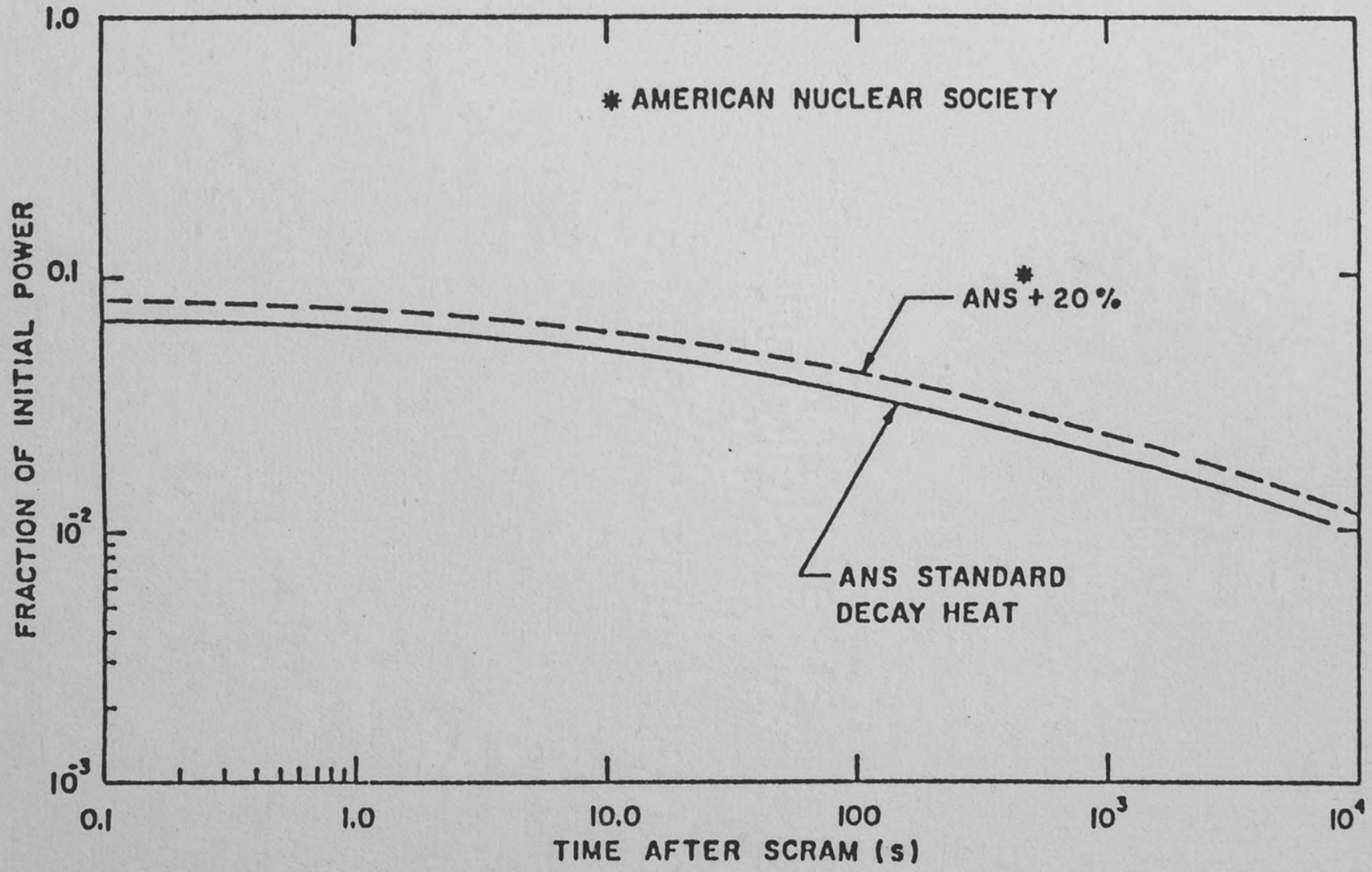

Figure 28. Decay Power Following Reactor Scram (Leung 1980)

analysis. The hypothetical accidents which manifest the major threat to nuclear safety are:

a. Loss of Flow Accidents (LOFA).

b. Loss of Coolant Accidents (LOCA)

c. Reactivity Initiated Accidents (RIA)

The characteristics of these relatively fast accident scenarios are explained in the following sections.

Characteristics of LOCA

The loss-of-coolant accident (LOCA) usually results from a breach in the primary system. The LOCA is also referred to as blowdown or rapid depressurization. A hypothetical LOCA in a water reactor result in a flow discharge at the break location and a rapid depressurization in the primary system. The LOCAs are usually classified depending upon the break size. If the ratio of the break size to pipe cross-sectional area is on the order 1 or over, the accident is named large break loss-of-coolant accident (LBLOCA). If the ratio is around 0.25 and less, it corresponds to a small-break loss-of-coolant accident (SBLOCA). The intermediate range is classified as intermediate-break loss-of-coolant accident (IBLOCA). Most of the work in the area of transient CHF has focused on LBLOCA. This may be due to the fact that, although very unlikely, a hypothetical LBLOCA results in the most rapid and severe thermal-hydraulic transient, especially in a pressurized water reactor (PWR).

A double-ended guillotine pipe break (200 percent break) in the inlet pipe (cold leg) of a PWR is shown in Figure 29. The fluid initially undergoes depressurization and reaches the saturated state;

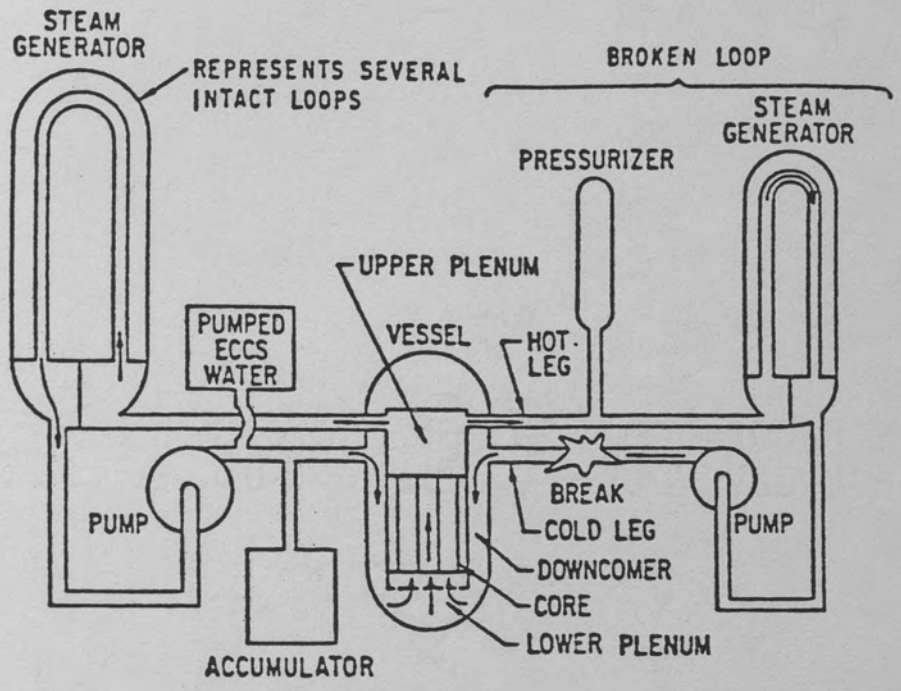

Figure 29. Schematic of a PWR System (Leung 1980)

this period is denoted as the subcooled blowdown. Since the cold-leg break allows a rapid depressurization of the lower plenum, a bidirectional flow configuration with fluid emptying at both ends of the reactor core will result. This will cause a CHF on the fuel rods as a result of liquid depletion. For a hot-leg break, however, the flow reversal does not occur.

Although, in terms of transient CHF analysis, most emphasis is placed upon LBLOCAs, certain IBLOCA and SBLOCA experiments have also been conducted. However, in these experiments, the CHF behavior is generally of secondary importance, and the major concern is the thermal-hydraulic response of the system.

Experimental Studies

Major blowdown experiments have been performed in the following experimental facilities within the U.S.A.:

Semiscale Program-INEL (Idaho Falls, Idaho) The Semiscale Mod-1 system (with 1½ loop) is a small scale, electrically heated model of four-loop PWR. The core contains 40 rods with a total heated length of 1.67 meters. The power steps provide an inlet-skewed axial-power shape. The following test series were within the interest of a LOCA study: Blowdown Heat Transfer Tests (Test Series 2), Steam Generator Tube Rupture Test (Test Series 29), Special Tests (Test Series 29), LOFT Counterpart Tests (Test Series 6). The Semiscale Mod-2A is a 2-loop model of PWR. The core contains 25 electrically-heated rods with 3.66 m of heated length. Experiments on intermediate and small-break LOCA's were conducted in this system. The Semiscale Mod-3 is

again a 2-loop model, with 25 electrically heated 3.66 m long rods. The rods simulate a symmetric chopped-cosine power profile. Blowdown data for test series 7 were obtained from Semiscale Mod-3.

Thermal Hydraulic Test Facility-THTF (Oak Ridge, Tennessee). The thermal-hydraulic test facility has an electrically heated core with 49 full-length (3.66m) rods. The axial power profile simulates a symmetric chopped-cosine function. Test series 100 consists of 6 blowdown tests.

Power Burst Facility-PBF (INEL, Idaho Falls, Idaho). The tests were conducted with four separately-shrouded nuclear fuel rods with an active length of 0.91m. The power has a skewed chopped-cosine profile. Tests series LOC-11 were conducted to investigate a PWR 200 percent cold-leg break.

CE/EPRI Blowdown Program (Combustion Engineering/Electric Power Research Institute at Columbia University-New York, New York). The test program emphasizes the hydraulic simulation of large, double-ended cold-leg breaks. The addition of an exit break area was also studied. The blowdown tests were conducted in the Columbia Rod Bundle Test Facility, where the system contains a 5 x 5 electrically-heated rod bundle. The axial-power profile is uniform. The heated length is 1.68 m.

LOFT Simulated Blowdown Program (Columbia University-New York, New York). The tests were conducted in the Columbia Rod Bundle Test

Facility of the University of Columbia. Therefore, the core design is the same as the CE/EPRI Blowdown Program.

J-Loop (Westinghouse). The facility is a single-loop simulation of a typical PWR system, containing a 5 x 5 bundle of electrically-heated rods. The rods have full length (3.66m). Supplementary auxiliary systems permit the flexibility to conduct both system-response blowdown tests and controlled heat-transfer studies. The effects of the following parameters have been tested in this program: pressure for constant pressure transients, depressurization rate, initial pressure for depressurization-type transients, flow rate, flow decay rate, inlet enthalpy, power, and flow direction. The program also includes tests designed to investigate the Griffith simple voiding theory (Smith 1976) and the Henry spontaneous nucleation theory (Henry 1977).

Freon Blowdown Test Facility (Argonne National Laboratory). This is a small-scale apparatus. The test fluid is Freon-11. Three electrically-heated test sections are used. A number of inlet and exit-break transients are conducted.

Blowdown CHF Models

The Slifer-GE correlation (Slifer 1971), although based on steady-state data, was subsequently adopted as a transient CHF correlation for BWR analysis by the commission acceptance criteria. The correlation is given in Appendix A.

Segev and Bankoff (1976) have proposed three models for blowdown CHF:

a. The multiple-bubble fast CHF model,

b. The bidirectional annular-flow model, and

c. The vapor-film model.

In the multiple-bubble fast CHF model, it is suggested that the CHF occurs because of the close packing of bubbles on the wall where a superheated liquid layer exists. This is the "near wall bubble crowding" CHF mechanism analyzed by Weisman and Pei (1983).

In the bidirectional annular-flow model, the core voidage is found to be strongly dependent on heat flux but much less on the rate of depressurization. The resultant differential equation for the voiding rate is obtainable.

The third approach, the vapor-film model, incorporates a modification of the Kutatelatze pool-boiling CHF criterion (Kutateladze 1963). This model uses the perfect gas law to predict the pressure at CHF. Therefore, the time to CHF can be estimated knowing the depressurization rate.

Hsu and Beckner (1978) proposed a transient CHF correlation which can handle both DNB and Dryout types for wide ranges of flow rates and pressures. This correlation is also given in Appendix A.

Mayinger and Belda (1974) proposed a simple model to estimate the time to CHF in a BWR system. Their final result, using a linear depressurization-rate transient, is given by a transcendental equation.

An elementary voiding theory was proposed by Smith and Griffith (Smith 1976). The time to CHF is considered to be simply the time required to increase the enthalpy of the initially subcooled liquid to the enthalpy of saturated vapor ($x = 1.0$). This simple model gives

very conservative results when compared to experimental data (Westinghouse 1982).

Henry and Leung (1977) proposed a model to predict the regions of the core which may experience limited efficient cooling during a PWR LOCA. The model suggests that the surfaces which experience fully-developed subcooled boiling during steady-state conditions will experience extended cooling during blowdown, due to their ability to provide preferred nucleation sites which can increase the heat removal capability by nucleate boiling. On the other hand, the surfaces which are mainly cooled by single-phase convection during steady-state will be unable to activate the nucleation sites until the surface temperature rises to a level of stable vapor blanketing via a spontaneous nucleation mechanism. This model is successful in predicting the experimental observations; it also explains the better cooling and longer time to CHF with reduced pressures, which was observed in the Semiscale experimental program. Validity of the theory has also been observed in the J - Loop Test Facility (Westinghouse 1982).

Characteristics of LOFA

The loss-of-flow accidents are characterized by a rapid reduction in the coolant mass-flow rate. It is usually due to a loss of power in one or more of the primary pumps.

LOFAs are not as widely investigated as LBLOCA, possibly due to the fact that they result in a slower transient. There have been several experimental investigations, however there is not yet a

theoretical model developed for CHF analysis in loss-of-flow accidents (LOFA).

Experimental Studies

Moxon-Edwards Test, SGHW Prototype Reactor - England (Moxon 1967). A series of experiments were carried out with forced convention, using water at 1000 psi. Four different test sections were used: uniformly heated tubes of 6 and 12 ft. lengths and uniformly heated 37-rod cluster of 12 ft. heated length. The flow transients were initiated by tripping the circulating pump. The pressure was held constant during the transient, and an exponential inlet flow decay was simulated.

Cumo's Tests, CISE - Italy (Cumo 1977). These were Freon-12 experiments conducted at equivalent PWR and BWR pressures. The test section was a uniformly heated round tube, and tests simulating exponential-flow decay were conducted.

Roumy Tests, CEA, Grenoble - France (Roumy 1974). Flow transient tests were conducted at constant pressure. The test section was a uniformly heated round tube.

ANL-Freon Blowdown Test Facility (Angonne National Laboratory). This test facility is described in the preceding section for blowdown test facilities.

J - Loop (Westinghouse) This test facility is also described in the preceding section for blowdown test facilities.

Characteristics of RIA

The rapid insertion of excess reactivity into a light water reactor (LWR) is recognized as one of the most dangerous accident situations, and it is classified as a reactivity initiated accident (RIA). To minimize the damage due to this type of an accident, there are some design requirements imposed on reactivity-control systems. These requirements imposed by the USNRC limit, are cited by MacDonald et al, (1980) as:

"The potential amount of reactivity increase to assure that the effect of postulated reactivity accidents can either (1) result in damage to the reactor-coolant pressure boundary greater than limited local yielding, (2) sufficiently disturb the core, its support structure, or other reactor-pressure vessel interals to impair significantly the capability to cool the core."

Worst case RIAs in commercial LWRs are postulated to result from the rapid removal of control-rod elements from the reactor core. In a PWR, a severe RIA might be caused by rupture of a control-rod drive mechanism, housing or control-rod drive nozzle, which results in a coolant-system pressure ejecting an inserted control rod from the core. In a BWR, a worst case RIA could be caused by the separation of an inserted control-rod drive from its cruciform control blade, the sticking of the control blade in the inserted position as the rod drive is withdrawn, and the rapid falling of the control blade to the withdrawn rod drive position.

Based on the review of fuel behavior experimental data prior to 1974, the NRC required that the LWRs operated within the United States must be designed such that the worst-case RIA will not result in a radial-average fuel enthalpy greater than 280 cal/g UO_2 at any axial location in the fuel rod. Much of the applicable pre-1979 RIA fuel-behavior experimental data were obtained in the SPERT (Capsule Driver Core) and TREAT test programs. Energy deposition and the resulting enthalpy increase in the test fuel was found to be the most important independent variable. Several test-rod designs indicated that the incident failure threshold has a stronger dependence on the energy depositon near the fuel surface than on the radial average energy deposition.

LWR fuel behavior during a severe RIA is characterized by an extremely rapid increase in temperatures. The fuel and the cladding temperatures become very high in relatively short periods of time. To illustrate the results of a severe RIA, the FRAP-T5 program is used. The calculations for 260 cal/g UO_2 peak-fuel enthalpy are shown in Figure 30. This figure represents the test power and the FRAP-T5 calculated-cladding surface, fuel surface, fuel centerline and peak-fuel temperatures during the first 300 msec of the transient. The figure also shows that the peak rod power reaches a value of 30,000 kW/m within 35 msec of the initiation of the transient. The fuel temperature rises very rapidly with the peak-fuel temperature (at a radial position near the fuel surface) reaching the UO_2 melting point (3100 K) within about 50 msec after initiation of the transient.

In order to further investigate the RIAs, to determine the fuel-failure thresholds, modes, and consequences as a function of energy

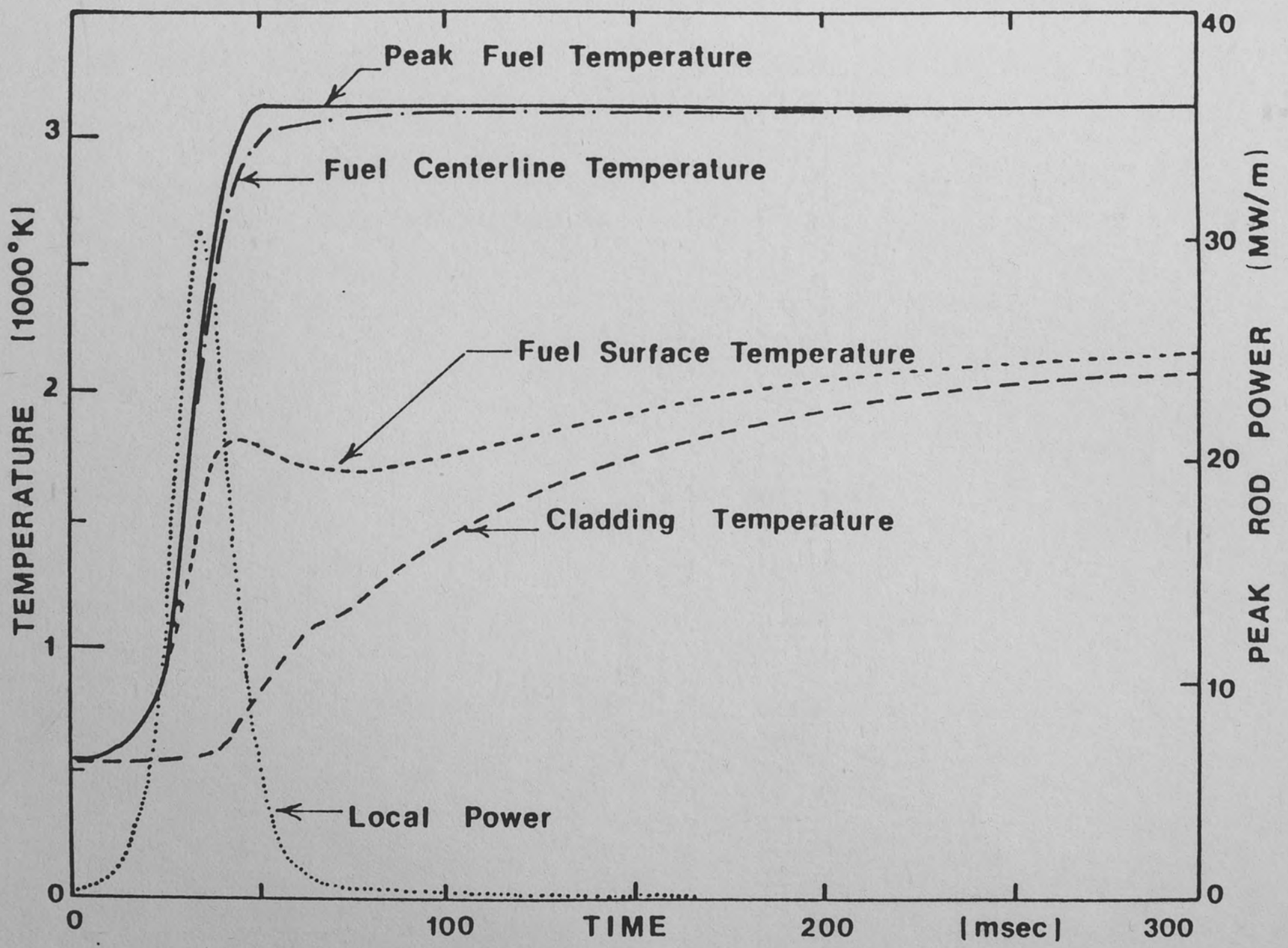

Figure 30. Fuel Rod Power and FRAP-T5 Calculated Temperatures During the First 300 msec of a 260 cal/g UO_2 RIA (Croucher and Loyd 1979)

deposition, irradiation history and fuel design, RIA tests series have been conducted in the INEL Power Burst Facility (PBF). In these experiments, nuclear fuel pellets were used as heating elements. Each fuel rod was inserted in a shroud, and each test had 4 shrouds. The heated length of fuel rods was 3 ft. and simulated a chopped-cosine power distribution.

Since the heat flux increases very rapidly, it is very likely that the CHF mechanism during an RIA is "near wall-bubble crowding and vapor blanketing." This is confirmed by power-transient experiments conducted by electrical heaters. A detailed summary of these experiments and a theoretical analysis of power transients are presented in Chapter VIII.

CHAPTER V

QUASI-STEADY APPROACH

The transient convection problem is one of the most challenging heat transfer problems. The difficulty in the transient convection problem arises because of its conjugate nature, i.e., the field equations in the fluid and the heat diffusion equation in the solid must be solved simultaneously, and the solutions must be coupled at the solid-fluid interface.

Even the simpler single-phase transient convection problem has been the subject of many analytical and experimental studies. The studies of Siegel (1963), Siegel and Perlmutter (1963), Adams and Gebhart (1964), Soliman and Johnson (1968), Sparrow and De Farias (1968), Koshkin et al. (1970), Sucec (1975), Kawamura (1977), Dorfman (1977), and Sucec (1981; 1985) are some examples of the transient single-phase convection problem. A review of these studies show that most of them use the so-called quasi-steady approach. There are experimental studies presented within the literature which try to set an empirical criterion for the application of the quasi-steady approach. The studies of Siegel (1960), Sparrow and Siegel (1960), Kawamura (1977), and Sucec (1981) are good examples of such attempts. In these studies various correlations are developed to determine the minimum time required to reach the quasi-steady conditions.

The so-called quasi-steady approach provides an approximate solution to the transient convection problem. It uses the steady-state convection heat transfer correlation applied on an instantaneous basis. To apply this approach, the local instantaneous values of the transient parameters are computed, and these values are used in a steady-state convective heat transfer correlation. Thus, the local instantaneous value of the convective heat transfer coefficient is determined and, in turn, used to solve the heat diffusion equation. The studies of Kawamura (1977) and Sucec (1981) show that the quasi-steady approach may be valid if the heat capacity of the solid is much greater than the heat capacity of the fluid. This means that the response time of the fluid (convective time constant) is much smaller than the response time of the wall. If this condition is satisfied, then the quasi-steady approach is valid.

The popularity of the quasi-steady approach to the transient convection problem stems from the fact that the steady-state convection problem has received extensive study. As a result, there are many correlations to estimate the steady-state convective heat transfer coefficient, as opposed to few (if any) transient convection correlations. But, as mentioned above, the quasi-steady approach is not always valid, and there are strict restrictions upon the use of such an approach. In the case of two-phase convection, these restrictions become even tighter. This is due to the fact that the time constant of two-phase convection is greater than the time constant of the single-phase convection, since the initiation, growth and

departure of the bubble require additional time. Therefore, the response time of the fluid during boiling heat transfer is greater than the response time of the single-phase fluid.

Mathematically, the total rate-of-change of the surface heat flux must be examined (Nelson and Duffy 1984) to determine when the quasi-steady approach becomes valid. For instance, the surface heat flux may be mathematically expressed in terms of the two-phase flow parameters, as

$$q = q\ (t,\ P,\ G,\ x,\ \text{etc.}) \tag{56}$$

and the total derivative of the heat flux with respect to time is given by:

$$\begin{aligned} dq/dt = (\partial q/\partial t)_{P,G,x} &+ (\partial q/\partial P)_{t,G,x}\ (dP/dt) \\ &+ (\partial q/\partial G)_{t,P,x}\ (dG/dt) \\ &+ (\partial q/\partial x)_{t,P,G}\ (dx/dt) + \ldots \end{aligned} \tag{57}$$

If $(\partial q/\partial t)_{P,G,x} \simeq 0$, then the quasi-steady conditions are satisfied, and the surface heat flux may be determined through an appropriate steady-state correlation as

$$q(t) = q_{ss}\ [\ P(t),\ G(t),\ x(t),\ \text{etc.}] \tag{58}$$

On the other hand, if $(\partial q/\partial t)_{P,G\ x}$ is not zero, then the quasi-steady approach is no longer valid, and a transient convective heat flux correlation must be developed as given in Equation 56. Obviously, for

a transient problem $\partial q/\partial t$ is never zero, but may be neglected when compared to the other terms of Equation 58, which then justifies the quasi-steady approach. If the wall responds slowly to any change in the convective parameters, then the term $\partial q/\partial t$ will be small. On the other hand, if the fluid responds rapidly, then the additional terms of Equation 58 will be large compared to $\partial q/\partial t$. Therefore, during the transient, the respond time of the wall being large is a necessary but not sufficient condition to justify the quasi-steady approach. In conjunction with the slow response of the wall, a fast response from the fluid is required.

When the problem is analyzed from this point of view, the applicability of the quasi-steady approach needs to be discussed in conjunction with the time and space averaging operators used in two-phase flow problems, as observed by Nelson and Duffey (1984). In the following section, a brief description of time and space averaging operators is given.

Time and Space Averaging Operations in Two-Phase Flow Problems

The necessity of time and space averaging operation in two-phase flow problems is dictated by the time and space averaged two-phase flow field equation. An excellent review of the development and the use of these equations is given by Delhaye (Bergles 1981). These equations are not repeated here. Instead, the definitions of time and space averaging operators, as applied to surface heat flux, are given.

If the local-instantaneous value of the surface heat flux is denoted by q_x^i, the area averaged instantaneous heat flux may be

obtained as

$$< q^i > = (1/A) \int_A q^i_{\tilde{\chi}} \, dA \tag{59}$$

The major question in the area averaging operator is how large an area is required for a meaningful average. This area, denoted by A*, must be large enough to include a sufficient number of the basic phenomena which control the convective heat transfer process. To illustrate this, the example of nucleate pool boiling over a flat surface may be examined. As shown in Figure 31, the minimum area must contain a sufficient number of active nucleation sites, so that it contains bubbles at different states involving initiation, growth, departure or collapse of the bubbles. If the area chosen is smaller than A*, then the area averaging cannot give meaningful results. For example, if the first half of the area A* in Figure 31 is used, the area averaged heat flux will be higher than the value averaged over A*, because this averaging process does not include the effect of departure and single-phase convection on the surface heat flux. To further understand this concept, $\partial < q^i > / \partial A$ must be examined. This derivative may be written in the limit form as

$$\frac{\partial < q^i >}{\partial A} = \lim_{\Delta A \to 0} [\, < q^i > |_{A^* + \Delta A} - < q^i > |_{A^*}] / \Delta A \tag{60}$$

where ΔA represents an arbitrary increment in the area. If A* is the minimum area for a meaningful averaging operation, then $\partial < q^i > / \partial A = 0$. Thus

$$< q^i > |_{A^* + \Delta A} = < q^i > |_{A^*} \tag{61}$$

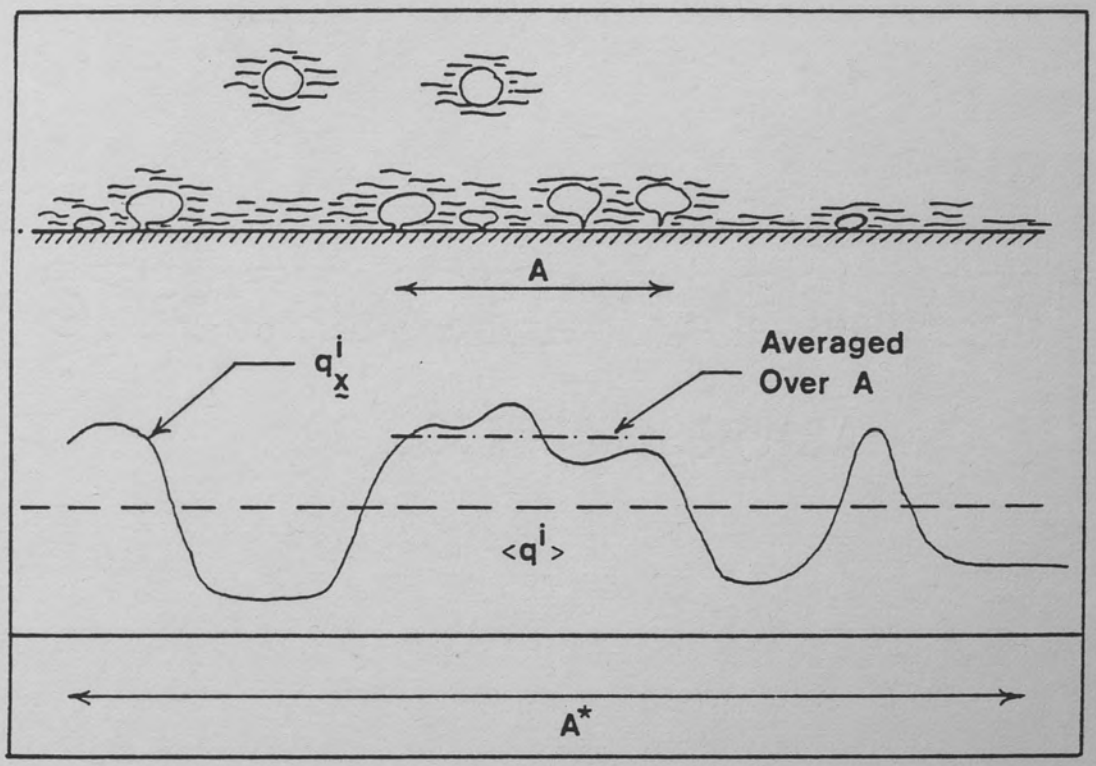

Figure 31. Area Averaged Heat Flux in Nucleate Boiling

for a finite consideration. Therefore, as long as an area larger than or equal to A* is chosen, it is of sufficient size to include a statistically sufficient number of basic phenomena.

The area-averaged surface heat flux is used in the volume-averaged two-phase flow energy equation, as shown by Delhaye (Bergles 1981). Delhaye (Bergles 1981) also shows that for certain problems, an area averaged energy equation may be required. In this case, the surface heat flux enters the equation as a line-averaged quantity. Two-phase duct flow is an example of such a problem where area-averaged field equations are used, because considerable changes may occur in the axial direction. In this problem, the heat flux must be averaged over the perimeter of the duct. Similar to the discussion about area-averaging, a minimum length is required for a meaningful line average.

Similar to area-averaging, a time-averaging operator may be applied to local-instantaneous heat flux in the following fashion:

$$\bar{q}_{\underset{\sim}{x}} = (1/\Delta t) \int_{\Delta t} q^{i}_{\underset{\sim}{x}} \, dt \tag{62}$$

As an analogy to a minimum area required for a meaningful-area average, there is a minimum time period denoted by Δt^*, over which the instantaneous values of the surface heat flux must be averaged. Δt^*, like A*, must contain a sufficient number of the periods of the controlling phenomenon in the boiling process. Going back to the example of steady-state pool boiling, Δt^* must contain a sufficient number of bubble initiation, bubble growth, and bubble departure (or collapse) periods. This is shown in Figure 32. Although not

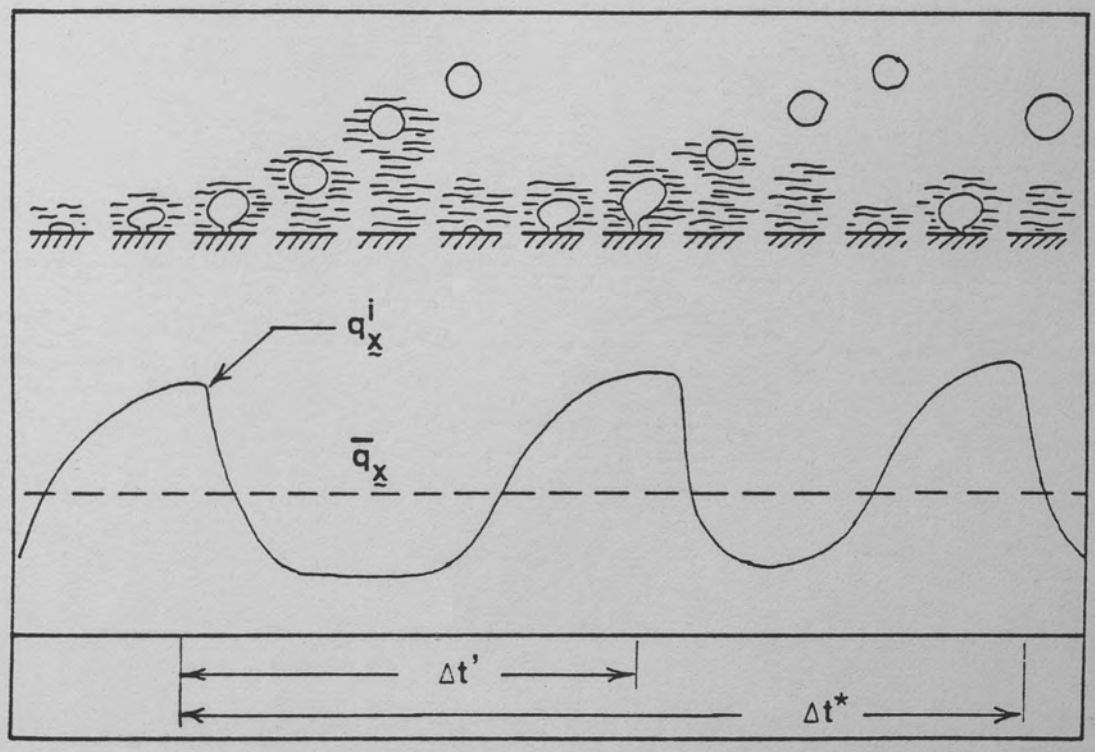

Figure 32. Time Averaged Heat Flux in Nucleate Boiling

quantified, figures 31 and 32 are drawn in accordance with the study of Yu and Mesler (1977) and Subbotin et al. (1974). If $\Delta t'$ denotes the sum of bubble initiation, growth and departure periods in steady-state saturated pool boiling, then

$$\Delta t^* = n^* \Delta t' \tag{63}$$

for a meaningful time average. For more insight into Δt^*, $\partial \bar{q}_{\underset{\sim}{x}}/\partial t$ must be examined in the integral form

$$\partial \bar{q}_{\underset{\sim}{x}}/\partial t = \lim_{\Delta t \to 0} (1/\Delta t) \left[\int_{\Delta t^*+\Delta t} q^i_{\underset{\sim}{x}} dt - \int_{\Delta t^*} q^i_{\underset{\sim}{x}} dt \right] \tag{64}$$

If Δt^* is large enough, the above averaging equation is independent of Δt ($\partial \bar{q}_{\underset{\sim}{x}}/\partial t = 0$) and Equation 64 yields, from a finite consideration

$$\int_{\Delta t^*+\Delta t} q^i_{\underset{\sim}{x}} \, dt = \int_{\Delta t^*} q^i_{\underset{\sim}{x}} \, dt \tag{65}$$

In the two-phase flow field equations, the time-averaged surface heat flux is used as a boundary condition, as noted by Delhaye (Bergles 1981).

Usually, in two-phase flow problems, the time and space averaging operators are used together. Delhaye (Bergles 1981) shows that the order of application of the averaging operators does not make any difference. From an experimental point of view, the necessity of using both operators arises because of the instrumentation in

measuring true local-instantaneous heat fluxes. The two-averaging operators may be related through the ergodic hypothesis (Tien 1978). The ergodic hypothesis states that if the phenomenon occurring at each point on the surface is a random occurrence relative to all other points, then the space average of any property is the same as the time average of that property for a single point. But, for the nucleate boiling example, the random occurrence is questionable. In the isolated bubble region, the bubbles grow at preferred nucleation sites but not at a random point over the surface. At fully-developed nucleate boiling, the bubbles grow and depart (or collapse) at a specific distance from each other, determined by the Taylor wavelength. The random occurrence in time is also physically incorrect, since the bubbles follow a certain frequency to grow and depart (or collapse). Therefore, necessity of using time and space-averaged operations simultaneously arises not only due to experimental restrictions, but also due to theoretical considerations.

However, from the previously considered examples of nucleate boiling, the time and space averaging operator may be inter-related. For example, if the area is chosen large enough to include many nucleations sites (or a number of Taylor instability wavelengths in fully-developed boiling), then the time required for time averaging operation may be minimized. The minimum time period may not be equal to zero, since there is no guarantee that the number of bubbles at different stages of growth is uniformly distributed over the area, no matter how large an area is used. But, if the area is large enough n^* in Equation 63 may be reduced to 1, meaning that one period including

the initiation, growth and departure (or collapse) will be enough for meaningful averaging.

In the present study q is used as the time-and space-averaged quantity, unless otherwise specified. It is used as synonymous to the quantity $< \bar{q} >$, obtained through the following operation:

$$< \bar{q} > = (1/\Delta t^*)(1/A^*) \int_{\Delta t^*} \int_{A^*} q \underset{\sim}{i} \cdot dA \, dt \qquad (66)$$

The average notations in the other chapters of the study are dropped for simplicity.

Effect of the Averaging Operators on the Quasi-Steady Approach

Since the present study is basically concerned with the transient convection problem in two-phase flow, the time-averaging operator is dominant in the analysis. The inherent assumption is that the problems considered here are of large geometry, so the geometry effects are neglected in the time-averaging process. Therefore, even during the transient, a meaningful area averaged heat flux can be obtained.

Then the question of interest is, "What happens if there is a drastic change in the area-averaged heat flux or in one (or more) of the area-averaged parameters affecting the area-averaged heat flux during the minimum time period Δt^*?" Since the fluid cannot respond to this change within this period, the criterion for quasi-steady approach is demolished. The change in the parameter and the fluid response to this change is schematically shown in Figure 33. In the first half of the curve, the parameter is changing quite rapidly over the time period Δt^*, and the fluid response is considerably lacking.

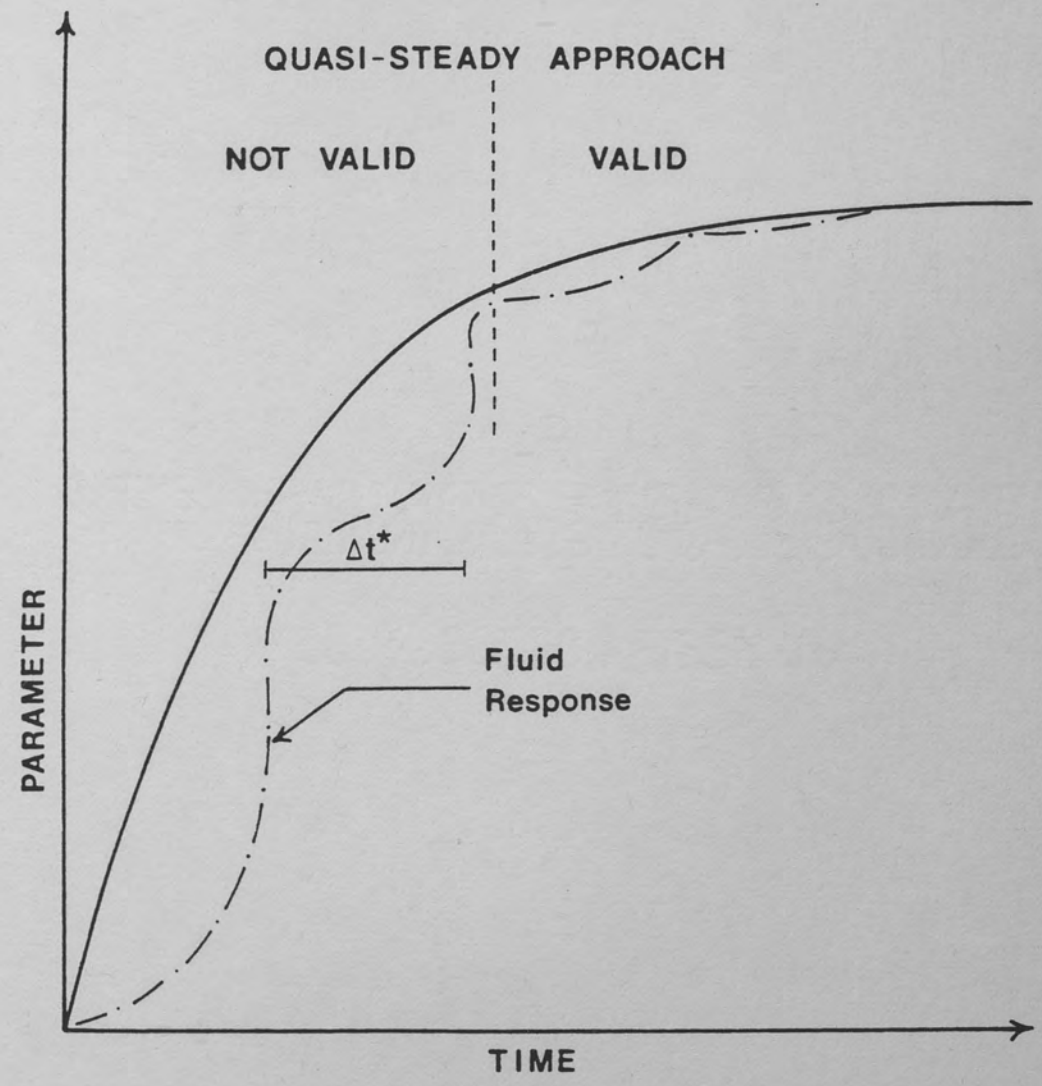

Figure 33. Qualitative Description of the Fluid Response to a Given Transient.

Therefore, the quasi-steady approach in this region is not possible, according to the criteria set. On the second half of the curve, however, the parameter is changing slowly and the fluid response is closer to the transient curve, in which case the quasi-steady approach may be possible. For the case of nucleate boiling, for instance, if the surface temperature of the heater is suddenly increased, the bubble which is originally at the surface must depart before the fluid can adjust itself to the new surface conditions. In reality, even the departure of one bubble is not enough; then some additional time is required for the temperature profile within the fluid to readjust.

Therefore, if there is a rapid change in one of the parameters during the time constant of the convective fluid, the fluid may not sense this change as rapidly, and the quasi-steady approach is not valid. From this point of view, the time constant of the convective fluid is equivalent to the minimum time over which the convective properties of the fluid are averaged.

CHAPTER VI

QUASI-STEADY APPROACH FOR TRANSIENT CHF

Based on the discussion of the previous chapter, it can be concluded that the critical heat flux (CHF) may be determined by a quasi-steady approach during transient conditions, if the rate-of-change of the transient parameter is slow as compared with the response time of the two-phase fluid. Unfortunately, the transient CHF problem has, in general, been restricted to quasi-steady treatment without considering whether or not the above condition is satisfied.

This fact is due to the complex nature of the CHF problem, which does not easily surrender to an analytical approach. Thus, most of the correlations used in determining the CHF in nuclear reactors are either empirical or semi-empirical, and they are usually based on steady-state, (or quasi-steady) CHF data. Since there is no transient CHF correlation developed over a wide range of data, the transient CHF may only be estimated by applying the steady-state CHF correlations through the quasi-steady approach.

The so-called quasi-steady approach in determining the CHF may be summarized as follows:

a. The local-instantaneous values of the CHF parameters are computed at a given axial location for a given time. Although these values are referred to as local-instantaneous, they are still average values, and they are averaged over the cross-section of

the channel as well as over the time-increment of the computer program.

b. These values of CHF parameters are used in a steady-state CHF correlation to determine the corresponding CHF.

c. The local-instantaneous value of the surface heat flux is also determined. Here the heat flux is also averaged over the perimeter of the channel and over the time increment of the computer program. Therefore, in items (a) and (c), local means the axial location and instantaneous means within the frame of the time increment of the computer program.

d. Finally, the ratio of the local-instantaneous heat flux to the CHF is computed. If the ratio is greater than 1, it means there is no CHF at that axial point. If the ratio is 1, it means CHF has just occurred, and if the ratio is smaller than 1, CHF has been exceeded.

The quasi-steady approach, as described above, is currently being used in all the system codes employed in the nuclear industry. The TRAC, RELAP, FRAP and COBRA codes are such examples. In the present study, the author used a simpler computer program, CODA, developed by Leung and Gallivan (1980). The details and a listing of the CODA code are given in Appendix B.

Using the CODA code Leung (1980) compared the result of eight steady-state CHF correlations to the data collected from flow-transients and blowdown tests. Table 5 shows the data-base of Leung (1980). The same blowdown data, with the exception of ANL and CE/EPRI single-tube test results, have been compared to some additional CHF correlations by Lo (1984) at Argonne National Laboratory (ANL) and by

TABLE 5

EXPERIMENTAL DATABASE OF LEUNG (1980)

Facility and Test No.	Reference
1. Flow Transients	
Moxon-Edward (AEEW)	(Moxon 1967)
Cumo (CISE)	(Cumo 1977)
Roumy (CEA Grenoble)	(Roumy 1974)
ANL	(Leung 1980)
2. Blowdown Tests	
ANL Single tube	(Leung 1980)
CE/EPRI Single tube	(Guerrero 1976)
CE/EPRI 5 x 5 Rod bundle	(Hsia 1977)
LOFT Columbia loop 5 x 5 rod bundle	(Gottula 1978)
PBF LOC-11 (PWR fuel in shroud tube)	(Buckland 1978)
ORNL THTF 7 x 7 rod bundle	
Test 105 (40% inlet-60% outlet)	(Clemons 1977)
Test 104 (50% inlet-50% outlet)	(Leon 1978)
Test 178 (32% inlet-28% outlet)	(Craddick 1976a)
Test 181 (20% inlet break)	(Craddick 1976a;b)
Test 177 (INEL code verification)	(Craddick 1980)
INEL Semiscale MOD-1 40 rod bundle	
Test S-02-1 (hot-let break)	(Crapo 1975)
Test S-02-9 (baseline series)	(Crapo 1976)
Test S-29-2 (reduced pressure)	(Crapo 1976 a;b)
Test S-28-1 (steam generator tube rupture	(Collins 1975)
Test S-06-6 (LOFT counterpart)	(Esparza 1977)
INEL Semiscale MOD-3 25 rod bundle	
Test S-07-3 (baseline series)	(Gillins 1978)
Test S-07-9 (baseline series)	(Miyasaki 1979)

Gunnerson, Pasamehmetoglu and Hosler (Gunnerson 1984) at the University of Central Florida. All the correlations compared to the blowdown data base are given in Table 6.

CODA Prediction of Flow Transients Data

The flow transient data have not been compared to CHF correlations by the author. Here, the results of Leung (1980) are summarized.

Moxon and Edwards' Tests

These are exponential flow decay experiments. In some experiments the flow decay is also accompanied by a power burst. Moxon and Edwards (1967) reported that their prediction of the time-to-CHF (t_{CHF}) was too early in all the experiments, compared to the experimental results. This indicates that the predicted CHF, by using the quasi-steady approach, is lower than the measured CHF. The discrepancy increases for faster transients.

Leung's study (1980) shows that the rapid CHF, which results from high initial heat fluxes and fast transients, is significantly overpredicted by the Biasi correlation and significantly underpredicted by Bowring, CISE correlations and Walley's theoretical model (1978b). The best results are obtained for slow CHF by using the Bowring correlation; Biasi correlation slightly overpredicts the data. Walley's analytical model underpredicts the CHF by 0.4 sec even for slow CHF. This result seems to be in contradiction with Collier's (1981) statement. According to Collier (1981), the results of Walley's prediction in the Moxon-Edwards tests are excellent. Results

TABLE 6

CHF CORRELATIONS COMPARED TO BLOWDOWN TEST DATA

Biasi	(Biasi 1967)
Local Barnett	(Barnett 1966)
Bowring	(Bowring 1972)
CISE	(Bertoletti 1965)
B & W - 2	(Gellerstedt 1969)
W - 3	(Tong 1968 a)
Griffith-Zuber	(Griffith 1977)
Modified Zuber	(Smith 1976)
GE	(Slifer 1971)
Condie Mod - 7	(Condie 1978)
Hsu - Beckner	(Hsu 1978)
BWC	(Lo 1984)
LOFT	(Eide 1977)
CE - 1	(CENDP 1977)
Savannah River	(Knoebel 1973)
Katto	(Katto 1978 through 1982)
EPRI	(Columbia University 1982 and 1983)

of the CHF prediction in the Moxon-Edwards test data are shown in Figure 34.

Roumy's Test

These tests were conducted at constant pressure and constant power. In the first test, the time to CHF is predicted (Leung 1980) by CISE, Biasi and Bowring correlations to within 0.1 second. The results are shown in Figure 35. In the second test, however, neither one of the above correlations predicted the time to CHF correctly. Actually, the correlation predicted no CHF, as shown in Figure 36, although the CHF is experimentally observed at 0.97 sec into the transient. According to Leung (1980), the incapability of predicting the CHF in this test is due to the discrepancy found in correlating the steady-state CHF data by the various correlations.

Cumo's Tests

These are exponential flow-decay tests at equivalent BWR and PWR pressures in a Freon-12 system. The CISE-Freon Correlation (Cumo 1972) is used to predict the CHF. The comparison of the measurements from the first 10 tests with the prediction of the correlation show very good agreement (Leung 1980). But, Cumo et al. (1978) reported that for fast transients a correction factor must be superimposed on the correlation. The study of Cumo et al. (1978) will be further discussed in the next chapter.

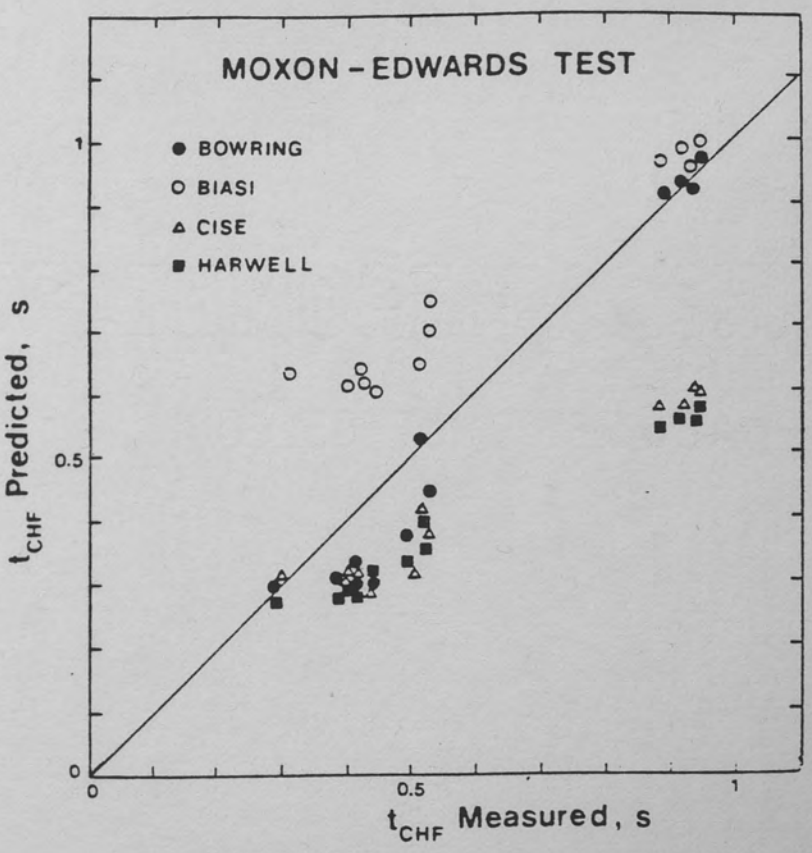

Figure 34. CHF Predictions in Moxon-Edwards Test (Leung 1980)

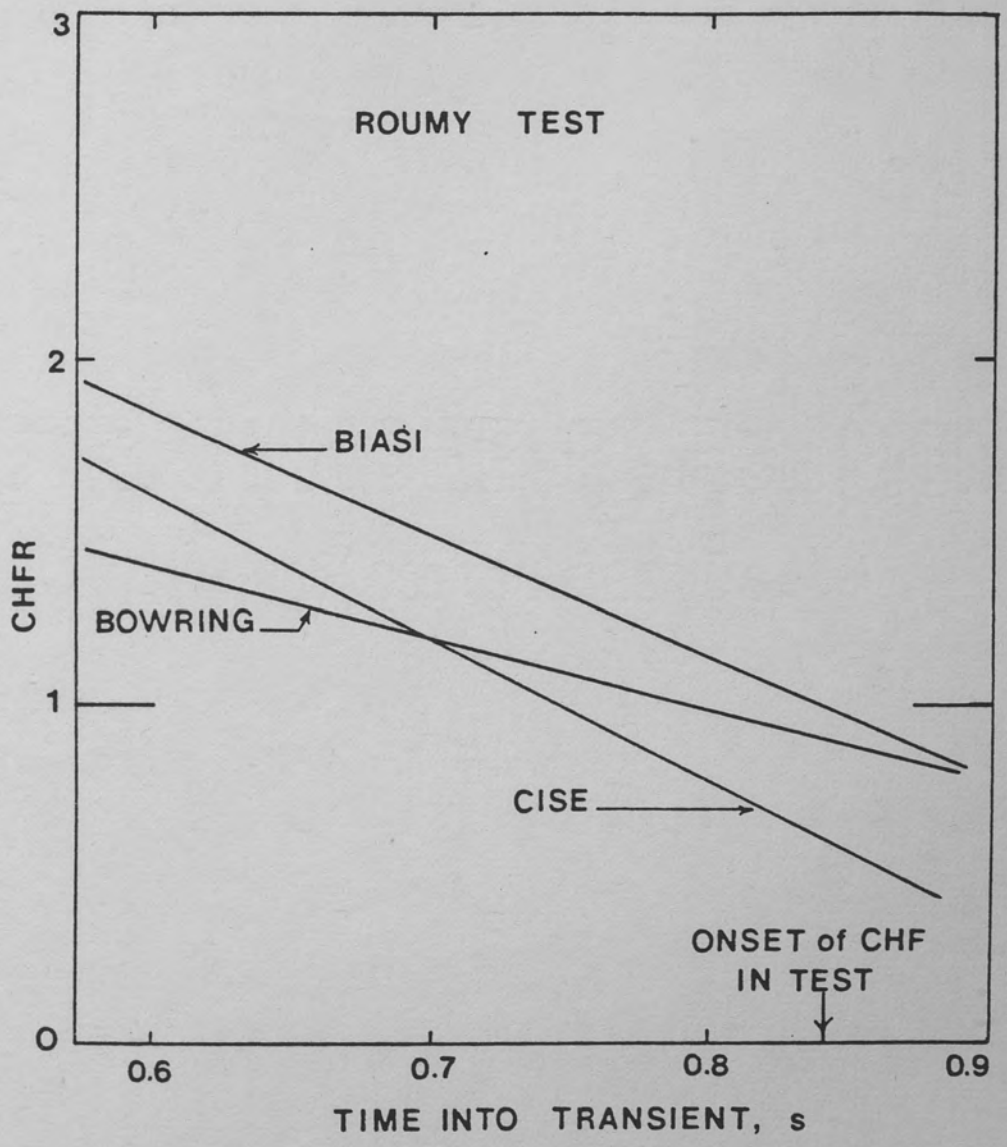

Figure 35. CHF Predictions in First Roumy Test (Leung 1980)

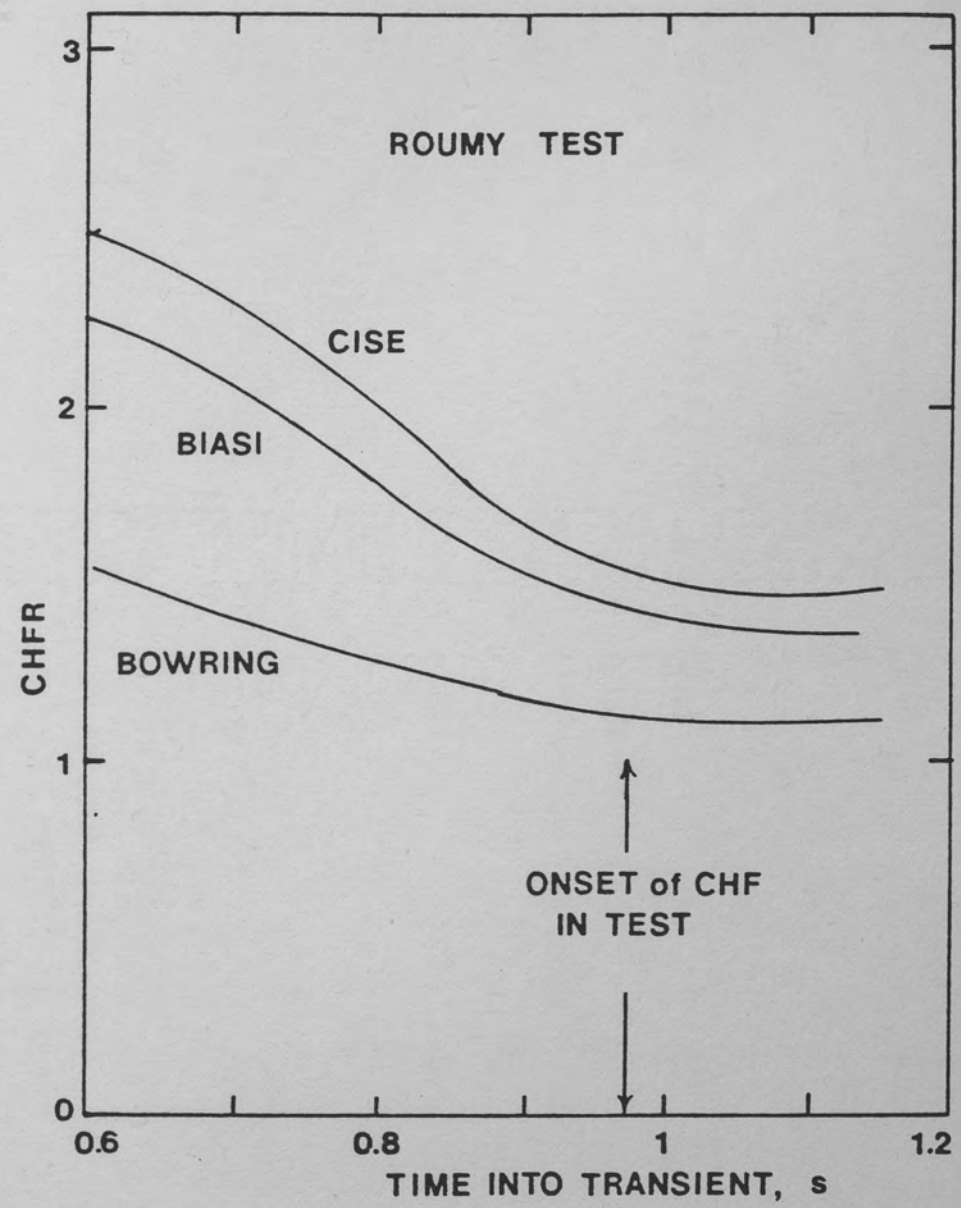

Figure 36. CHF Predictions in the Second Roumy Test (Leung 1980)

ANL Flow Transient Tests (Leung 1980)

The working fluid in these tests is Freon-11. In most tests a 4 percent linear flow decay is used. These are relatively slow transients and the comparison between calculated and measured time-to-CHF values is quite good. The CISE-Freon correlation is again used for comparison.

CODA Prediction of Blowdown Data

In this section, the results of blowdown experiments shown in Table 5 (with the exception of CE/EPRI and ANL Single-Tube Tests) are compared to steady-state CHF correlations shown in Table 6. This section summarizes the study of Leung (1980), Lo (1984), and the supplementary study conducted at the University of Central Florida (Gunnerson 1984). The initial conditions of these experiments are shown in Table 7.

CE/EPRI 5 x 5 Rod Bundle Test (Hsia 1977)

An inlet break was simulated, and no CHF was detected during the test. All the studied correlations were successful in predicting no CHF, except Savannah River, BWC, and Katto Correlations.

LOFT Columbia Loop 5 x 5 Bundle Test (Gottula 1978)

In this experiment, a double-ended guillotine break was simulated. The power was kept constant during the experiment (no scram). CODA's CHF prediction is summarized in Figure 37. As seen in Figure 37, quite a number of correlations were successful in predicting the data, including the $x = 1$ criterion. The latter condition is an

TABLE 7

INITIAL CONDITIONS OF LOSS-OF-COLLANT EXPERIMENTS (Leung 1980)

FACILITY	TEST	PRESSURE Mpa	INLET TEMPE-RATURE C	MASS FLOWRATE kg/s
CE/EPRI (5 x 5) (Uniform Axial Heat Flux)	BHT-25	13.7	296	9.3
LOFT COLUMBIA (5 x 5) (Uniform Axial Heat Flux)	2-5 & 2-12	15.2	257	4.2
PBF(Shrouded fuel rod) (Choped-Cosine)	LOC-11C	15.3	325	2.63
THTF (7 x 7) (Choped-Cosine)	105	15.5	285	19.9
	104	15.5	287	20.0
	178	15.9	277	19.6
	181	14.2	267	13.4
	177	15.4	276	21.0
SEMISCALE MOD-1 (40 rod bundle) (Choped-Cosine)	S-02-1	15.6	286	7.8
	S-02-9	15.5	283	7.4
	S-29-2	12.2	283	7.4
	S-28-1	15.8	284	6.8
	S-06-6	15.8	290	4.9
SEMISCALE MOD-3 (5 x 5) (Choped-Cosine)	S-07-3	15.9	285	9.5
	S-07-9	16.1	284	8.6

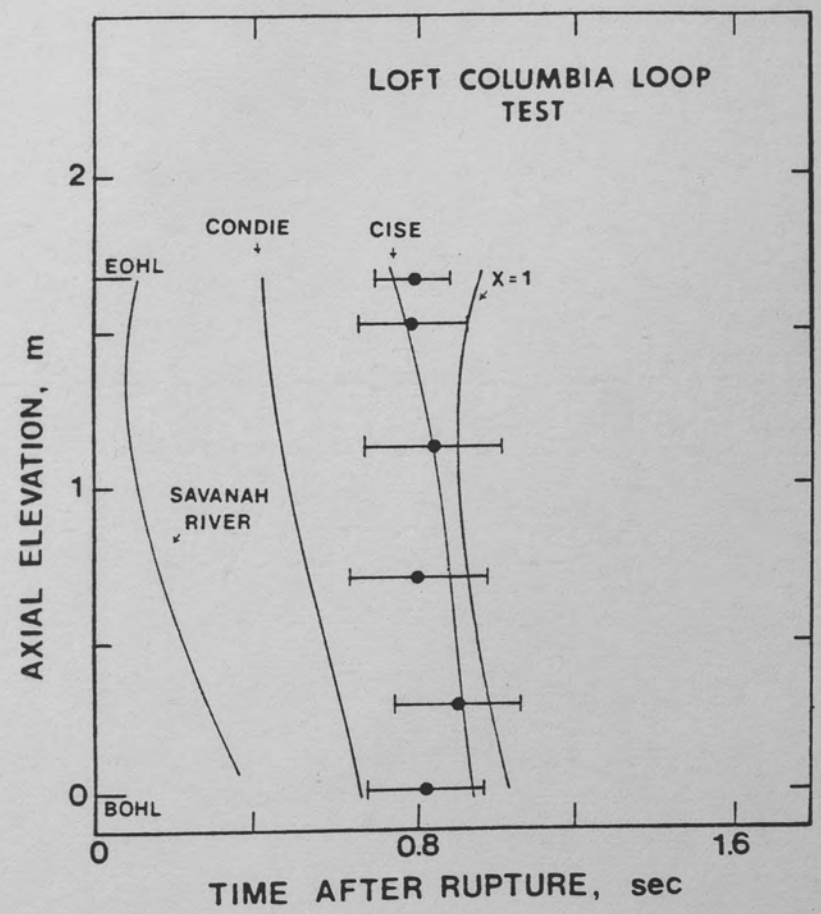

Figure 37. CHF Predictions in LOFT Columbia Test

indication of almost complete dryout within the core. In Figure 38, a 20 percent error band is shown for some of the correlations. This error band is obtained by plotting the loci of CHFR at 0.8 and 1.2.

PBF, LOC-11 (Shrouded Fuel Rods) (Buckland 1978)

A double-ended guillotine break was simulated. A delayed CHF was measured at the single thermocouple location. Since the CHF occurred at very low-mass velocity, there were only a few correlations which predicted CHF, as shown in Figure 39.

ORNL THTF - 105 (Clemons 1977)

This test was conducted with a 40 percent inlet - 60 percent outlet break configuration. A number of correlations gave close results, but the CHF is best predicted by the x = 1 criterion. The results are shown in figures 40 and 41.

ORNL THTF - 104 (Leon 1978)

The test conditions were similar to the THTF - 105 Test. In this test, a 50 percent inlet - 50 percent outlet break was simulated. Therefore, a stronger flow reversal was experimented. None of the correlations was able to predict the delayed CHF; the early CHF is predicted by a number of correlations, including the x = 1.0 criterion, as shown in figures 42 and 43.

ORNL THTF - 178 (Craddick 1976a)

This test was accomplished by introducing a 32 percent inlet - 28 percent outlet break. Coda code predictions are shown in figures 44

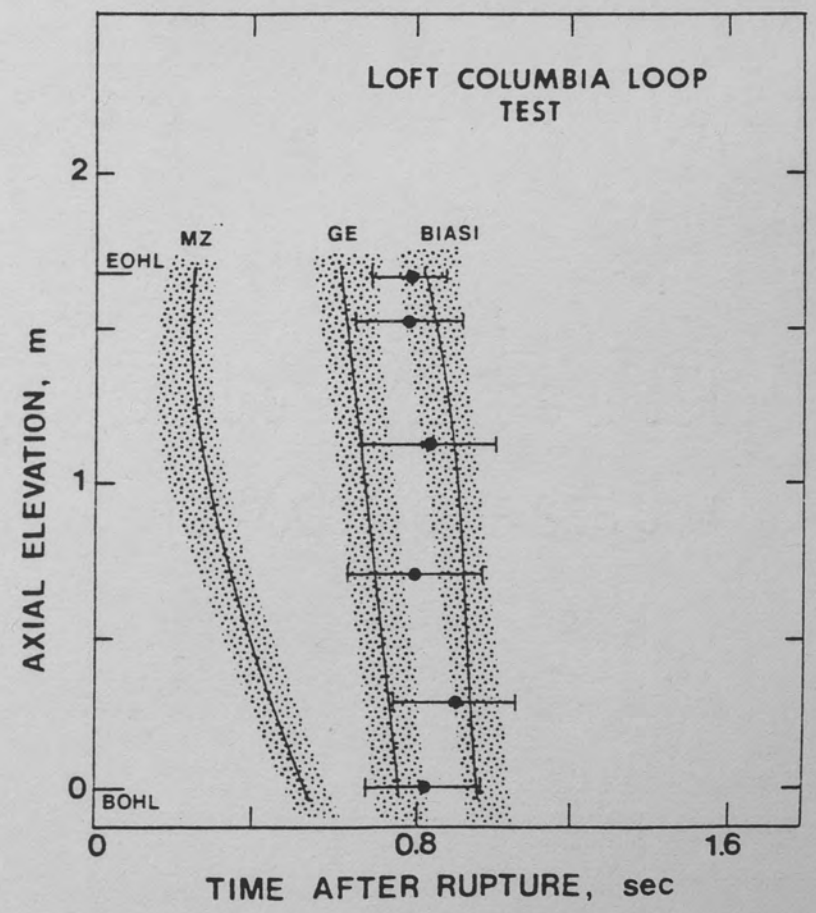

Figure 38. CHF Predictions in LOFT Columbia Test with Error Bands

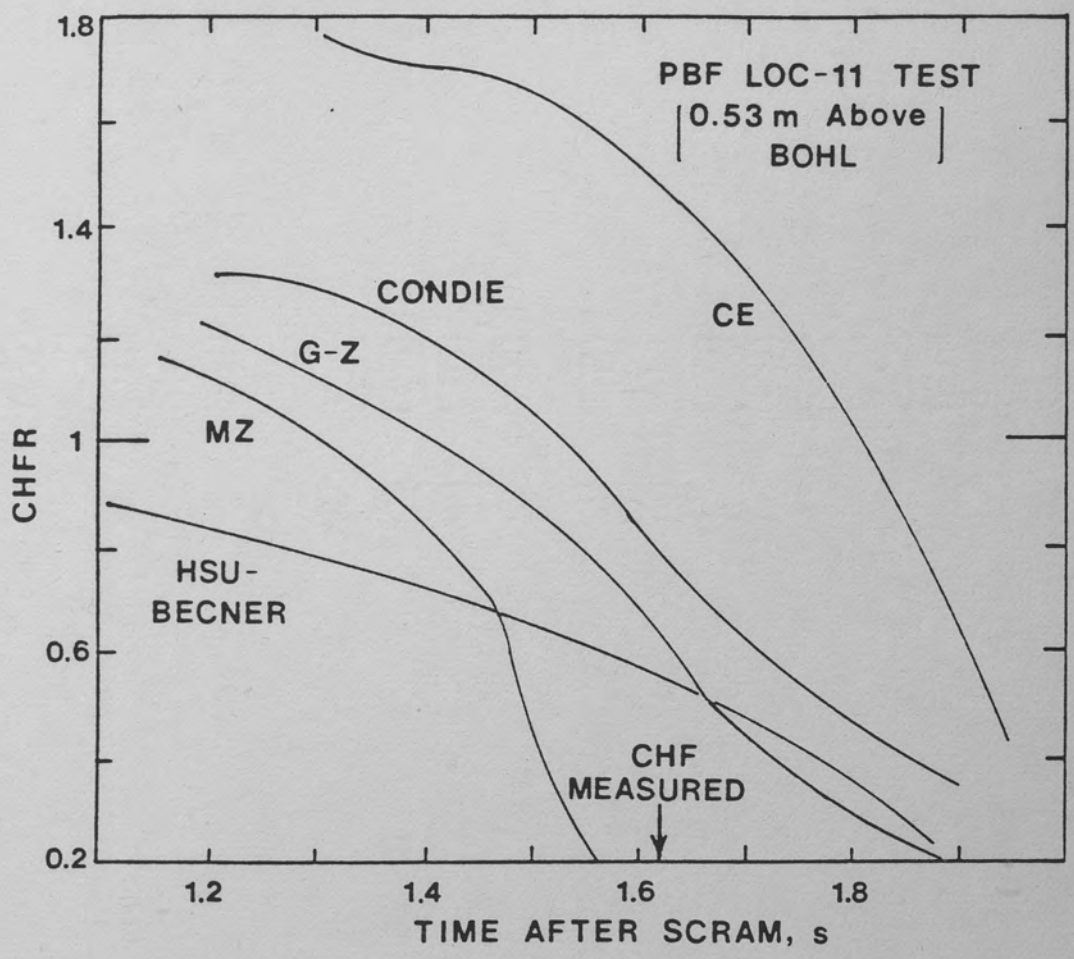

Figure 39. CHF Predictions in PBF LOC-11 Test

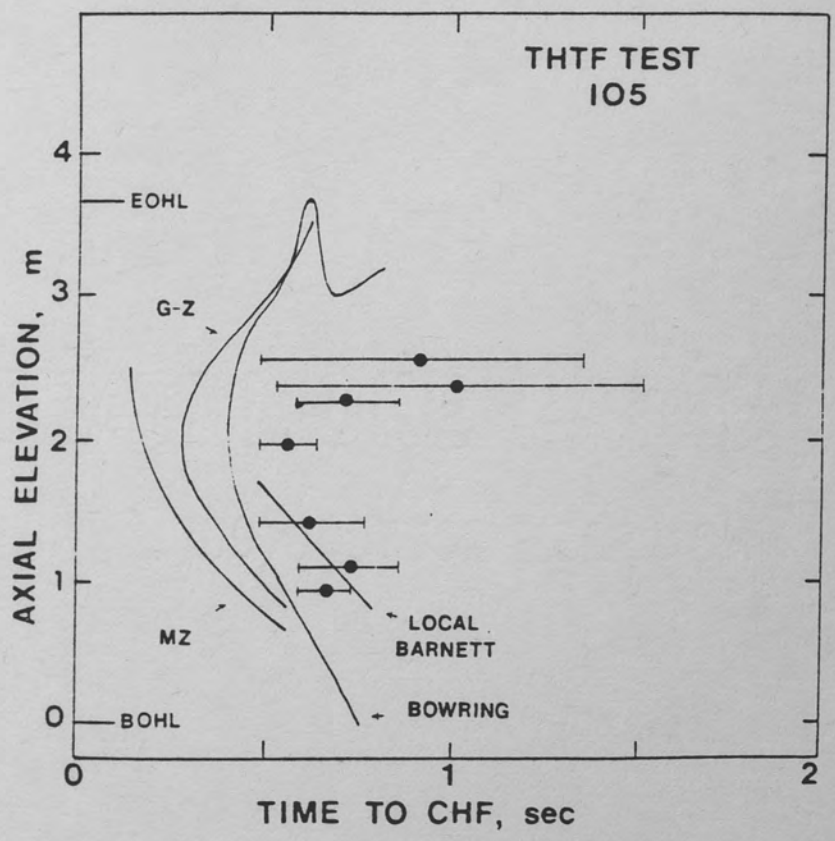

Figure 40. CHF Predictions in THTF-105 Test

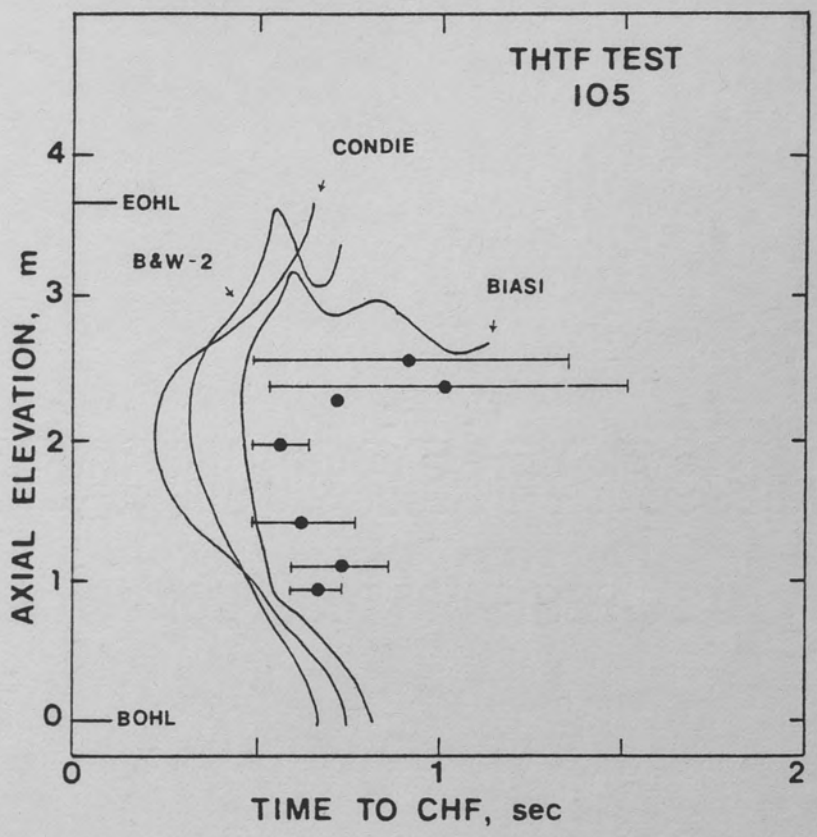

Figure 41. CHF Predictions in THTF-105 Test

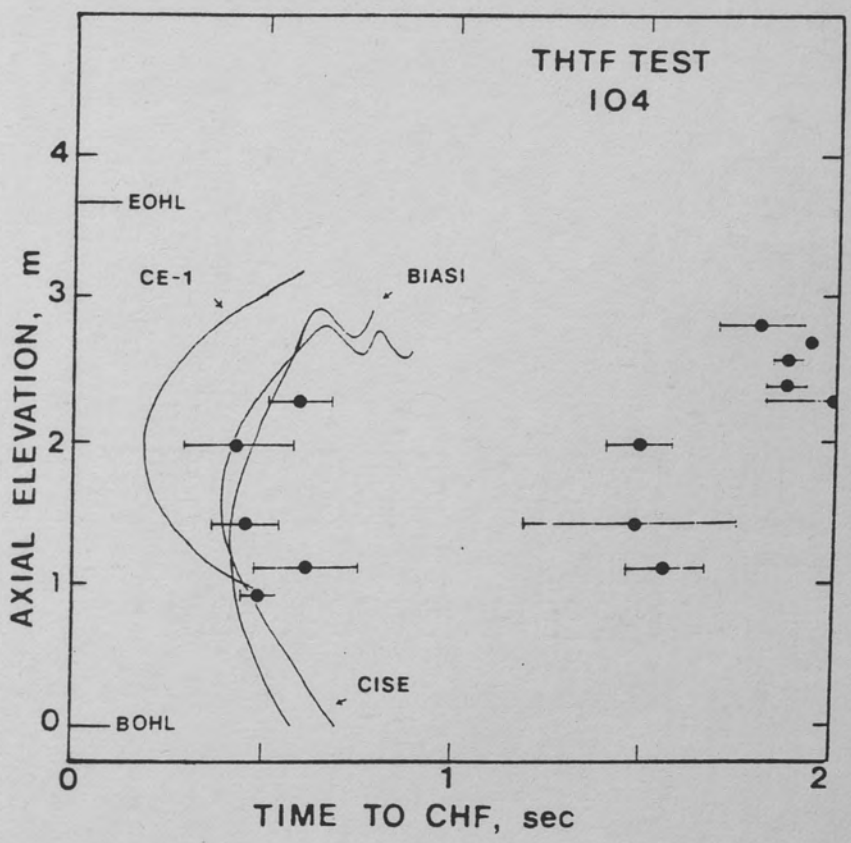

Figure 42. CHF Predictions in THTF-104 Test

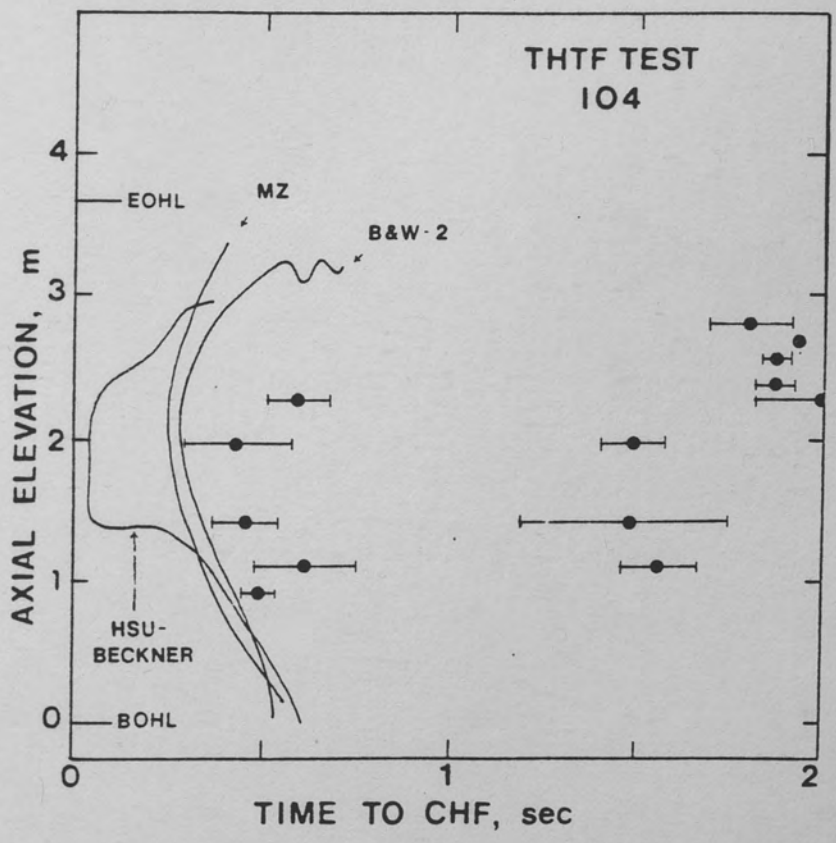

Figure 43. CHF Predictions in THTF-104 Test

and 45. Due to the limited number of data points, statistical calculations on thermocouples could not be performed (Leung 1980).

ORNL THTF - 181 (Craddick 1979b)

This test was a mild transient with a 20 percent inlet break. It is a small-break LOCA. As shown in Figure 46, the Biasi, CISE and x = 1 correlations are quite successful in predicting the CHF in this test.

ORNL THTF - 177 (Craddick 1980)

The test conditions were identical to the THTF - 178 test. Thus, the results were similar as shown in figures 47 and 48.

INEL Semiscale Mod-1, S-02-1 (Grapo 1975)

This was a double-ended hot-leg break test. No flow reversal was observed. The CHF first occurred 24 seconds into the transient. All the correlations failed to predict the data, except the Griffith-Zuber correlation, as shown in Figure 49.

INEL Semiscale Mod-1, S-02-9 (Crapo 1976)

This was a 200 percent, double-ended cold-leg break test. The results of CODA calculations are shown in figures 50 and 51. Again, a number of CHF correlations performed well for this test.

INEL Semiscale Mod-2, S-29-2 (Crapo 1976 a & b)

This test was also a double-ended cold-leg break test, but at a

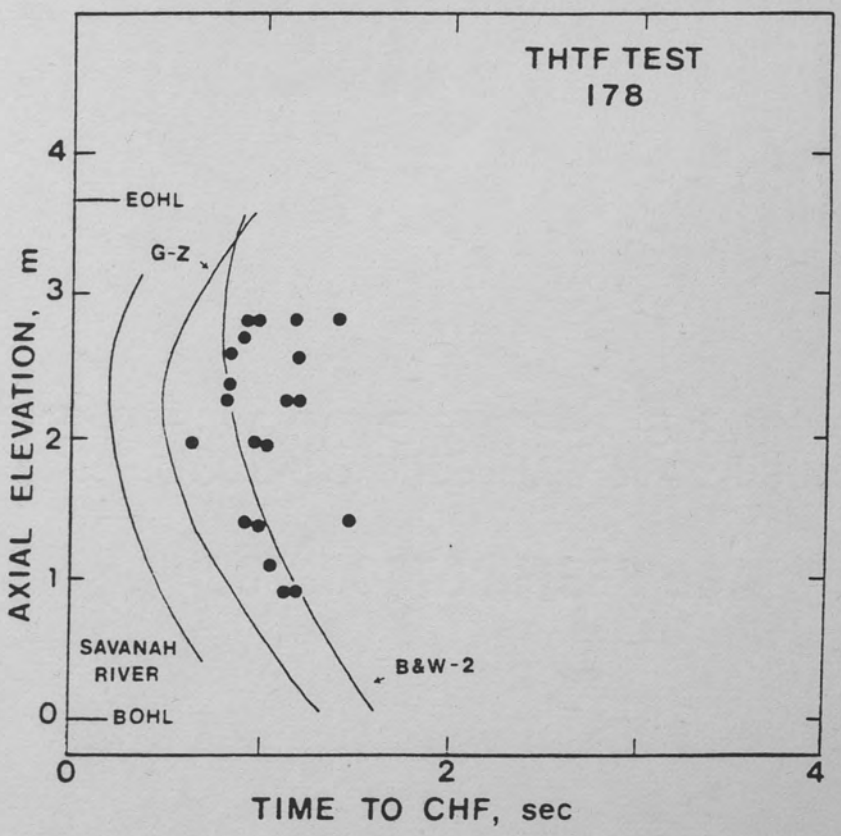

Figure 44. CHF Predictions in THTF-178 Test

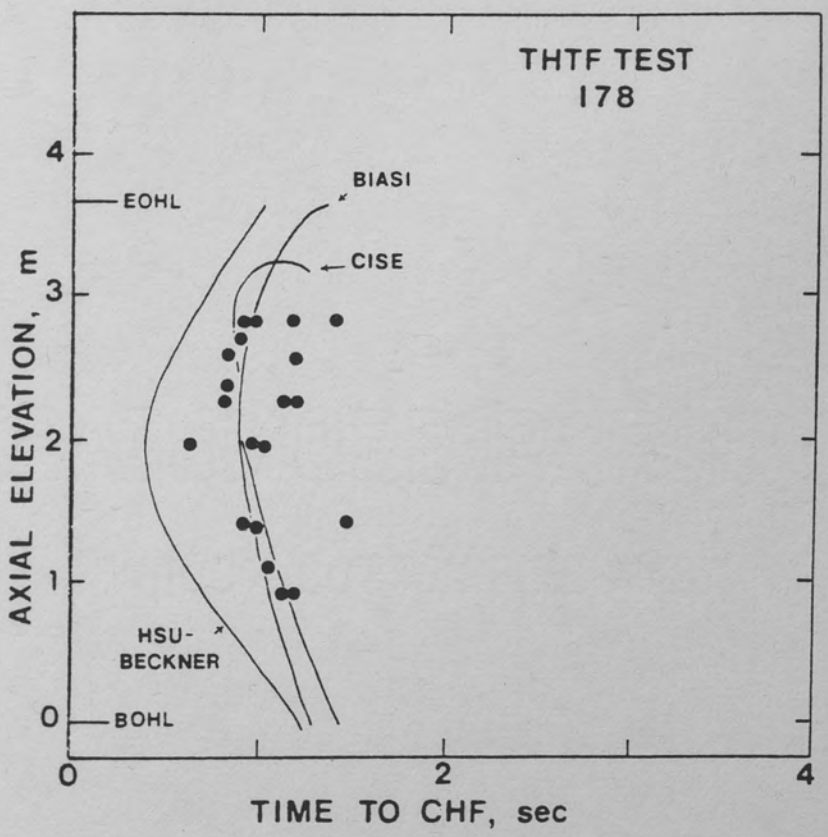

Figure 45. CHF Predictions in THTF-178 Test

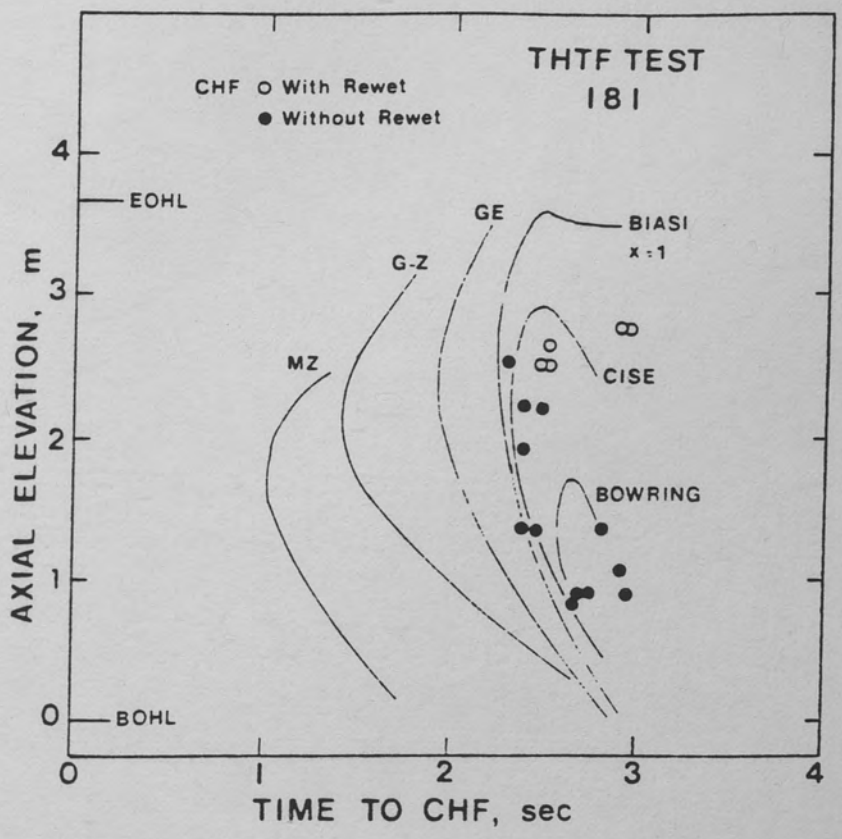

Figure 46. CHF Predictions in THTF-181 Test

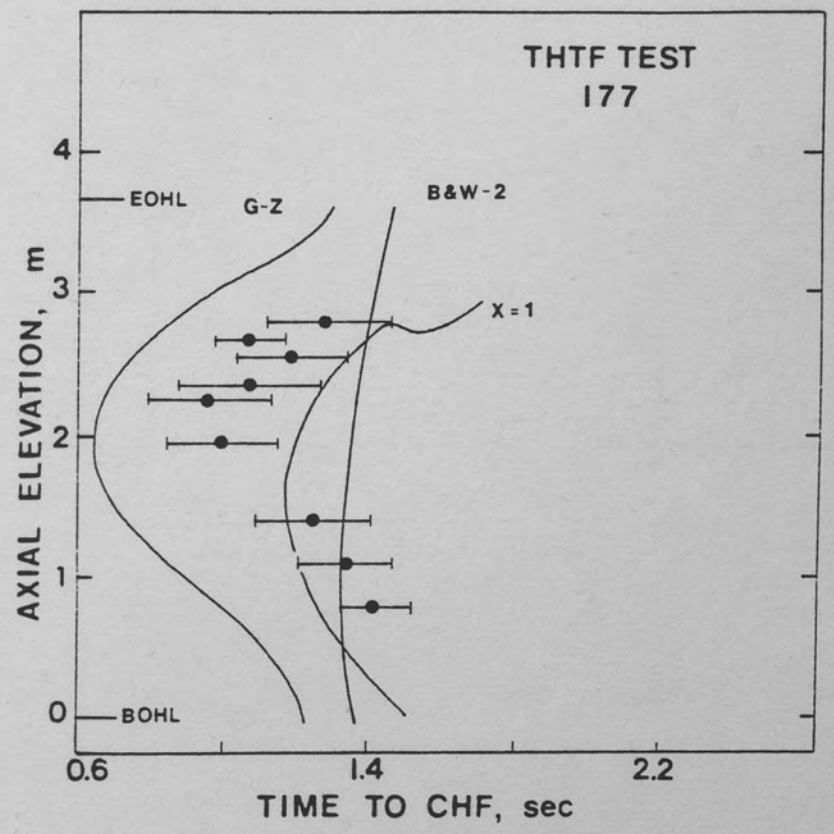

Figure 47. CHF Predictions in THTF 177 Test

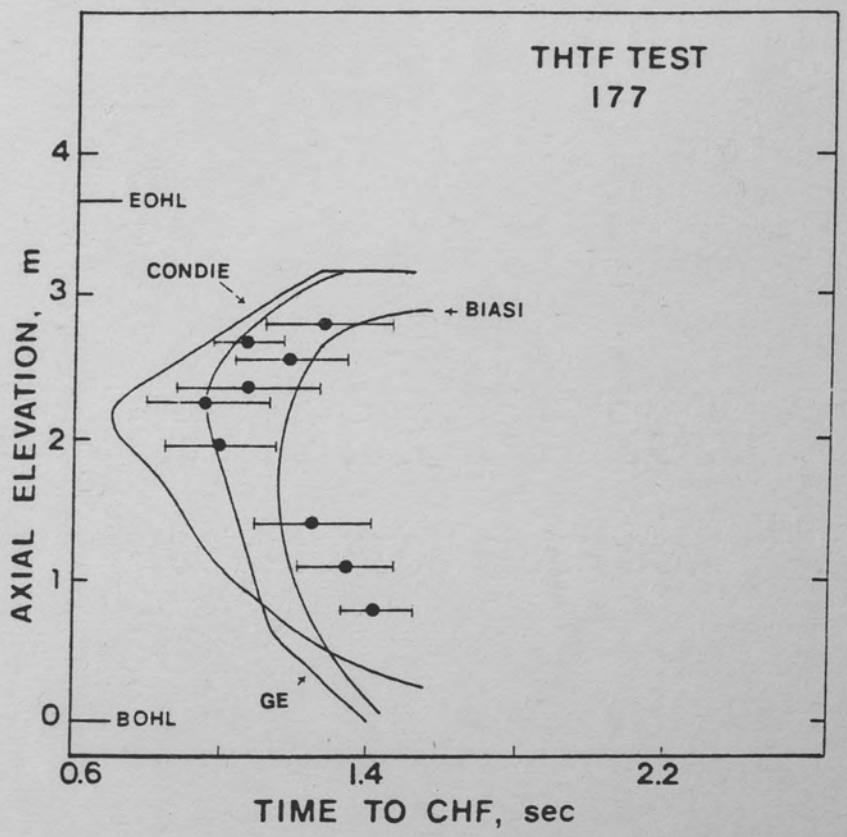

Figure 48. CHF Predictions in THTF 177 Test

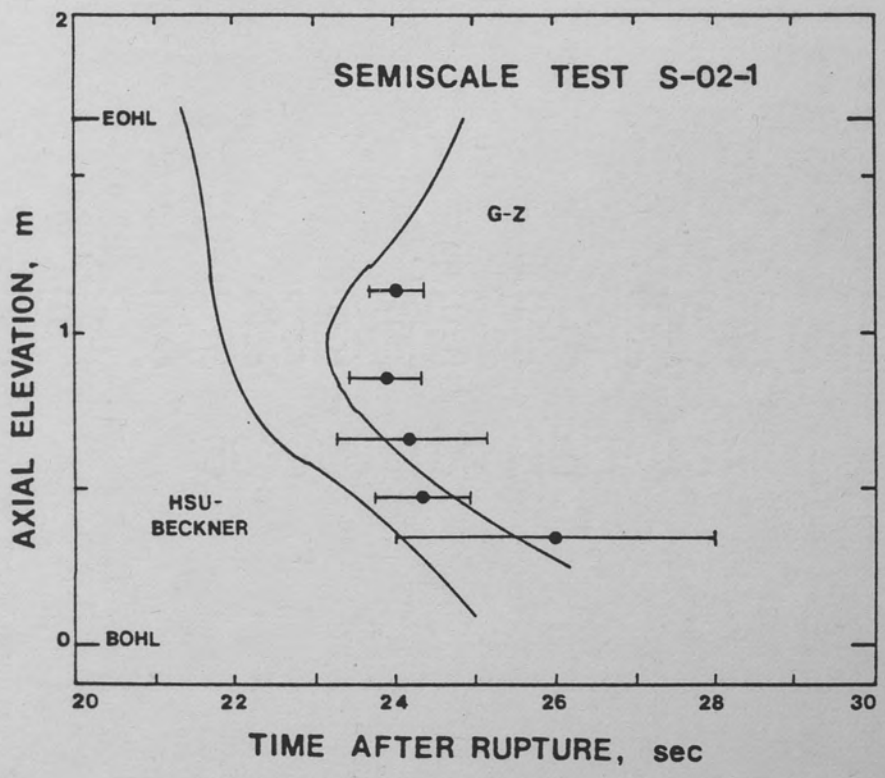

Figure 49. CHF Predictions in S-02-1 Test

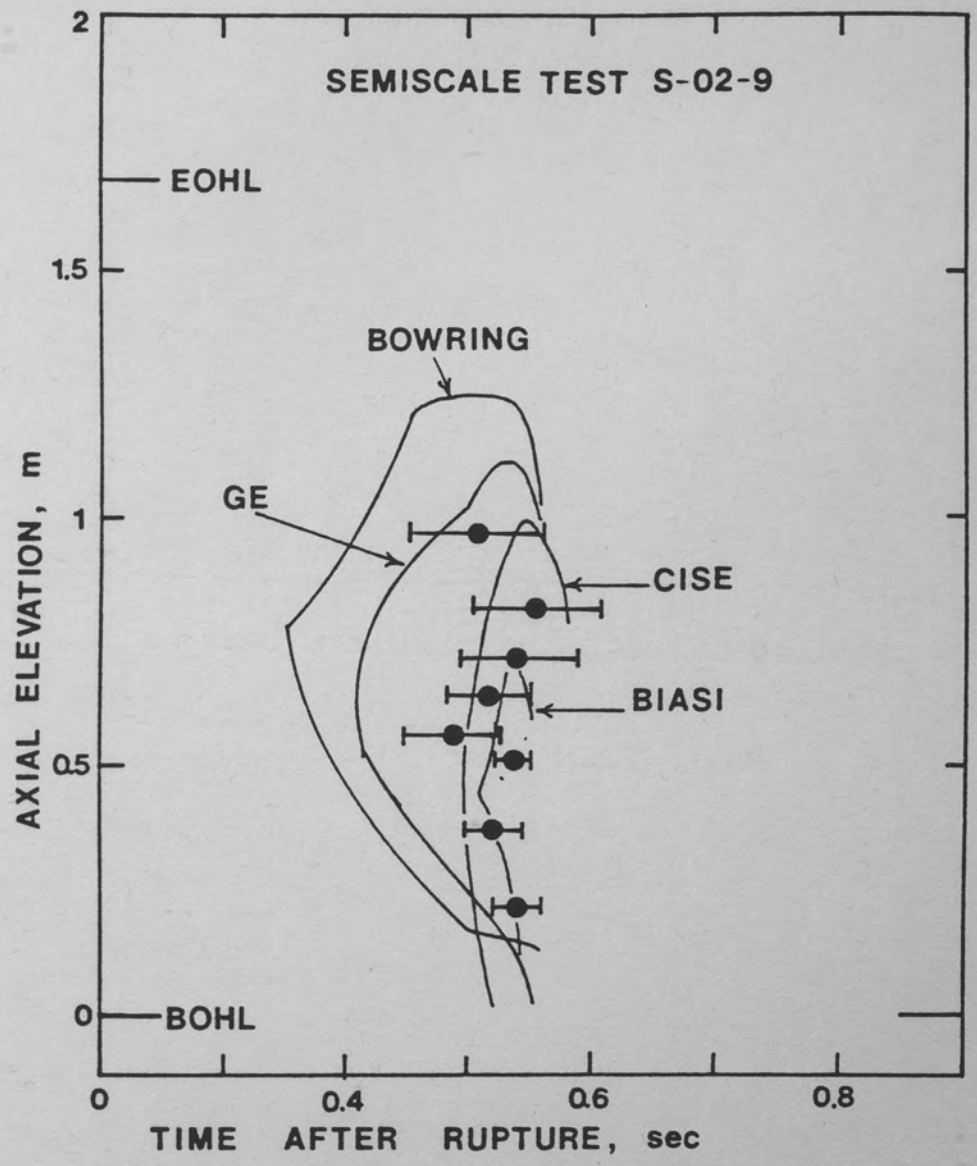

Figure 50. CHF Predictions in S-02-9 Test

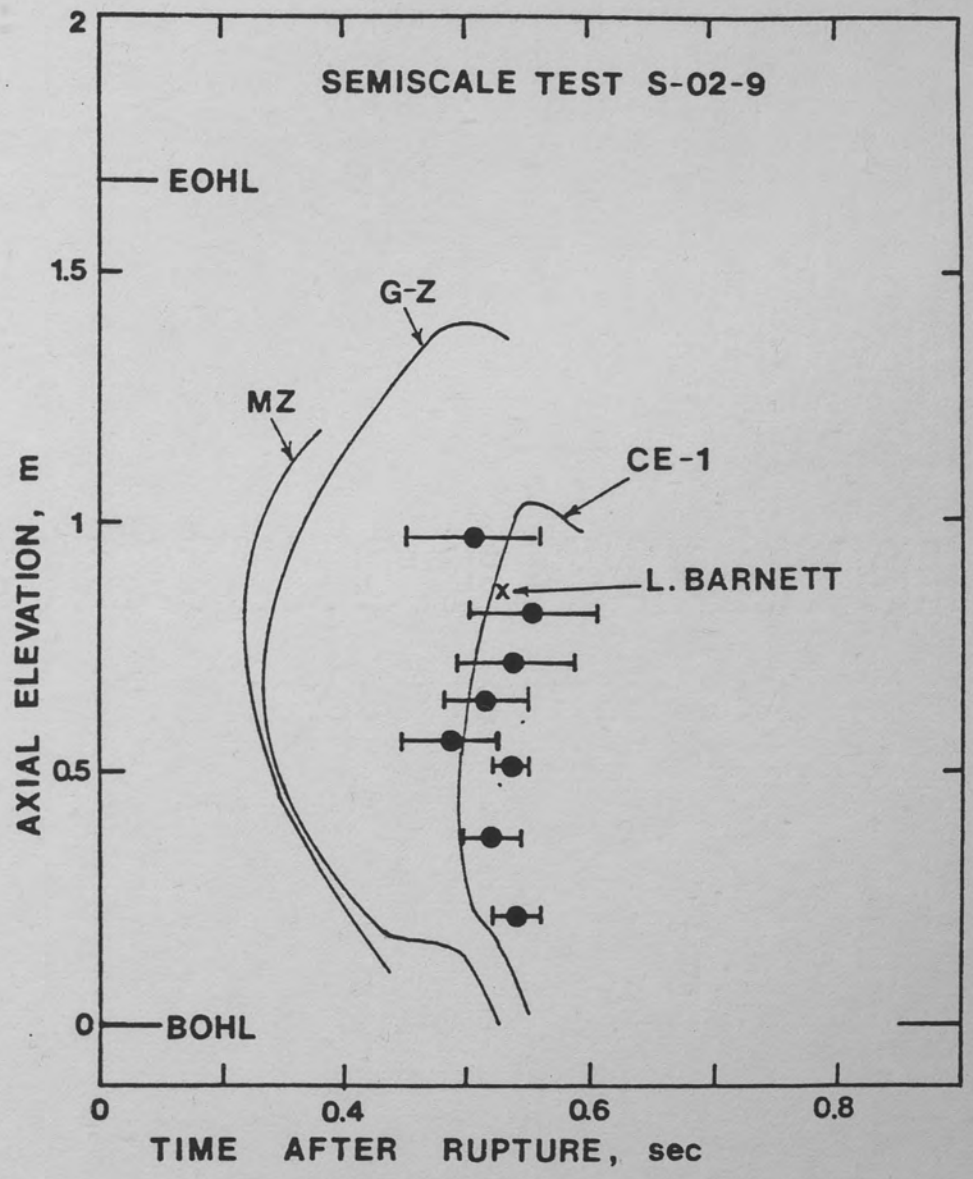

Figurre 51. CHF Predictions in S-02-9 Test

reduced pressure. The results are similar to the S-02-9 test, but time-to-CHF is slightly underpredicted, as shown in figures 52 and 53.

INEL Semiscale Mod-1, S-28-1 (Collins 1971)

In this double-ended cold-leg break test, early and delayed CHF were observed. A number of correlations are able to predict the early CHF; but only the GE correlation is successful in predicting the delayed CHF, as shown in figures54 and 55.

INEL Semiscale Mod-1, S-06-6 (Esparza 1977)

In this last Semiscale Mod-1 experiment, a double-ended cold-leg break was simulated. The results of CODA predictions are shown in Figure 56. Only the Condie Mod-7 correlation is successful in this test.

INEL Semiscale Mod-3, S-07-3 (Gillins 1978)

This is also a double-ended cold-leg break test in a full-scale 5 x 5 PWR assembly. The results are shown in figures 57 and 58. In this experiment, the CHF occurred at a high-quality ($x \simeq 1$).

INEL Semiscale Mod-3, S-07-9 (Miyasaki 1979)

This was a test similar to S-07-9. The results are also similar and are shown in figures 59 and 60. In figures 37 through 60 the empty on darkened circles represent the experimental data.

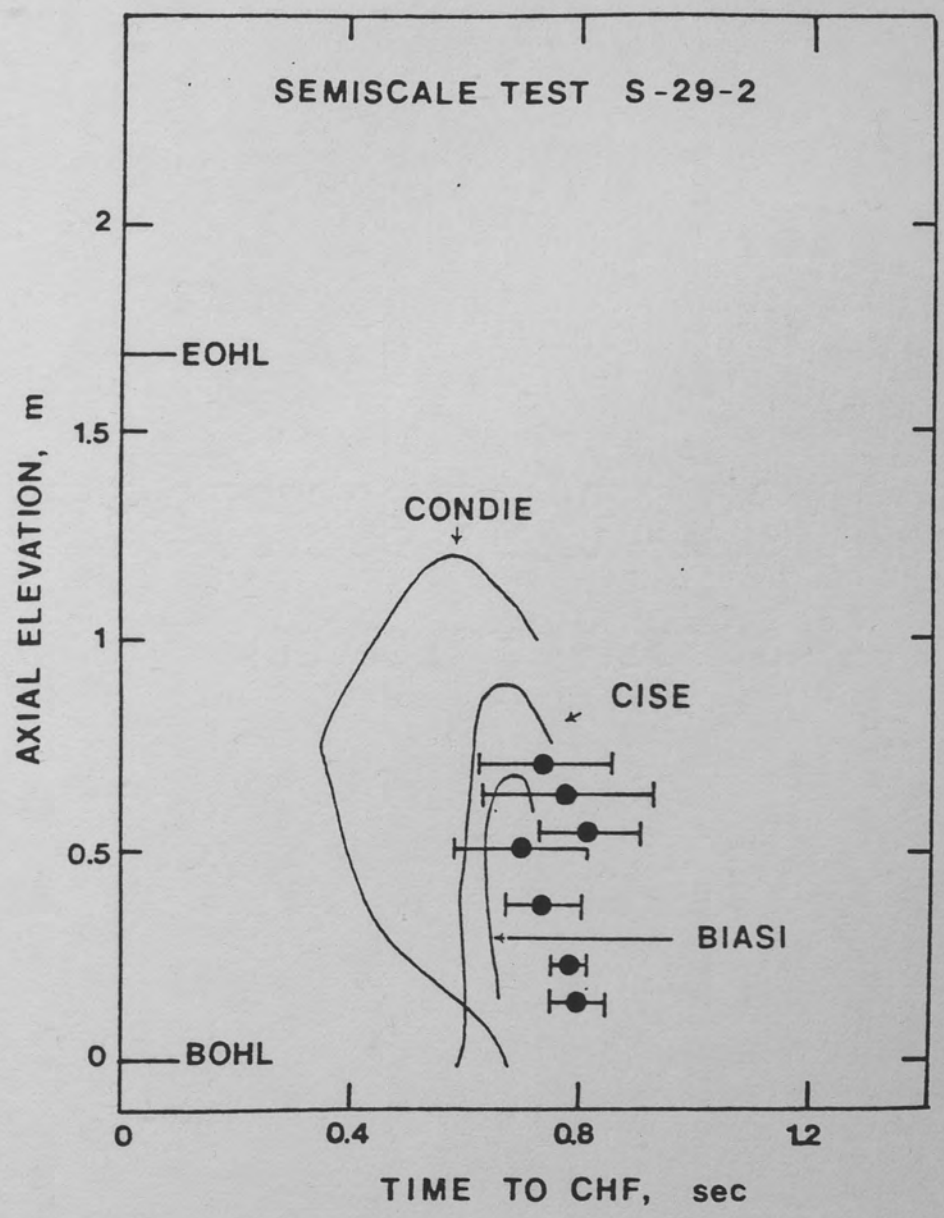

Figure 52. CHF Predictions in S-29-9 Test

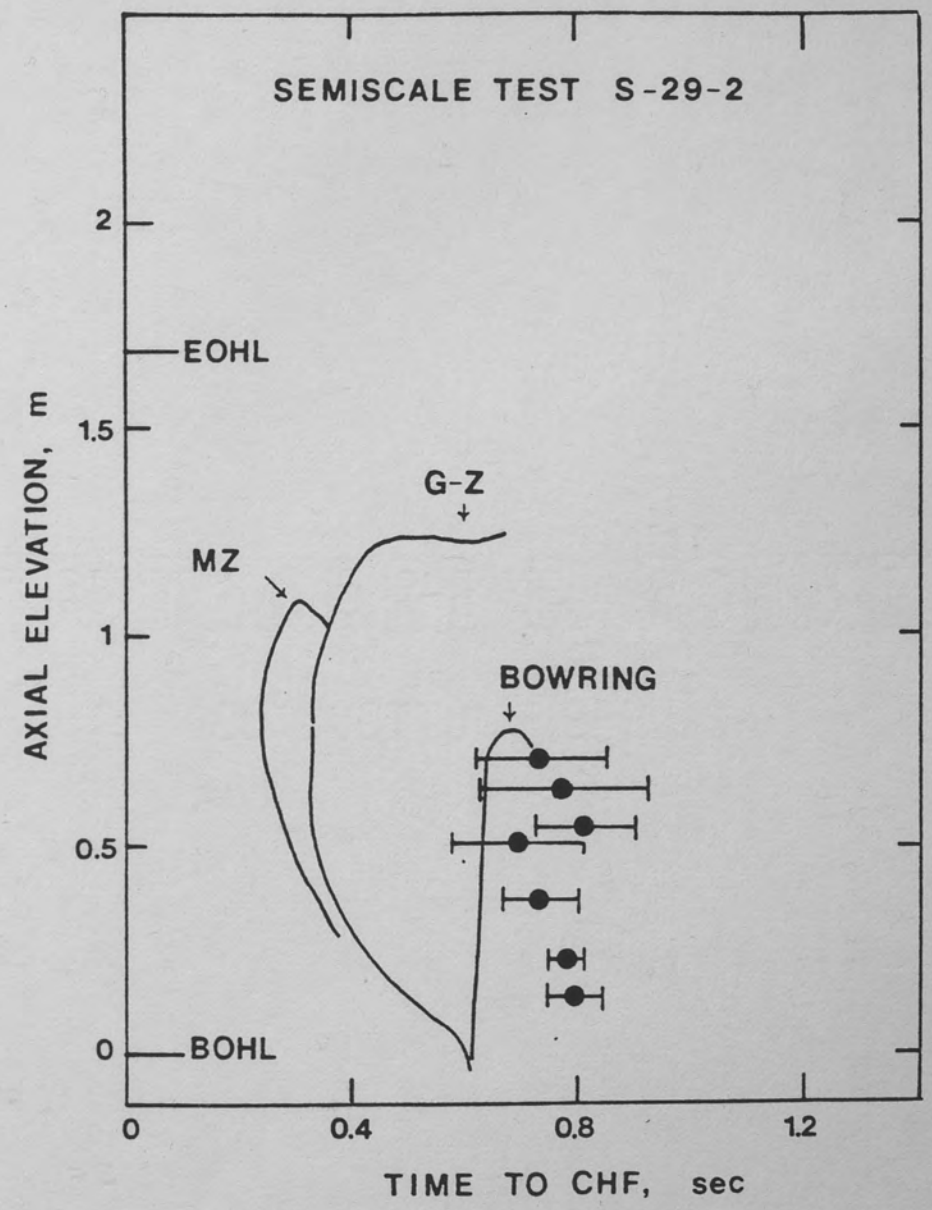

Figure 53. CHF Predictions in S-29-2 Test

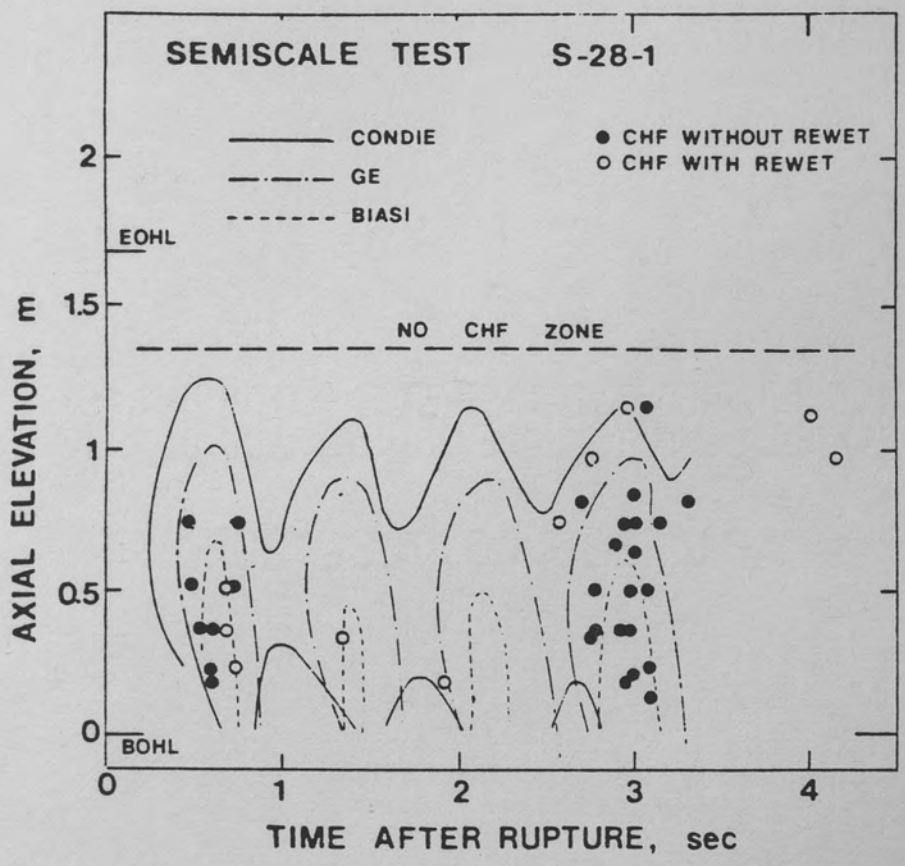

Figure 54. CHF Predictions in S-28-1 Test

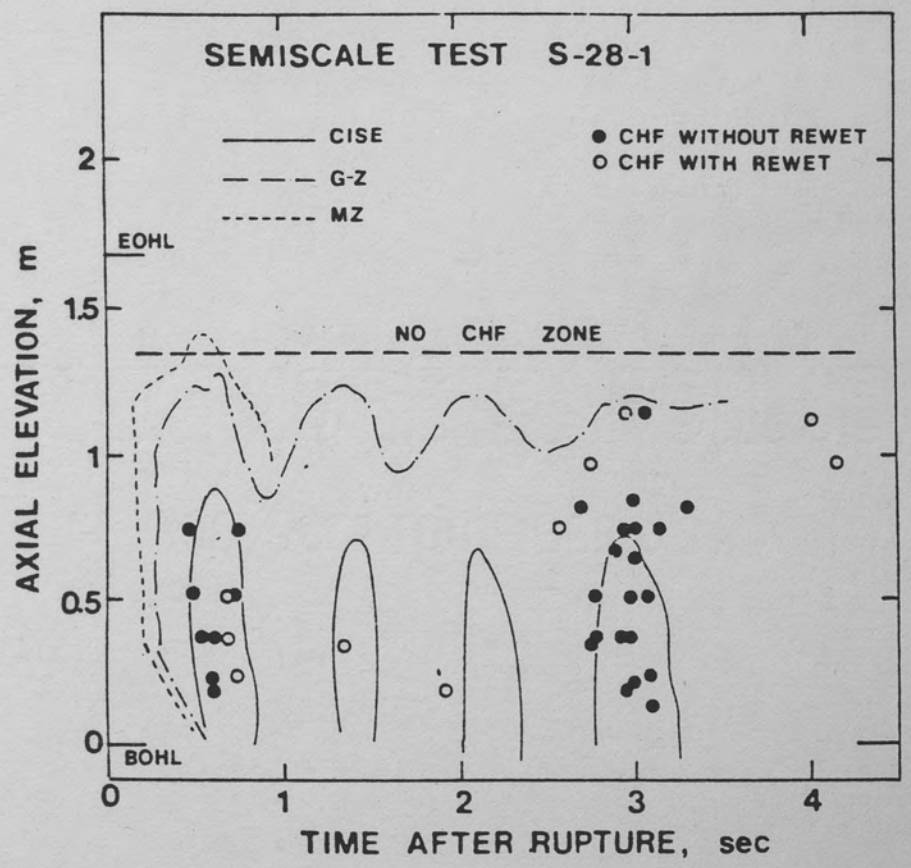

Figure 55. CHF Predictions in S-28-1 Test

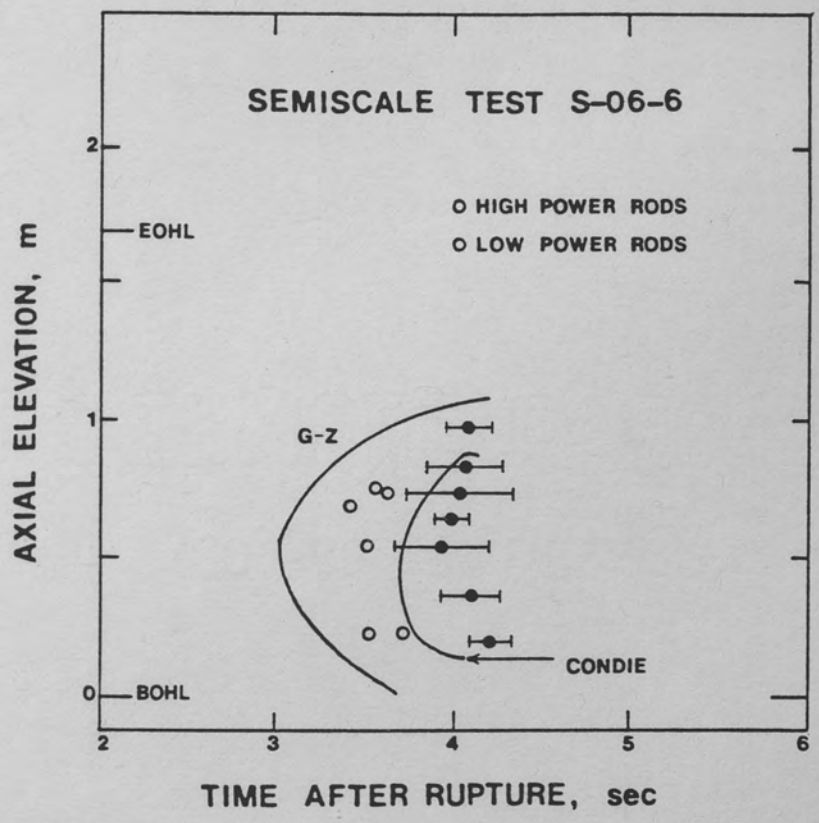

Figure 56. CHF Predictions in S-06-6 Test

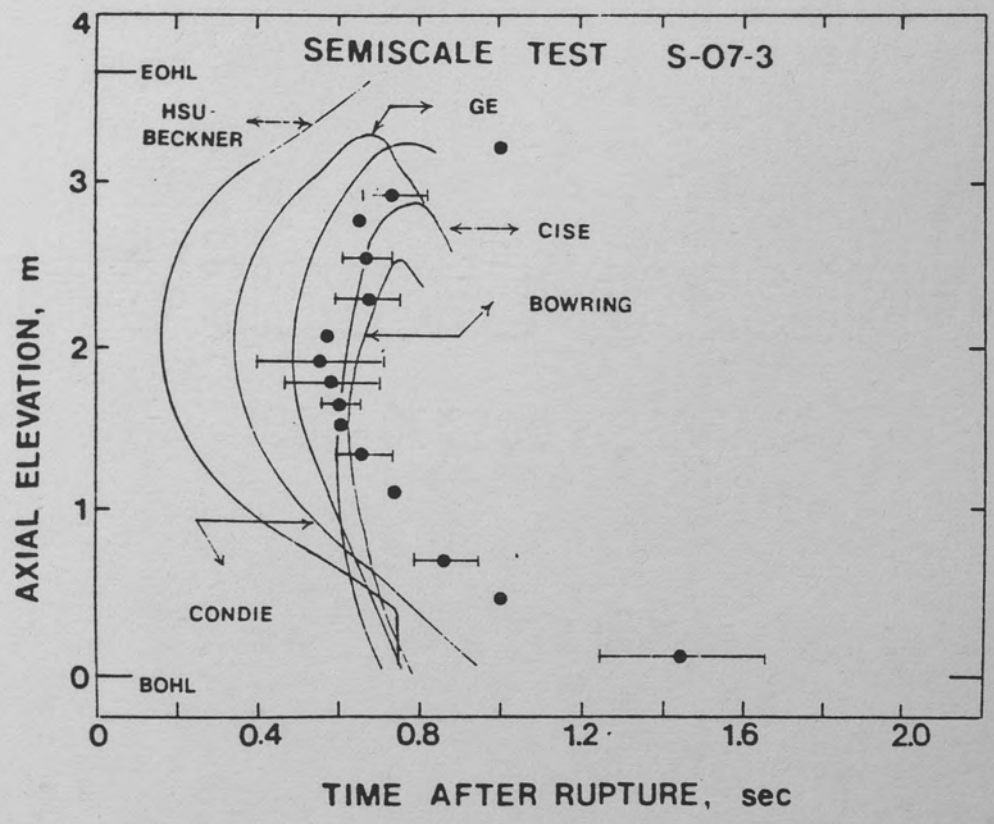

Figure 57. CHF Predictions in S-07-3 Test

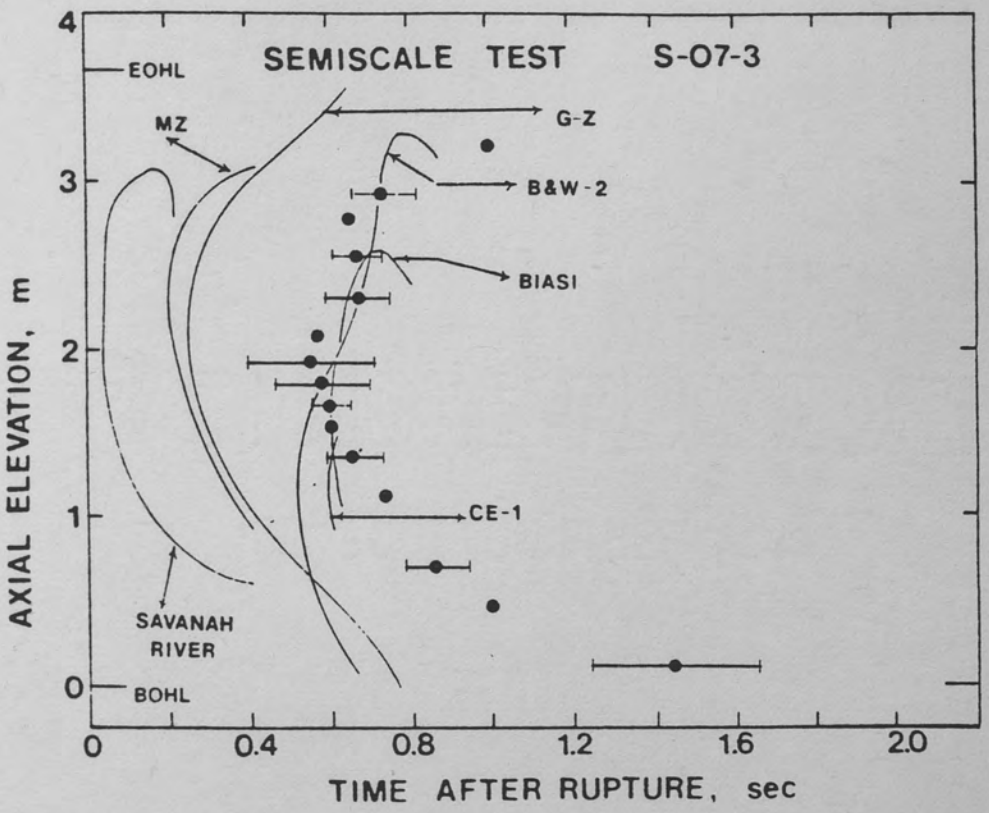

Figure 58. CHF Predictions in S-07-3 Test

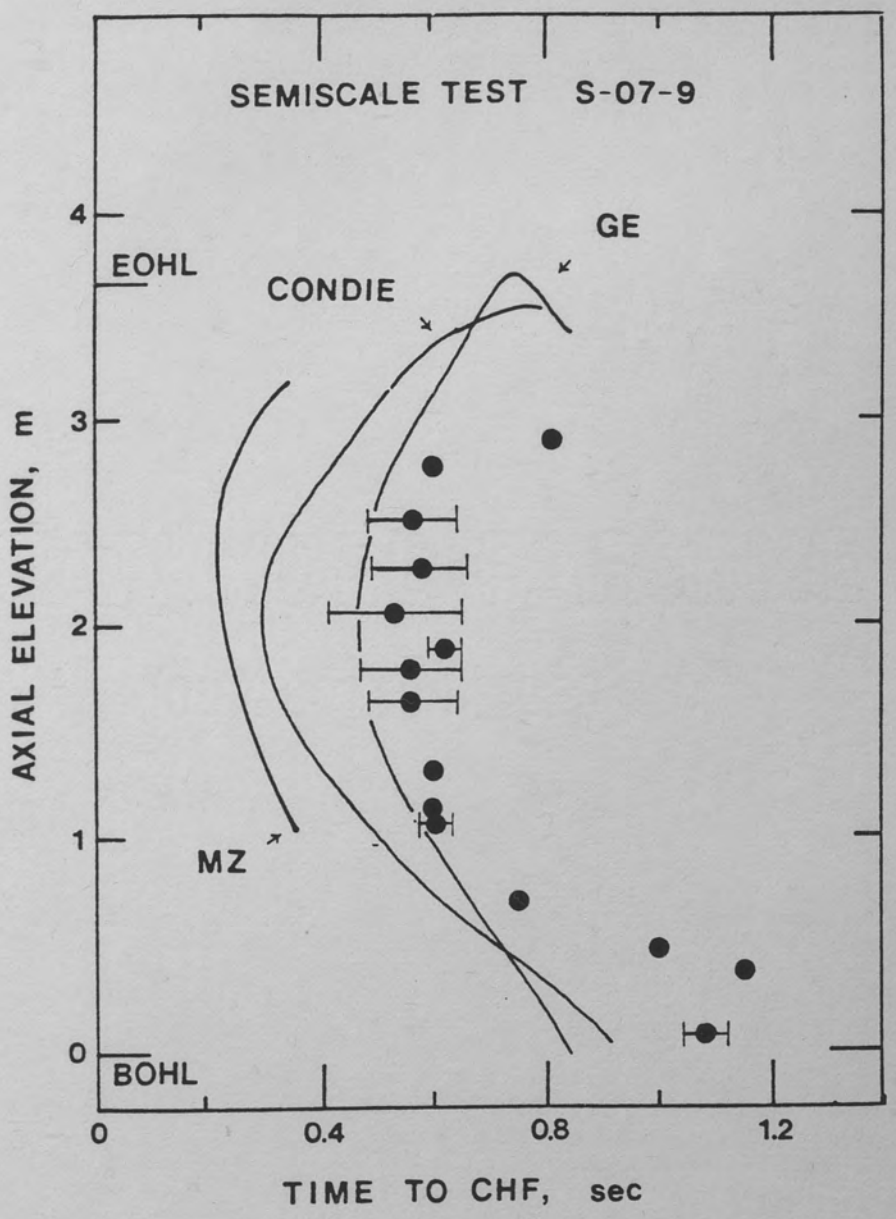

Figure 59. CHF Predictions in S-07-9 Test

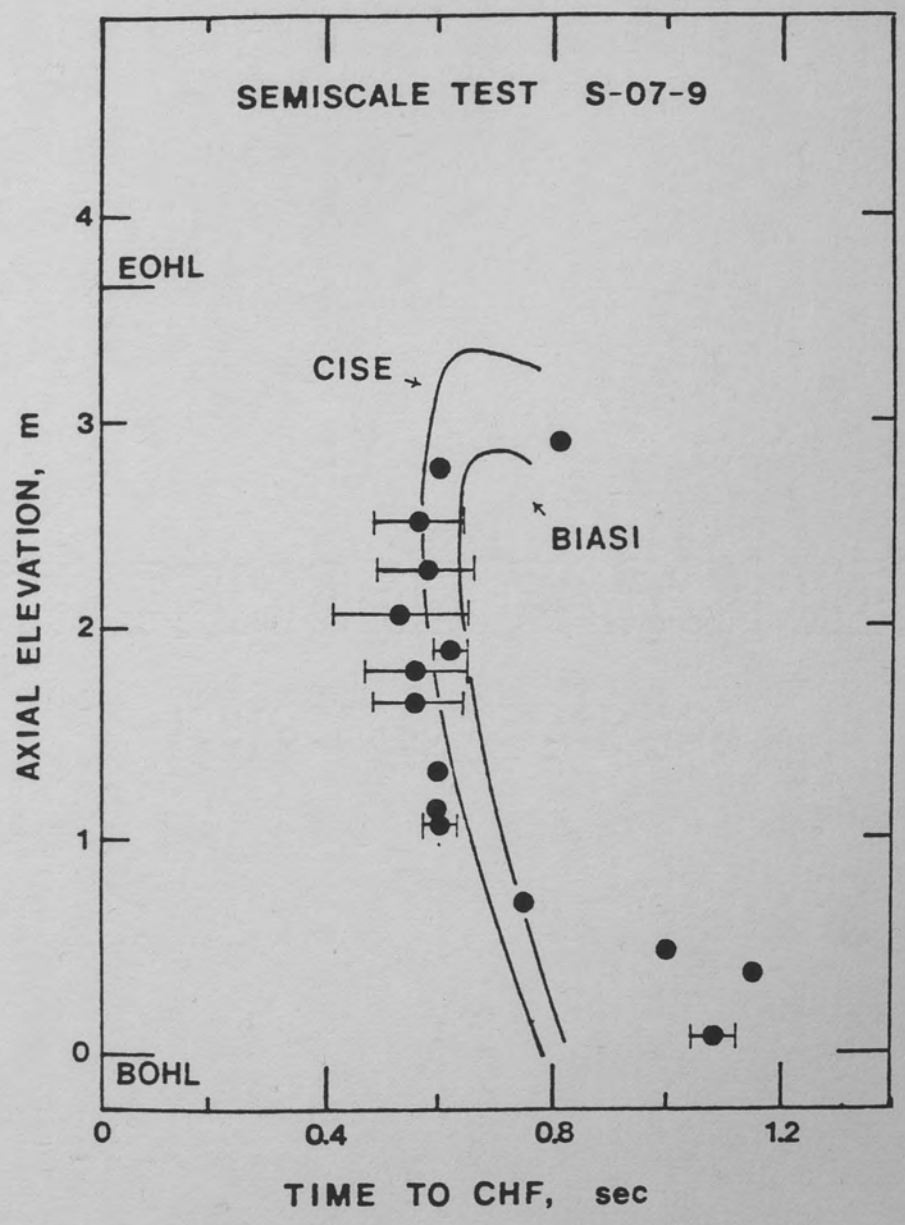

Figure 60. CHF Predictions in S-07-9 Test

Summary of CODA Predictions

Table 8 summarizes the results of CODA predictions in flow decay experiments. For blowdown experiments, a summary of the prediction results is presented in Table 9.

In general, the early CHF (t_{CHF} ~ 1 s) were best predicted by round-tube correlations. In general, the CISE and Biasi correlations were successful in a number of experiments. The Bowring correlation, although inferior to the CISE and Biasi correlations, yielded successful results in some experiments. The local Barnett, CE-1, and GE correlations were also successful in predicting the early CHF.

Although correlated over the rod-bundle data, Condie Mod-7 correlation performed very marginally over the blowdown data. It tends to correlate the delayed CHF better than the early CHF. The Hsu-Beckner correlation is correlated using blowdown data but yielded poor predictions over the data studied. The Savannah River, B & W-2, LOFT, and BWC correlations are found to be very unsuccessful.

The Griffith-Zuber and modified Zuber correlations were successful to predict the delayed CHF in the following range of mass velocity:

$$-240 < G < 100 \text{ kg/m}^2\text{-s}$$

In general, the Griffith-Zuber correlation performed better than the modified Zuber correlation. However, as suggested by Leung (1980), it should be kept in mind that this mass-velocity criterion is strongly affected by the measured mass flow, and that mass velocity of such low

TABLE 8

SUMMARY OF CHF RESULTS IN FLOW TRANSIENTS

TEST	Best Correlation(s)
Moxon-Edwards	None (Fast CHF) Bowring, Biasi (Slow CHF)
Roumy	CISE, Bowring, Biasi (1st Test) None (2nd test)
Cumo	CISE - Freon Correlation
ANL	CISE - Freon Correlation

TABLE 9

SUMMARY OF BLOWDOWN CHF RESULTS

Tests and Specifications	Bowring	Biasi	CISE	Griffith-Zuber	GE	Condie Mod-7	B&W-2	Hsu-Beckner	x-1.0	Savannah River	CE-1	Local Barnett	LOFT	BWC	Modified Zuber
CE/EPRI Rod-Bundle BHT-25	○	○	○	○	○	○	○	○	○	●	○	○	○	●	○
LOFT Columbia Loop	○	○	○	●	○	▲	○	●	○	●	○	○	●	●	●
PBF LOC-11C	●	●	●	○	○	○	●	●	●	●	●	●	●	●	▲
THTF Bundle #1															
Test 105	▲	○	○	▲	○	▲	▲	●	○	●	▲	○	○	●	●
Test 104	○	○	○	▲	○	▲	▲	●	○	●	▲	○	▲	▲	▲
Test 178	○	○	○	▲	▲	▲	▲	▲	○	●	●	▲	●	●	▲
Test 181	▲	○	○	▲	▲	▲	●	▲	○	●	●	●	●	●	●
Test 177	●	○	○	○	○	▲	●	▲	○	●	●	●	●	●	▲
Semiscale Mod-1															
S-02-1	●	●	●	○	●	●	●	▲	●	●	●	●	●	●	●
S-02-9	○	○	○	●	▲	▲	○	●	●	●	○	○	●	●	●
S-29-2	○	▲	○	●	▲	▲	▲	●	●	●	○	○	●	●	●
S-28-1 (Early and delay CHF)	○●	○▲	○▲	●○	○○	▲●	○▲	▲●	●●	●●	○●	○▲	●●	●●	●○
S-06-6	●	●	●	▲	●	○	●	▲	●	●	●	●	●	●	●
Semiscale Mod-3															
S-07-3	○	○	○	●	○	▲	○	●	▲	●	○	●	●	●	●
S-07-9	○	○	○	▲	▲	▲	▲	▲	▲	●	●	●	●	●	▲

NOTATION: ○ GOOD PREDICTION ▲ ACCEPTABLE (USUSALLY EARLY t_{CHF} PREDICTED) ● UNACCEPTABLE (MANY CASES NO CHF PREDICTION)

magnitude is very difficult to measure accurately in blowdown experiments.

The W-3, Katto and EPRI correlations are not included in Table 9, because they performed very poorly when compared with blowdown data. In many instances, they resulted in a negative CHF. But this poor performance is due to the nature of the correlations, rather than their inaccuracy. All three correlations are written in terms of the inlet quality (or inlet subcooling). In all the cold-leg break experiments, a flow reversal was observed. In this case, the inlet becomes ambiguous. If the inlet is defined at the flow-reversal point, then the quality at this point is much greater than the inlet quality range specified for these correlations. For the single hot-leg break test, although there was not a flow reversal, the correlations still performed poorly due to the high inlet quality. Especially the W-3 correlation has a very narrow quality range, since it is strictly a DNB correlation, whereas, in all of the above experiments, the CHF mechanism was an annular-flow dryout.

None of the correlations were able to predict the CHF after rewet. This is expected, since the prediction of rewet is difficult and it is not simulated in the CODA code.

The salient results of this and the previous studies indicate the following with respect to blowdown transient CHF modeling via steady-state correlations:

(i) The Biasi and CISE correlations, in general, provided the best predictions for most hot-leg and cold-leg LBLOCA conditions where significant coolant flow continued. Both

of these correlations, however, could not model the low flow CHF.

(ii) For conditions of low flow the Griffith-Zuber (1977) correlation predicted best.

It is, therefore, suggested that a simple combination of the Biasi and Griffith-Zuber correlations may be used for a best "first-estimate" of the LBLOCA transient CHF. A more elaborate steady-state correlation package may be possible to enhance the predictive accuracy, but within the uncertainty of the correlations themselves and the uncertainty of the experimental data, such endeavors may be only academic. A detailed discussion of the results is given in the following section.

Discussion of CODA Code Predictions

The results obtained through the CODA code analysis of the blowdown CHF data look promising in terms of the application of the quasi-steady approach to the transient CHF problem. However, there are questions which remain ambiguous. In this section, some of these questions are addressed.

a. In using the CHF correlations, it is the general consensus that a low-quality CHF (DNB) may be predicted by using the local conditions approach, whereas, at high-quality dryout the correlation must take the history effects into account, which is referred to as the boiling length approach. All the CHF data resulting from a blowdown belong to the annular flow dryout type, with non-uniform axial heat flux in many instances. Therefore, the general expectancy, under these conditions, is that a boiling

length correlation must be used in predicting the data. However, the result of the CODA code suggests that the relatively successful correlations are all based on the local conditions approach.

b. The relatively successful correlations, namely BIASI, CISE, Bowring and GE for early CHF, and Griffith-Zuber for delayed CHF, have the same common form. In all these correlations, the CHF may be expressed in the following form:

$$q_{CHF} \sim (B - x) \tag{67}$$

where B is either 1 (Biasi correlation at high quality and Griffith-Zuber correlation) or a number close to 1 (GE, where b = 0.84 or 0.80), or a function of pressure and mass velocity which results in a number close to 1 over the correlation range (CISE, Bowring). In the Griffith-Zuber correlation, the quality, x, in Equation 67 is substituted by void fraction α_v. In all the blowdown experiments, the CHF was experienced at high quality. In fact, in many experiments the x = 1 criterion was as successful as any of the above correlations. This, obviously, suggests that the CHF was reached at very low heat flux level (almost zero). Under these conditions, the above correlations may only be given credit for yielding the right limit at high quality. But a more general statement about the success of these correlations requires more caution.

c. The occurrence of the CHF at such high quality is possibly due to the fact that, in all the experiments, the critical heat flux ratio (CHFR or DNBR) at the onset of the transient was 2 or even

greater. Right after the onset of the transient, the rate of change of the CHF parameters is also relatively fast and it tends to level up with time. In all the experiments, the CHF was reached at relatively slower rates-of-change. The rate of change of the transient parameters, as shown as a function of time for all the blowdown experiments analyzed, is given in Appendix C. It is believed that if the heat flux level was closer to the steady-state CHF at the onset of the transient, the CODA code results would be different. This is schematically illustrated in Figure 61, with reference to the time-constant of the CHF phenomenon (Δt^*) discussed in the previous chapter. If the local heat flux curve followed q_2, instead of q_1 as it did in the experiments analyzed, then the CHF could have been reached at an earlier time. In that case, the quality would have been lower and the merit distribution among the steady-state CHF correlations could have been different. In addition, the quasi-steady approach could completely fail, since the rate-of-change of the transient parameter is relatively high in this time period.

d. In blowdown experiments, there is more than one parameter under transient. For instance, in a blowdown experiment with scram, the pressure (P), the mass velocity (G) and the power generation rate (Q) are all under transients. These parameters may have opposing effects on the transient CHF. For example, a rapid depressurization may result in a lower CHF, whereas, a rapid reduction in mass velocity may tend to increase the CHF. But when applied together, they may compensate each other and result

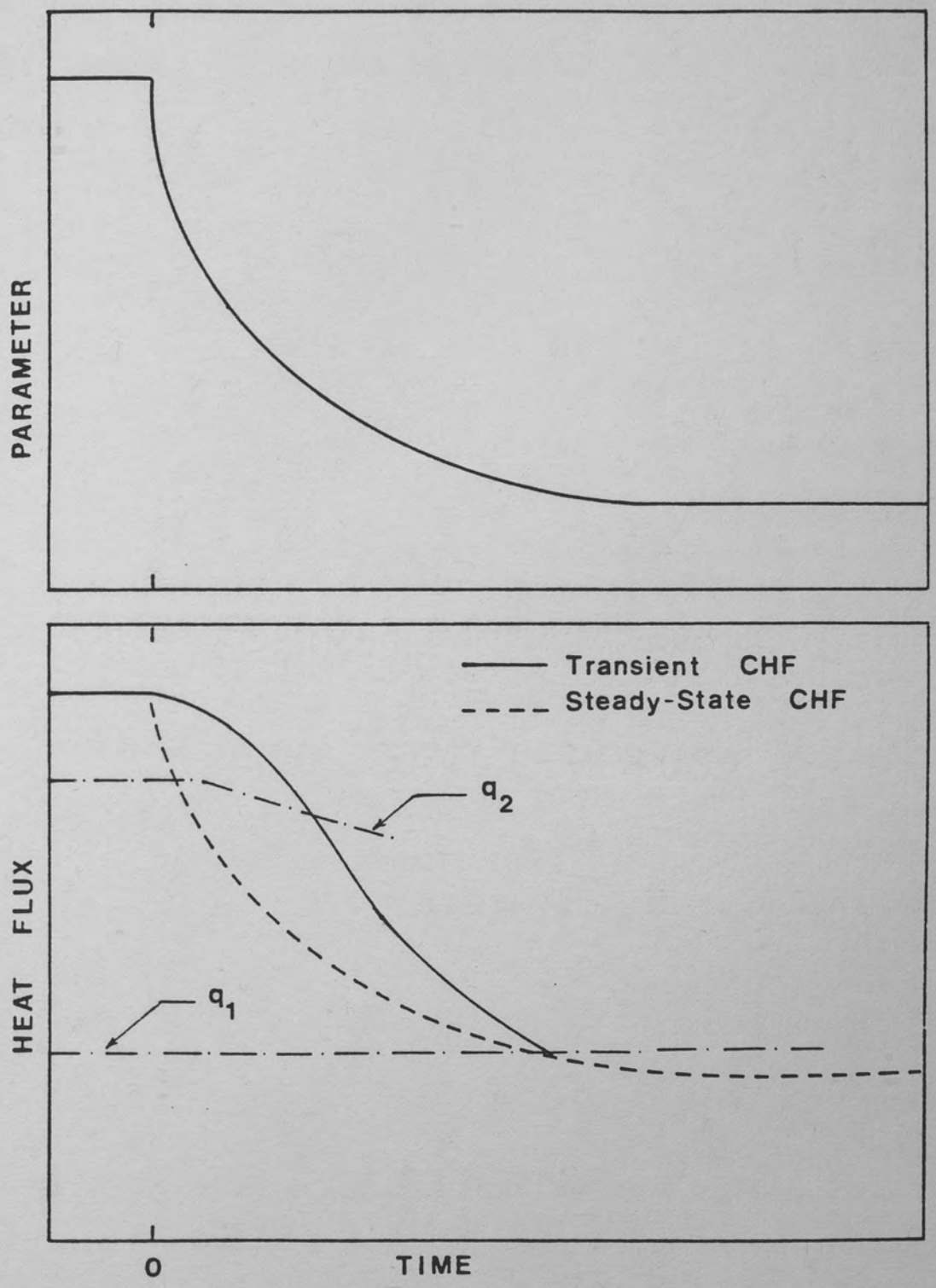

Figure 61. Conceptual Transient CHF Curve

in a transient CHF, which is close to a steady-state CHF. This hypothesis, referred to as the coincidence hypothesis (Gunnerson 1984) will be further discussed in the last chapter. But, in summary, the coincidence hypothesis states that the effect of individual transients must be carefully analyzed before making a statement in terms of a quasi-steady approach in combined effect transients such as the blowdown case.

e. The accuracy of a rather simple computer code as CODA is also questionable in terms of estimating the two-phase flow parameters. The CODA code assumes a homogenous flow with no slip between the phases. In complex situations, such as a blowdown with flow reversal, the drift fluxes may be quite important and these are neglected in the CODA formulation. Also, the CODA code does not differentiate between the CHF in upward and downward flows. This assumption also needs to be justified, especially for low mass flow rates.

f. A CHF surface may be generated using best-estimate correlations as suggested by the results of CODA. Figures 62 and 63 show such CHF surfaces at two different pressures as a function of the mass velocity and quality. The Biasi and Griffith-Zuber correlations are used to generate these surfaces. Using the CISE correlation instead of the Biasi correlation results in a similar surface. As observed in these figures, the two correlations used do not yield to each other at the suggested boundary ($G = 100\ kg/m^2 - s$) Even at high quality, the Biasi correlation results in a CHF value, which is a few times larger than the result of the Griffith-Zuber correlation. For instance, at 1000 psi and at 80

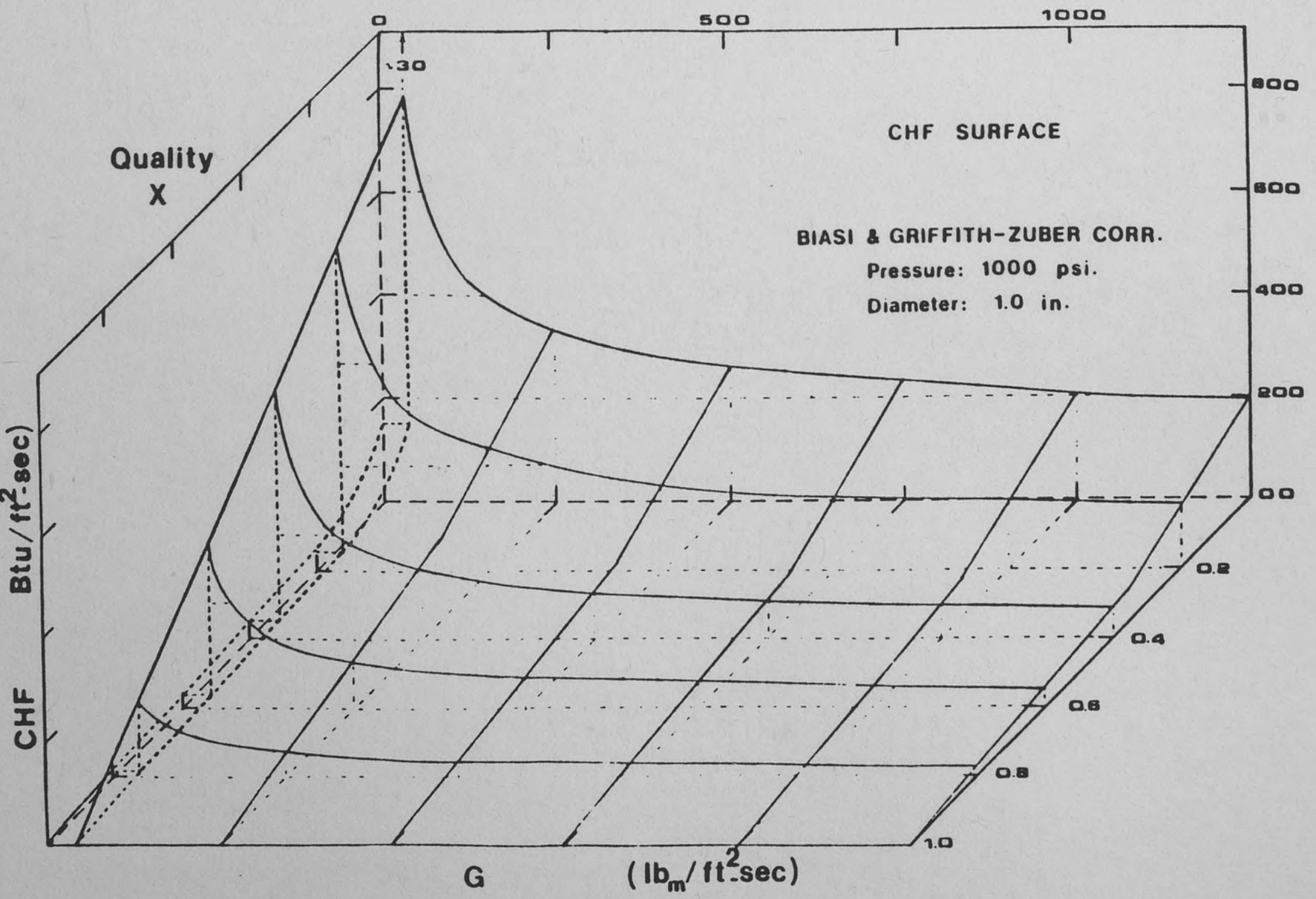

Figure 62. CHF Surface for 1000 psi Pressure Generated from Biasi and Griffith-Zuber Correlations

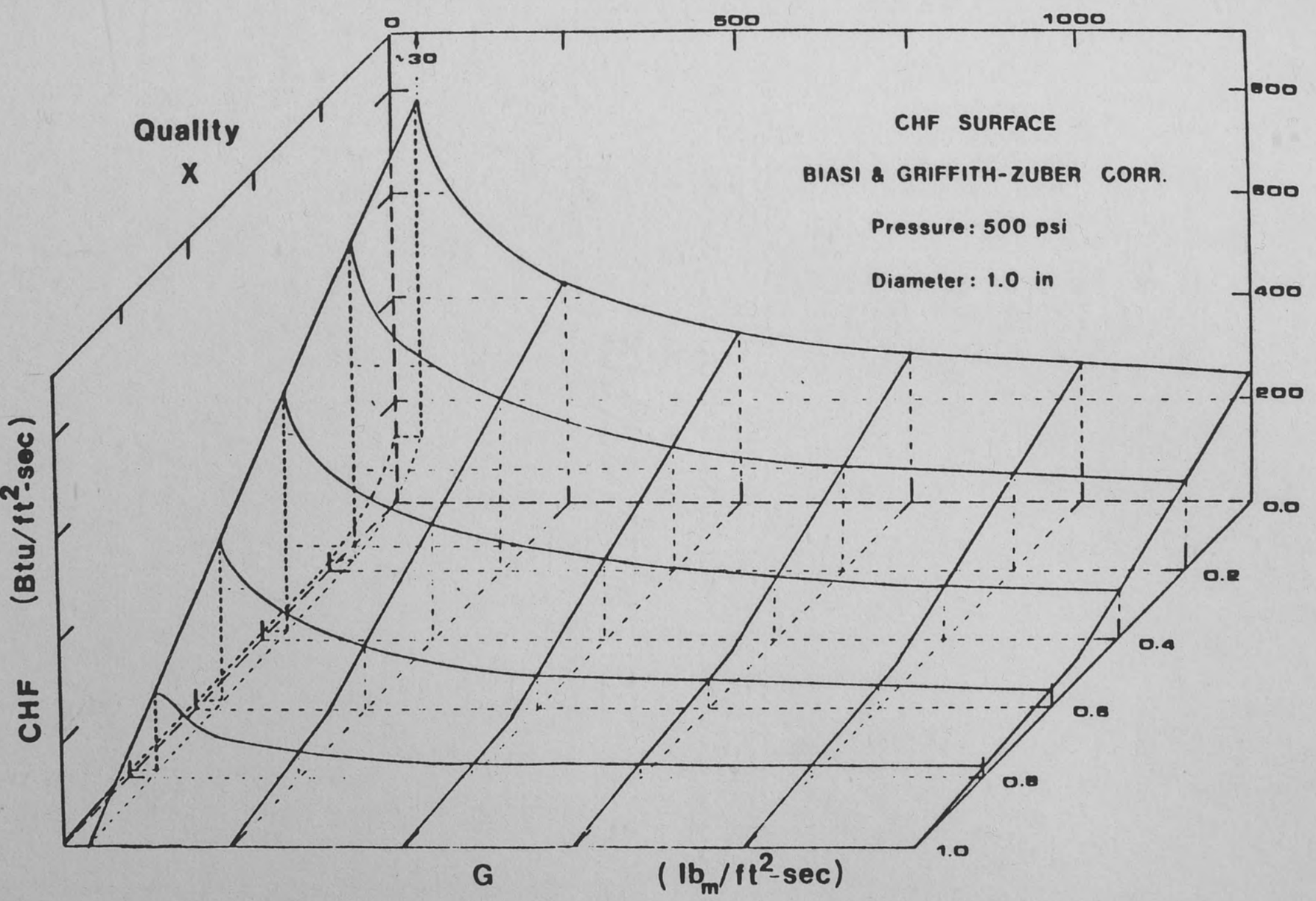

Figure 63. CHF Surface for 500 psi Pressure Generated from Biasi and Griffith-Zuber Correlations

percent quality, the result of Biasi correlation is an order of magnitude greater than the result of Griffith-Zuber correlation at the interface. Therefore, there is a considerable uncertainty in applying the CODA code suggestions in this specific region.

g. Finally, it is known that there is a considerable difference between correlations, even though all the parameters may be within their suggested range. Therefore, the author thinks that applying various correlations to transient CHF data without checking for consistency may be very erroneous. A positive result may be purely coincidental, and an extrapolation of this result to different situations may be completely wrong. The best check for consistency must be the steady-state tests. Only the correlations which can predict the steady-state CHF in a given experimental facility for a given set of conditions should be used in comparison with the transient CHF data for the same facility. This way, a positive statement made in the quasi-steady approach may have some dependability.

The results of this discussion show that the studies of Leung (1980), Lo (1984), and the author (Gunnerson 1984) in applying the steady-state CHF correlations to blowdown CHF through a quasi-steady manner raise more open-ended questions than satisfactory answers. It is the author's strongest belief that the subject must be treated more in detail, with more emphasis on basic physics to obtain any satisfactory answer to the transient CHF. This is done in the upcoming chapters.

Additional Experiments Considered

The results discussed in the previous sections are restricted to flow transient and blowdown data. In order to extend the database for The CODA program used to examine the blowdown data, some additional experiments are addressed by the author. Unfortunately, most of the domestic experiments related to SBLOCA's and RIA's were not specifically conducted to analyze the CHF behavior. Most of these experiments were designed for thermal-hydraulic code development and verification or for assessing fuel-rod behavior. The experiments considered are shown in Table 10.

In these experiments, the CHF behavior was of secondary importance, and neither the experiments nor the reports were instrumented or documented to detail the CHF behavior. The prediction of local instantaneous CHF parameters like pressure, mass flux, and local heat flux becomes a difficult task in many instances. In almost all these experiments, the number of thermocouples per channel was only one or two (there were no thermocouples in many subchannels).

The thermal-hydraulic response in SBLOCAs and IBLOCAs is quite different from the thermal-hydraulic response in LBLOCAs (blowdown), as reported by Boucher and Dimenna (1983). Since the thermal-hydraulic response of the system, i.e., the determination of two-phase flow parameters under transient conditions prior to CHF, is not the scope of the present study, the data analysis of these experiments is omitted. A simple code CODA may not be capable of handling this problem, considering the difficulties encountered by Leung (1980) in the analysis of the THTF-181 Test, which was a SBLOCA. The author thinks that a CODA code analysis of these experiments would not bring

TABLE 10

ADDITIONAL LWR TRANSIENTS ADDRESSED

Test	Reference
SBLOCA	
INEL: Semiscale Mod-2A	
UHI/SBLOCA	Shimeck (1983)
INEL: Semiscale Mod-3	
S-SB-2A	Fauble (1980)
S-SB-P1	Dingman (1980)
S-SB-P2	Dingman (1980)
S-SB-P3	Cozzual (1980)
S-SB-P4	Cozzual (1980)
S-SB-P7	Dingman (1980)
IBLOCA	
INEL: Semiscale Mod-2A	
IBTS	Boucher (1983)
RIA	
INEL: PBF	
RIA 1-1	Inabe (1978) Martinson (1978 a) Buckland (1979) Seiffert (1980)
RIA 1-2	Inabe (1978) Martinson (1978 b) Zimmermann (1979) Cook (1981)

any noticeable insight into the transient CHF problem. Theoretically and experimentally, it has been observed that the validity of the quasi-steady approach in determining the transient CHF depends upon the magnitude of the rates-of-change of CHF parameters. For a higher rate of change, the quasi-steady approach is more questionable. Since for SBLOCAs and IBLOCAs, the magnitude of the rates-of-change of the major CHF parameters like pressure (P) and mass velocity (G) are smaller than the magnitude of the rates-of-change of the same parameters for LBLOCAs, this leads to the logical conclusion that, if the quasi-steady approach is valid for LBLOCAs, it must be valid for IBLOCAs and SBLOCAs. Another commonly discussed hypothetical accident, the RIA, is theoretically analyzed in Chapter VIII.

CHAPTER VII

NON QUASI-STEADY EXPERIMENTS

A wide literature search of transient CHF studies prior to 1980 is provided by Leung (1978; 1980). Since 1980, there have been some additional CHF studies. The most comprehensive experimental study in terms of direct reactor application is probably the one by Westinghouse Electric Corporation (Westinghouse 1981; 1982). But a detailed literature search is not presented in this chapter. Since the present study is mostly concerned with fast transients where the quasi-steady approach is unable to predict the CHF, a brief overview of such experiments is presented.

Power Transients

The CHF during power transients is important in the nuclear industry, since they are typical of reactivity initiated accidents (RIA). Other than full-scale RIA experiments referred to in the previous chapter, there are simpler power-transient studies aimed towards the fundamental understanding of boiling heat transfer during power transients. The studies of Schrock (1966), Johnson (1971), Aoki et al. (1973; 1974), Tachibana et al. (1968), Sakurai et al. (1970), Kawamura et al. (1970), Sakurai and Shiotsu (1977a;b), Kataoka et al.

(1983) and Serizawa (1983) are examples of such studies. In this section, a few of these studies are summarized.

Tachibana et al. (1968) experimentally studied the CHF in saturated pool boiling at atmospheric pressure under transient power conditions. The heating elements were flat strips of nickel submerged vertically in water. The strips were 50 mm long, 6 mm wide and of variable thickness (0.01, 0.05, 0.1 mm). The heat generation rate per unit surface area was linearly increased as follows:

$$Q_s(t) = Q_{s,o}(t/\tau) \tag{68}$$

where $Q_{s,o} = 10^6$ kcal/m^2-hr (1.16 MW/m^2)

This experiment showed that, for values of τ smaller than 100 msec, the transient CHF was considerably greater than the steady-state CHF, and the difference increased with decreasing ramp period τ. As τ increases, the transient CHF asymptotically approaches the steady-state CHF. The reason for the increase of the CHF with shortening ramp period is explained by Tacibana et al. (1968) as follows:

> "The first bubble appears as the surface temperature reaches a certain level. Since the surface temperature rises at a higher rate in the shorter period transient, more bubbling sites can be expected to come into being before one bubble grows and extends over the surrounding nucleation sites. In this manner, the short period transients allow more bubbles to exist on the heating surface at higher superheat. This is what provides for a higher

heat flux in the nucleate boiling region, including the case of the critical heat flux condition."

Another interesting result of the experiment (Tachibana 1968) is the response of the surface heat flux to the change in power generation during the nucleate boiling regime. During steady-state conditions, the heat flux is equal to the heat generation rate. But, during power transients, this quasi-steady relation does not hold. Until the initiation of boiling, the surface heat flux lags the power generation rate and after the initiation of boiling it increases at a higher rate up to the CHF. Therefore, for small values of ramp period, a linear increase in the power generation rate does not imply a linear increase in the surface heat flux. The increase of the surface heat flux becomes more linear with increasing value of the ramp period. Figure 64 illustrates this concept. This figure is not quantified, but drawn according to the observations of Tachibana et al. (Tachibana 1968). In both figures, the ribbon thickness is assumed the same. In Figure 64a, τ is in the order of 100 msec, and in Figure 64b, τ is in the order of 10 msec. Obviously, this relation between the surface heat flux and the heat generation rate is also affected by the ribbon thickness H, but this effect is not shown in Figure 64.

Sakurai et al. (1970) made a similar experiment for pool boiling under atmospheric pressure. As a heater they used a vertical platinum ribbon of 0.1 mm in thickness, 2.5 mm in width and 15 mm in length. The heat generation rate was represented by

$$Q(t) = Q_0 \exp (t/\tau) \qquad (69)$$

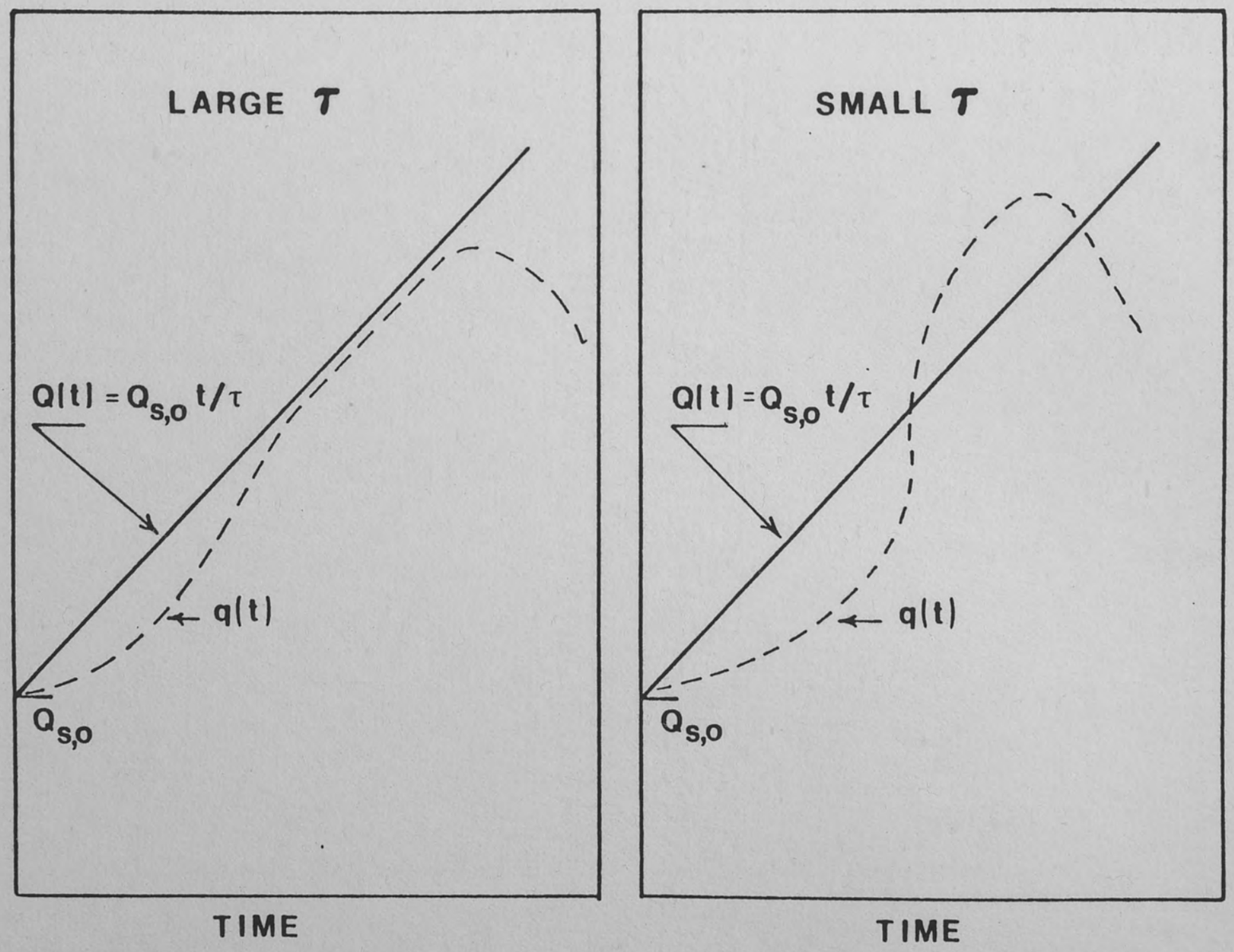

Figure 64. The Relation Between the Heat Generation Rate and the Surface Heat Flux.

They obtained transient CHF data for 75, 50, 25° subcooled and saturated water conditions. They correlated their data in the following empirical form:

$$q_{CHF,TR} - q_{CHF,SS} = K \tau^{-b} \qquad (70)$$

where the values of K and b are given in Table 11.

TABLE 11

THE CONSTANTS AND $q_{CHF,SS}$ VALUES IN EQUATION 70

Water Temperature	$q_{CHF,SS}$ (MW/m^2)	K x 10^{-4}	b
298 °K	7.36 ± 0.28	45.0 ± 2.8	0.52 ± 0.05
323 °K	3.71 ± 0.12	40.5 ± 1.3	0.55 ± 0.02
348 °K	2.84 ± 0.06	1.05 ± 0.08	1.15 ± 0.05
373 °K	0.67 ± 0.05	0.66 ± 0.10	1.11 ± 0.09

Sakurai et al. (1970) reported that the heat flux increased along the steady nucleate boiling curve and its linear extension up to the transient critical heat flux. They pointed out that the quasi-steady nucleate boiling existed with a certain lifetime on the linear extension of the steady nucleate boiling curve, and they also measured the lifetime. However, this experiment was not adequate in explicitly exploring the effects of power transients on the CHF, because of the geometry effects present. The length of the ribbon heater used was 15

mm. For water at atmospheric pressure, the Taylor instability wavelength is in the order of 20 mm. Therefore, CHF measurements for such geometries is very much geometry dependent, and the known CHF correlations fail to predict such CHF (Leinhard 1981).

Kawamura et al. (Kawamura 1970) obtained transient CHF data for pool boiling of water at atmospheric pressure. They also used stainless steel and nickel flat-ribbon heaters of 60 mm in length, 6.8 mm in width, and 0.01 to 0.8 mm in thickness. The heater was placed with the heat transfer surface being vertical to the water. In their experiments, Kawamura et al. (1970) tested different power functions which were linear, exponential, and squared hyperbolic secant. They also measured the transient CHF with 70, 40, and 20°C subcooling. Some of their results may be summarized as follows:

a. In a short-period transient, many small bubbles cover the surface; in a long-period transient, a few large bubbles cover it.

b. In subcooled pool boiling, a great number of small bubbles grow and collapse repeatedly on the heating surface.

c. When power maintains a non-zero level before the transient starts, the transient CHF in subcooled boiling is reduced considerably.

Sakurai and Shiotsu made a more detailed investigation of the transient pool boiling heat transfer (Sakurai 1977a;b). They experimentally investigated the transient pool boiling under saturated conditions. The heat generation rate was increased exponentially according to Equation 69. They obtained transient CHF data for periods ranging from 5 msec to 10 sec and for pressures ranging from

0.1 to 2.1 MPa. The heater was a horizontally supported thin platinum wire with effective length of 32.2 mm and with diameter of 1.2 mm. For periods less than 100 msec., they correlated their experimental data as follows:

$$(q_{CHF,TR} - q_{CHF,SS})/q_{CHF,SS} = 0.079\ \tau^{-0.6} \qquad (71)$$

Sakurai and Shiotsu (1977a) observed that there are two boiling patterns that can exist in transient boiling. The one they called the regular process has a maximum heat flux after reaching and following the steady boiling curve and its linear extension. The irregular process, on the contrary, has its maximum heat flux without ever reaching and following the steady boiling curve and its linear extension. The regular boiling is the most important one to the nuclear industry, since the regular process changes to an irregular process with decreasing period, and as the pressure increases, this change occurs at shorter exponential periods. This limiting period is very short ($\tau << 5$ msec) for the pressure range which is of interest to the nuclear industry, as reported by Sakurai and Shiotsu (1977b). In this regular boiling, the heat transfer coefficient after the initiation of boiling becomes lower than the steady one at the same heat flux level. This may be explained by the time lag of a slow activation process of originally flooded cavities in the low heat flux region. Then it recovers before the maximum heat flux is reached. The maximum heat flux is higher for a shorter period and for a higher system pressure. However, for irregular processes, the heat transfer coefficient never recovers to the steady boiling curve, and the maximum heat flux first

decreases to a minimum value (as low as the steady maximum heat flux) with the decrease in the period and then it increases. The reason why the heat flux increases along the extension curve up to the maximum heat flux in the regular process, is due to the fact that the vapor patch does not form immediately after the steady CHF, until a certain amount of thermal energy is stored in the vicinity of the heater surface. Thermal energy, transferred to the water during the time between steady-state CHF and transient CHF, is the threshold value for the vapor patch formation.

The transient boiling heat transfer under forced convection is experimentally investigated by Kataoka et al. (1983). They obtained the data by exponentially increasing the heat input which was supplied to a platinum wire in water flowing upward in a round tube at pressures from 0.143 to 1.503 MPa, and at various subcoolings. They correlated this data in a non-dimensional form similar to Katto's approach (1978) as follows:

$$(q_{CHF,TR} - q_{CHF,SS})/q_{CHF,SS,OO} = 0.083\tau^{-0.63} \qquad (72)$$

where $q_{CHF,SS}$ is the steady-state CHF and is given by:

$$\frac{q_{CHF,SS}}{G\,h_{fg}} = 0.03740\,(\rho_v/\rho_l)^{0.66}\left(\frac{\sigma\rho_l}{G^2 L_o}\right)^{0.40}$$

$$\times\left\{1 + \left[0.0368\,(L_o/d_{HE})^{-0.20}\,(\rho_v/\rho_l)^{-0.79} + \varepsilon\right]\frac{(\Delta h_{SUB})_i}{h_{fg}}\right\} \qquad (73)$$

where L_o is the Laplace coefficient and is given by

$$L_o = \{\sigma/[g(\rho_1 - \rho_v)]\}^{\frac{1}{2}} \tag{74}$$

and $\varepsilon = 0$ for $(\Delta T_{SUB})_i = 0 - 40°K$

$$\varepsilon = 0.00808\ (\rho_v/\rho_1)^{-1.09}\left[\frac{(\Delta h_{SUB})_i - (\Delta h_{SUB})_{i,\ at\ 40°K}}{(\Delta h_{SUB})_i}\right] \tag{75}$$

for $(\Delta T_{SUB})_i = 40 - 70°K$

$q_{CHF,SS,OO}$ is the steady-state CHF with zero subcooling and zero flow. It is given by:

$$\frac{q_{CHF,SS,OO}}{h_{fg}\ \rho_v} = 0.16\ [\sigma g(\rho_1 - \rho_v)\ /\rho_v{}^2]^{0.25} \tag{76}$$

Note that Equation 76 is similar to Zuber's (1958) equation with a coefficient of 0.16 as suggested by Kutatelatze (1963).

Equation 72 is a simplified version of a more accurate equation, where the constant 0.083 is replaced by a pressure dependent term. The accurate form of this equation is as follows:

$$(q_{CHF,TR} - q_{CHF,SS})q_{CHF,SS,OO} = 1.274\ (\rho_v/\rho_1)^{-0.30}$$
$$\times\ \{\tau[\sigma g(\rho_1-\rho_v)/\rho_v^2]^{0.25}/L_o\}^{-0.63} \tag{77}$$

But within the pressure range studied, Kataoka et al. (1983) observed that the pressure dependence can be neglected, which yielded Equation 72.

Serizawa (1983) proposed a correlation to theoretically predict the maximum heat flux in power transients. In his study, Serizawa mentioned four different boiling patterns. These patterns are shown in Figure 65. The A-type boiling in this figure corresponds to the regular process of Sakurai and Shiotsu (1977). The B-type boiling curve may be looked on as an intermediate process between the regular and irregular processes. Serizawa (1983) started from the postulate that the DNB heat flux in the power transients is specified by closely-packed vapor bubbles covering the whole area of the heated surface. The analysis is applicable to A-type (regular) boiling, shown in Figure 65, which is of interest to the nuclear industry. The model is based on the formation and consumption of a thin liquid layer between the vapor blanket and the heated surface. Figure 66 shows the proposed simple physical model of the transient burnout.

At time A, a stable vapor blanket covers a considerable portion of the heated surface. Underneath the vapor blanket, there exists a liquid micro-layer. The thickness of the liquid layer is considered to decrease with an increase of the heat flux. As the liquid layer evaporates, the consumption of the liquid is compensated by the continuous supply of liquid from the surrounding medium, as expressed by the following equation:

$$\Delta E_v = E_v - W_f = 0 \qquad (78)$$

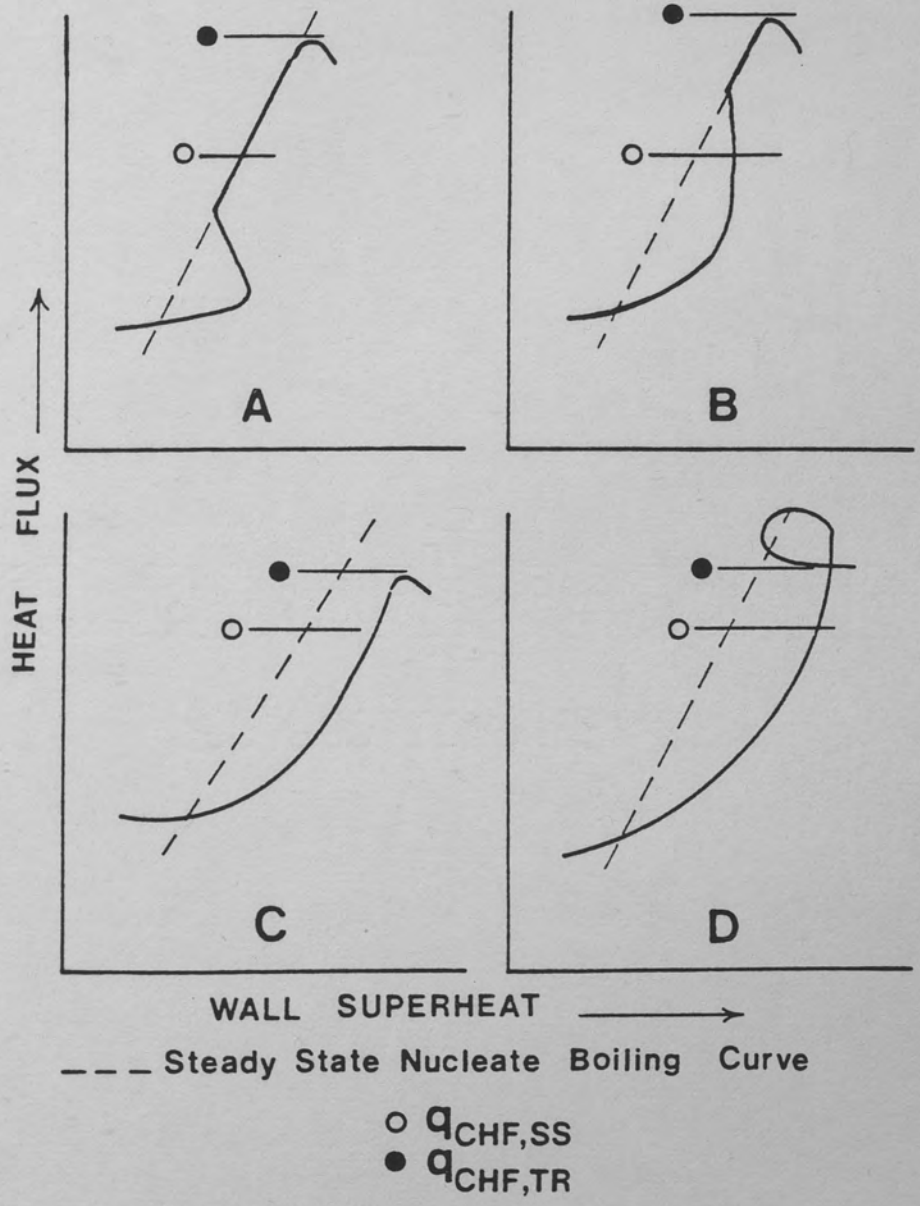

Figure 65. Boiling Patterns in Power Transients (Serizawa 1983)

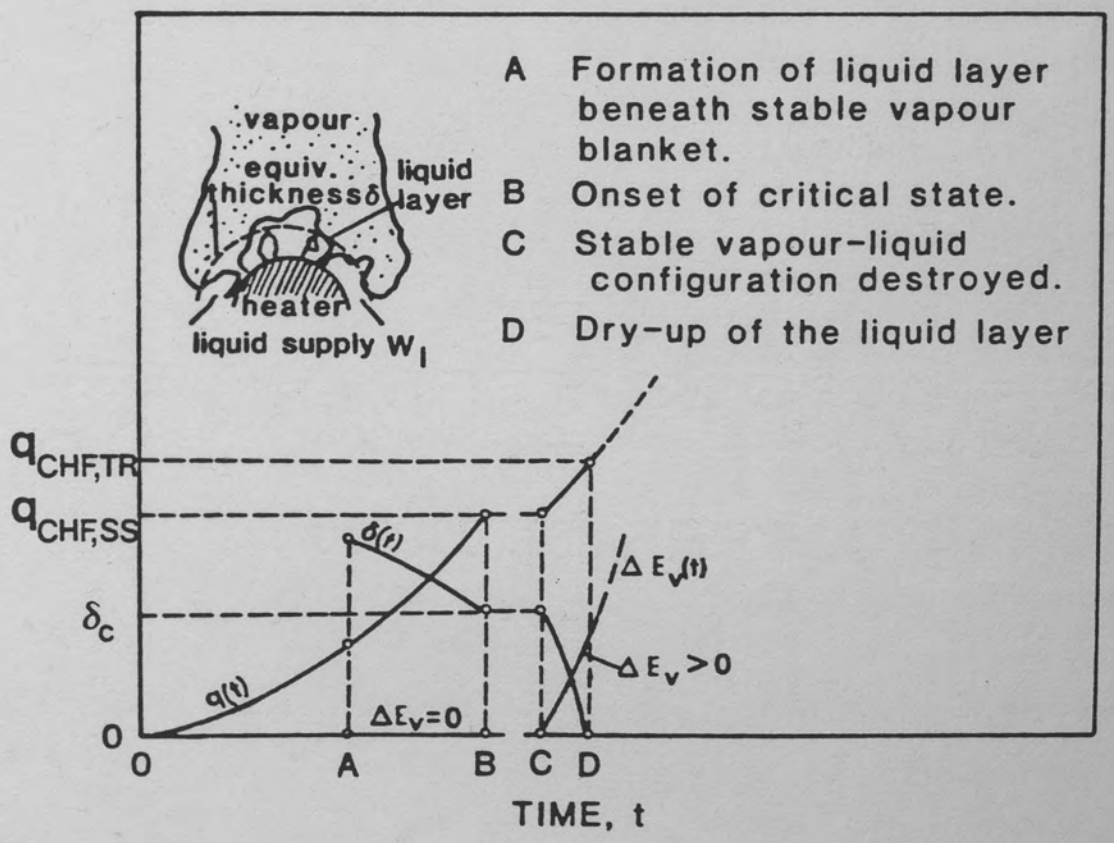

Figure 66. Physical Model of CHF (Serizawa 1983)

Where $E_v = A_f\, q/\, h_{fg}(1 + C_p\, \Delta T_{SUB}/h_{fg})$, is the rate of evaporation and W_f is the rate of liquid supply. The value of W_f is assumed not to exceed a critical value determined by the thermal-hydraulic conditions around the heater.

At time B, when the heat flux reaches a value q_{CHF}, which is the steady-state critical heat flux, ΔE_v is still equal to zero, but W_f reaches its critical value. At this point, the micro-layer thickness remains constant at q_{CHF} and the boiling is stable.

If $\Delta E_v > 0$, the boiling is no longer stable and the liquid layer will be consumed. Therefore, the surface will eventually be dried out at time D. The corresponding heat flux is the transient critical heat flux.

Based on this simple model, through the mathematics it is concluded that the liquid layer thickness is a primary influence on the transient CHF behavior, together with the liquid supply to the layer. According to Serizawa's (1983) model, the steady-state CHF is formulated as

$$A_f\, q_{CHF,SS} = (h_{fg} + C_p\, \Delta T_{SUB})\, W_{fs} \tag{79}$$

Whereas, the transient CHF is formulated as

$$A_f \int_{t_{CHF,SS}}^{t_{CHF,TR}} q(t)\, dt = A_f \rho_l h_{fg} \delta_c + (h_{fg} + C_p \Delta T_{SUB}) \int_{t_{CHF,SS}}^{t_{CHF,TR}} W_f(t) dt \tag{80}$$

Serizawa (1983) assumed that W_f (t) is constant within the time period from $t_{CHF,SS}$ to $t_{CHF,TR}$. Thus, W_{fs} may be obtained from Equation 79.

Substituting this value of W_{fg} into Equation 80, the governing equation becomes

$$\int_{t_{CHF,SS}}^{t_{CHF,TR}} q(t)dt = \rho_l h_{fg} \delta_c + q_{CHF,SS}(t_{CHF,TR} - t_{CHF,SS}) \quad (81)$$

The burnout behavior during a given transient may be determined from Equation 81, once q(t) and δ_c are known. Serizawa (1983) states that a quasi-steady conduction model may be assumed as long as A-type boiling occurs. The quasi-steady conduction model consists of relating the surface heat flux to the heat generation rate through a simple volume to surface-area ratio as follows:

$$q(t) = V/S \; Q(t) \quad (82)$$

Serizawa took an empirical approach in determining the liquid layer thickness δ_c. In the process, transient CHF data from power transient experiments with horizontal wire and flat ribbon heaters in pool boiling, and also with vertical cylindrical heaters in forced convective boiling, are used. Therefore, the good prediction obtained in correlating the various data is not surprising, and the validity of the assumptions used in the derivation is not very clear. For example, although the experiment of Tachibana et al. (1968) does not result in a quasi-steady conduction relation, by using this approximation Serizawa's (1983) model predicts Tachibana's (1968) data perfectly. The assumption of W_f being independent of time is also questionable. But, further discussion of Serizawa's correlation is

presented in Chapter VIII, where power transients are further analyzed.

Pressure Transients

Rapid depressurization is a phenomenon that occurs during loss-of-coolant accidents (LOCA). In a LOCA the rapid depressurization is accompanied by a rapid flow reduction and, with a scram, the power is also transient. All the blowdown experiments considered in the previous chapter belong to this category of combined transients. There are also studies dealing with rapid depressurization alone, to investigate the physical foundations of such transients. The studies of Westinghouse Electric Corporation (Westinghouse 1981; 1982), Aoki et al. (1974) and Sakurai et al. (1980) are examples of such studies.

In the J-Loop test facility, Westinghouse Electric Corporation (1981; 1982) performed rapid depressurization experiments where mass velocity was kept constant. Tests 301, 302, 303, 313 and 314 are the rapid depressurization tests. The initial pressures of 12.1 MPa (Test 301 and 302), 15.5 MPa (Test 303) and 13.8 MPa (Test 313 and 314) are used. The depressurization rate was kept constant at 2.41 MPa/sec during the tests, except in Test 302, where the depressurization rate was 0.689 MPa/s. The mass velocity in all those tests were kept constant at 3424 kg/m^2-s).

The experimental CHF values obtained in these tests were compared to the prediction of various correlations. Two different codes were used for this purpose. The MAYU 04 code was used for a bundle-averaged fluid conditions type of analysis and the COBRA-IV code was used for a subchannel analysis. Although the subchannel analysis gave

better results in terms of thermal-hydraulic parameters, the extent of the CHF was not predicted by any of the correlations during these depressurization tests. The Biasi correlation did not predict any CHF (except for Test 313, where it predicted the CHF too late) for these tests, although the CHF occurs within the first few seconds into the transient. The reason the Biasi Correlation is specifically mentioned, is due to the fact that it is one of the correlations recommended in predicting the blowdown CHF data, as discussed in the previous chapter.

Aoki et al (1974). experimentally studied the problem of CHF during rapid depressurization in forced convective boiling. The test section was an annular vertical upward flow channel, consisting of a pyrex tube of 8 mm inside diameter and a heater made of a stainless tube of 4.6 mm outside diameter and of 0.2 mm thickness. The effective heating length was 92 mm. The power was kept constant through each experiment. There was no coolant loss associated with rapid depressurization. The depressurization was from 0.3 MPa to atmospheric pressure. The rate of depressurization was dependent on the subcooling. At higher subcooling, the pressure reached the atmospheric pressure faster. This is shown in Figure 67. For smaller initial subcoolings, the drop of wall temperature after depressurization became slower. In this case, a shorter time-to-CHF was observed. The experiments were conducted at different flow velocities. It was observed that t_{CHF} decreased as the flow velocity increased. Under the complex interaction of the above parameters, the following general trends were observed:

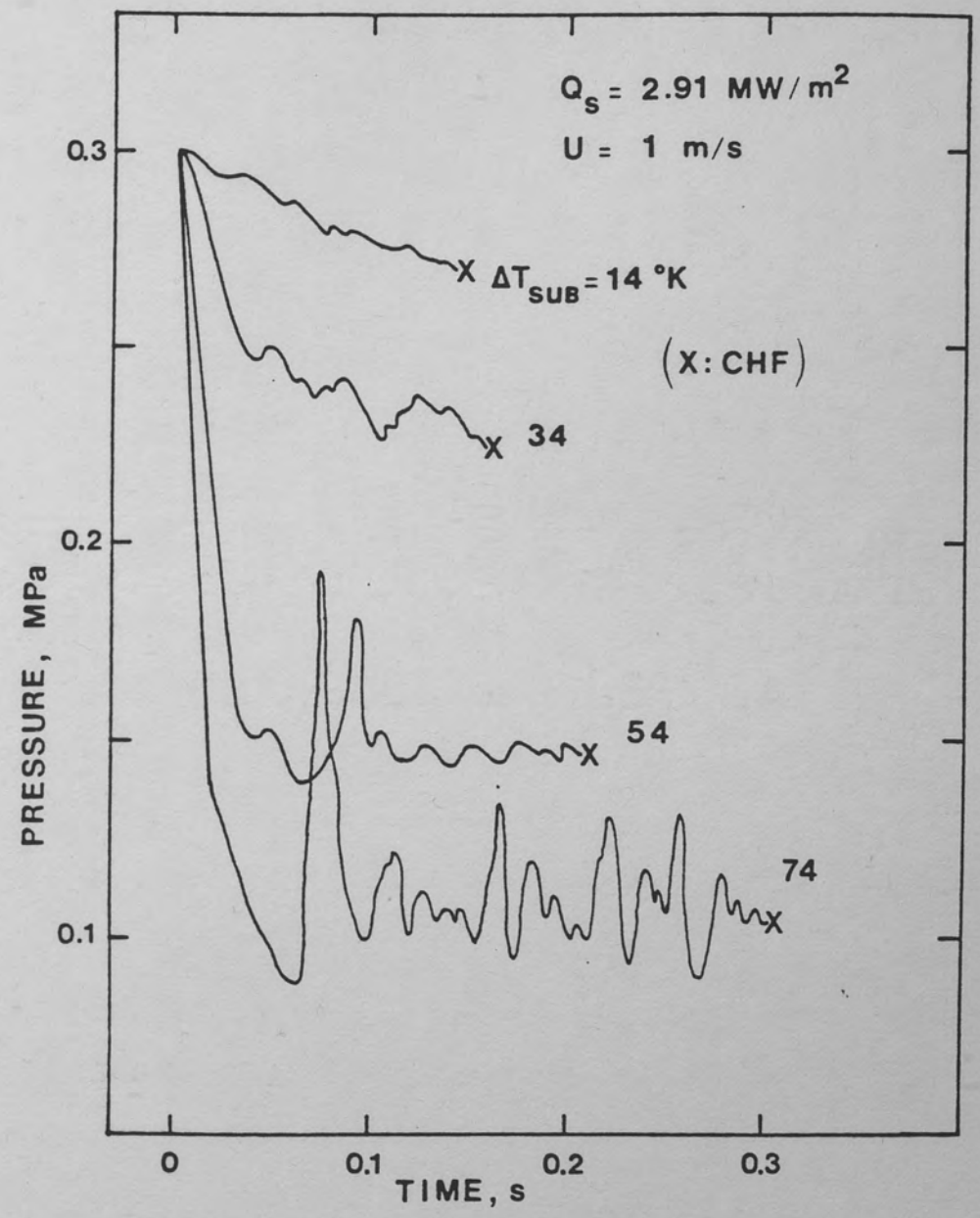

Figure 67. The Rate of Depressurization as a Function of Subcooling for the Depressurization Experiment of Aoki et al. (1974)

a. The boiling heat transfer was very well established during the depressurization process.

b. The CHF was reached during the period that the second generation bubbles appeared on the surface. No CHF was observed right after the blowdown during the existence of first-generation bubbles.

c. The transient CHF was larger than the steady-state CHF at the released pressure. The difference between $q_{CHF,TR}$ and $q_{CHF,SS}$ was a function of the initial subcooling and the flow velocity.

At this point, the hypothetical experiment of Lahey and Moody (1979) may be introduced. The hypothetical experiment simulates a one-second depressurization test at 200 psi/sec depressurization rate. This simple pressure decay and the results of a transient computer code are shown in Figure 68. In this figure, the exit quality versus time is plotted. During the time it takes the control volume that initially was at the boiling boundary to exit the test section, the exit quality decreases. This is due to the rapid expulsion of the two-phase fluid as a result of the flashing process. After that, the quasi-equilibrium state is reached and the exit quality monotonically increases. When the blowdown is terminated, the transient quality rises to the new equilibrium value at 800 psi. This simplified analysis of Lahey and Moody (1979) may help explain why there normally is no premature CHF during depressurization and why the CHF frequently occurs just after blowdown ceases.

To gain further understanding of rapid depressurization on the CHF, the pool boiling experiment of Sakurai et al. (1980) may be

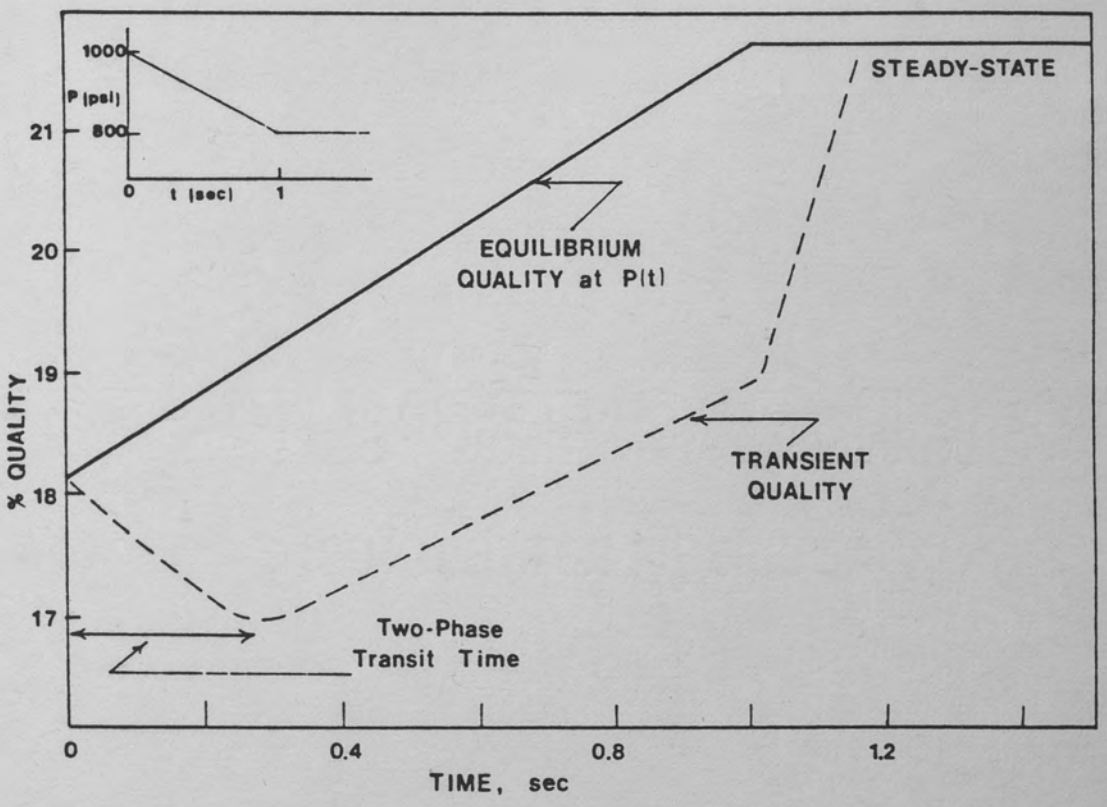

Figure 68. Hypothetical Depressurization Experiment of Lahey and Moody (1979)

examined. Sakurai et al. (1980) studied the transient boiling phenomena caused by rapid depressurization on a test heater which was initially in a non-boiling state in a pool of water. The test heater, which was a platinum wire of 1.2 mm in diameter and 71.6 mm in length, was placed in a pool of subcooled water, and the heat generation rate was held constant throughout each experiment. The change in system pressure was adjusted such that it followed an exponential decay given by

$$P = P_o \exp(-t/\tau) \tag{83}$$

The pressure transients were performed for the initial pressures 0.59, 1.08, and 1.90 MPa and for the water temperatures of 353 and 373°K. The pressure reduction period, τ, was varied from 3 msec to 60 msec. For τ = 3.5 msec, the pressure and surface temperature histories are shown in Figure 69. After the onset of nucleate boiling, the heat flux was observed to follow an almost linear increase until it reached the transient CHF value. The results of these experiments showed that the CHF was strongly dependent on the initial heat flux and the rate of depressurization, and it was always lower than the corresponding steady-state CHF. As shown in figures 70, 71, and 72, the ratio of transient CHF to steady-state CHF decreases as the initial heat flux decreases and as the exponential period τ decreases. For initial heat fluxes lower than the initial heat flux shown in figures 70 and 71, and for τ greater than 10 msec as shown in Figure 72, no CHF was observed.

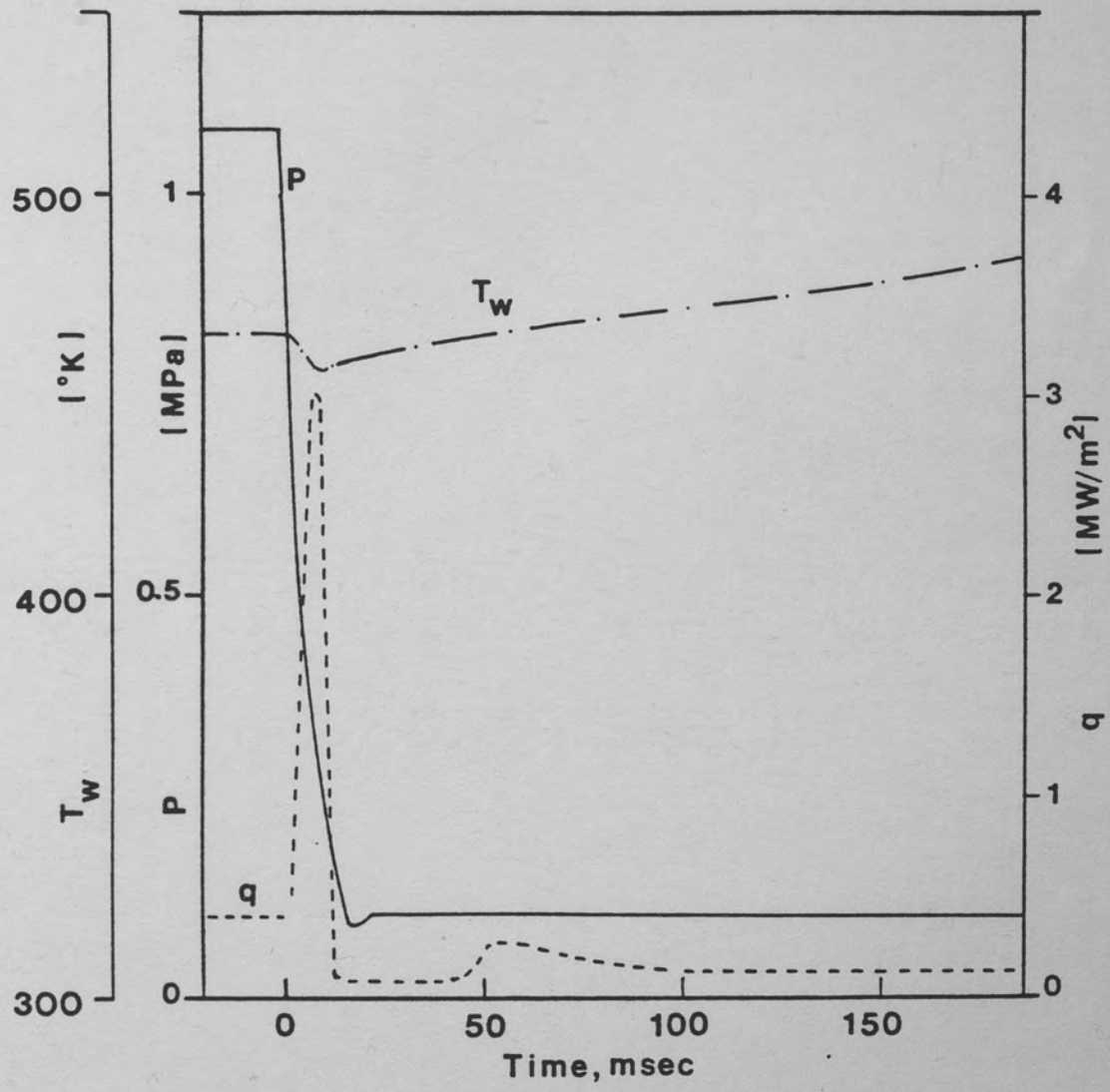

Figure 69. Pressure, Surface Temperature and Surface Heat Flux Histories During Rapid Depressurization (Sakurai 1980)

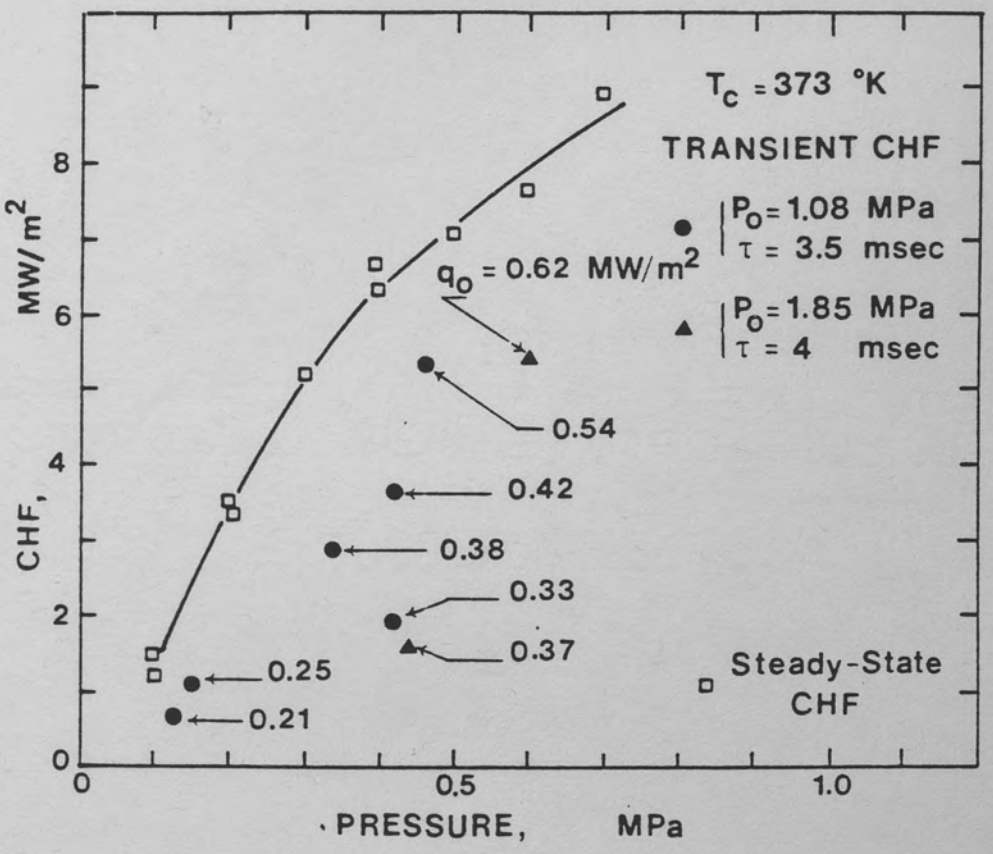

Figure 70. The Results of Depressurization Experiments (Sakurai 1980)

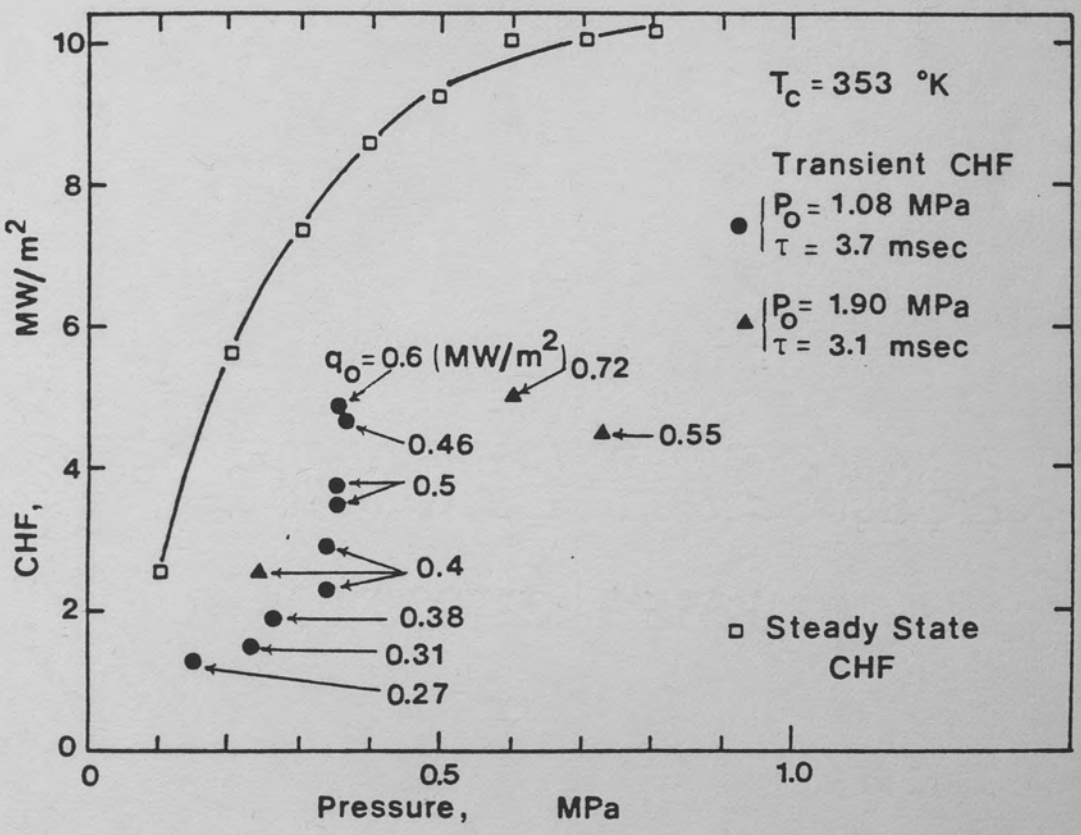

Figure 71. The Results of Depressurization Experiments (Sakurai 1980)

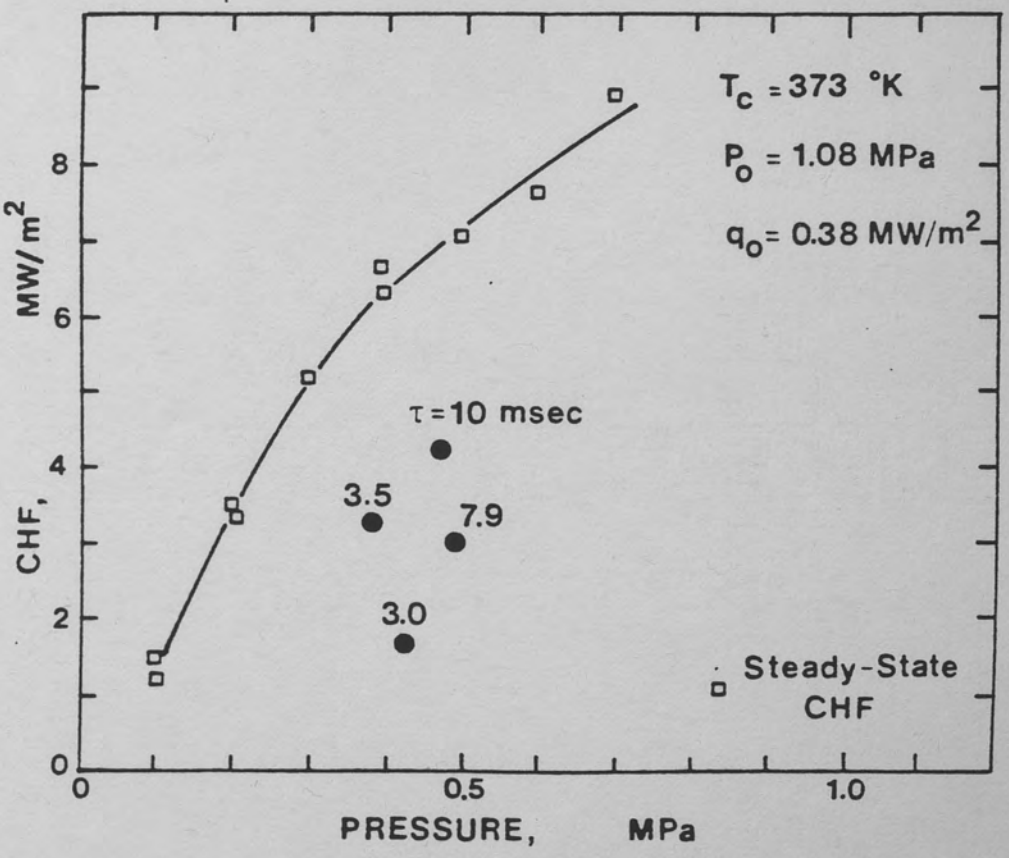

Figure 72. The Results of Depressurization Experiments (Sakurai 1980)

For short reduction periods, the heater surface temperature drops rapidly as the boiling initiates. The thermal boundary layer of the initial steady state may not vary as rapidly as the reduction of the surface temperature; therefore, the change in the temperature at some position away from the heater surface may be delayed. And, as the saturation temperature decreases due to pressure reduction, this will result in a thicker layer of superheated liquid than that in steady nucleate boiling. According to Sakurai et al. (1980), these factors as well as the reduction in subcooling, which is more effective for shorter periods and lower heat fluxes, lower the value of the CHF.

Flow Transients

Some of the flow transient experiments have been analyzed by Leung (1980), and the results were summarized in Chapter VI. In those experiments, as well as in the flow reduction tests conducted by Westinghouse Electric Corporation (Westinghouse 1981 ; 1982), it was observed that the quasi-steady approach was fairly successful in predicting the transient CHF. But there are also examples in the literature where the transient CHF is considerably different from the CHF predicted by the quasi-steady approach. The studies of Cumo and his co-workers (Cumo 1978 ; Celata 1986) and Ishigai et al. (1974) are such examples.

The influence of abrupt flow change on the CHF in the high-quality steam water flow is experimentally studied by Ishigai et al. (1974). The test section was a stainless steel tube of 8 mm I.D. and 1 mm thickness. The test section consisted of a 1135 mm adiabatic section, followed by a 750 mm heated section. A two-phase mixture was

fed into the test tube; the inlet steam quality ranged from 0.5 to 0.8 in various tests. The exit pressure was kept at 5 atmospheres during the tests.

In these experiments, the dryout occurred at heat fluxes lower than the corresponding steady-state CHF for sudden flow deceleration. The difference between the transient CHF and the steady-state CHF increased as the deceleration increased. The abrupt change was applied on the mass-flow rate of vapor phase. Therefore, the flow transient was characterized by the shear stress change in time. Ishigai et al. (1974) referred to this type of transient CHF as the premature dryout, and they theoretically analyzed the premature dryout by applying the modified kinematic wave theory on the liquid film-vanishing hypothesis. Ishigai et al. (1974) related the ratio η of transient CHF to steady-state CHF to the ratio of the shear-stress before and after the transient. After certain simplifying assumptions, the ratio η was formulated through the simple rotation:

$$\eta = (q_{CHF,TR}/q_{CHF,SS}) = (\tau_{s,1}/\tau_{s,o}) \tag{84}$$

The experimental results and the predictions of Equation 84 are shown in Figure 73. In their analysis, Ishigai et al.(1974) accounted for the effect of the inlet quality by using the ratio η and the shear stress ratio. At low-mass flow rate the decrease in the critical heat flux was considerable, where at high-mass flow rate the decrease was little.

The effect of mass-flow rate transients on CHF is also experimentally investigated by Cumo et al. (1978). They obtained experimental

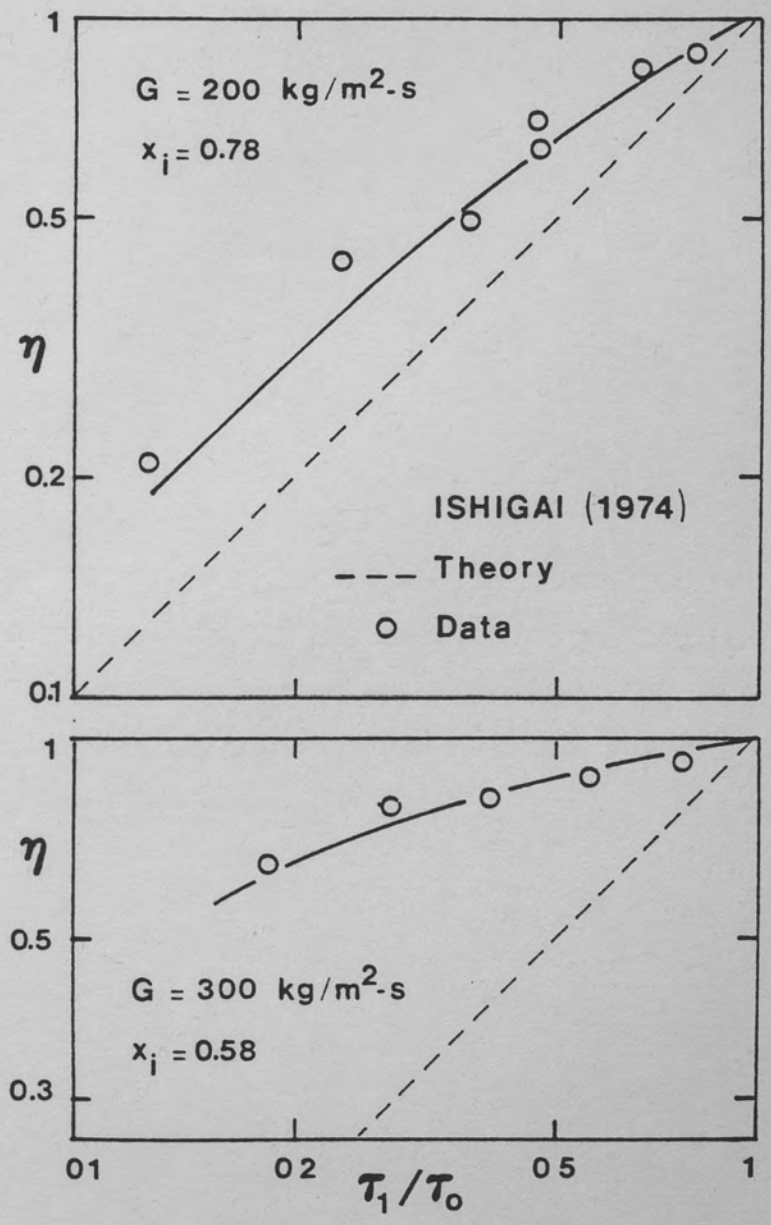

Figure 73. The Effect of Abrupt Flow Change on CHF (Ishigai 1974)

CHF data with constant pressure and uniform heat flux in a freon loop simulating an exponential flow decay, which is typical of LOFA conditions. In these experiments, the fluid, Freon-12, entered at subcooled conditions and flowed upward through a uniformly-heated test section of stainless steel with heated length of 2 m, inner diameter of 7.8 mm, and wall thickness of 1 mm. Some of these experiments are compared to the CISE-freon steady-state CHF correlation by Leung (1980). As summarized in Chapter VI, the results were successful; but only the relatively slow experiments were studied by Leung (1980). By studying all the experiments, including the relatively-fast ones, for an exponential flow decay, Cumo et al. (1978) correlated the transient CHF data in the following form:

$$q_{CHF,TR} = q_{CHF,SS} + C.F. \tag{85}$$

where the correction factor, C.F. is given by

$$C.F. = 0 \text{ if } \frac{t_{0.5}\, q_{CHF,TR}\, (P_{cr}/P)^{2.2}}{q_{CHF,SS}(G_o)} > 24 \text{ sec.} \tag{86}$$

$$C.F. = \left| q_{CHF,SS}\,(G_o) - q_{CHF,SS}\,[G_i(t)] \right| \exp(-gt)$$

$$\text{where } g = 0.82\,(t_{0.5})^{0.15}\,(P_{cr}/P)^{\frac{1}{2}}$$

where $t_{0.5}$ is the time required for 50 percent reduction in flow.

This correlation suggests that for rapid flow reduction, the transient CHF is higher than the corresponding steady-state CHF. In

the above correlation, the steady-state CHF is correlated by using the CISE-Freon correlation.

More recently, Cumo and his co-workers (Celata 1986) performed a similar experimental study for transient CHF during flow reduction. Celata et al. (1986) used a similar test section which was a stainless steel tube 2300 mm in length, 7.5 mm inner diameter, and 0.9 mm wall thickness. The test section was uniformly heated. In all the tests, the inlet subcooling was kept constant and equal to 23°C. Four parameters have been varied during these tests. The test matrix is shown in Table 12. For each test the parameters were kept constant, except for the mass-flow rate which was well-approximated by the following characteristic function:

$$[G_i(t)/G_o] = \gamma_1/(1 + \gamma_2\, e^{t/\tau}) \tag{87}$$

In the data analysis, Celata et al. (1986) used a parameter referred to as the "time transit parameter," defined as

$$t_t = \rho_{lo}[L/G_o] \tag{88}$$

Celata et al. observed that the critical heat flux data was dependent on the following ratio:

$$\tau' = t_{0.5}/t_t \tag{89}$$

TABLE 12

THE EXPERIMENTAL TEST MATRIX OF CELATA ET AL. (1986)

P (MP_a)	1.2 ;	1.5 ;	2.0 ;	2.75				
q (W/m^2)	Ranging between 32,000 and 85,000							
$G_{i,o}$ (kg/m^2-s)	1000;	1250;	1470					
$t_{0.5}$ (s)	0.4;	1.0;	2.0;	3.0;	4.0;	5.0;	7.0;	10.0

and correlated their data in the following form:

$$\frac{G(t_{CHF,TR})}{G(t_{CHF,SS})} = 1-\exp\left|-0.87\ (P/P_{cr})^{-0.57}(\tau')^{0.54}[q/q_{CHF,SS}(G_o)]^{2.8/\tau'}\right| \quad (90)$$

Since the CHF decreases as the mass-flow rate decreases for fixed inlet subcooling, Equation 90 shows that for small values of τ' the transient CHF is greater than the corresponding steady-state CHF. The inaccuracy of the steady-state prediction becomes important for values of τ' less than 2.

CHAPTER VIII

THEORETICAL PREDICTION OF THE CHF DURING POWER TRANSIENT

The study of boiling with time-dependent heat input is a major concern for many applications of boiling heat transfer, especially in light-water-reactor (LWR) technology. The prediction of critical heat flux (CHF) in the safety evaluation of reactivity initiated accidents (RIA) in LWRs is important to the nuclear industry. These types of accidents are associated with a sudden increase in power generation and may occur in a nuclear reactor under a variety of conditions, as discussed in Chapter IV. Along with power burst experiments, referenced in Chapter IV and VI, simulating RIA in full-scale reactors, there have been several experiments aimed toward a fundamental understanding of the CHF phenomena caused by power transients. Some of these studies were summarized in Chapter VII.

In this chapter, the transient CHF caused by a time-dependent heat source is investigated from basic principles. In the first section, the transient CHF for saturated pool boiling during power transients is studied. In the following sections, the effects of liquid supply, subcooling, and forced convective boiling on the transient CHF are investigated.

Transient CHF in Saturated Pool Boiling During Power Transients

The multi-step model of Haramura and Katto (1983), summarized in Chapter III, is the most complete formulation of the CHF problem in saturated pool boiling and is used in the development of the transient CHF correlation. The time-dependent nature of the heat generation rate makes it necessary to couple the developed CHF model with an appropriate conduction model, which is also included in this section.

Theoretical Transient CHF Correlation

The CHF for steady-state saturated pool boiling is formulated by Haramura and Katto (1983) as

$$\tau_d \, q_{CHF,SS,OO} = \rho_f \delta_{c,o} (1 - A_v/A_w) \, h_{fg} \tag{91}$$

where $\delta_{c,o}$ is the critical liquid layer thickness underneath the bubble and τ_d is the hovering period of the bubble, as discussed in Chapter III. The ratio A_v/A_w represents the fraction of the surface area covered by vapor to the total heated area. When the heat flux reaches the steady state CHF value, the liquid layer thickness is formulated (Haramura and Katto 1983) as

$$\delta_{c,o} = f_1(P)/q^2_{CHF,SS,OO} \tag{92}$$

where,

$$f_1(P) = 0.5\pi\sigma[(\rho_f + \rho_g)/(\rho_f \rho_g)] \, (A_v/A_w)^2 \, (\rho_g h_{fg})^2 \tag{93}$$

as summarized in Chapter III. If the local heat flux is kept at this level, the liquid layer will dry out at the end of τ_d. Using equations 91 and 92, the hovering period may be written as

$$\tau_d = f_2(P) f_1(P) / q^3_{CHF,SS,OO} \tag{94}$$

where

$$f_2(P) = \rho_f \, h_{fg} \, (1-A_v/A_w) \tag{95}$$

In power transient situations, however, the local heat flux increases during τ_d, which causes the complete evaporation to take place sooner than τ_d. By the time the surface is essentially dried, the local heat flux reaches a value higher than $q_{CHF,SS,OO}$ which is $q_{CHF,TR}$.

During the evaporation process there is no liquid supply to the liquid layer; thus, the rate of change of the liquid layer thickness is governed by either one of two mechanisms: the hydrodynamic instability which dictates the maximum thickness of the stable liquid layer for a given surface heat flux, or evaporation. This may mathematically be expressed as

$$(d\delta/dt) = \text{MAX} \{ |(\partial \delta_{c,o}/\partial q)(dq/dt), \, |q/f_2(P)| \} \tag{96}$$

where the first term on the RHS corresponds to hydrodynamic thinning and the second term to evaporation. This hypothesis is illustrated in Figure 74. Figure 74 shows that if the heat flux is kept constant at

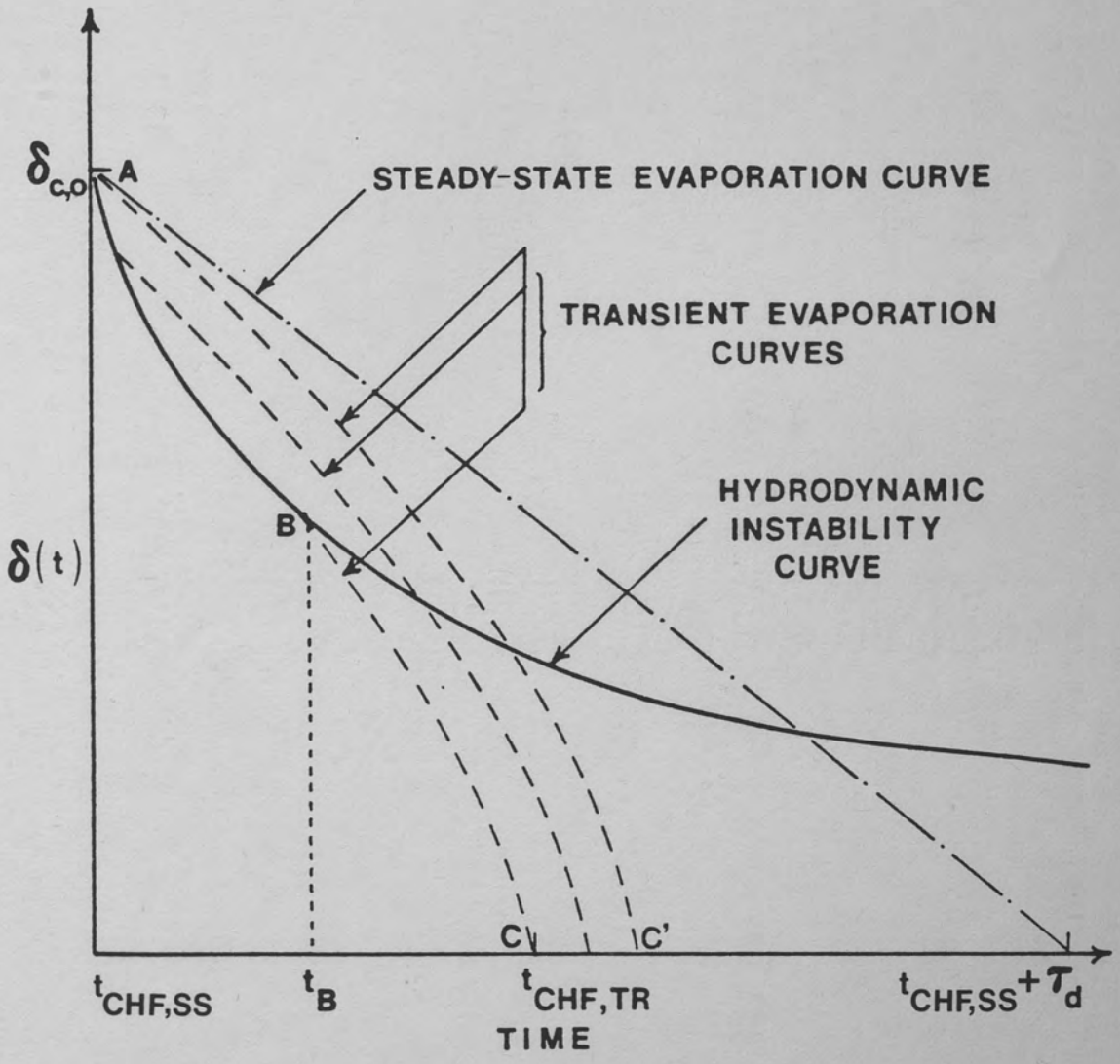

Figure 74. The Change in Liquid Layer Thickness Due to Hydrodynamic Instability and Evaporation

the steady-state CHF level, the liquid layer will evaporate at the end of the hovering period τ_d. But, since the heat flux increases with time, the rate of evaporation also increases, as shown by the dotted lines. However, an increase in the heat flux also causes a decrease in the thickness of the stable liquid film, as shown by the solid line. The slope of the evaporation line and the critical liquid thickness line determine the dominant mechanism. Figure 74 shows that between points A and B the hydrodynamic instability is dominant; whereas, at point B the evaporation starts dominating until the complete evaporation of the liquid layer thickness. Therefore, the liquid layer thickness follows the curve ABC rather than AC', as suggested by Serizawa (1983). In order to estimate the time-to-CHF accurately, the point B must be estimated. This switch-over point between the two mechanisms may be calculated by setting the slopes of evaporation and hydrodynamic instability lines equal, such that

$$(\partial \delta_{c,o}/\partial q)(dq/dt) = -q/f_2(P) \qquad (97)$$

The critical liquid layer thickness may be related to the surface heat flux through Equation 92. Equation 92 is developed (Haramura and Katto 1983) by estimating the Helmholtz instability wavelength in the vapor stems for a steady-state surface heat flux. By assuming that the vapor velocity in the stems accelerates instantaneously to its magnitude dictated by the increasing surface heat flux, the same equation may be used for transient surface heat flux. This assumption is thought to be reasonable, since the total distance traveled by the vapor (the length of the vapor stems) is very small (on the order of

10 to 100 microns). Therefore, using Equation 92, the heat flux at the switch-over point may be calculated as

$$q_B = \{ 2 f_1(P) f_2(P)(dq/dt)_{q=q_B} \}^{\frac{1}{4}} \quad (98)$$

Using Equation 94, Equation 98 may be written as

$$q_B = q_{CHF,SS,OO} B_s \quad (99)$$

where B_s is the dimensionless parameter which determines the switch-over between the two mechanisms and is given by

$$B_s = \left[2 \tau_d (dq/dt)_{q=q_B} / q_{CHF,SS,OO} \right]^{\frac{1}{4}} \quad (100)$$

If B_s is less than or equal to 1, the decrease in the liquid layer between $t_{CHF,SS}$ and $t_{CHF,TR}$ is controlled by evaporation alone. However, if B_s is greater than 1, the effect of the hydrodynamics on the decrease of liquid layer thickness must be included in the analysis. Once the surface heat flux is known as a function of time, the switchover heat flux, q_B, may be calculated through equations 99 and 100. Hence, the transient CHF may be predicted through the following integrals:

$$(\delta_{c,o})_{t=t_{CHF,SS}} = \int_{t_{CHF,SS}}^{t_B} [2f_1(P)(dq/dt)/q^3]dt + \int_{t_B}^{t_{CHF,TR}} [q/ f_2(P)] \, dt \quad (101)$$

if $B_s > 1$, and

$$(\delta_{c,o})_{t=t_{CHF,SS}} = \int_{t_{CHF,SS}}^{t_{CHF,TR}} [q/f(P)]dt \tag{102}$$

if $B_s \leq 1$.

If the surface heat flux q is known as a function of time, Equations 101 and 102 may be integrated. If the surface heat flux increases linearly, it may mathematically be expressed as

$$q(t) = q_o + (dq/dt)t \tag{103}$$

For a linear increase, Equation 101 may be integrated to yield

$$(\delta_{c,o})_{t=t_{CHF,SS}} = [f_1(P)/q^2_{CHF,SS,OO}] - [f_1(P)/q_B^2] + (q_{CHF,TR} + q_B)(t_{CHF,TR} - t_B)/(2f_2P) \tag{104}$$

Using equations 91, 92, 95, 99 and 100, $t_{CHF,TR} - t_B$ may be written as

$$t_{CHF,TR} - t_B = 2\tau_d/[B_s^2 (B_s + \eta)] \tag{105}$$

where $\eta = q_{CHF,TR}/q_{CHF,SS,OO}$ Finally, for a linear increase in the heat flux, $t_{CHF,TR} - t_B$ may be expressed in terms of $q_{CHF,TR}$ and q_B through Equation 103, as follows:

$$t_{CHF,TR} - t_B = (q_{CHF,TR} - q_B)/(dq/dt) \tag{106}$$

Equating the RHS of equations 105 and 106, and substituting q_B from Equation 99, the transient CHF correlation may be obtained as

$$\eta = \sqrt{2}B_s^2 \tag{107}$$

For $B_s \leq 1$, Equation 102 may be integrated through a similar procedure to yield

$$\eta = (1 + B_s^4)^{\frac{1}{2}} \tag{108}$$

Thus, the transient CHF correlation for a linear increase in the local heat flux may be written as

$$\eta = \left[1 - H(B_s - 1)\right](1 + B_s^4)^{\frac{1}{2}} + \left[H(B_s - 1)\right](\sqrt{2}B_s^2) \tag{109}$$

where $H(B_s - 1)$ is the Heavyside step-function.

If the surface heat flux increases exponentially as given by

$$q(t) = q_o \exp(t/\tau) \tag{110}$$

then, Equation 100 reduces to

$$B_s = (2\tau_d/\tau)^{1/3} \tag{111}$$

If B_s is greater than 1, Equation 101 may be integrated to yield

$$(\delta_{c,o})_{t=t_{CHF,SS}} = [f_1(P)/q^2_{CHF,SS}] - [f_1(P)/q^2_B] + \tau\,[q_{CHF,TR} - q_B]/f_2(P) \quad (112)$$

Using equations 91, 92, 95 and 99, Equation 112 may be written as

$$\tau_d/\tau = B_s^2\,(\eta - B_s) \quad (113)$$

Finally, using Equation 111, the transient CHF correlation may be written as

$$\eta = 1.89\,(\tau_d/\tau)^{1/3} \quad (114)$$

for $\tau_d/\tau \geq 0.5$

For $\tau_d/\tau \leq 0.5$, Equation 102 may be integrated to yield

$$\eta = 1 + \tau_d/\tau \quad (115)$$

Therefore, the transient CHF correlation for an exponential increase in the surface heat flux may be written as

$$\eta = \left[1 - H(\tau_d/\tau - 0.5)\right](1 + \tau_{d/\tau}) + \left[H(\tau_d/\tau - 0.5)\right]\,1.89(\tau_d/\tau)^{1/3} \quad (116)$$

where $H(\tau_d/\tau - 0.5)$ is the Heavyside step-function.

The Conduction Within the Heater During Power Transients

The transient CHF correlations developed in the previous section are based on the rate-of-change of the local heat flux. During power transients, however, the rate-of-change of the heat generation rate is the major parameter, and it is often directly measured. Therefore, in order to use the above CHF correlations, a relation between the heat generation rate Q and the surface heat flux q must be established. In this section, the transient conduction problem of a cylindrical heater in a pool of liquid is considered. The heat generation rate is assumed to increase exponentially according to

$$Q(t) = Q_o \exp(t/\tau) \tag{117}$$

Neglecting the temperature variations in the axial and circumferential directions, the energy equation in terms of temperature variation in cylindrical coordinates becomes

$$\rho C_p \frac{\partial T}{\partial t} = k\left[\frac{1}{r}\frac{\partial}{\partial r}\left(r \frac{\partial T}{\partial r}\right)\right] + Q_o e^{t/\tau} \tag{118}$$

subject to the following boundary conditions:

$$\text{at} \quad r = 0 \qquad \frac{\partial T}{\partial r} = 0 \tag{119}$$

and

$$\text{at} \quad r = R \qquad T = T_w \tag{120}$$

If the second boundary condition in Equation 111 is known as a function of time, an analytical solution to the problem may be obtained using the appropriate transform techniques. But this boundary condition is supplied from the solution of the conjugate convection problem. For nucleate boiling, however, this becomes a difficult task. Therefore, in this section, certain approximations and their implications are discussed. When non-dimensionalized, using the variables given in the nomenclature, equations 118, 119, and 120 yield, respectively

$$\left[\frac{\rho\, C_p\, R^2}{k\,\tau}\right]\frac{\partial T'}{\partial t'} + \left[\frac{\rho\, C_p\, R}{h_c \tau}\right]\frac{dT_w'}{dt'} - e^{t'} = \frac{1}{r'}\frac{\partial}{\partial r'}\left(r'\,\frac{\partial T'}{\partial r'}\right) \tag{121}$$

$$\text{at } r' = 0 \qquad \frac{\partial T'}{\partial r'} = 0 \tag{122}$$

$$\text{at } r' = 1 \qquad T' = 0 \tag{123}$$

For electrical heater wires with low heat capacity, high thermal conductivity and small radius, the coefficient of the first term becomes small, except for very small values of τ. Therefore, the first term of Equation 121 may be dropped, compared to the other terms in the LHS of the equation. With this approximation Equation 121, subject to the conditions given by Equations 122 and 123, may be solved to yield the temperature profile as a function of time t and radial coordinate r. By using the Fourier law, the surface heat flux may be obtained as

$$q' = \frac{1}{2}\left[e^{t'} - \left(\frac{\rho\ C_p\ R}{h_c \tau}\right)\frac{dT_w'}{dt'}\right] \tag{124}$$

During the solution procedure, h_c is treated as constant; but, in fact, it is a function of time. Depending upon the time interval considered and the value of h_c within this interval, Equation 124 may have the following implications:

1. For high values of h_c, when dT_w'/dt' is on the order of dT'/dt', the last term of Equation 124 may be dropped, as compared to the first term. Then, Equation 124 reduces to:

$$q' = e^{t'}/2 \tag{125}$$

Thus,

$$q = (RQ_o\ e^{t/\tau})/2 \tag{126}$$

The heat flux is related to the heat generation rate through the simple relation:

$$q = Q(V/S) \tag{127}$$

where V is the heater volume and S is the heater surface area. Hereafter, this case will be referred to as the quasi-steady conduction model.

2. For low values of h_c, all the heat conducted to the surface may not be convected away, and the quasi-steady conduction model will overpredict the surface heat flux, i.e.,

$$q < Q(V/S) \tag{128}$$

3. If a sudden increase in h_c occurs (for instance, right after the initiation of boiling), there may not be enough heat generated and conducted to the surface to compensate for the convection. Thus, some of the previously stored energy starts being convected away, which results in a decrease of the surface temperature ($dT'_w/dt' < 0$). This, in turn, implies

$$q > Q(V/S) \tag{129}$$

The time interval which is of interest to the present study is the period between the time the surface heat flux reaches the steady state CHF value and the time it reaches the transient CHF value. The experimental studies of Sakurai and Shiotsu (1977a) and Serizawa (1983) on the boiling patterns during a power transient, show that all three cases considered previously are possible within this specific time interval. The boiling patterns corresponding to each case are shown in Figure 75. Figure 75-a may correspond to the quasi-steady conduction model described as case 1, whereas, the boiling pattern of Figure 75-b may result in case 2. The temperature shoot-back in the time interval from steady state CHF to transient CHF, as shown in Figure 75-c, is likely to cause the conditions in case 3.

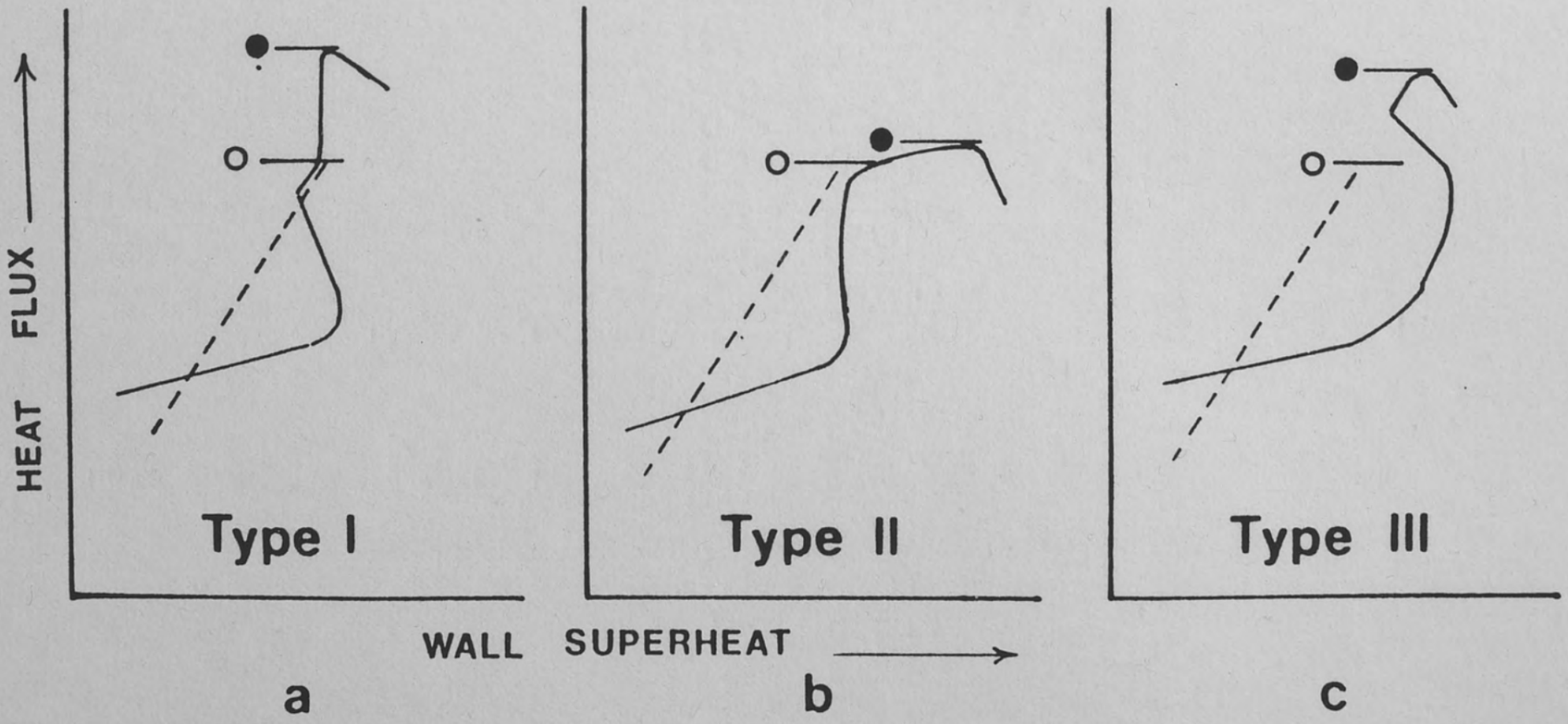

Figure 75. The Different Types of Boiling During Power Transients.

Since, depending upon the geometry, pressure, exponential period, and heater material, all the different patterns in Figure 75 are possible, the use of an appropriate conduction model in the transient CHF correlations becomes crucial. Hereafter, the boiling patterns shown in figures 75-a, 75-b, and 75-c are referred to as Types I, II, and III, respectively.

Comparison With Data

The transient CHF correlations developed for saturated pool boiling are compared to the data from the experiments of Sakurai and Shiotsu (1977b), Kuroda (1979), Tachibana et al. (1968), Sakurai et al. (1970), Kawamura et al. (1970), and Kataoka et al. (1983).

Figures 76 through 81 show the comparison of Equation 116 with the data of Sakurai and Shiotsu (Sakurai 1977b) at various pressures. The experimental conditions of this study were summarized in Chapter VII. The results are quite successful for high pressure. The data is slightly overpredicted for lower values of τ. This is possibly due to the fact that the quasi-steady conduction is not present for such rapid transients. The developed theory is also very dependent upon the magnitude of τ_d. For comparison with the data, the value of τ_d is calculated through Equation 15, which may introduce some error. On the other hand, for 0.196 and 0.101 MPa, the correlation overpredicts the data for values of τ less than 50 msec. This is expected, since Sakurai and Shiotsu (1977b) experimentally observed that at low pressure and small exponential period the boiling pattern of Type II is present. In the figures 76 through 81, the dotted line represents

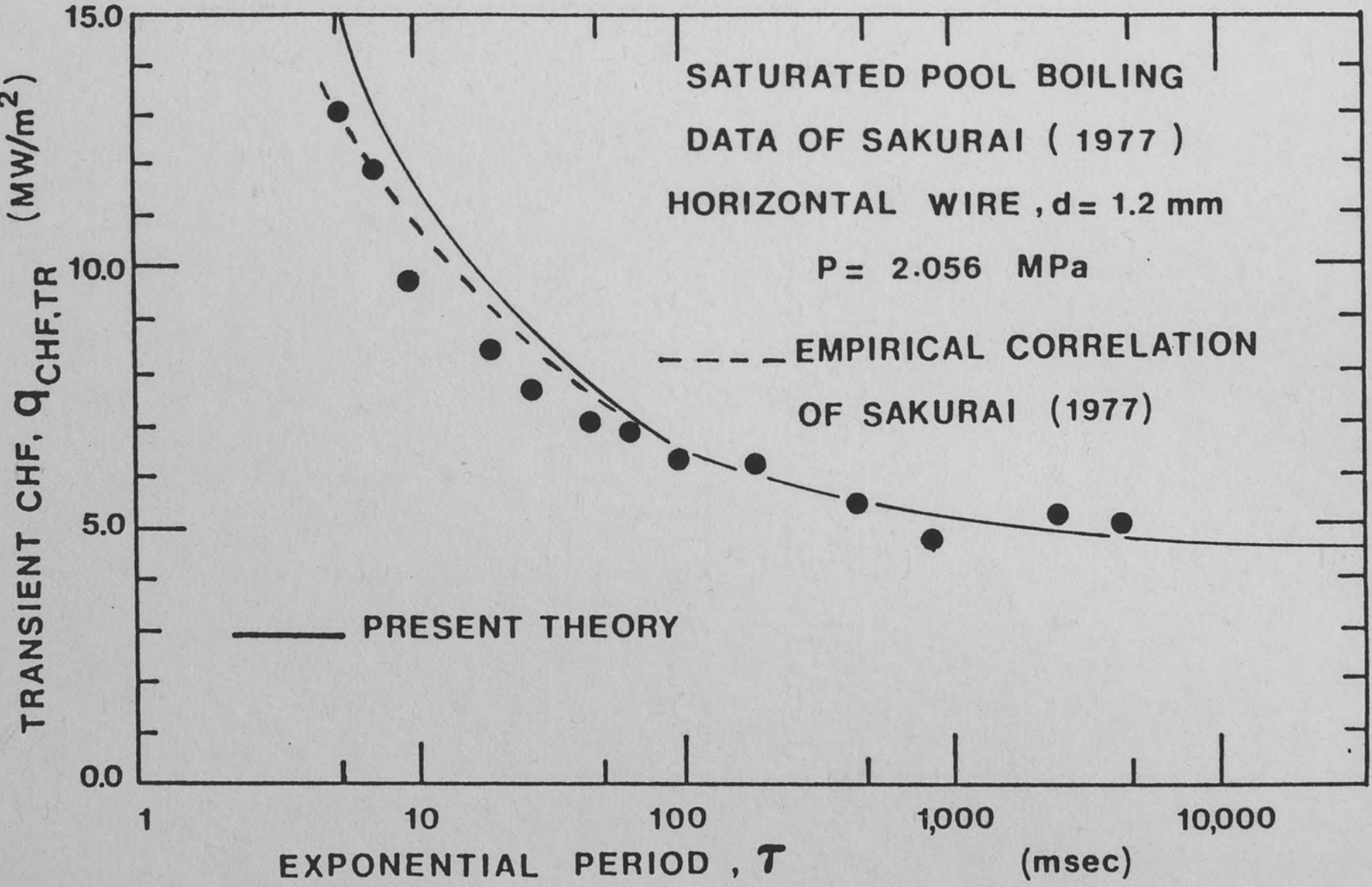

Figure 76. Comparison of the Present Theory with the Data of Sakurai and Shiotsu (1977)

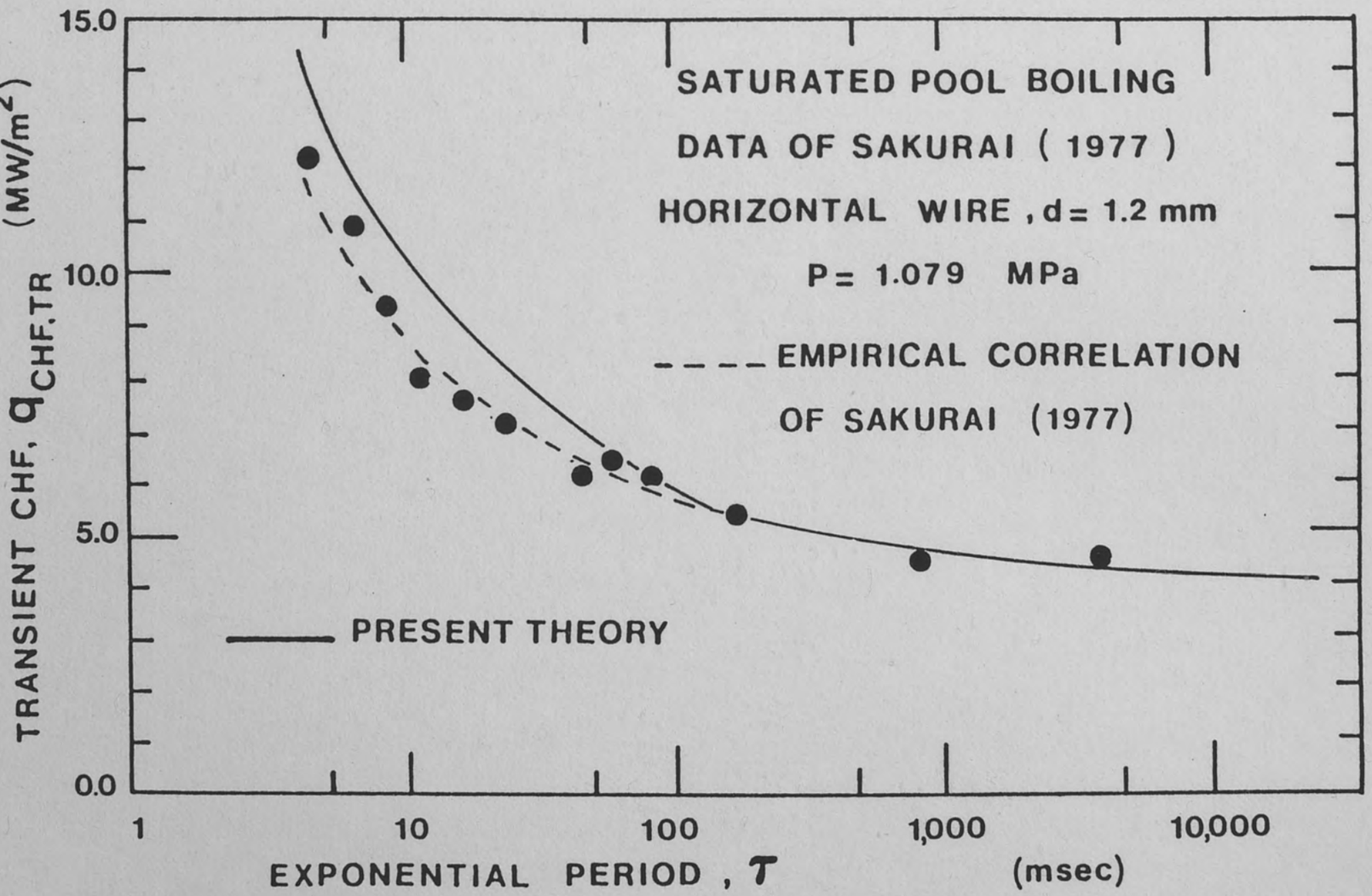

Figure 77. Comparison of the Present Theory with the Data of Sakurai and Shiotsu (1977)

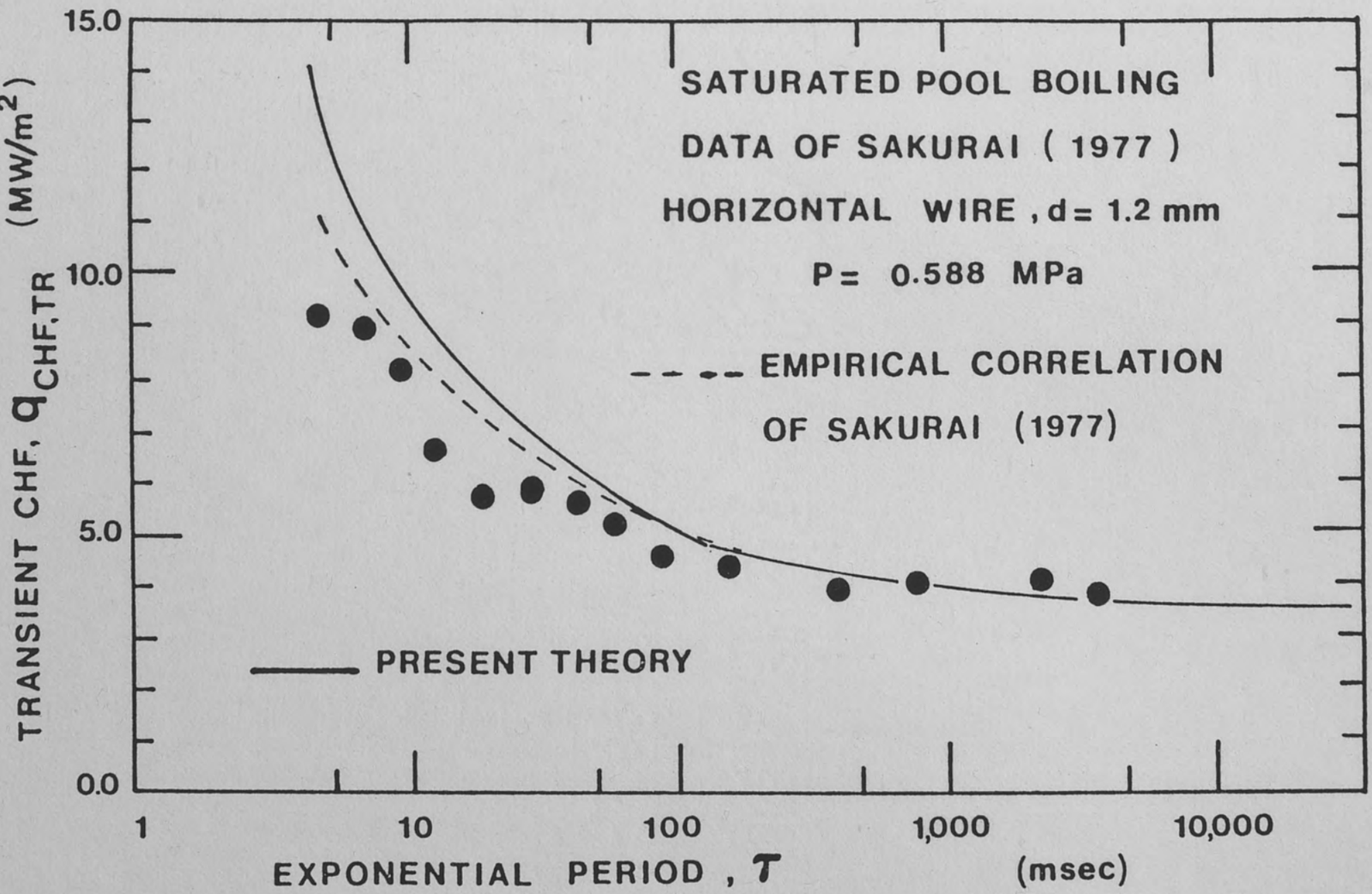

Figure 78. Comparison of the Present Theory with the Data of Sakurai and Shiotsu (1977)

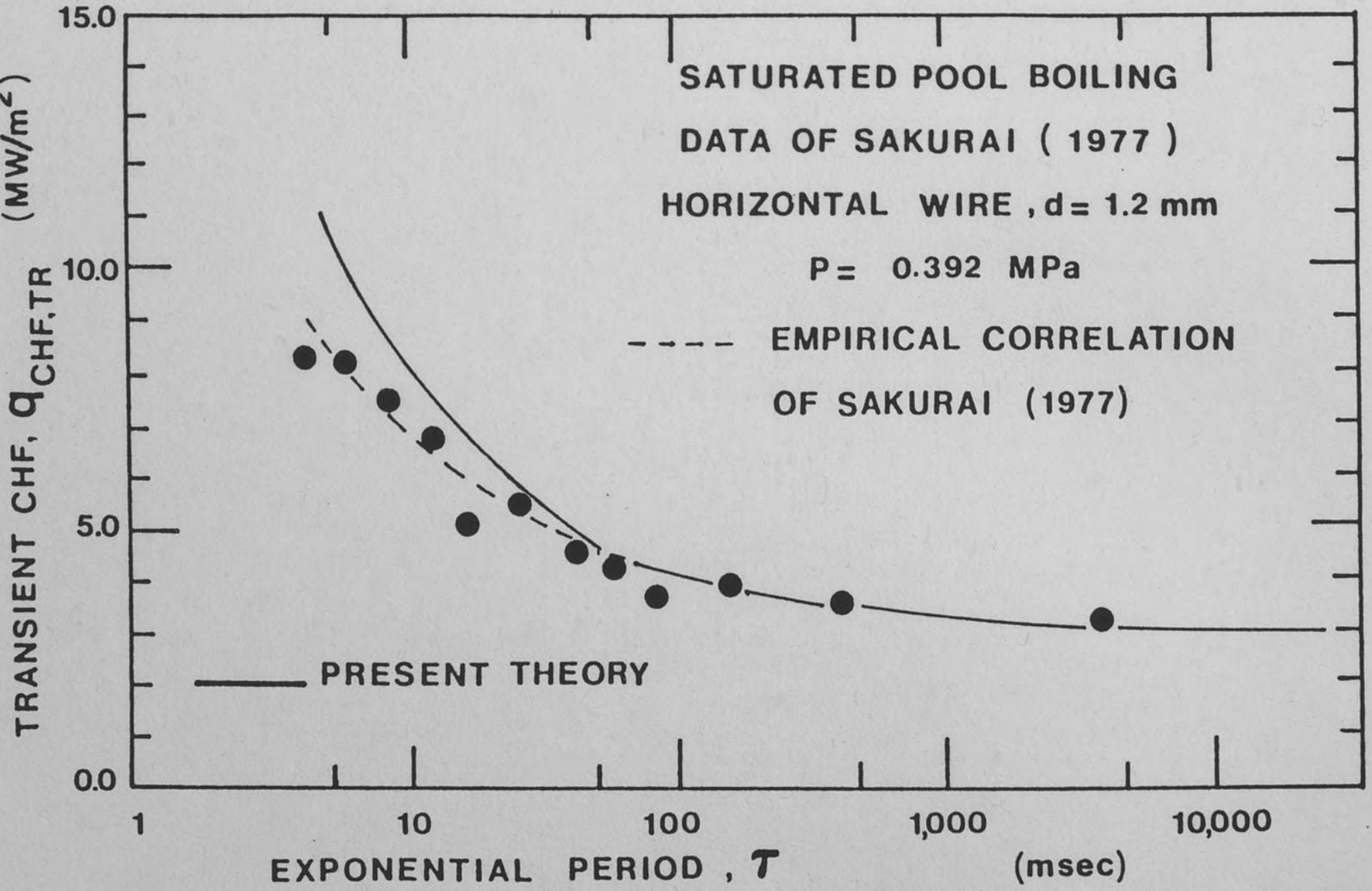

Figure 79. Comparison of the Present Theory with the Data of Sakurai and Shiotsu (1977)

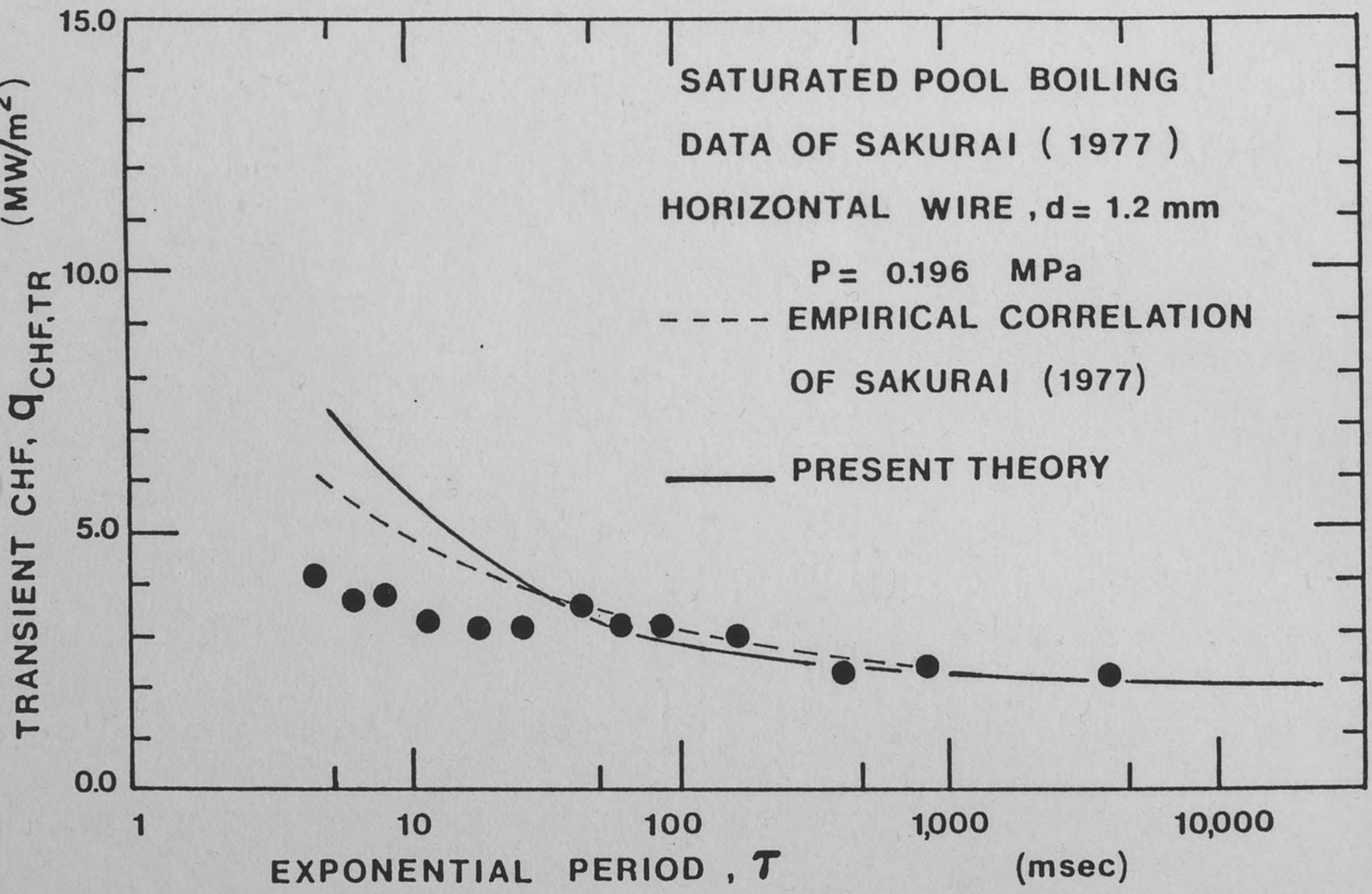

Figure 80. Comparison of the Present Theory with the Data of Sakurai and Shiotsu (1977)

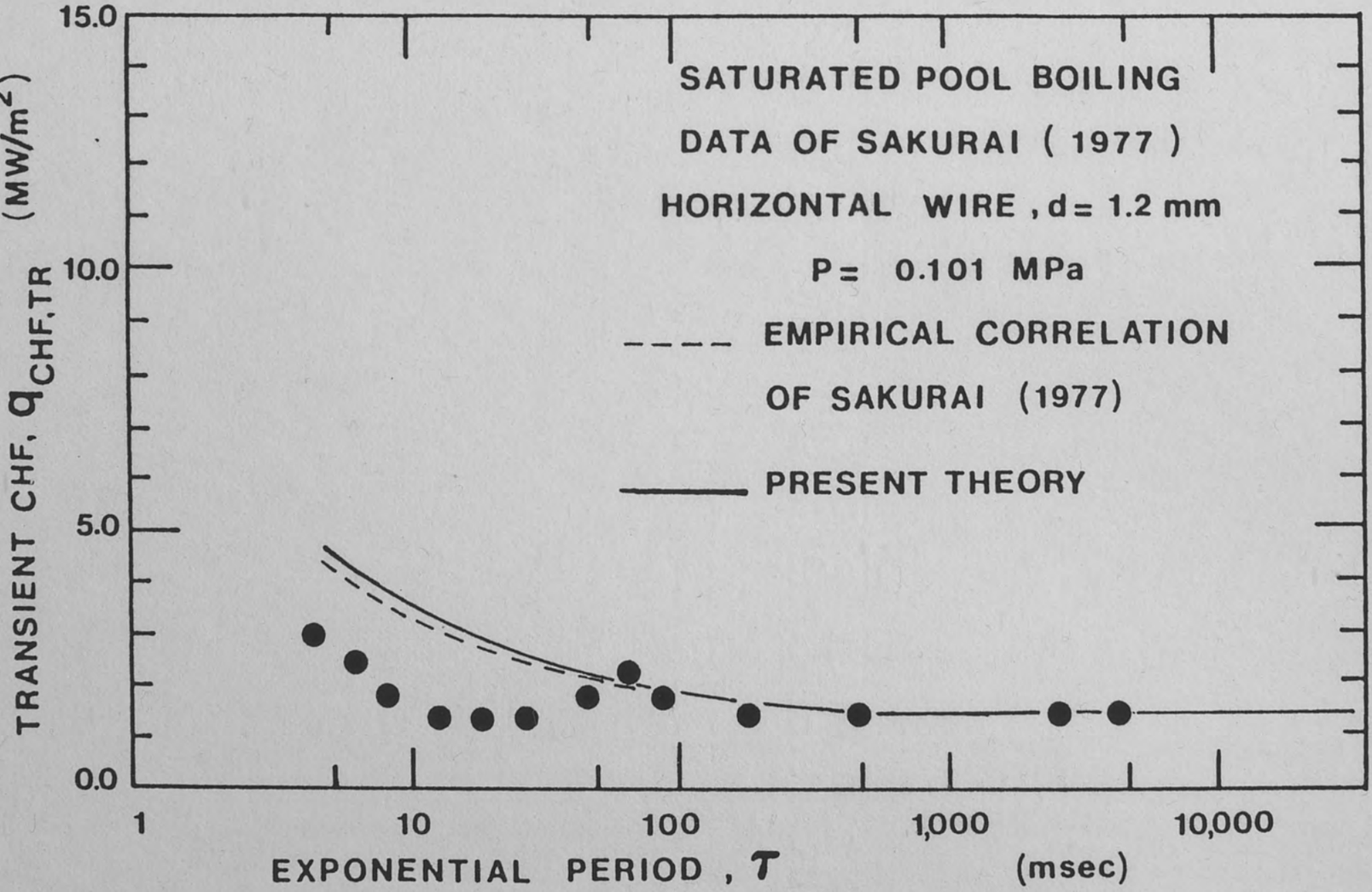

Figure 81. Comparison of the Present Theory with the Data of Sakurai and Shiotsu (1977)

the empirical correlation of Sakurai and Shiotsu (1977b), which is given by Equation 71 in Chapter VII.

Figure 82 shows the comparison of the present correlation with the data of Kuroda (1979). The results are the same as the results of the comparison with the data of Sakurai and Shiotsu (1977b), since the same experimental set-up was used. The data of Kuroda (1979) for subcooled boiling is analyzed in the next section.

The present theory is also compared to the data of Tachibana et al. (1968), as shown in Figure 83. In this experiment, flat ribbon heaters were used and the heat generation rate per unit surface area was increased linearly, as summarized in Chapter VII. Assuming that the quasi-steady conduction model may be used, Equation 109 is used to evaluate η, and the result is shown by the solid line. But, the experimental observations of Tachibana et al. (1968) show that the surface heat flux does not increase linearly as the heat generation rate per unit surface area does and dq/dt is greater than dQ_s/dt after the initiation of boiling. This is illustrated by Figure 64 in Chapter VII. The present correlation overpredicts the data, which may be due to unknown hydrodynamics of the flat ribbon heater. In addition to the effect of non-quasi-steady conduction which was experimentally observed, the discrepancy between the data and the present theory is possibly due to the inappropriate steady-state CHF model employed. For flat ribbon heaters, no liquid supply to the liquid layer during the bubble growth may not be very realistic. Furthermore, the calculation of τ_d using a circular cylinder model is erroneous by itself.

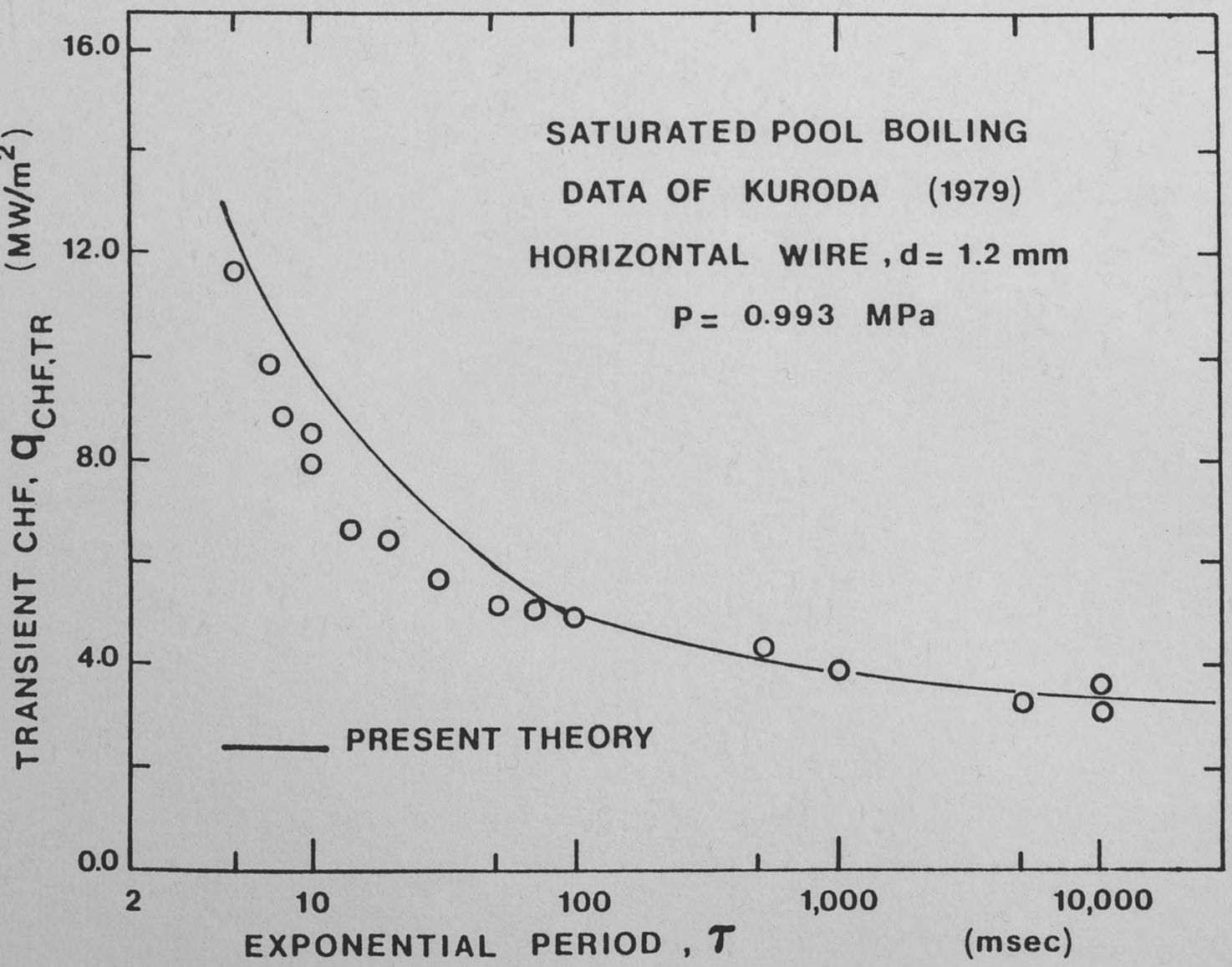

Figure 82. Comparison of the Present Theory with the Data of Kuroda (1979)

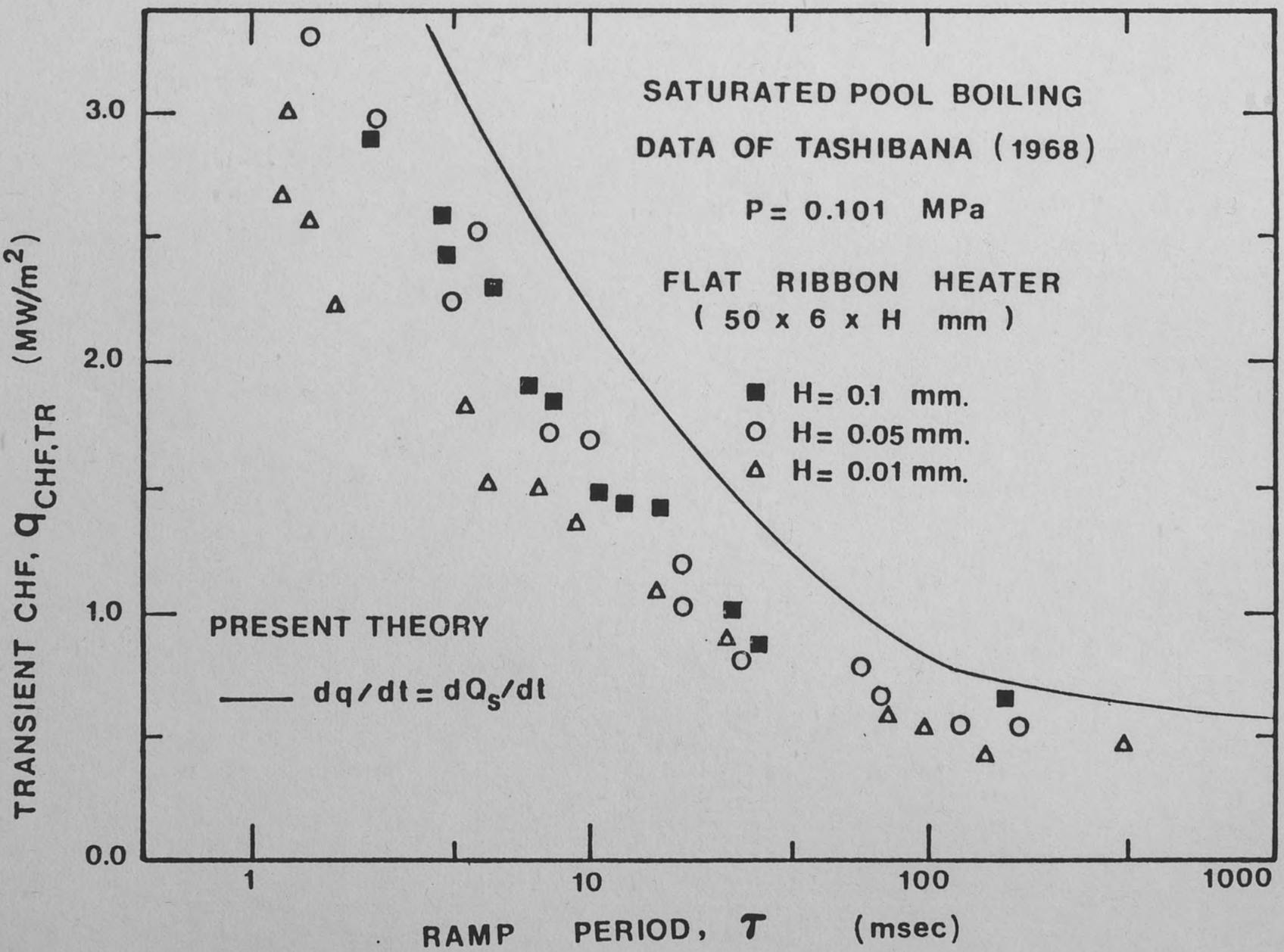

Figure 83. Comparison of the Present Theory with the Data of Tachibana et al. (1968)

The experimental study of Kawamura et al. (1970) was very similar to the experiment of Tachibana et al. (1968). Thus, the results as compared to the present theory are the same. Since Kawamura et al. (1970) investigated the effect of subcooling also, the data analysis is shown in the section where the effect of subcooling is theoretically studied.

The data of Sakurai et al., (1970) are also compared to the present correlation, as shown in Figure 84. In this experiment, flat ribbon heaters of very small geometry (0.1 x 2.5 x 15mm) are used. Since the unstable Taylor wavelength is larger than the longest dimension, the geometry effects become dominant and the hydrodynamics become very complex. The experiments were simulating an exponential power increase; therefore, Equation 116 is used to calculate n. The present theory, in conjunction with the quasi-steady conduction model, is only good in predicting the general trend of the data, as shown in Figure 84. The discrepancy is expected to be due to theoretical difficulties mentioned above. Especially, the geometry effects due to such small heater geometries are thought to be the major source of error, since even the steady-state CHF is overpredicted by any of the commonly used correlations. Therefore, since the geometry effects are beyond the scope of the present study, the data analysis of this experiment for subcooled CHF is skipped.

The experimental setup of Kataoka et al. (1983) was designed to study the transient CHF during forced convective boiling. In this setup, which consists of a vertical wire placed in a vertical flow channel, Kataoka et al. (1983) also obtained a set of data with zero flow and zero subcooling. The comparison of the present theory to

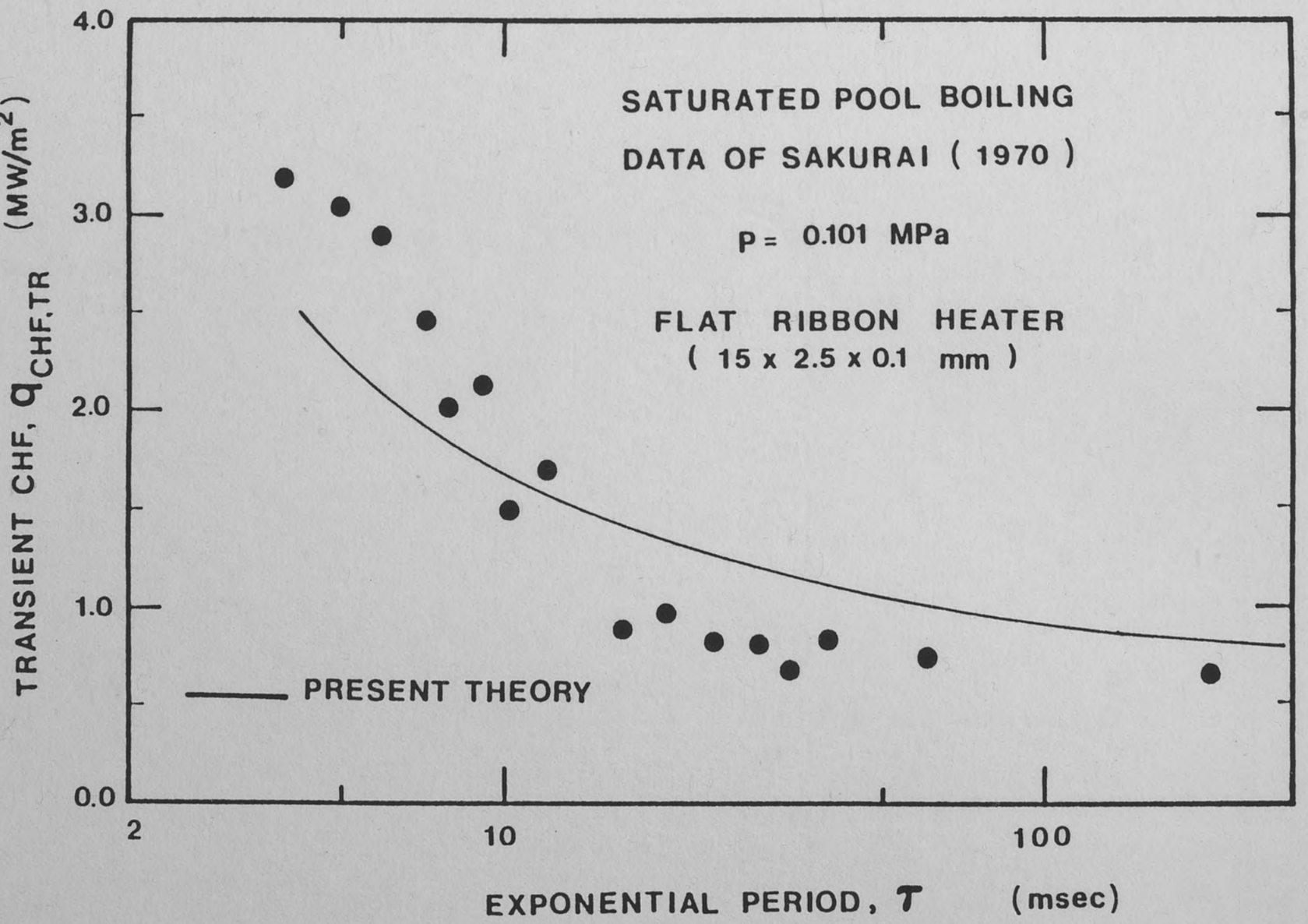

Figure 84. Comparison of the Present Theory with the Data of Sakurai et al. (1970)

this set of data is shown in Figure 85. Both the present theory and the empirical correlation of Kataoka et al. (1983) overpredict the data at 0.143 MPa. This is due to Type II boiling present at this low pressure. At 0.594 MPa, the present theory slightly overpredicts the data for values of τ less than 50 msec. This may be attributed to the presence of non-quasi steady conduction. In Figure 85, the dotted line represents the empirical correlation of Kataoka given by Equation 72 in Chapter VII.

Transient CHF In Subcooled Pool Boiling During Power Transients

The relation between the CHF and the subcooling is formulated by Ivey and Morris (Ivey 1962), as given by Equation 28 in Chapter III. If the variation of liquid density and liquid specific heat, with respect to the degree of subcooling are neglected, Equation 28 shows that the ratio of CHF in subcooled pool boiling to CHF in saturated pool boiling is a linear function of ΔT_{SUB}. In the context of the present study, the question of interest is whether the subcooling has the same quantitative effect on the transient CHF or not.

Experimentally, it has been observed that, for a given pressure, as the subcooling increases, η decreases for the same rate of change of the surface heat flux. This result is also expected theoretically. A careful analysis of Equations 109 and 116 shows that, in each case, η is an increasing function of τ_d, which is defined as the hovering period of the bubble. For subcooled boiling, however, it has been observed (Fand 1974) that the initiation, growth, and collapse of a bubble is faster than the initiation, growth, and departure of the

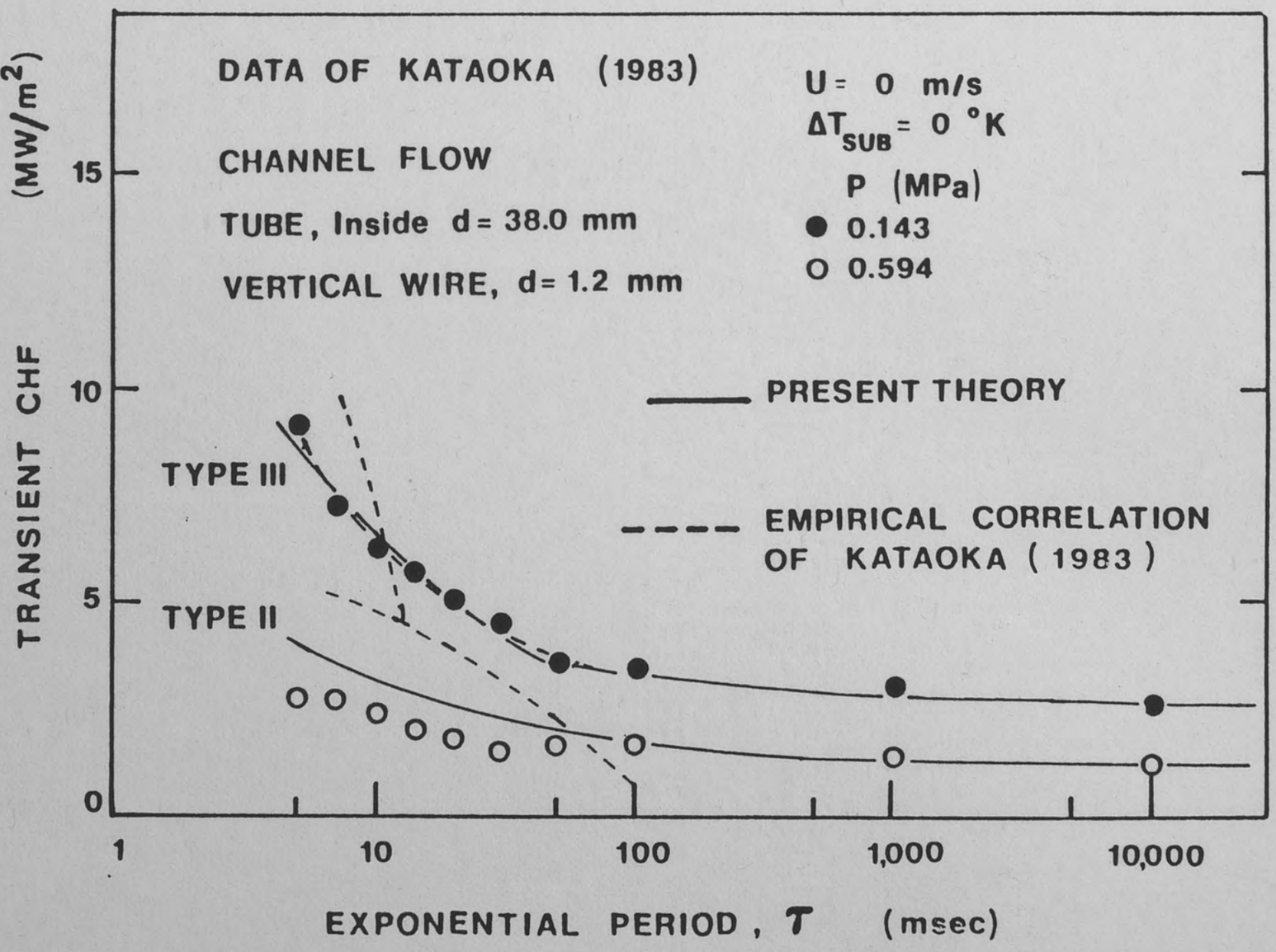

Figure 85. Comparison of the Present Theory with the Data of Kataoka et al. (1983) for Zero Flow and Zero Subcooling.

bubble for saturated boiling at the same pressure. Since the quantity τ_d is smaller for subcooled boiling, η is also smaller. In the rest of this section, a transient CHF correlation is developed. But this task requires an appropriate steady state CHF model for subcooled pool boiling.

Steady-State CHF Model For Subcooled Pool Boiling

Here, an attempt is made to model the subcooled pool boiling CHF in a similar fashion to the model of Haramura and Katto (1983). The model is based on the following postulates:

a. The density and the specific heat of the subcooled liquid is a weak function of temperature, and they can be approximated by their value at the saturation temperature for the given pressure. This assumption is commonly used in thermodynamics, and it is considered to be quite accurate for moderate subcooling.

b. Based on the first postulate, the ratio A_v/A_w may be assumed to be unaffected by the subcooling, since it is a function of the liquid density and it does not depend on the surface heat flux (Haramura 1983).

c. The liquid layer thickness is dictated by Helmholtz' instability, and it is inversely proportional to the square of the surface heat flux, as stated by Haramura and Katto (1983), for saturated pool boiling.

d. At high heat fluxes, near the CHF, the surface is crowded by many bubbles growing and collapsing continuously.

e. During the bubble growth, there is no liquid supply to the liquid layer. The liquid layer receives some liquid when the bubble

collapses. The temperature of the supplied liquid is equal to the temperature of the bulk liquid in the pool.

f. The initiation of the new bubble after the collapse of the previous one is almost instantaneous.

g. The CHF is reached if the liquid layer completely evaporates during the bubble growth period.

Based on these postulates, the CHF may be mathematically formulated as

$$\tau_g \, q_{CHF,SS,0} = \rho_l \, h_{fg} \, \delta_{c,s} (1 - A_v/A_w)(1 + C_{pl} \, \Delta T_{SUB}/h_{fg}) \qquad (130)$$

where τ_g is the growth period of the bubble, and $\delta_{c,s}$ is the liquid layer thickness at CHF for subcooled boiling. This formulation assumes no liquid supply to the liquid layer during the growth period τ_g, and when the liquid is supplied right before the growth period, it is at the bulk temperature. These are extreme idealizations. In reality, there may be a little liquid supply to the liquid layer during the growth period, which will tend to increase the CHF. On the other hand, when the liquid is supplied to the liquid layer, it is warmer than the bulk liquid, since part of the supply is from the thermal boundary layer. This effect tends to decrease the CHF. Furthermore, the liquid needs to be superheated over its saturation temperature before evaporation. Therefore, these assumptions have counter-acting effects on the steady-state CHF. For the purpose of transient CHF analysis, the net effect of these assumptions is thought to be negligible.

In Equation 130, the quantity τ_g is difficult to estimate, since the hydrodynamics of subcooled boiling are not well understood. Therefore, an empirical approach is used to quantify τ_g. The other terms of Equation 130, however, may be quantified by using the previously stated postulates. ρ_l is the liquid density in the liquid layer, and it is assumed to be equal to the density of saturated liquid at the same pressure, due to postulate (a).

The critical liquid layer thickness may be related to the critical liquid layer thickness for saturated pool boiling, $\delta_{c,o}$, at the same pressure, through the following relation:

$$\delta_{c,s} = \delta_{c,o}(q_{CHF,SS,OO}/q_{CHF,SS,O})^2 \qquad (131)$$

This relation makes use of postulates (a) and (c).

Using postulate (b), the quantity $(1 - A_v/A_w)$ is assumed to be independent of the subcooling. Therefore, it remains the same as for saturated boiling. In order to estimate τ_g, the following form is assumed:

$$\tau_g = f_3(P, \Delta T_{SUB})(q_{CHF,SS,O}/q_{CHF,SS,OO})^{1/5} \tau_d \qquad (132)$$

The dependence of the growth period on the 1/5 power of the surface heat flux is carried over from the formulation of τ_d by Haramura and Katto (1983).

Now, substituting Equations 131 and 132 into Equation 130, the following relation may be obtained:

$$f_3(P, \Delta T_{SUB}) = [\rho_f h_{fg} \delta_{c,o}(1 - A_v/A_w)/\tau_d]$$

$$x(q_{CHF,SS,OO}/q_{CHF,SS,O})^{11/5} (1/q_{CHF,SS,O}) \qquad (133)$$

$$x(1 + C_{pf} \Delta T_{SUB}/h_{fg})$$

The term within the brackets on the RHS of Equation 133 may be recognized as $q_{CHF,SS,OO}$ from Equation 91. Thus, Equation 133 yields

$$f_3(P, \Delta T_{SUB}) = (q_{CHF,SS,OO}/q_{CHF,SS,O})^{16/5}(1 + C_{pf} \Delta T_{SUB}/h_{fg}) \qquad (134)$$

Now the ratio $q_{CHF,SS,OO}/q_{CHF,SS,O}$ may be obtained by using the semi-empirical correlation of Ivey and Morris (1962), which is given by Equation 28 in Chapter III. Therefore, combining equations 28, 128 and 123, the growth period of the bubble in subcooled boiling may be related to the growth period of the bubble in saturated boiling at the same pressure. But, since the main objective of the present study is to investigate the transient CHF rather than developing a steady-state CHF model or testing the accuracy of the correlation by Ivey and Morris (1962), the ratio $q_{CHF,SS,OO}/q_{CHF,SS,O}$ will be left in the final form of the equation for τ_g, as follows:

$$\tau_g = (q_{CHF,SS,OO}/q_{CHF,SS,O})^3(1 + C_{pf} \Delta T_{SUB}/h_{fg})\tau_d \qquad (135)$$

In all the transient CHF experiments analyzed in this study, the steady-state CHF for saturated conditions and at various subcoolings are also measured. Therefore, the measured quantities may be used for

comparison purposes, rather than relying on the semi-empirical correlation (Ivey 1962) given by Equation 28.

Transient CHF Correlation

Using the proposed steady-state CHF model, a transient CHF correlation may be developed, using a procedure similar to the one used for developing the transient CHF correlation in saturated pool boiling. The total rate of change of the liquid layer thickness $\delta_{c,s}$ may be written as

$$(d\delta/dt) = MAX[|(\partial\delta/\partial q)(dq/dt)|, |q/f_2'(P)|] \quad (136)$$

where

$$f_2'(P) = \rho_l h_{fg}(1 - A_v/A_w)(1 + C_p \Delta T_{SUB}/h_{fg}) \quad (137)$$

Equation 136 may be integrated through the same procedure as the integration of Equation 96, for linear and exponential increases of the surface heat flux. The resulting equations of η are exactly the same as equations 109 and 116, if τ_d is replaced by τ_g and $q_{CHF,SS,OO}$ is replaced by $q_{CHF,SS,O}$. Therefore, using the above substitutions, equations 109 and 116 may be used to predict the transient CHF in subcooled pool boiling.

In the next sub-section, the correlations are compared to experimental data. For comparison, the heat generation rate is again related to the surface heat flux through the quasi-steady conduction model discussed earlier.

Comparison With Data

In Figure 86, the present theory is compared to the data of Kuroda (1979). The predictions are usually good, although the data is slightly underpredicted for 40 and 60 °K subcoolings. Considering the various simplifying assumptions made in the steady-state CHF model, this discrepancy is expected. For the most part, the prediction is within 10 percent. Between the simplifying assumption of the steady-state model, the estimation of τ_g and the quasi-steady conduction, the prediction is quite successful.

The theory is also compared to the data of Kawamura et al. (1970). In these experiments, the heater was a flat ribbon. Figure 87 shows that even the saturated pool boiling data is poorly predicted by the present theory. The same poor prediction is found to be pertinent for the subcooled pool boiling data. The comparison at 40° subcooling is also shown in Figure 87. The comparisons at 20° and 70° subcoolings are similarly poor. The discrepancy in this case is very high, and the effect of the various boiling patterns may not be the unique reason for this. It is thought that the hydrodynamic model used is erroneous for flat ribbon problems. This matter is further discussed later in this chapter.

Transient CHF in Forced Convective Boiling During Power Transients

The problem of transient CHF in forced convective boiling during power transient is theoretically studied by Serizawa (1983). Although Serizawa must be recognized for his unique and original approach to the problem, the author thinks that his method is unsatisfactory in

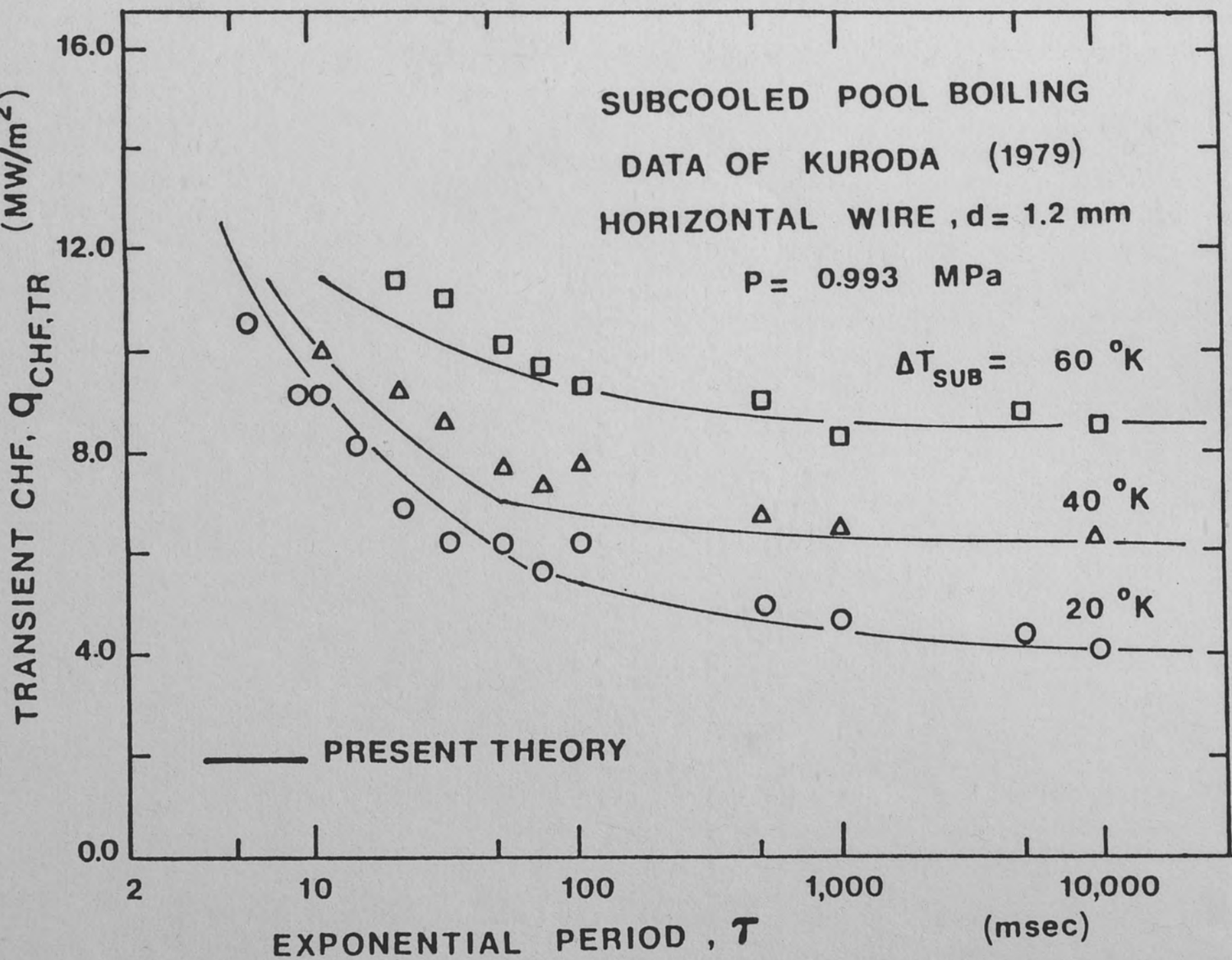

Figure 86. Comparison of the Present Theory with the Data of Kuroda (1979)

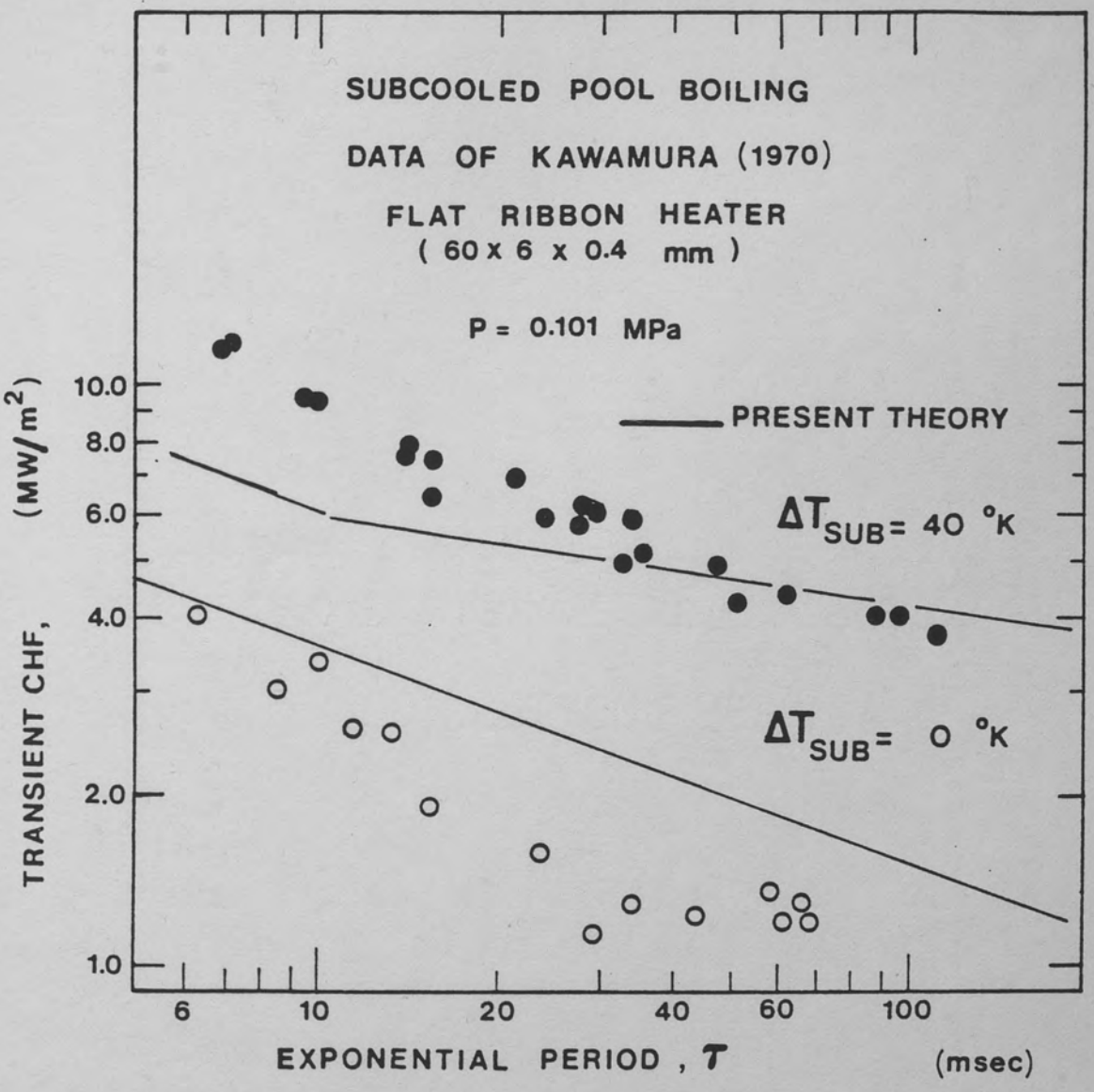

Figure 87. Comparison of the Present Theory with the Data of Kawamura et al. (1970)

certain aspects of the problem. At this point, it may be necessary to discuss the ambiguities of Serizawa's approach before making an attempt for a new formulation.

As summarized in Chapter VII, Serizawa (1983) formulates the steady-state CHF in the following form:

$$q_{CHF,SS} A_w = W_{fs} (h_{fg} + C_p \Delta T_{SUB}) \qquad (138)$$

where W_{fs} is the liquid supply rate at the steady state CHF level. Although this formulation is thought to be appropriate for forced convective boiling for vertical heater geometry and for pool boiling with long vertical heaters, it cannot be generalized. Equation 138 suggests that, if W_{fs} is zero, $q_{CHF,SS}$ must be zero. This is obviously not true, based on the previous discussion of saturated pool boiling CHF. In saturated pool boiling, the steady-state model of Haramura and Katto (1983) proposes no liquid supply to the liquid layer during the hovering period of the bubble at high heat fluxes near the CHF. By using this steady-state model, the author is able to predict the transient CHF quite accurately for horizontal heating surfaces, as seen in the previous sections. Therefore, Serizawa's attempt to extend the formulation of Equation 138 to saturated pool boiling conditions and to try to correlate the data for such problems is thought to be possible, only because of the empiricism incorporated into the model.

Furthermore, Serizawa (1983) postulates a model for transient CHF:

$$A_f \int_{t_{CHF,SS}}^{t_{CHF,TR}} q(t)dt = A\,\rho_l h_{fg} \delta_c + (h_{fg} + C_p \Delta T_{SUB}) \int_{t_{CHF,SS}}^{t_{CHF,TR}} W_f(t)dt \qquad (139)$$

If W_f is assumed constant between $t_{CHF,SS}$ and $t_{CHF,TR}$, Equation 139 yields the following:

$$\int_{t_{CHF,SS}}^{t_{CHF,TR}} q(t)dt = \rho_l\, h_{fg}\, \delta_c + q_{CHF,SS}\,(t_{CHF,TR} - t_{CHF,SS}) \qquad (140)$$

In addition to the knowledge of q(t), the above formulation requires an explicit knowledge of the critical liquid layer thickness δ_c. Serizawa relates q(t) to Q(t) through the quasi-steady conduction model as previously discussed. The critical liquid layer thickness δ_c is empirically correlated by Serizawa by directly comparing the above model to transient CHF data. Besides this empiricism, Serizawa's model may also be questioned because of neglecting the hydrodynamic effect on the rate of change of the liquid layer thickness. As proposed by Haramura and Katto (1983), the liquid layer thickness is a function of the Helmholtz instability wavelength, which is, in turn, a strong function of the surface heat flux. Therefore, between $t_{CHF,SS}$ and $t_{CHF,TR}$ the liquid layer thickness changes not only due to evaporation but also due to the change in the vapor velocity within the stems, which affects the Helmholtz instability wavelength.

Finally, the author thinks that a constant liquid supply to the liquid layer is not realistic. This liquid supply, W_f, is related to

radial velocity fluctuations at the bubbly layer-core interface, and only the fluctuations larger than the vapor velocity flowing away from the surface can penetrate the bubbly layer, as postulated by Weisman and Pei (1983). Since the vapor velocity is a function of the surface heat flux, then W_f is a function of surface heat flux, which is, in turn, a function of time.

In the following section, the above discussed items are incorporated into the transient CHF formulation.

Transient CHF Correlation

Similar to the earlier correlations for pool boiling, the rate-of-change of the liquid layer thickness may be written as

$$d\delta/dt = MAX\{|(\partial\delta/\partial q)(dq/dt)|, |[q/f_2'(P)] - W_f/[\rho_f(1-A_v/A_w)A_w]|\} \quad (141)$$

where

$$f_2'(P) = \rho_f h_{fg} (1 - A_v/A_w)(1 + C_p \Delta T_{SUB}/h_{fg}) \quad (142)$$

This equation is similar to Equation 136 with the addition of the liquid supply term. As in the previous discussions, δ_c is related to the surface heat flux through the following relation:

$$\delta_c = f_1(P)/q^2 \quad (143)$$

The first two terms on the RHS of Equation 141 have the same physical meaning as in Equation 96. However, Equation 141 has an additional

third term on the RHS which mathematically models the liquid supply to the liquid layer. In order to integrate Equation 141, q and W_f must be known as a function of time. For an exponential power transient, using the quasi-steady conduction model, the surface heat flux may be expressed in the same exponential form, as given by Equation 110. In this section, the transient CHF correlation is developed for an exponential increase of the surface heat flux.

Evaluation of the Liquid Supply Term, W_f. W_f is related to the radial velocity fluctuations for a given flow field. These radial velocity fluctuations are a function of the distance from the heater wall and the flow velocity outside the boundary-layer. The velocity fluctuations which are of interest to the present problem are the ones at the liquid-bubbly layer interface. The bubble boundary layer, during power transients, may not be as well developed as in steady-state conditions. Therefore, the boundary-layer thickness may be less than for steady-state conditions, but this thickness remains constant between the time the surface heat flux reaches $q_{CHF,SS}$ and the time it reaches $q_{CHF,TR}$. This is due to the fact that both phenomena occur during the same generation of bubbles. Thus, between $t_{CHF,SS}$ and $t_{CHF,TR}$, the bubbly layer thickness is constant, and furthermore, the flow velocity U does not change appreciably because of the nature of the transient, which implies that the radial velocity fluctuations remain essentially unchanged during this period. However, this does not necessarily mean that the quantity W_f remains unchanged. W_f includes the only radial velocity fluctuations which can enter the bubbly layer. Weisman and Pei (1983) postulate that the only radial

velocity fluctuations that can enter the bubbly-layer are those which are larger than the vapor velocity v_v which, in turn, is directly proportional to the surface heat flux.

In order to evaluate W_f, the expected value of the radial velocity fluctuations which enter the bubbly layer must be computed. It is assumed that the liquid which enters the bubbly layer eventually reaches the heater surface, due to the high turbulence within the bubbly layer. This assumption was successfully used by Weisman and Pei (1983) in the analytical formulation of steady-state CHF at low qualities. The expected value of v(t) may be expressed by

$$E(v) = \int_{v_v}^{\infty} (v - v_v)p(v)dv \tag{144}$$

where p(v) is the probability density function for the radial velocity fluctuations. A normal distribution for v is a realistic assumption (Weisman 1983). But, for the purpose of the present study, a normal distribution creates some computational difficulties. Here, a simpler distribution is assumed as:

$$p(v) = C_1/v^{n'} \tag{145}$$

where C_1 is a constant and n' is an integer, such that $n' \geq 3$. This approximation may be quite accurate, if v_v is larger than three standard deviations, i.e., the integration of Equation 144 is over the upper tail of the normal distribution. In the present problem, since

the surface heat flux is high, v_v is expected to satisfy the above conditions. This approximation is illustrated in Figure 88. The term n' is restricted to values larger than 3 to yield the right probabilistic limit in Equation 144. Using equations 144 and 145, the following results may be obtained:

$$E[v(t)]/E[v(t_{CHF,SS})] = [v_v(t_{CHF,SS})/v_v(t)]^n \qquad (146)$$

where $n = n' - 2$. Since W_f is directly proportional to v, which is, in turn, directly proportional to q, W_f may be formulated as:

$$W_f(t) = [q_{CHF,SS}/q(t)]^n W_{f,s} \qquad (147)$$

where n is an integer such that $n \geq 0$. For $n = 0$, this obviously corresponds to the condition when $W_f(t)$ is constant between $t_{CHF,SS}$ and $t_{CHF,TR}$. $n = \infty$ corresponds to the condition where the liquid supply is equal to zero.

Formulation of Transient CHF Correlation. In order to integrate Equation 141, first the switch-over point between the instability mechanism and the evaporation mechanism must be calculated. Similar to the procedure followed for saturated pool boiling, this point may be obtained by equating the slope of the instability line to the slope of the net evaporation line as follows:

$$(\partial\delta/\partial q)(dq/dt) = -[q/f'(P)] + W_f/[\rho_f A_W(1 - A_v/A_W)] \qquad (150)$$

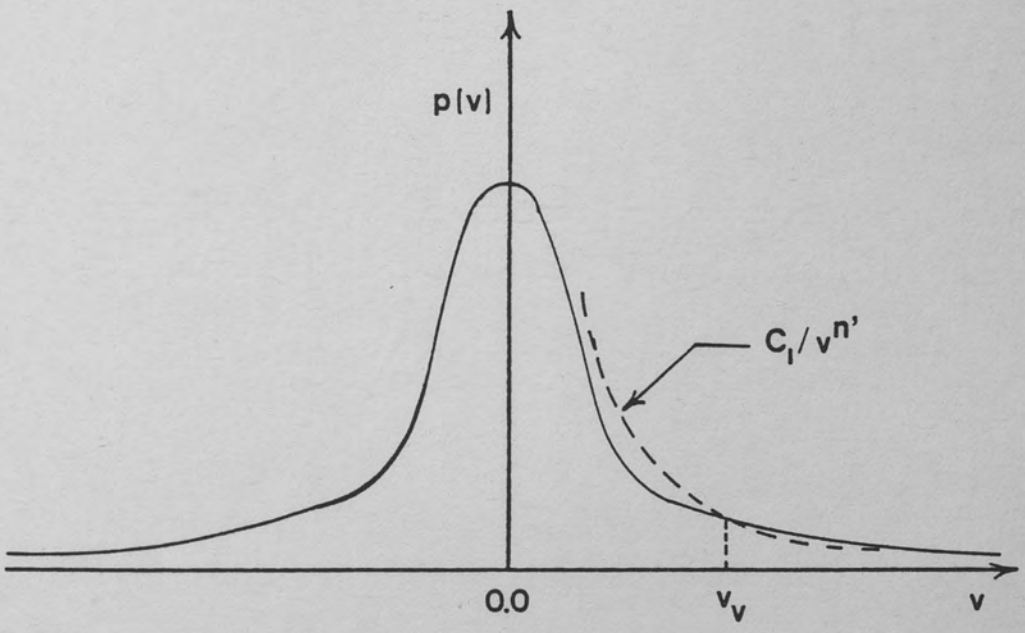

Figure 88. Probability Density Function for Radial Velocity Fluctuations.

By using equations 110, 142, 143 and 149, Equation 150 may be written as

$$-2f_1(P)/(q_B^2\tau) = - q_B/f_2'(P) + q_{CHF,SS}^{n+1}/[q_B^n f_2'(P)] \qquad (151)$$

Defining the time constant of the CHF phenomenon for forced convective boiling, τ_c, as

$$\tau_c = \delta_c\, f_2'(P)/q_{CHF,SS} \qquad (152)$$

using Equation 143 and substituting q_B by $B_s\, q_{CHF,SS}$, as suggested by Equation 99, Equation 151 yields

$$B_s^{n+1} - (2\tau_c/\tau)B_s^{n-2} = 1 \qquad (153)$$

When solved for B_s, Equation 153 always yields $B_s > 1$, for any positive, finite value of n, with two possible exceptions: if $\tau \to \infty$, B_s is always equal to 1, but this case corresponds to the steady-state problem; and if $n \to \infty$, the liquid supply term in Equation 150 vanishes and Equation 111 is recovered from Equation 153. Since B_s is always greater than 1, the following integral must be evaluated to determine the transient CHF:

$$(\delta_c)_{t=t_{CHF,SS}} = \int_{t_{CHF,SS}}^{t_B} [2f_1(P)(dq/dt)/q^3]dt \qquad (154)$$

$$+ \int_{t_B}^{t_{CHF,TR}} [q/f_2'(P)]dt - \int_{t_B}^{t_{CHF,TR}} W_f/[\rho_f(1 - A_v/A_w)A_w]dt$$

For an exponential power increase, and with the use of equations 142, 143 and 149, the above integral may be evaluated to yield

$$\delta_c(q_{CHF,SS}/q_B)^2 = [\tau/f_2'(P)](q_{CHF,TR} - q_B)$$

$$+ (1/n)[q_{CHF,SS}\ \tau/f_2'(P)][(1/q^n_{CHF,TR}) - (1/q_B^n)] \qquad (155)$$

Finally, defining $q_B = B_s\ q_{CHF,SS}$ and using Equation 152, the final transient CHF correlation for forced convective boiling may be obtained as follows:

$$\eta^{n+1} - \{[(n\tau_c/\tau) + nB_s^3 + B_s^2]/(nB_s^2)\}\ \eta^n + B_s^n/n = 0 \qquad (156)$$

This equation, along with Equation 153, may be solved for η once the value of n is determined. In the above Equation, τ_c is the time constant of the CHF phenomenon in forced convective boiling for the DNB mechanism. It is defined by Equation 152, and it physically represents the time required for the complete evaporation of the liquid layer, once the steady-state CHF level is reached.

If the same heater is horizontally placed in a pool of saturated liquid, τ_c becomes τ_d, as previously defined. Mathematically, τ_c may be related to τ_d as follows:

$$\tau_c = (q_{CHF,SS,OO}/q_{CHF,SS})^3(1 + C_p \Delta T_{SUB}/h_{fg})\tau_d \qquad (157)$$

The Effect of n on Transient CHF Correlation. Equations 153 and 156 show that the value of η depends upon the choice of n. Therefore, before these equations can be compared to data the value of n must be determined. Another governing variable in equations 153 and 156 is the ratio τ_c/τ. The effect of n on the transient CHF for various values of τ_c/τ is shown in Table 13. In this table, n = o, n = 1, n = 2, and n = ∞ are considered. Obviously, n is not restricted to integer values and may assume any positive real value.

When n = o, this corresponds to constant liquid supply conditions. Equations 153 and 156 reduce to

$$B_s^2 (B_s - 1) = 2\tau_c/\tau \qquad (158)$$

$$\eta - \log(\eta/B_s) = [B_s^3 + (\tau_c/\tau)]/B_s^2 \qquad (159)$$

For n = 1 equations 153 and 156 reduce to

$$B_s (B_s^2 - 1) = 2\tau_c/\tau \qquad (160)$$

$$\eta^2 - \{[(\tau_c/\tau)/B_s^2] + B_s + 1\}\eta + B_s = 0 \qquad (161)$$

For n = 2, equations 153 and 156 reduce to

TABLE 13

THE EFFECT OF n ON η FOR VARIOUS VALUES OF τ_c/τ

τ_c/τ	η for n=o	η for n=1	η for n=2	η for n=∞
5	3.75	3.61	3.51	3.23
3	3.20	3.11	3.10	2.44
2	2.89	2.77	2.70	2.26
1	2.4	2.29	2.20	1.89
0	1	1	1	1

$$B_s = [\ 1 + 2\tau_c/\tau]^{1/3} \tag{162}$$

and

$$\eta^3 - [(3B_s^3 + B_s^2 - 1)/(2B_s^2)]\eta^2 + (B_s^2/1) = 0 \tag{163}$$

When $n \to \infty$ Equation 153 becomes

$$B_s = (2\tau_c/\tau)^{1/3} \tag{164}$$

and Equation 156 yields

$$\eta = 1.89(\tau_c/\tau)^{1/3}\ , \text{ for } B_s \leq 1 \tag{165}$$

For $B_s < 1$, η is given by

$$\eta = 1 + \tau_c/\tau \tag{166}$$

Since $n = \infty$ corresponds to no liquid supply, the resemblance of equations 164, 165, and 166 to equations 111, 114 and 115 is not surprising. The solutions of equations 158 through 166 are given in Table 13 for various values of τ_c/τ.

Figure 89 shows the present correlation as compared with the data of Kataoka (1983) for various values of n. This set of data corresponds to forced convective boiling data with saturated liquid flowing at a velocity U = 2.67 m/s and at a pressure 0.594 MPa. The data shows that for best predictions, n must be chosen between 2 and ∞, but $n = \infty$ gives a close prediction. Hereafter, for comparing the correlation with the data, $n = \infty$ is used. Again, $n = \infty$ means that there is no liquid supply.

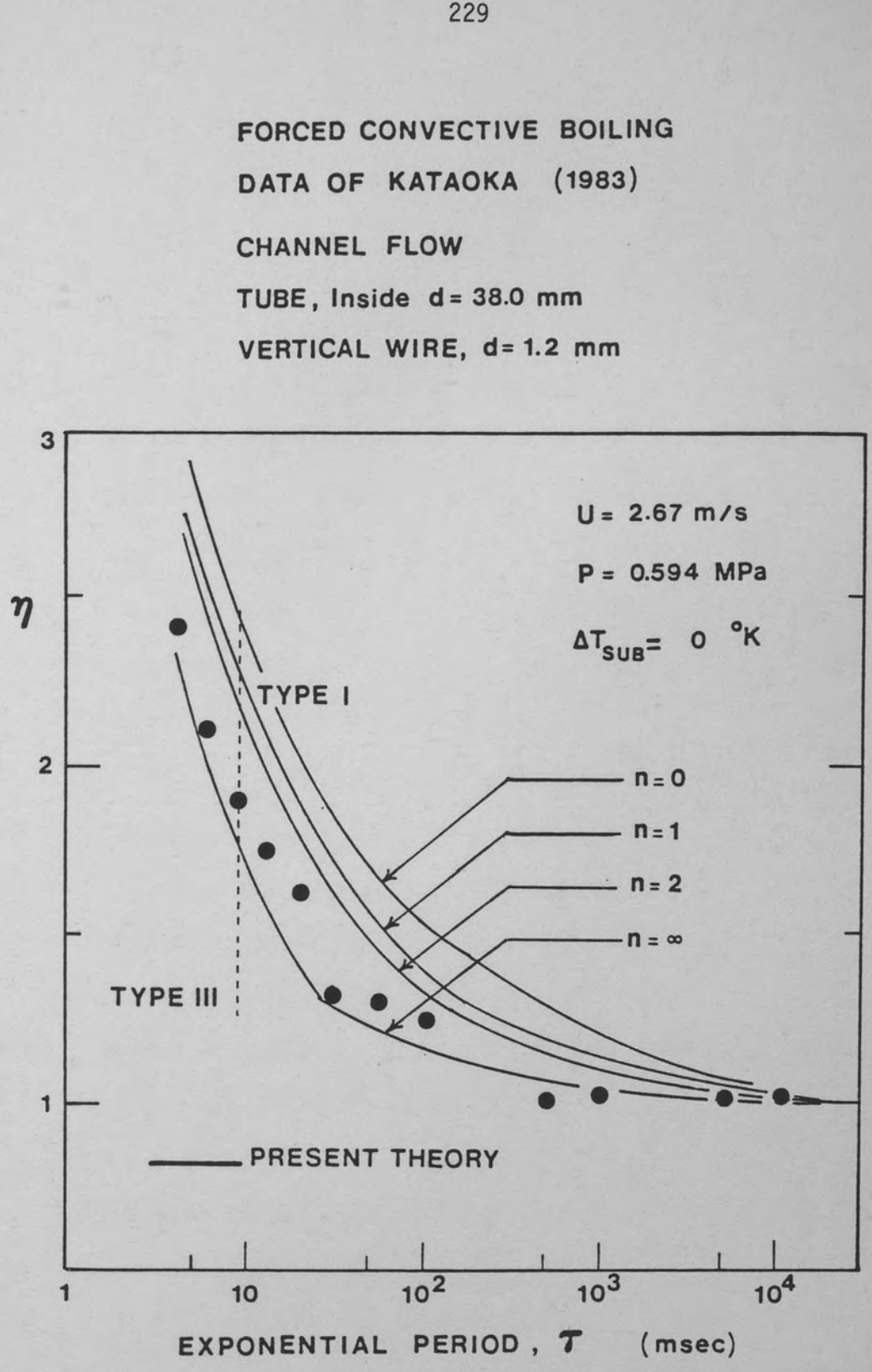

Figure 89. Comparison of the Present Theory with the Data of Kataoka et al. (1983) for Various Values of n.

Comparison with Data

When n is set equal to ∞, Equation 156 reduces to Equation 116. This equation is valid when the surface heat flux is increasing exponentially with an exponential period τ. This situation is present when the power generation rate increases exponentially and when the quasi-steady conduction model may be used to relate the surface heat flux to the power generation rate. In the rest of this section, Equation 116 is compared to forced convective boiling data, assuming the quasi-steady conduction model may be used. Figures 90 through 100 show the present correlation compared to the data of Kataoka et al. (1983). The experimental setup of Kataoka et al. (1983) is summarized in Chapter VII. The figures are self-explanatory in terms of experimental conditions like pressure, flow velocity, subcooling, and heater geometry. In all the cases, the agreement between the data and the present correlation is good. In general, the slight deviation between the data and the present theory may be attributed to various simplifying assumptions made in analyzing the effect of subcooling as well as to the assumed choice of ∞ for n in Equation 156. In these figures, the dotted lines show the empirical correlation of Kataoka et al. (1983) given by Equation 72.

The present theory is also compared with the data of Aoki et al. (1974). In this experiment, vertical flow in an annulus was tested. The vertical heater of 5 mm diameter which experienced an exponential power transient was placed inside a tube with an inner diameter of 8 mm. The minimum exponential period tested was about 50 msec. Since the subcooling was low during these experiments, saturated conditions

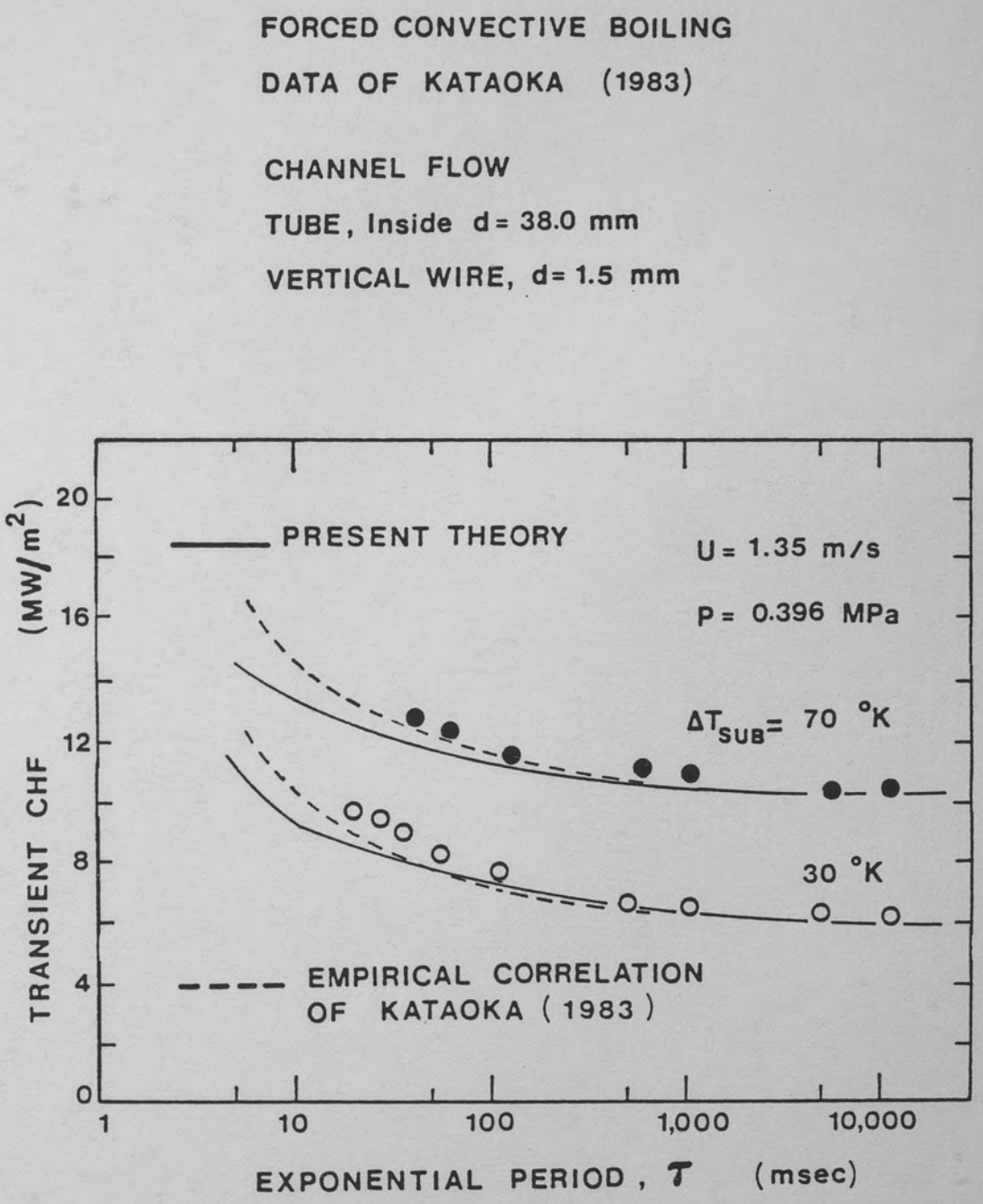

Figure 90. Comparison of the Present Theory with the Data of Kataoka et al. (1983)

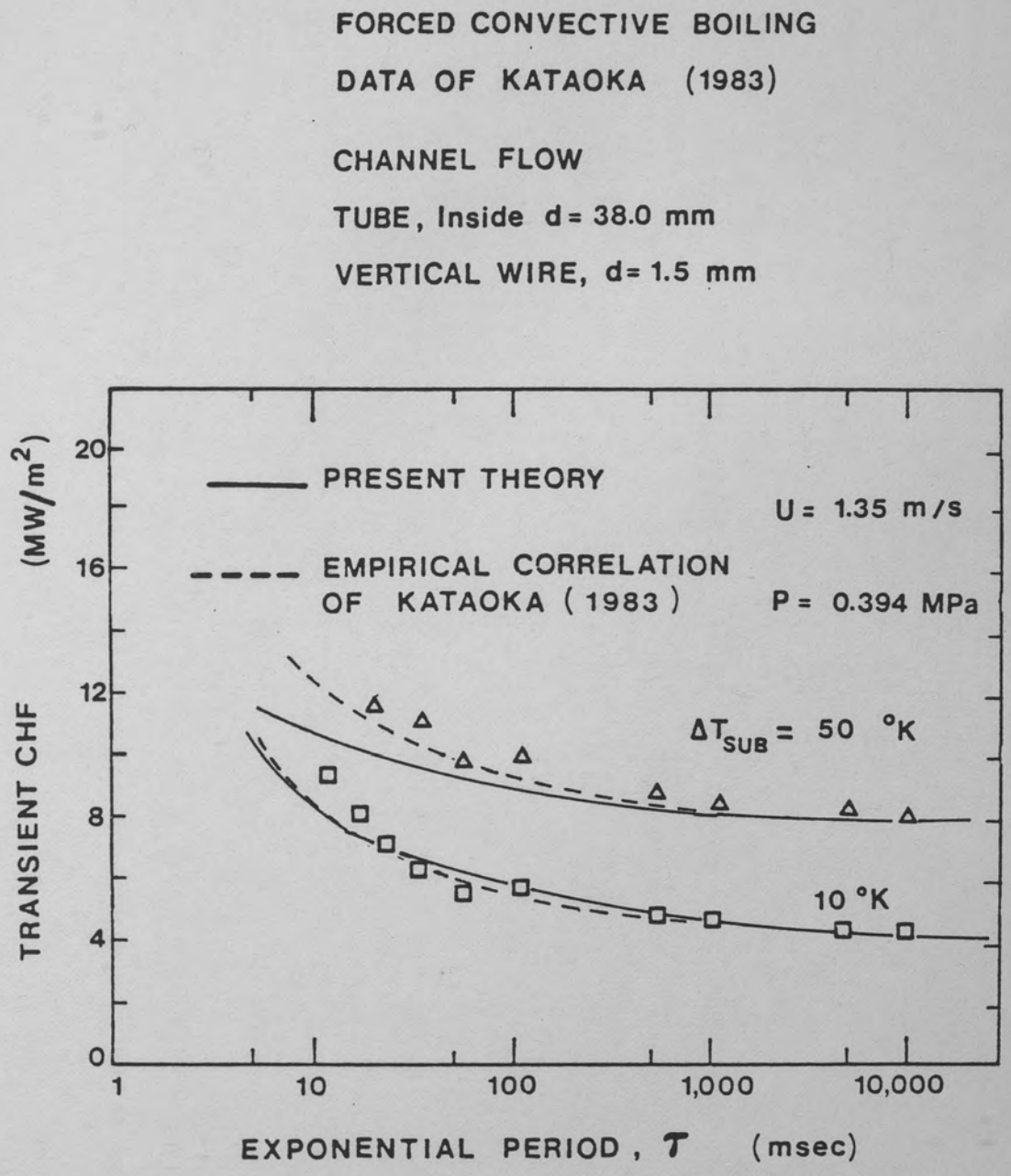

Figure 91. Comparison of the Present Theory with the Data of Kataoka et al. (1983)

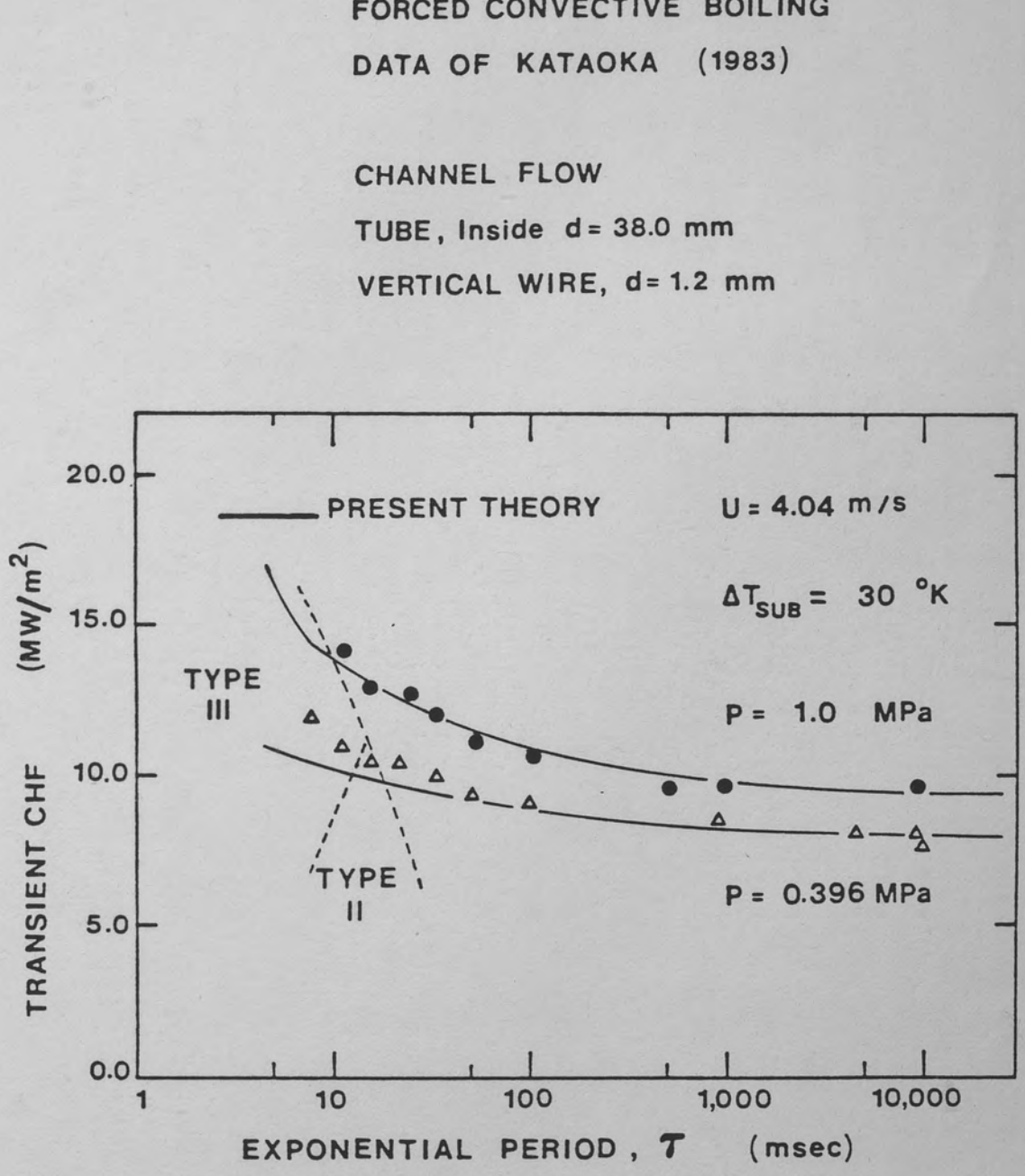

Figure 92. Comparison of the Present Theory with the Data of Kataoka et al. (1983)

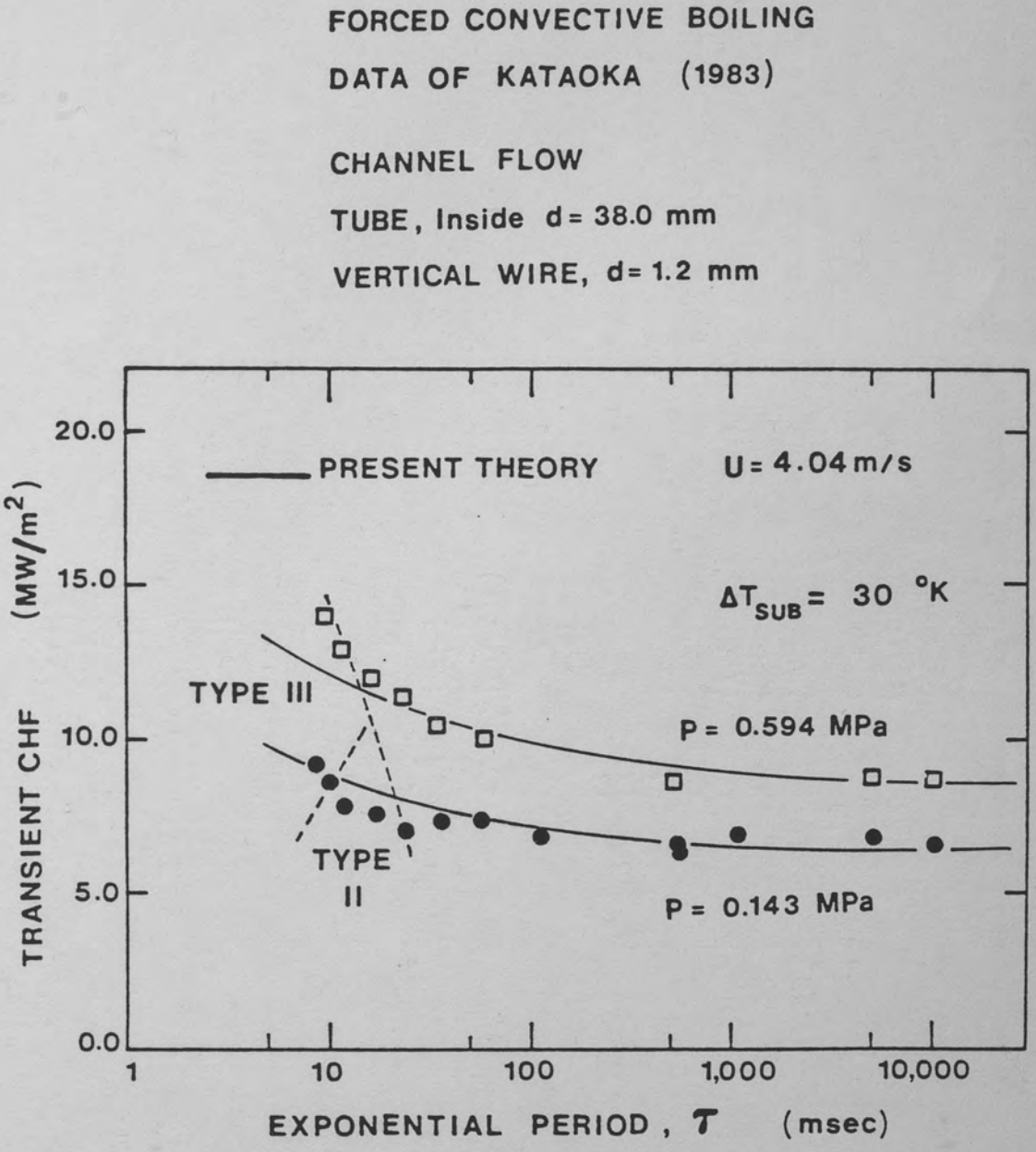

Figure 93. Comparison of the Present Theory with the Data of Kataoka et al. (1983)

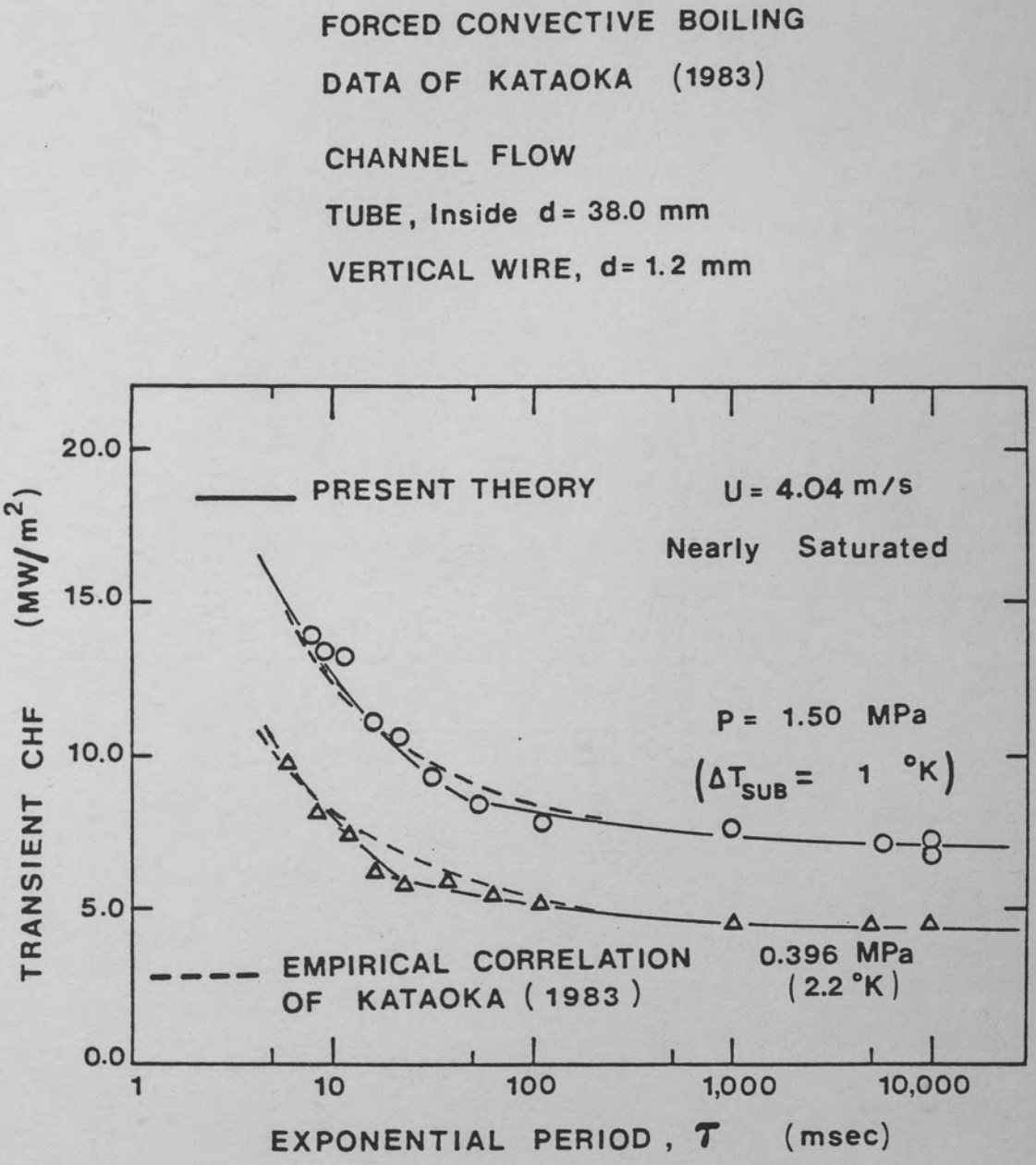

Figure 94. Comparison of the Present Theory with the Data of Kataoka et al. (1983)

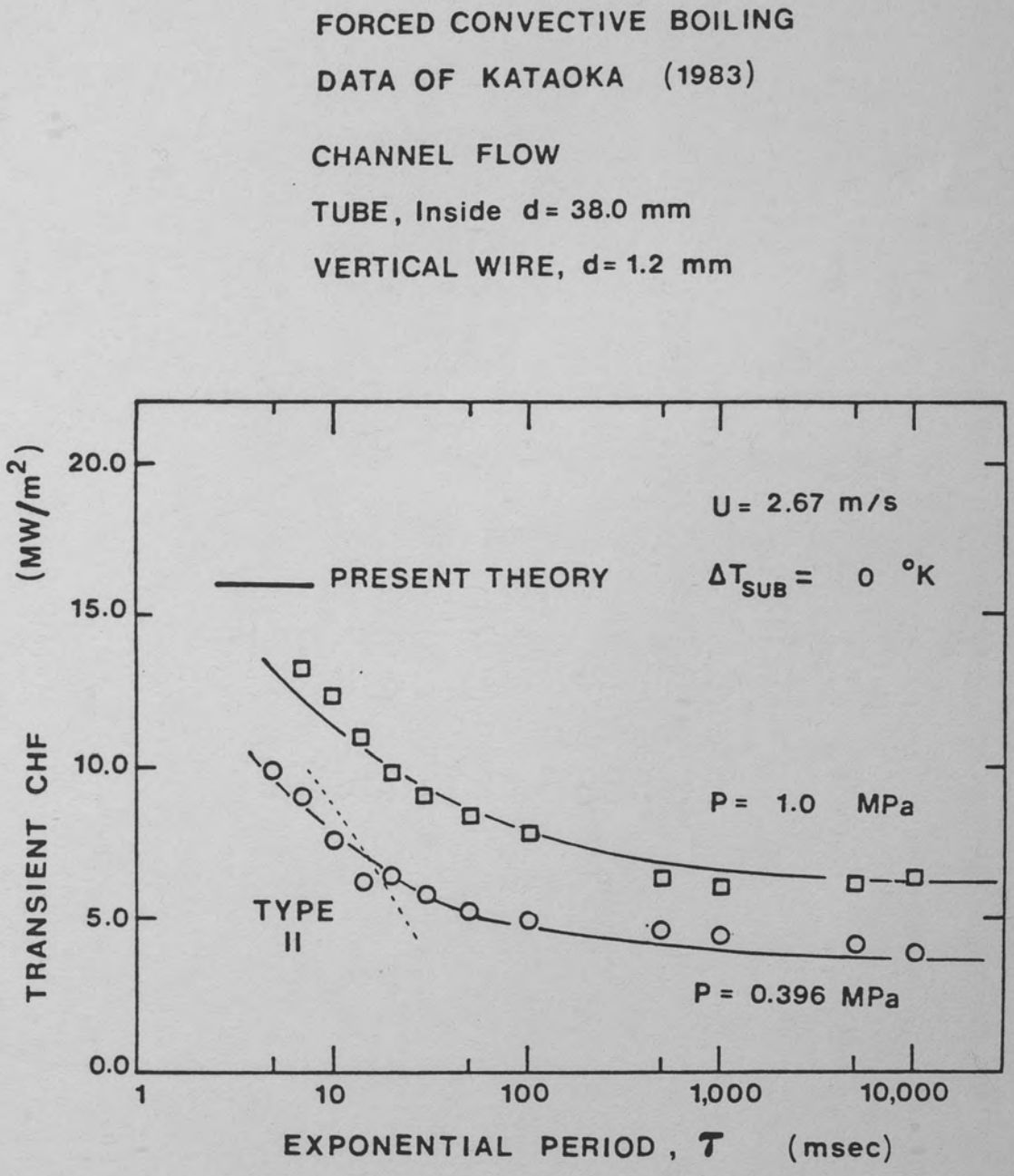

Figure 95. Comparison of the Present Theory with the Data of Kataoka et al. (1983)

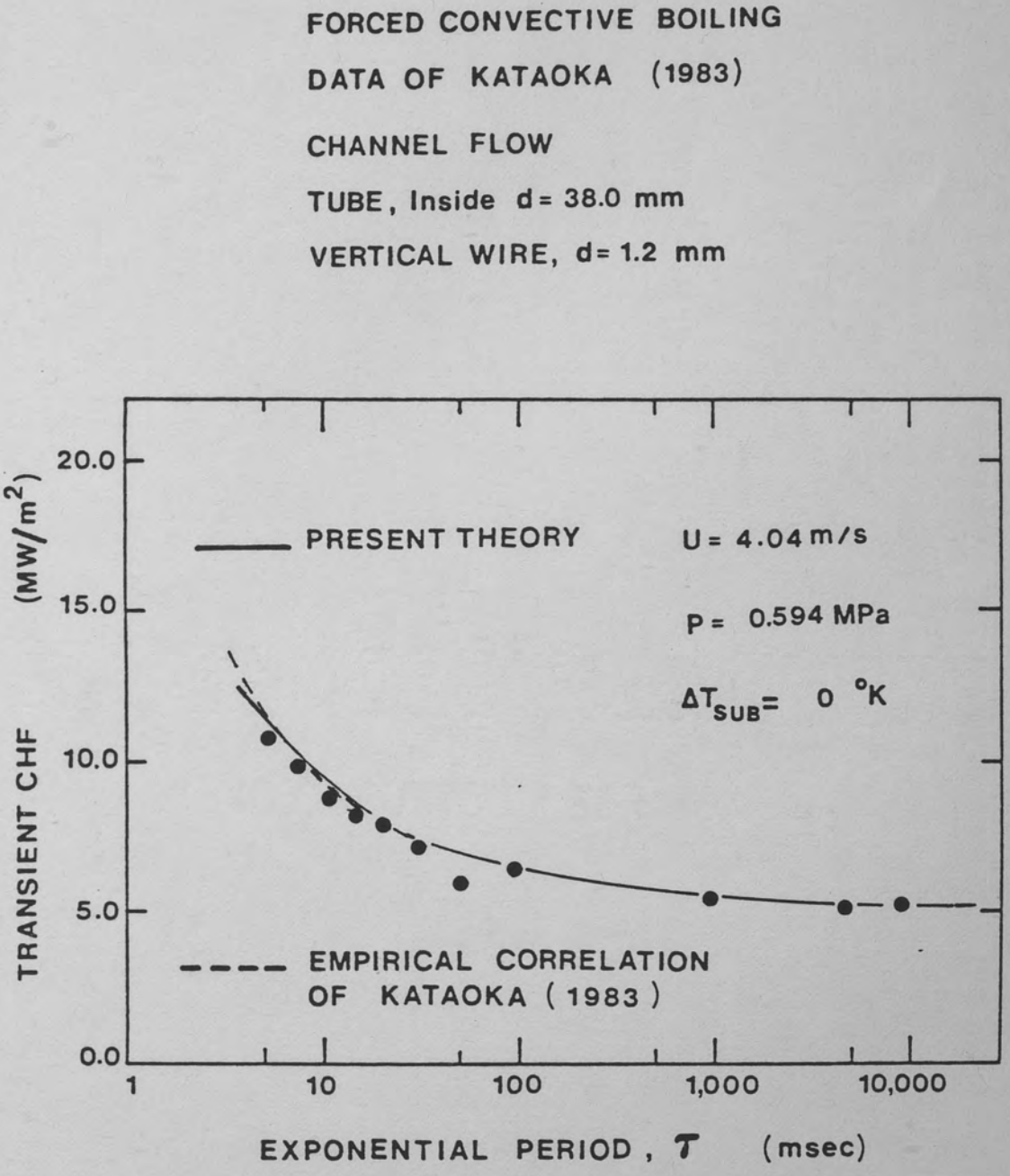

Figure 96. Comparison of the Present Theory with the Data of Kataoka et al. (1983)

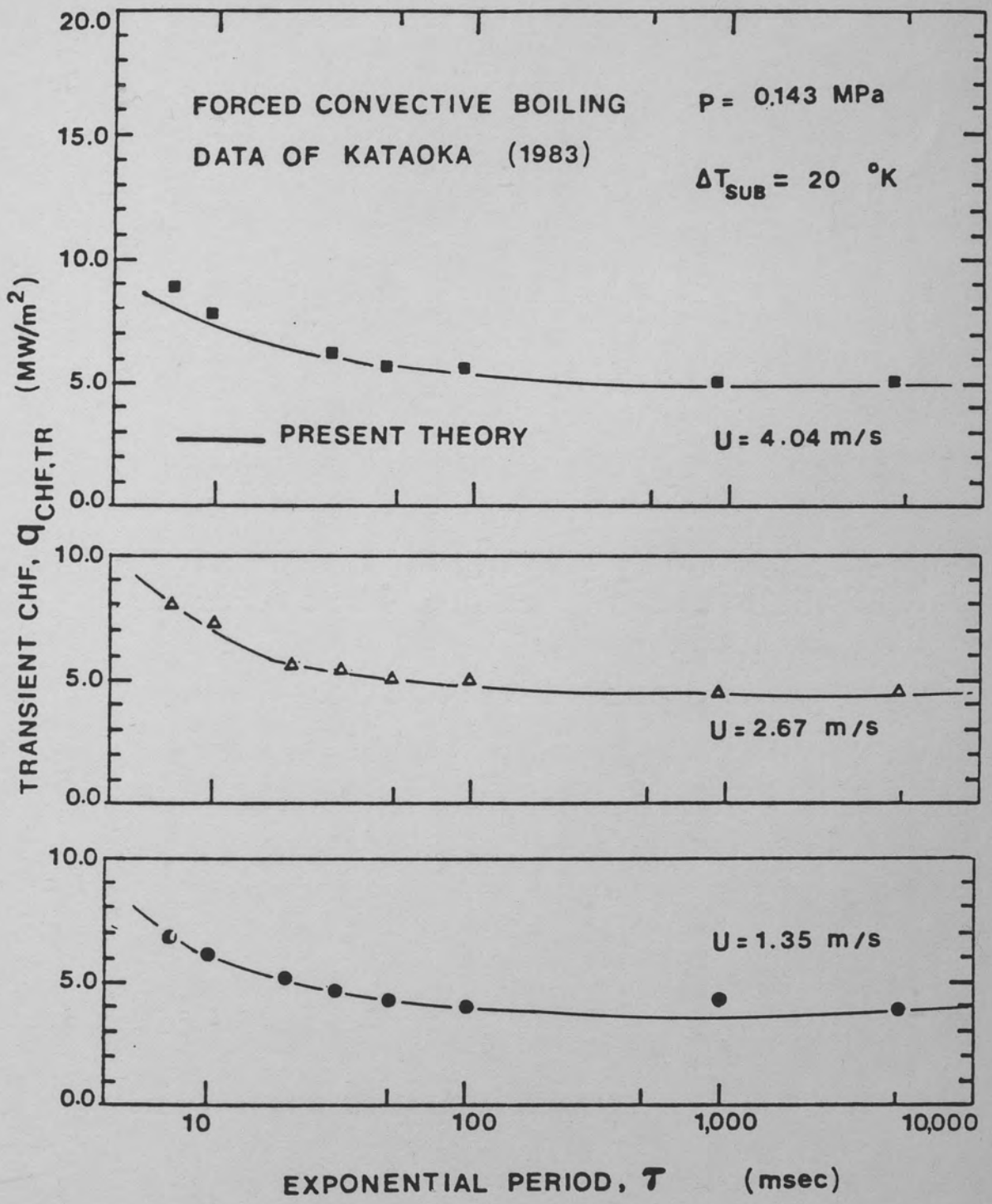

Figure 97. Comparison of the Present Theory with the Data of Kataoka et al. (1983)

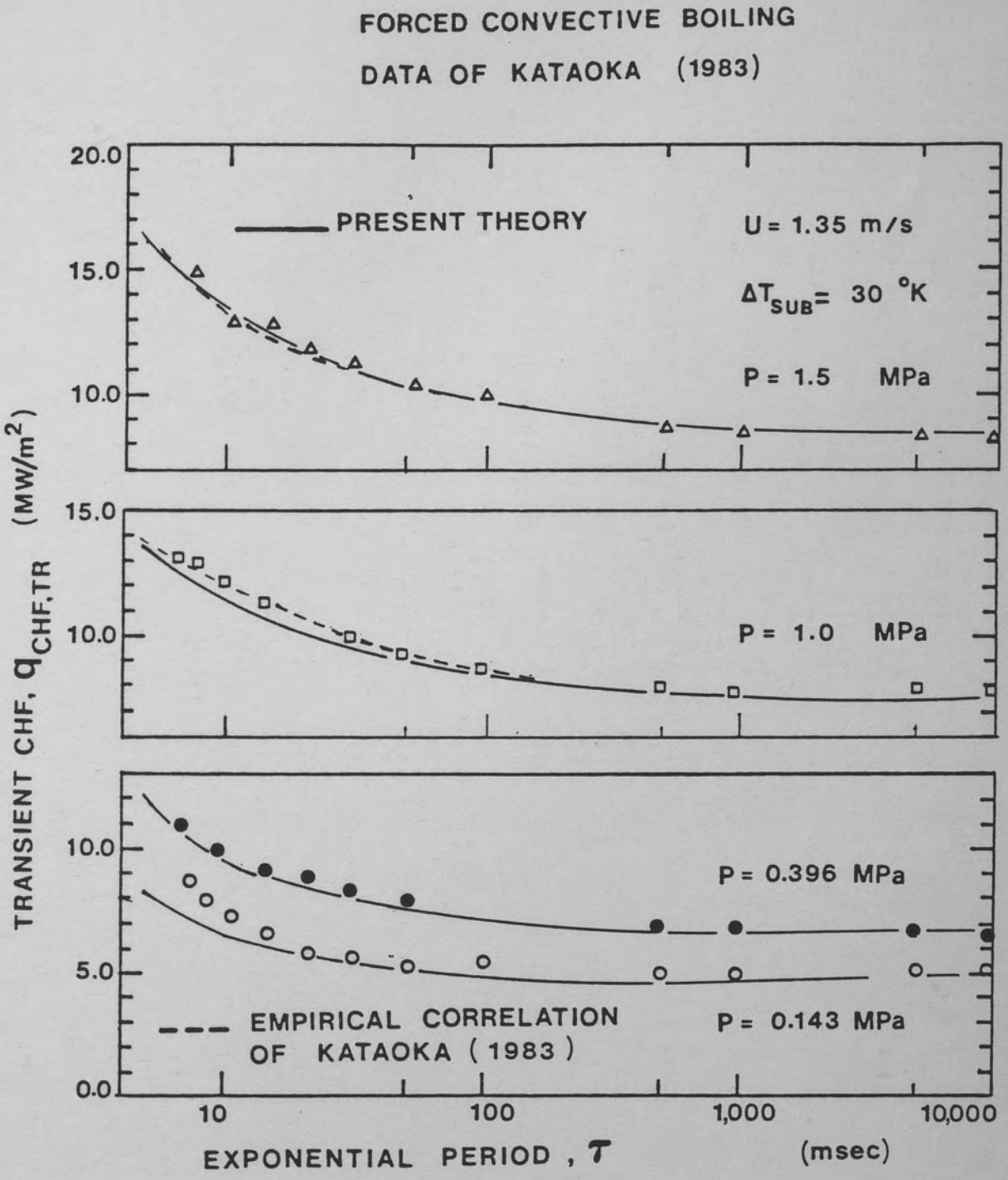

Figure 98. Comparison of the Present Theory with the Data of Kataoka et al. (1983)

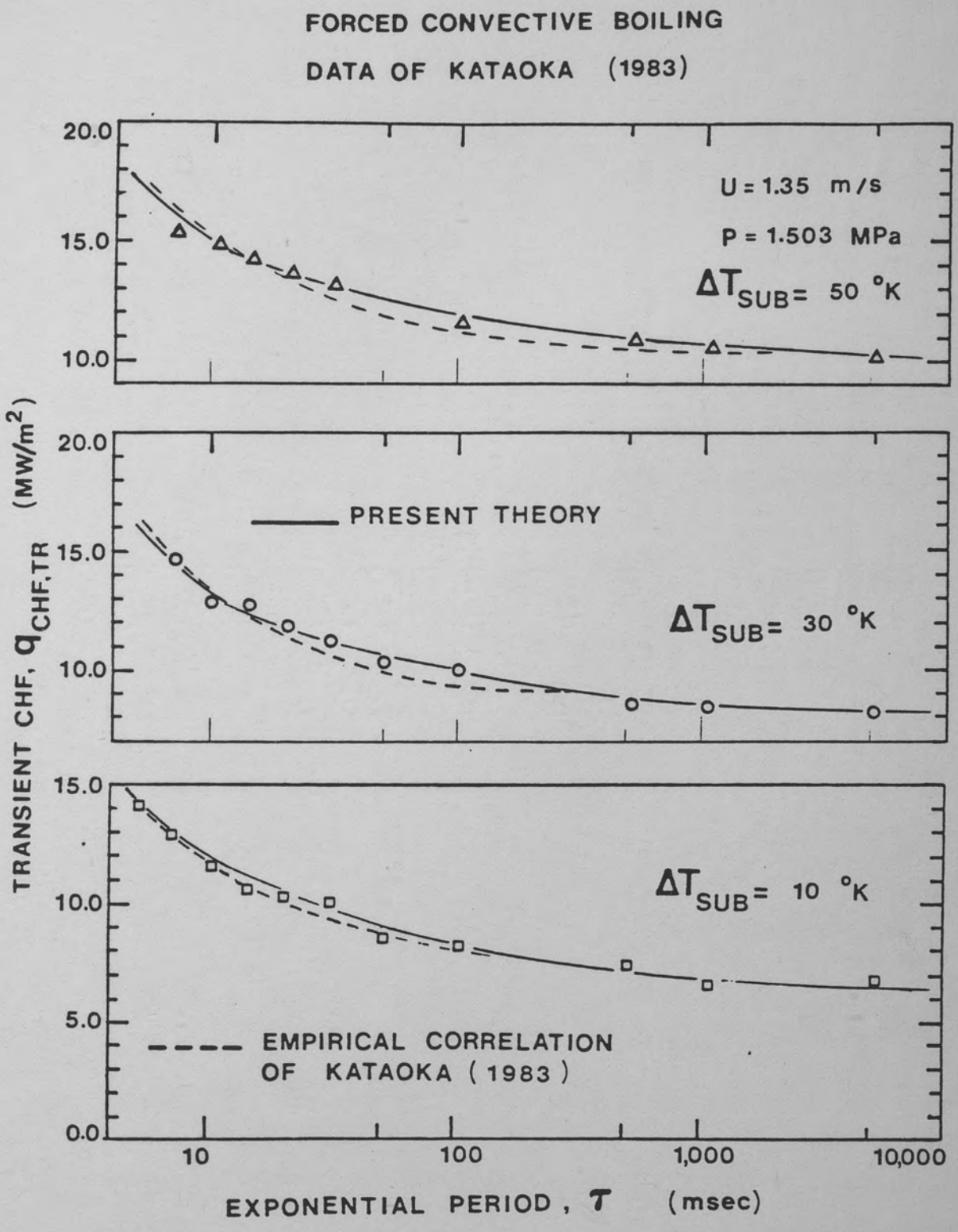

Figure 99. Comparison of the Present Theory with the Data of Kataoka et al. (1983)

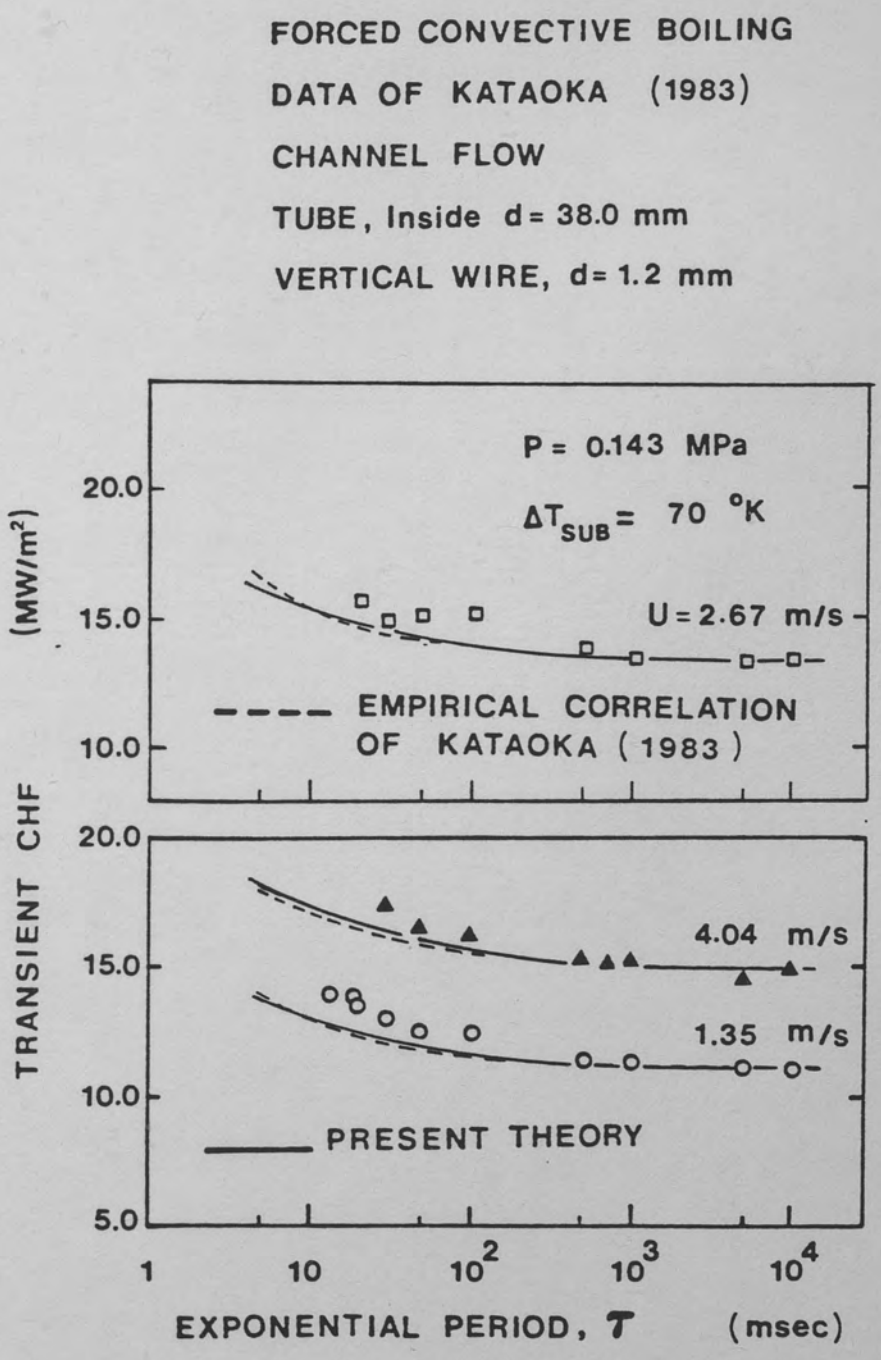

Figure 100. Comparison of the Present Theory with the Data of Kataoka et al. (1983)

are assumed in plotting the present correlation. The agreement is again quite favorable, as shown in Figure 101.

Summary of the Theoretical Transient CHF Predictions

In this chapter, a transient CHF theory was developed for horizontal heaters in pool boiling and vertical heaters in pool and forced convective boiling. For these two problems, it is observed that the mechanisms which lead to CHF during steady state conditions are different. The CHF mechanisms are illustrated in Figure 102. For pool boiling on horizontal heaters, the CHF is mathematically formulated by equations 91 and 121. In this mechanism, there is no liquid supply to the liquid layer underneath the bubble during the bubble growth period. When the bubble departs from the surface, or when it collapses, the liquid layer replenishes to its maximum thickness determined by the Helmholtz instability. However, for boiling over the vertical surfaces with or without forced convective flow, the bubbles do not depart from the surface. They travel parallel to the heater surface, forming a bubble boundary layer. In this configuration, the liquid layer may not be reformed after the bubble departs, but it is continuously fed from the bulk liquid. Therefore, the liquid supply becomes the dominant CHF parameter, and the steady state CHF is formulated by Equation 138 as suggested by Serizawa (1983). In this chapter, the transient CHF is formulated by taking the liquid supply into account, and a general expression is developed as given by equations 153 and 156. However, the comparison of Equation 156 to transient CHF data suggests that n must be large and $n = \infty$ is quite successful in correlating the data. Physically, this suggests that

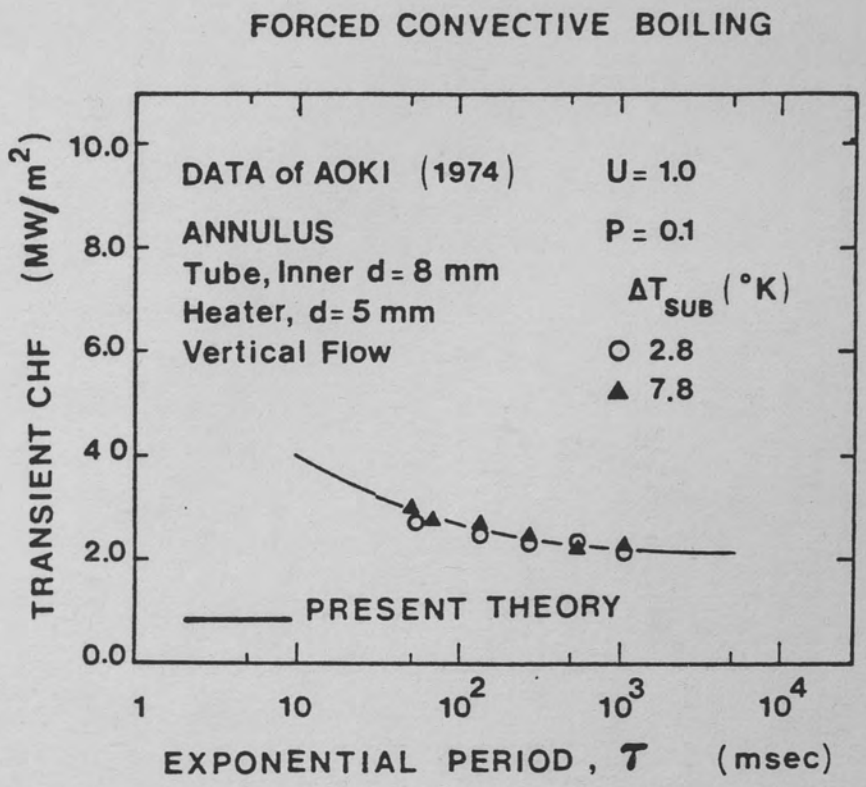

Figure 101. Comparison of the Present Theory with the Data of Aoki et al. (1974)

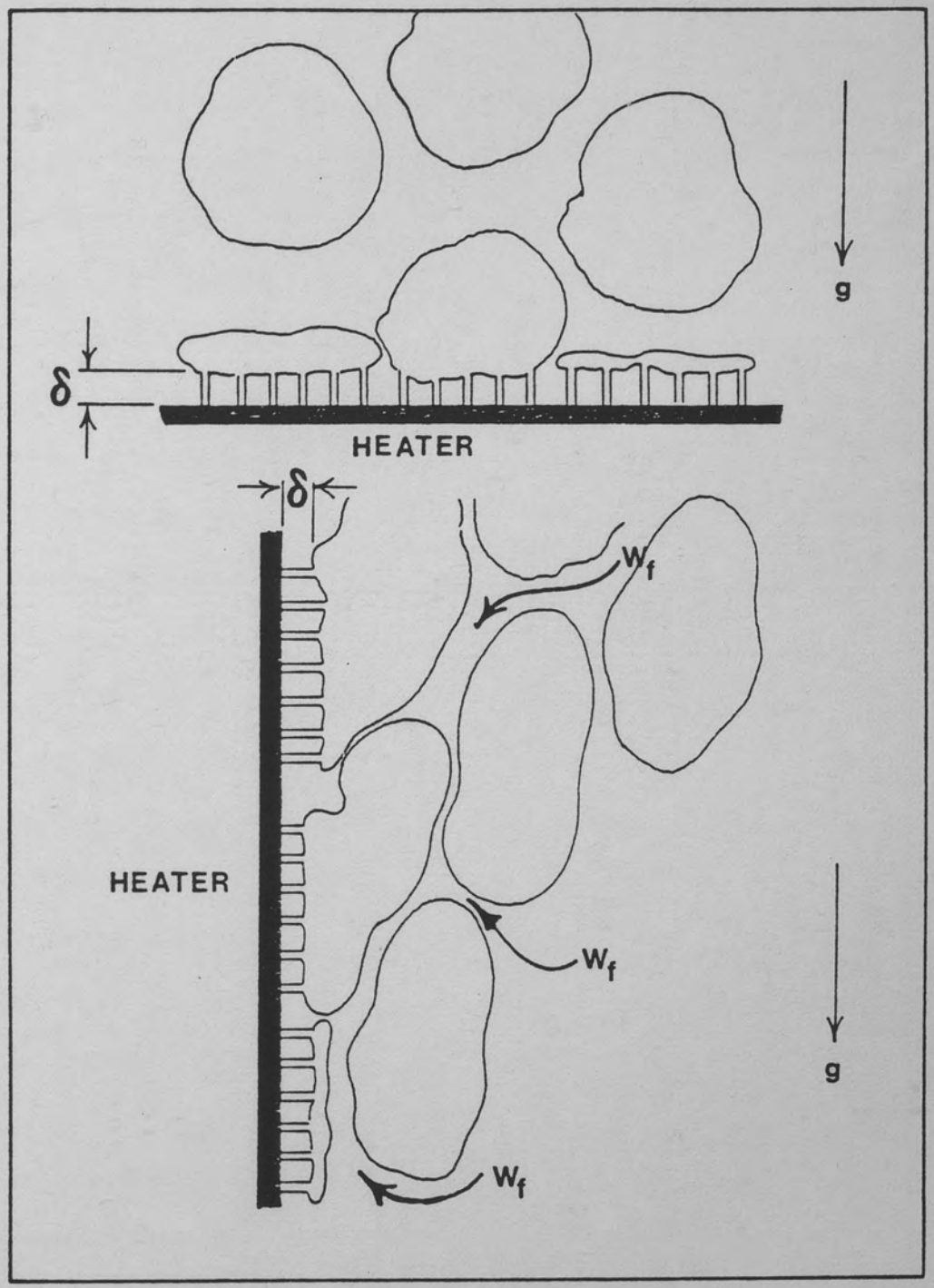

Figure 102. The Different CHF Mechanisms Considered By the Present Theory

there is very little or no liquid supply to the liquid layer between $t_{CHF,SS}$ and $t_{CHF,TR}$. Therefore, the liquid supply, although important during nucleate boiling, has minimal effect on the transient CHF. Therefore, these two situations are the extreme cases. There may be problems in which both mechanisms may be equally important. Small disk heaters placed in a pool of water, inclined surfaces with or without forced convective flow, horizontal surfaces with forced convective flow, flat ribbon heaters with small width and placed vertically in a pool of water are such candidates.

The present theory has difficulty in correlating the data from flat ribbon heaters. This geometry is shown in Figure 103. In this problem with small vertical dimension, both mechanisms are important. There is a continuous liquid supply to the liquid layer from the bottom. On the other hand, when the bubble departs, the liquid layer may be reformed, since the bubbles do not block the bubble liquid. Therefore, for such a problem, the steady state CHF must be formulated to include both mechanisms. This, in turn, affects the transient CHF formulation. A further analysis of this problem is possible, but, since this geometry is not of specific interest to the nuclear industry, such an effort may be too academic, and it is not included here.

For the problems mentioned above, with an exponential increase in the surface heat flux, the present theory may be expressed as follows:

$$\eta^{n+1} - \{[(n\,\tau_c/\tau) + nB_s^3 + B_s^2]/(nB_s^2)\}\eta^n + B_s^n/n = 0 \qquad (167)$$

where B_s is given by:

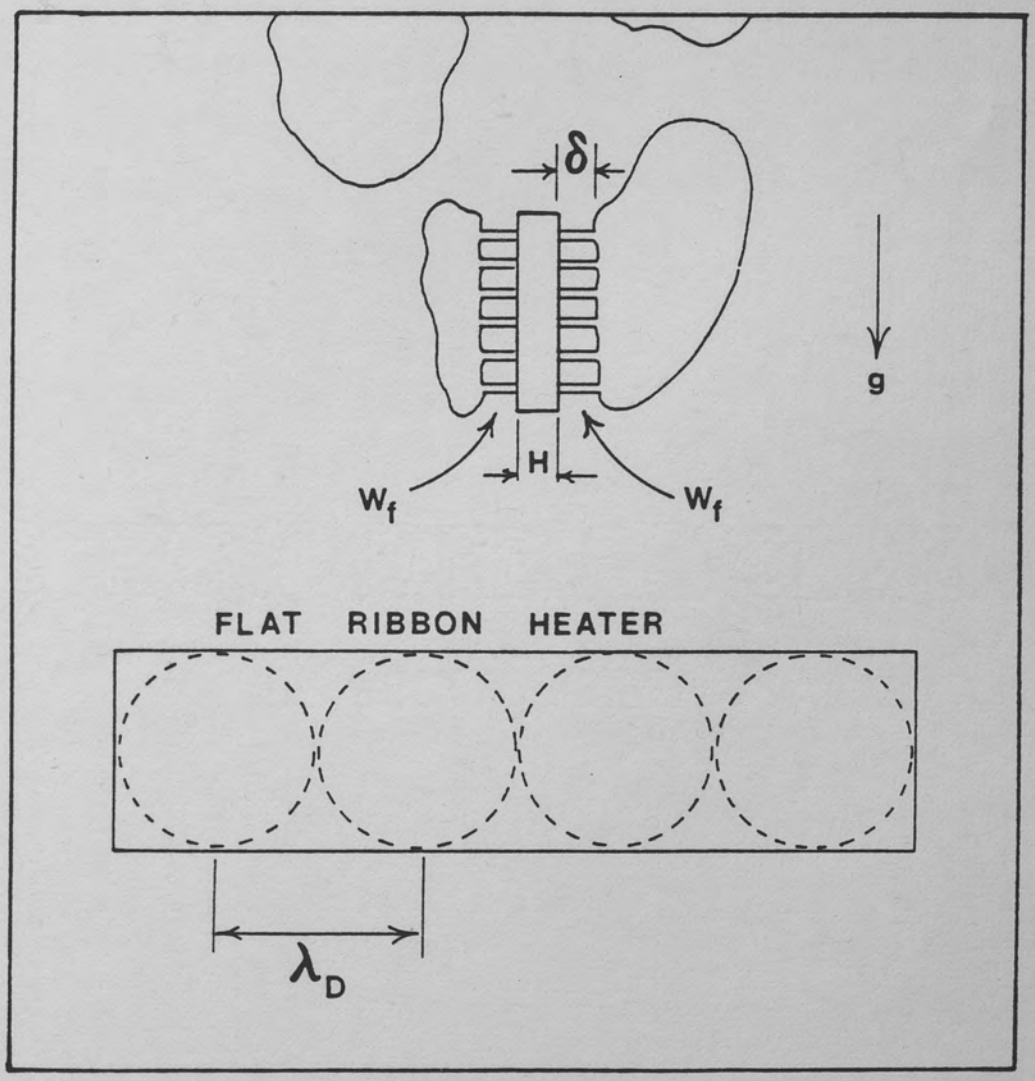

Figure 103. CHF Mechanism for Flat Ribbon Heaters

$$B_s^{n+1} - (2\tau_c/\tau)B_s^{n-2} = 1 \qquad (168)$$

For pool boiling over horizontal surfaces and forced convective boiling over vertical heaters, n is equal to ∞ is assumed, and the above equation reduces to Equation 116.

When n = 0, Equation 168 reduces to Equation 159, which corresponds to the physical situation where the liquid supply to the liquid layer is constant. This situation may arise in external flow situations, where liquid is supplied to the liquid layer either from the heater surface or by a liquid jet supplied through a nozzle located near the surface. No comparison with data is made for this case.

In general, the present theory is quite successful in highlighting the governing physics of the transient CHF during power transients. It is quite successful in correlating the DNB data, and it is possibly more complete than the theory developed by Serizawa (1983), due to the following reasons:

a. It is purely analytical, as opposed to extensive empiricism used by Serizawa (1983) in formulating the liquid layer thickness.
b. It incorporates the effect of Helmholtz instability wavelength on the liquid layer thickness, which is ignored by Serizawa (1983). If evaporation is assumed to be the only mechanism controlling the liquid layer thickness, as suggested by Serizawa (1983), the data is very much overpredicted.
c. The present theory suggests that the effect of liquid supply to the liquid layer is zero (or minimal).

The present theory, however, requires further improvements. The

following items are the ambiguous points of the present theory:

a. The accuracy of Equation 15 in quantifying τ_d must be investigated.

b. The use of an equivalent diameter for flat ribbon heaters in calculating τ_d may not be very appropriate.

c. The various simplifying assumptions employed in calculating τ_g in subcooled boiling need to be justified in terms of their net contribution.

d. The validity of the quasi-steady conduction requires further study.

e. Finally, once all the above ambiguities are clarified, the exact value of n by direct comparison to data may be obtained. Thus, the effect of the liquid supply may be determined.

The geometry of concern in nuclear reactors is a vertical heater with forced convective flow around it. Therefore, Equation 167 in conjunction with Equation 168 may be used to predict the transient CHF during power transients. As the subcooling and the flow velocity increase, the ratio of transient CHF to steady-state CHF, denoted by η, decreases for a given exponential period τ. Furthermore, in nuclear fuel rods, the quasi-steady conduction model is not as valid as in electrical heaters. During the conduction analysis of the problem, it is observed that the quasi-steady conduction model is possible if the dimensionless group $[\rho C_p R^2/(k \tau)]$ is very small. In nuclear fuel rods, however, the radius is larger than the electrical heaters of the experiments studied here, and the thermal diffusivity $(k/\rho C_p)$ is smaller. Therefore, the quasi-steady conduction model is only possible for large exponential periods, in which case the steady-

state CHF is close to the transient CHF. For small values of τ, the above dimensionless group becomes large, and most of the generated energy remains stored within the fuel pellets. Thus, the surface heat flux increases at a slower rate than the heat generation rate, which again results in the transient CHF close to the steady-state CHF. Therefore, during power transients in nuclear fuel elements, the quasi-steady approach in determining the transient CHF is more accurate than in electrical heaters.

The present theory is concerned with DNB mechanism. This is due to the fact that, if there is not an annular flow at the onset of a rapid transient, the flow will not have enough time to adjust itself to an annular flow. However, if the annular flow already exists at the onset of transient, the above theory needs to be modified. Essentially, the liquid layer thickness δ_c needs to be redefined and the liquid supply term must be written in terms of deposition and entrainment coefficients.

Finally, it must be understood that the present theory is directly aimed towards the prediction of η. The author makes no claim of predicting the steady-state CHF through a preferred CHF correlation. Therefore, for comparison with the data, the experimental values of steady-state CHF are incorporated into the present theory. However, by using an appropriate CHF correlation, it was also possible to predict these values within a reasonable margin, except for flat ribbon heaters.

CHAPTER IX

THEORETICAL CONSIDERATIONS OF HYDRODYNAMIC TRANSIENTS

One major type of transient which is of interest to the nuclear industry, i.e., the power transients, is analyzed in the previous chapter. Rapid depressurization and rapid reduction of coolant mass flow rate are two other major transients which concern the nuclear industry. These transients, referred to as hydrodynamic transients, are analyzed in the present chapter. The analysis, however, is restricted to first principles. Closed form transient CHF correlations are not developed for hydrodynamic transients as is done for power transients. Although they are relatively more complex by nature, such correlations are not impossible and are suggested as future research. First, the rapid depressurization experiments are analyzed.

Transient CHF During Rapid Depressurization

The two experimental studies aimed towards a fundamental understanding of transient CHF during rapid depressurization are the ones by Sakurai et al. (1980) and Aoki et al. (1974). These two studies yield conflicting results. The experiments of Sakurai et al. (1980) suggest that the transient CHF is smaller than the steady-state CHF, whereas, the experiments of Aoki et al. (1974) suggest the

opposite. In these two experiments, the nature of the boiling heat transfer problem is different. The study of Sakurai et al. (1980) is concerned with pool boiling, whereas, Aoki et al. (1974) studied forced convective boiling in channel flow. But the major disagreement between the results may not be attributed to this. In fact, there are important differences in the transient parameters which directly affect the results. These are:

1. In the experiment of Sakurai et al. (1980), the transient is initiated at a non-boiling state, whereas, in the experiments of Aoki et al. (1974), the transient starts from a boiling state (or the heat flux is very close to the value for the initiation of boiling). Obviously, this results in considerable differences between the initial values of the CHF parameter in these problems. The maximum initial heat flux used by Sakurai et al. (1980) is 0.60 MW/m^2, and the initial heat flux used by Aoki et al. (1974) is 2.90 MW/m^2. The initial subcooling in the experiments of Sakurai et al. (1980) ranged from ~ 80° to ~ 130°C. Aoki et al. (1974) used a maximum inlet subcooling as 74°C. At the exit, the subcooling was lower than this value.
2. The initial pressures in the two experiments were also significantly different. Sakurai et al. (1980) used 1.90 and 1.08 MPa as initial pressures, whereas, the initial pressure for the experiment of Aoki et al. was ~ 0.3 MPa. In both experiments, the released pressure was the atmospheric pressure (0.1 MPa).
3. The pressure reduction is faster in the study of Sakurai et al. (1980). The exponential periods range from 3.5 to 10 msec. In

the experiment of Aoki et al. (1974), the fastest reduction occurs for 74° inlet subcooling. The pressure reduction period corresponding to this case is ~ 25 msec. This value is approximated from Figure 67.

4. The experimental results reflect the effects of these different parameters on the boiling mechanism. The transient CHF occurs during the growth of the first generation bubbles in the experiments of Sakurai et al. (1980). However, the transient CHF occurs during the growth of the second (or later) generation of bubbles in the experiments of Aoki et al. (1974).

5. The results may also be compared in terms of the time constant of the CHF phenomenon. In Chapter 8 for power transients, this time constant is shown to be related to the bubble growth period for pool boiling and to the complete evaporation of the liquid layer in forced convective boiling. They are on the same order of magnitude, but with strong functions of pressure and subcooling. Therefore, the time constant of the CHF phenomenon is variable during rapid depressurization. But, at the released pressure with zero (or lower) subcooling, it is on the order of 20 to 30 msec. In all the tests of Sakurai et al. (1980), the pressure reaches the atmospheric pressure in less than 25 msec, and the CHF occurs within 10 msec into the transient. However, in the experiments of Aoki et al. (1974), the fastest CHF is experienced at ~ 100 msec into the transient.

6. Furthermore, in some tests the transient CHF reported by Sakurai et al. (1980) is not truly a CHF but may be referred to as a

temporary CHF. In all the tests of Sakurai et al. (1980), the power generation rate was kept constant. Thus, the quasi-steady surface heat flux must be constant. But, during the rapid transient, because of the imbalance in the response time, the surface heat flux increases and reaches the transient CHF. When the pressure reaches the atmospheric pressure, the depressurization stops and the pressure remains constant. At this point, the boiling mechanism corresponds to transition boiling. But, since for heat flux controlled surfaces transition boiling is unstable, the boiling either returns to nucleate boiling or goes into the stable film boiling. The latter case is shown by Figure 69 in Chapter VII. The former case is illustrated by Figure 104. As seen in Figure 104, the temperature excursion which is typical of the CHF is not experienced for this case, and the heat flux recovers the quasi-steady value with further decrease in the surface temperature. Thus, although transition boiling is temporarily experienced in this test, it is difficult to refer to the peak heat flux as CHF, since nucleate boiling is recovered at a later time into the transient.

As this discussion suggests, the mechanism that leads to the transient CHF is rather complex and results from a complex interaction of various parameters. A complete analytical study of this problem is beyond the scope of this chapter; however, certain fundamentals are illustrated.

The experimental studies of Sakurai et al. (1980) and Aoki et al. (1974) suggest that the governing variable in the study of the transient CHF during rapid depressurization is

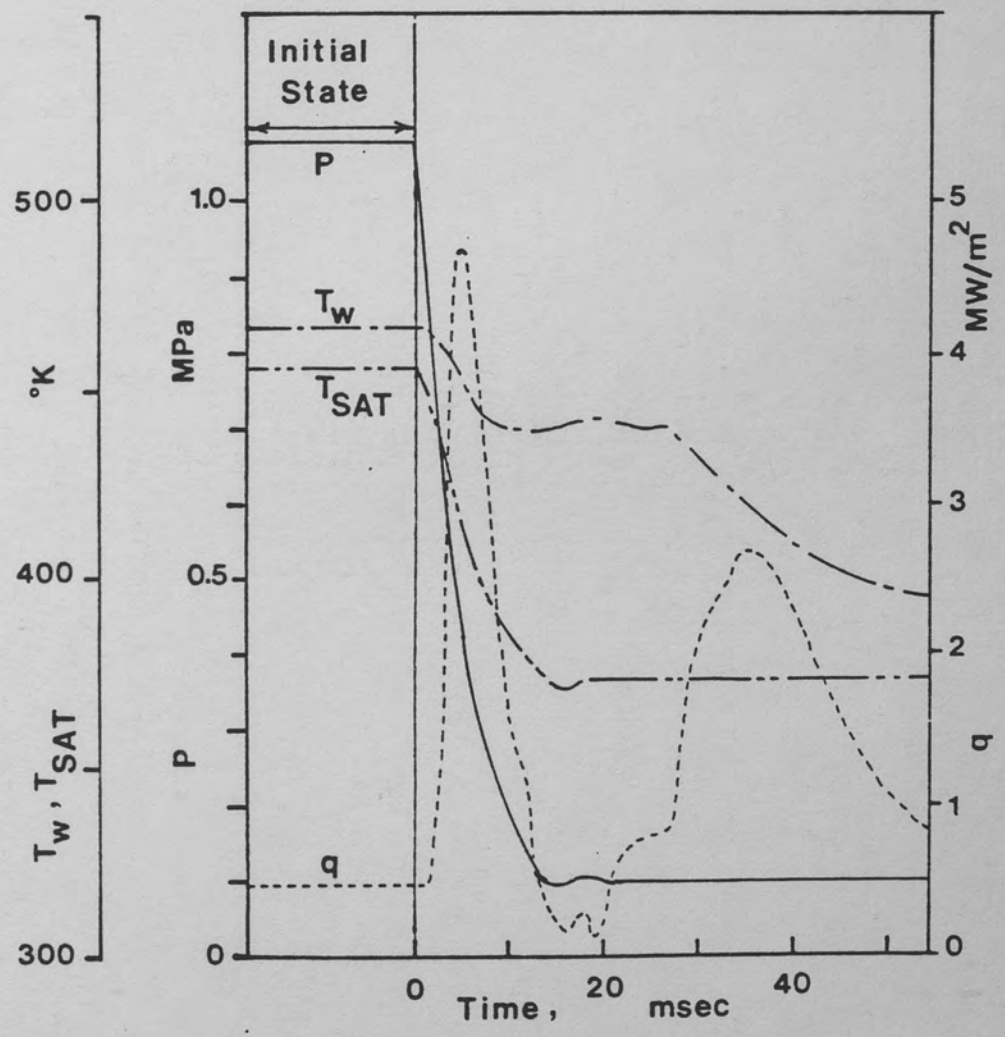

Figure 104. Pressure, Surface Heat Flux and Surface Temperature Histories During Rapid Depressurization (Sakurai 1980)

$$\Delta T_{SAT}(t) = T_W(t) - T_{SAT}(t) \tag{169}$$

During depressurization, the saturation temperature of the coolant decreases due to the decrease in pressure. At the same time, the heater wall temperature also decreases due to an increase in the convective heat transfer coefficient h_c. But, the relative measures of the rate of decrease in these temperatures is the dominant CHF parameter. If during the transient $(\Delta T_{SAT})_{CHF}$ is reached, then the surface temperature becomes too high to sustain a stable liquid film, and the surface undergoes transition boiling.

For small diameter heaters with low thermal storage capacity and high thermal conductivity, the heat balance equation may be written as

$$\rho C_p(dT_W/dt) = Q_o - 2q(t)/R \tag{170}$$

In Equation 170 Q_o may be expressed in terms of the initial surface heat flux as

$$Q_o = 2q_o/R \tag{171}$$

Then, Equation 170 becomes

$$(\rho C_p R/2)(dT_W/dt) = q_o - q(t) \tag{172}$$

where q(t) may be expressed as:

$$q(t) = h_c(t)[T_W(t) - T_c(t)] \tag{173}$$

The coolant temperature, T_c, is a function of time due to the removal of latent heat during homogeneous nucleation. In rapid depressurization homogeneous nucleation becomes possible, since a thicker layer of liquid becomes superheated due to rapid decrease in saturation temperature. But, this decrease in the coolant temperature may be negligible as compared to the other time dependent temperature terms. Thus

$$d(T_W - T_c)/dt \simeq dT_W/dt \tag{174}$$

Using equations 173 and 174, the rate of change of the surface heat flux may be written as

$$(dq/dt) = (T_W - T_c)(dh_c/dt) + h_c(dT_W/dt) \tag{175}$$

If the transient is slow enough, the surface heat flux remains constant, since the heat generation rate is constant. Therefore, for quasi-steady conditions

$$(1/h_c)(dh_c/dt) = -[1/(T_W - T_c)](dT_W/dt) \tag{176}$$

if $(1/h_c)(dh_c/dt) > -[1/(T_W - T_c)](dT_W/dt)$, then $dq/dt > 0$ and the surface heat flux increases. Since dh_c/dt is positive before the onset of the CHF, Equation 176 shows that dT_W/dt must be negative. If, during this period $(\Delta T_{SAT})_{CHF}$ is reached, the surface will undergo transition boiling. At that point, dh_c/dt becomes negative and dT_W/dt becomes positive. Thus, the heat flux starts decreasing. When the

pressure reaches the released pressure and the transient stops, if $q(t)$ is less than q_o, the boiling cannot return to nucleate boiling, since this requires an additional increase in h_c. This is the case illustrated in Figure 69. However, if $q(t) \geq q_o$ at the end of the transient, it is very likely that the boiling will return to nucleate boiling. This is a qualitative explanation of the experimental results of Sakurai et al. (1980). The strong dependence of the results on the initial heat flux q_o may also be explained through Equation 172.

On the other hand, if $(\Delta T_{SAT})_{CHF}$ is not reached within the bubble growth period, the first generation bubbles will be able to depart or collapse without the destruction of the stable liquid film on the heater surface. Under such conditions, the thermal boundary layer has ample time to readjust itself, and a quasi-steady temperature profile may be established. Thus, the average value of the surface heat flux reaches a constant which is the initial heat flux. In this case, in order to observe a CHF, the initial heat flux must be larger than or equal to the CHF at the released pressure. Consequently, the transient CHF is higher than the steady state CHF, since CHF is not an instantaneous phenomenon. Once the CHF conditions are reached, a short period of time is required for the complete evaporation of the stable liquid layer over the heater surface. During this period of time, however, the pressure continues to decrease. If the pressure decay follows the ascending half of the CHF versus pressure curve as shown in Figure 9, the steady-state CHF corresponding to the pressure at complete dryout is lower than the actual CHF. This is illustrated by Figure 105.

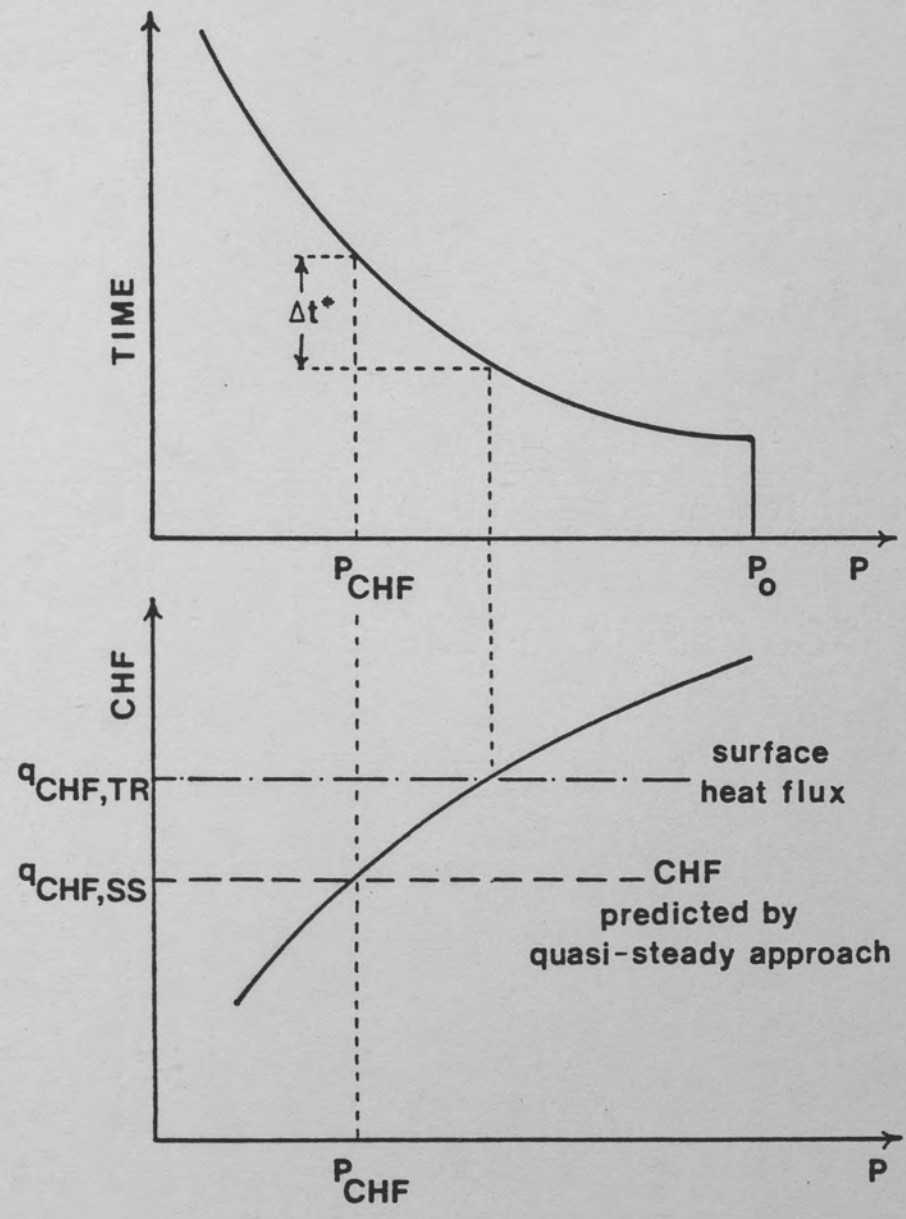

Figure 105. Qualitative Illustration of the Difference Between Steady-State CHF and Transient CHF in Rapid Depressurization

They are not quantified, but the above basic principles may be used to analyze the data. Although a semi-empirical approach may be incorporated into the above analysis through the data of Sakurai et al. (1980) and Aoki et al. (1974), such an effort is considered unnecessary by the author, simply because of certain inconsistencies observed in the data. For instance, Aoki et al. (1974) report that in a number of tests the transient CHF data was irreproducible. In the study of Sakurai et al. (1980), Figure 72 contradicts the conclusion of Sakurai et al. (1980), which states that the difference between the transient CHF and the steady-state CHF increases with decreasing exponential period τ. As observed in Figure 72, the transient CHF corresponding to an exponential period of 7.9 msec is lower than the transient CHF corresponding to 3.5 msec, although all the other experimental variables are almost the same.

The above analysis is basically applicable to bubbly flow and pool boiling, since the analyzed data correspond to such problems. During a LOCA where the rapid depressurization becomes an important transient CHF parameter, the two-phase flow is of annular type. The same type of approach may, however, be valid for an annular flow the dryout. For an annular flow to be established before the onset of CHF, the surface temperature and heat flux histories must be similar to the results of Aoki et al. (1974). In this case, a similar result may be anticipated, where the transient CHF is greater than the steady-state CHF. This is due to the fact that, after the onset of CHF conditions, some small period of time is required for a complete dryout of the liquid film. During this time, however, the pressure continues decreasing; thus, the steady-state CHF is lowered. The

difference, however, may be negligible for low values of dP/dt. In LOCA experiments, such low values are observed. Actually, this is expected, since obtaining an annular flow during a transient which is initiated at a non-boiling state may only be possible during relatively slow transients. Finally, although dP/dt is an important CHF parameter during LOCA, it is not the only parameter, and the rapid reduction in mass flow rate may be of equal importance. Thus, a complete understanding of LOCA requires knowledge of the effect of rapid flow reduction on the CHF. This is investigated in the following section.

Transient CHF During Rapid Flow Reduction

Flow transients are not studied in detail during the research. Furthermore, a systematic set of data for fast flow transients is not readily available in the literature. The studies of Cumo (1978) and his co-workers (Celata 1986) try to correlate the CHF in terms of the instantaneous inlet mass velocity. In doing so, for relatively faster transients, they need to attach a correction factor to the prediction of the steady-state correlation. However, this is not quite a correction factor to the quasi-steady prediction. In the quasi-steady approach, the local-instantaneous value of the mass velocity is calculated through a computer program, and this value is used in the steady-state correlation. In the experiments of Cumo et al. (1978) and Celata et al. (1986), the CHF mechanism is annular flow dryout. For this mechanism, with uniform heat flux, the CHF is expected at the tube exit even during transient conditions. However, at a given time, the exit mass velocity is greater than the inlet mass velocity, since

the former is the inlet mass velocity at a time earlier by one time-transit parameter. This is shown in Figure 106. In this case, a prediction of CHF based on the inlet mass velocity is expected to be lower than the actual CHF, since the actual occurs at a location where the mass velocity is higher. This is a qualitative analysis of the correction factor in the empirical correlation of Cumo et al. (1978). A quantitative prediction of this correction factor, however, is not very easy, and it has to remain empirical as in Equation 86. The difficulty arises due to the fact that dryout is very much dependent on history effects. Since the mass velocity is different at each axial location, the effect of this variable mass velocity on the deposition and entrainment parameters must be considered. Then, an integration must be carried over the entire channel length. The estimation of entrainment and deposition is a difficult task during transient conditions.

Nevertheless, the correction factor may be empirically correlated as done by Cumo et al. (1978), or the actual mass velocity at time-to-CHF may be empirically obtained, as done by Celata et al. (1986). However, these experiments do not bring any insight into the quasi-steady approach. The fastest flow transient simulated in these experiments has a half-life period of 0.4 s. This corresponds to an exponential period of ~ 600 msec. This exponential period is much greater than the time constant of the CHF phenomenon, which is calculated to range from a few milliseconds to ~ 60 msec, depending upon the pressure, subcooling, and heater geometry. Thus, it is very likely that the quasi-steady approach is valid for these experiments, once the local-instantaneous mass velocities are calculated. For

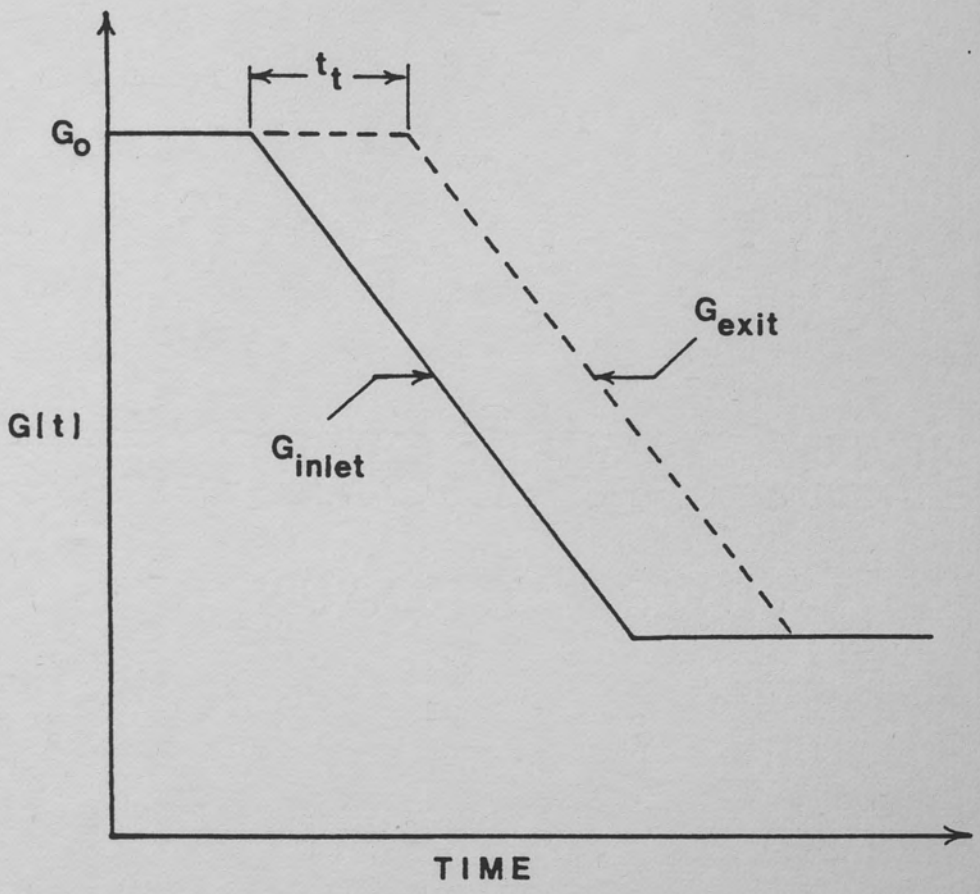

Figure 106. The Difference Between Inlet and Exit Mass Velocities in Flow Transients

faster transients, the flow may not have time to transform into an annular flow. In a DNB mechanism, the transient CHF may be larger than the CHF predicted by the quasi-steady approach. This is due to the fact that, once the CHF conditions are set, additional time is required for the complete evaporation of the liquid layer. But, during this period, the mass velocity continues decreasing. Thus, at the instant of CHF, the quasi-steady approach predicts a lower CHF, resulting from this lower mass velocity. This is illustrated in Figure 107.

Finally, the experiment of Ishigai et al. (1974) may be an example of a non quasi-steady CHF. But, in this experiment, the flow rate of the liquid phase is kept constant. The transient occurs as the rapid deceleration of the vapor core. The measured CHF is smaller than the predicted CHF. Ishigai et al. (1974) theoretically and experimentally show that the difference between the steady-state CHF and the transient CHF is strongly related to interfacial shear stress. This automatically shows that the phenomenon is controlled by deposition and entrainment, rather than evaporation. The experiment of Ishigai et al. (1974) brings more insight into pressure transients than mass flow transients. In pressure transients, the drift fluxes may be quite important and may have a noticeable effect on the CHF.

In this chapter, no closed form correlations for hydrodynamic transients are presented. However, even the above simple discussions may show the danger in blindly applying the quasi-steady approach to a rather complex situation such as a LOCA.

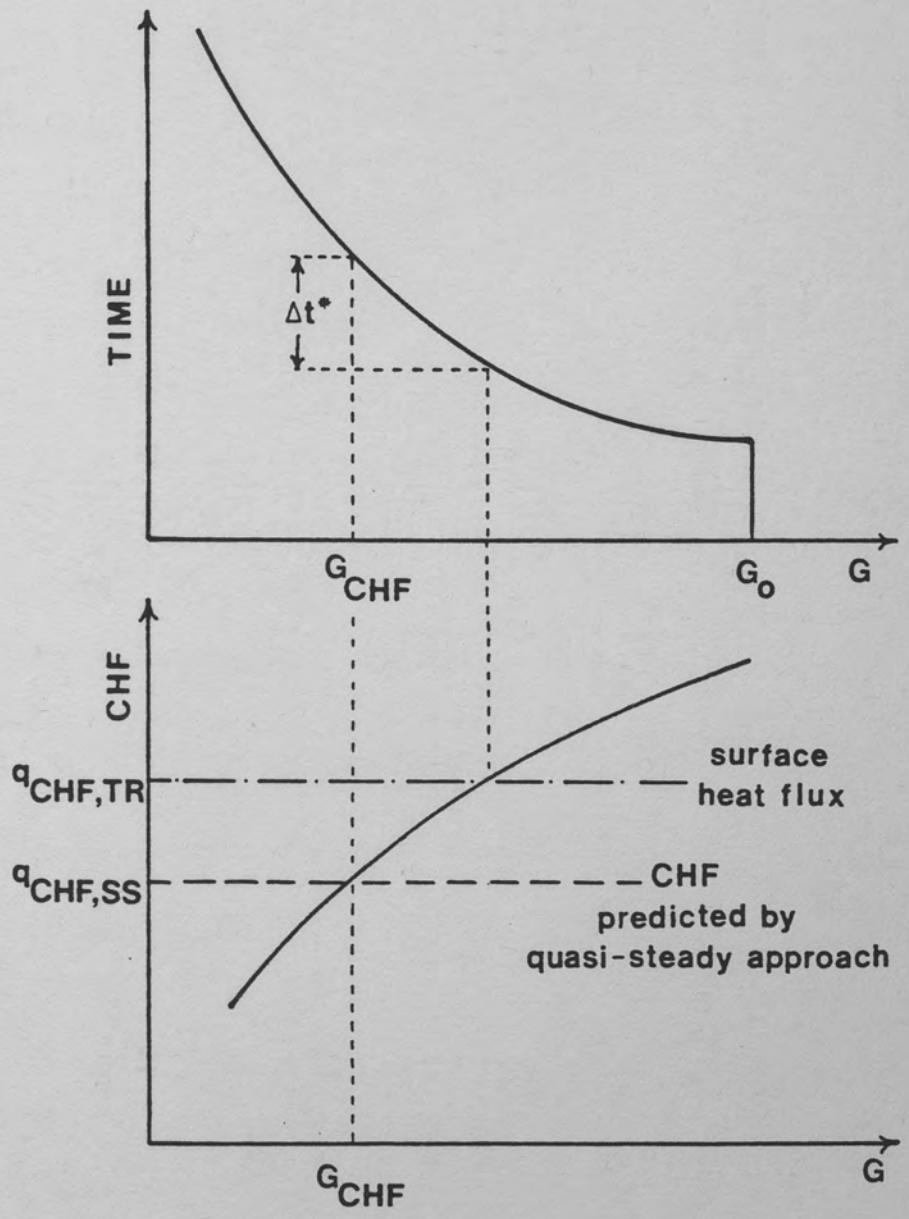

Figure 107. Qualitative Illustration of the Difference Between Steady-State CHF and Transient CHF in Rapid Flow Reduction

CHAPTER X

A MATHEMATICAL MODEL FOR A TRANSIENT CHF CORRELATION

In this chapter, a generalized transient CHF correlation is proposed. The correlation only suggests a general structure, and a complete quantification of such correlation requires a considerable amount of additional transient CHF data. For rapid depressurization and rapid flow reduction, the transient CHF data is limited. Thus, it is very difficult to empirically correlate the transient CHF for a wide range of parameters. Therefore, in this chapter, a relatively simple correlation is developed to best correlate transient CHF behavior. This development is based on the theoretical and analytical observations presented in the previous chapters.

Based on the material provided within previous chapters, the following additional CHF parameters may be used in a transient CHF correlation: the rate-of-change of the transient parameter, $d\alpha/dt$, the minimum time over which the steady-state heat fluxes are averaged, Δt^*, the initial value of the transient parameter at the onset of the transient, α_o, the initial heat flux, q_o, and the value of the CHF at the onset of transient $(q_{CHF,SS})_{t=0}$. Here α denotes a general parameter under transient such as pressure (P), mass velocity (G), or the power generation rate (Q).

For steady-state CHF, Katto (1978; 1979a; 1979c), Ahmad (1973), Shah (1978), and many others have successfully used dimensionless groups in their empirical correlations. For a dimensionless transient CHF correlation, however, the following dimensionless groups can be used in addition to the steady-state groups: $[q_{CHF,TR}/q_{CHF,SS}]$, $[|(dP/dt)|\ \Delta t^*/P(t)]$, $[|(dG/dt)|\ \Delta t^*/G(t)]$, $[|(dQ/dt)|\ \Delta t^*/Q(t)]$, $[P(t)/P_o]$, $[G(t)/G_o]$, $[Q(t)/Q_o]$ and $[(q_{CHF,SS})_{t=0}/q_o]$.

Assuming that any of the parameters P, G, or Q, denoted by α, follows an exponential transient in the form

$$\alpha = \alpha_o \exp(\pm t/\tau) \tag{177}$$

Then $|d\alpha/dt|$ becomes

$$|d\alpha/dt)| = \alpha(t)/\tau \tag{178}$$

Under exponential transients, therefore, the recommended dimensionless groups reduce to

$$|(d\alpha/dt)|\ \Delta t^*/\alpha(t) = \Delta t^*/\tau \tag{179}$$

where Δt^* is the time constant of the CHF phenomenon and τ is the time constant of the transient. If the time constant of the transient is much greater than the time constant of the phenomenon, which can mathematically be stated as:

$$\tau >> \Delta t^* \tag{180}$$

$$\Delta t^*/\tau \simeq 0 \tag{181}$$

then the additional dimensionless number vanishes and the quasi-steady modeling of CHF becomes possible, as discussed by Nelson (Dahlquist 1985). Thus, for exponential transients or for any type of transient where the time constant is defined accordingly as

$$\tau = \frac{\alpha(t)}{d\alpha/dt} \tag{182}$$

the proposed dimensionless groups physically compares the time constant of the transient to the time constant of the phenomenon.

The dimensionless groups $[\alpha(t)/\alpha_o]$ measure the time into the transient. For an exponential transient given by Equation 177, the time into the transient is given by

$$t = \pm \tau \log (\alpha/\alpha_o) \tag{183}$$

where log denotes the natural logarithm. Therefore, the dimensionless groups $[|(d\alpha/dt)|\ \Delta t^*/\alpha(t,]$ and $[\alpha(t)/\alpha_o]$ may be used together to compare the time-into-the-transient, t, to the time constant of the CHF phenomenon, Δt^*, as follows:

$$(\Delta t^*/t) = \pm [|(d\alpha/dt)|\ \Delta t^*/\alpha(t)]/\log(\alpha/\alpha_o) \tag{184}$$

The other dimensionless group $L(q_{CHF,SS})_{t=0}/q_o]$ is related to the safety margin to CHF at the onset of a transient, and finally

$[q_{CHF,TR}/q_{CHF,SS}]$ represents the relative inaccuracy of the quasi-steady approach to transient the CHF problem.

Therefore, a generalized transient CHF correlation may be written in terms of the steady-state CHF parameters plus the above transient parameters, as

$$[q_{CHF,TR}/q_{CHF,SS}] = \eta \{ [q_{CHF,SS,0}(t)/G(t)h_{fg}(t)], [L/d], [\rho_v(t)/\rho_l(t)], [(\Delta h_{SUB})_i(t)/h_{fg}(t)], [|(d\alpha/dt)|\ \Delta t^*/\alpha(t)], [\alpha(t)/\alpha_o], [(q_{CHF,SS})_{t=0}/Q_o]\}_{t=t_{CHF}} \quad (185)$$

In Equation 185, α represents all the transient variables and the dimensionless groups containing α must be repeated for each variable. One physical trend Equation 185 needs to manifest is that as dP/dt, dG/dt and dQ/dt go to zero simultaneously while $q_{CHF,TR}$ needs to approach $q_{CHF,SS}$; thus η approaches 1.

To develop an empirical transient CHF correlation, the data from a combined effect test where more than one parameter is under transient may be difficult to analyze. For this reason, separate effect test data where only one parameter is under transient are more convenient. In separate effect test data, if the database is large enough, the effect of $d\alpha/dt$ on the transient CHF may be explicitly investigated. To do so, the data must be selected such that all the parameters are the same except $d\alpha/dt$. For an α transient, Equation 185 may be written as

$$\eta = 1 + \phi_\alpha \tag{186}$$

where ϕ_α is the transient contribution to the CHF, due to an α transient and it is a function of all the terms on the RHS of Equation 185. The form of Equation 186 suggests that when $d\alpha/dt$ goes to zero ϕ_α goes to zero. This type of an approach is very common in the literature for expressing various non-equilibrium quantities, which may be expressed as an equilibrium quantity plus a perturbation term. Using the same concept, the proposed correlation expresses the transient CHF, which is a non-equilibrium quantity, as the quasi-steady CHF, which is an equilibrium quantity, plus a perturbation term, ϕ_α.

Theoretical and experimental observations suggest that when all the other parameters are fixed, ϕ_α is a monotonically increasing or decreasing function of $[|(d\alpha/dt)|\ \Delta t^*/\alpha(t)]$, or $(\Delta t^*/\tau)$, as specifically applied to exponential transients. To correlate such data, the common "best-fit" forms are as follows:

$$\phi_\alpha \sim \exp(\Delta t^*/\tau) \tag{187}$$

$$\phi_\alpha \sim B_\alpha^{(\Delta t^*/\tau)} \tag{188}$$

$$\phi_\alpha \sim (\Delta t^*/\tau)^{a_\alpha} \tag{189}$$

Another observation based on the previous chapters is that η is a slowly increasing or decreasing function of $(\Delta t^*/\tau)$. Thus

$$d\phi_\alpha/d(\Delta t^*/\tau) << 1 \tag{190}$$

This stems from the fact that Δt^* is usually a small quantity, on the order of milliseconds. Among equations 187, 188, and 189, the latter is more likely to satisfy this criterion over a wider range of τ, with a proper choice of a_α. Therefore, ϕ_α may be written as

$$\phi_\alpha \simeq \Psi_\alpha \cdot (\Delta t^*/\tau)^{a_\alpha} \tag{191}$$

where Ψ_α is the proportionality parameter and it is a function of the dimensionless groups on the RHS of Equation 185, except $[|(d\alpha/dt)| \Delta t^*/\alpha(t)]$. The term Δt^* in Equation 181 is not readily available. As defined earlier, it is the time constant of the CHF phenomenon, and it is equivalent to the time required for complete evaporation of the stable liquid layer in a bubble crowding mechanism and the time required for complete dryout of the liquid film in annular flow, after the onset of CHF conditions. The term Δt^* is a function of various steady-state CHF parameters; therefore, it can be incorporated into the Ψ_α term without a loss of generality. Hence

$$\phi_\alpha \sim \Psi_\alpha \cdot (\tau/\tau^*)^{-a_\alpha} \tag{192}$$

Since Equation 192 yields a linear relation on a logarithmic scale, a standard least-square method may be used to correlate the data, over a given range of τ.

To further investigate the form of Equation 192, the Taylor series of ϕ_α may be analyzed

$$\phi_\alpha = \sum_{i=1}^{\infty} (d\phi_\alpha/d\tau)_{\tau=\tau_1} (\tau - \tau_1)^i/i! \qquad (193)$$

where τ_1 is chosen large enough so that the quasi-steady approach is valid and $\phi_\alpha(\tau_1)$ is equal to zero plus or minus the allowable percent error in estimating the CHF (say 15 percent). With the previous assumptions such that ϕ is a monotonically and slowly increasing (or decreasing) function of τ, it is likely that the above Taylor series is rapidly convergent. For instance, the range of τ may be chosen such that over this range the data may exhibit an almost constant curvature. The curvature of a function at a given point may be written from elementary calculus as

$$\text{CURVATURE} = d^2 \phi_\alpha/d\tau^2/[1 + (d\phi_\alpha/d\tau)]^{3/2} \qquad (194)$$

Previously, it was assumed that

$$| d \phi_\alpha /d(\Delta t^*/\tau) | << 1 \qquad (195)$$

Then, Equation 195 may be written in terms of $d\phi_\alpha/d\tau$ by using the chain-rule, so that

$$| d \phi_\alpha/d(\Delta t^*/\tau) | = (\tau^2/\Delta t^*) | d \phi_\alpha/d\tau| \qquad (196)$$

Since Δt^* is a small quantity, for many relatively fast practical problems of practical interest τ is on the same order as Δt^*. In this case, the following conclusion may be drawn:

$$|(d\phi_\alpha/d\tau)| << 1 \tag{197}$$

Consequently:

$$\text{CURVATURE} \simeq d^2\phi/d\tau^2 \tag{198}$$

Therefore, if the data is correlated over a τ range where the curvature is almost constant, then in the Taylor series expansion of Equation 193, the terms with $i > 2$ drop. Thus

$$\phi_\alpha \simeq (d\phi_\alpha/d\tau)_{\tau=\tau_1} (\tau - \tau_1) + (d^2\phi_\alpha/d\tau^2)_{\tau=\tau_1}(\tau - \tau_1)^2/2 \tag{199}$$

Now, if ϕ_α is approximated by Equation 192, Equation 199 yields

$$\phi_\alpha \simeq -a_\alpha \Psi_\alpha (\tau_1/\tau^*)^{-a_\alpha-1} (\tau - \tau_1) +$$

$$a_\alpha (a_\alpha + 1) \Psi_\alpha(\tau_1/\tau^*)^{-a_\alpha-2} (\tau - \tau_1)^2/2 \tag{200}$$

where $\tau_2 \leq \tau \leq \tau_1$, such that in this range, the curvature remains constant. Furthermore, the above Taylor series approximation suggests that

$$\Psi (\tau_1/\tau^*)^{-a_\alpha} \simeq 0 \tag{201}$$

which, in turn, suggests

$$\tau^* << \tau_1 \tag{202}$$

But this is expected since τ^* is on the order of Δt^*.

The above manipulations obviously do not constitute a rigorous proof to the proposed structure. The validity of this form for power transients is supported by the empirical correlations reported in Chapter VII and the theoretical considerations of Chapter VIII. However, a similar abundance of data for pressure and mass flow rate transients is not available, and similar empirical correlations are missing in the literature. Nevertheless, it is the author's contention that the proposed form, although it may not be the most accurate form, may be used as an improvement to the quasi-steady approach over a given range of variables which are of interest to practical problems. In other words, the term ϕ_α may be regarded as an approximate correction factor on the quasi-steady approach. Therefore, for a separate effect transient, the following form is suggested:

$$\eta = 1 + \phi_\alpha \tag{203}$$

where

$$\phi_\alpha \simeq \Psi_\alpha \, (\tau/\tau^*)^{-a_\alpha} \tag{204}$$

The parameters Ψ_α, a_α and τ^* remain to be empirically determined for various transients of interest, such that α is either P, G, or Q.

Once the functions Ψ and the constants a and τ^* are empirically determined, the empirical correlations for power, flow rate and pressure transients may be obtained separately. Although these separate effect correlations may be useful in some problems, most

practical problems arise as combined transients. In case of a LOCA with scram, for instance, the pressure, mass velocity, and local heat flux are all varying at the same time. Therefore, a more general combined effect transient correlation is required. Assuming that the transients are applied on a one-at-a-time basis, the following form for a combined transient correlation is suggested:

$$\pi = (1 + \phi_P)\ (1 + \phi_G)\ (1 + \phi_Q) \tag{205}$$

where ϕ_P , ϕ_G and ϕ_Q correspond to pressure, flow, and power transients, respectively. Physically, Equation 205 implies that the combined transient CHF behavior may be modeled as a combination of the separate effects on the CHF. The above combination form is suggested mathematically if one-at-a-time applications of the separate effects may be assumed. Such an assumption, therefore, the form of Equation 205, may not be absolutely correct. This remains to be further investigated by direct data comparison. However, it is believed that the above simple form may bring considerable improvement on the quasi-steady approach. This form is obtained by first applying the pressure transient, for instance. Then the transient CHF becomes

$$q_{CHF,TR} = q_{CHF,SS}(1 + \phi_P) \tag{206}$$

Now, taking this value of transient CHF as the steady-state value and applying the mass velocity transient, it gives

$$q_{CHF,TR} = q_{CHF,SS}(1 + \phi_P)\ (1 + \phi_G) \tag{207}$$

And finally applying the power transient, the transient CHF assumes the form given by Equation 205.

Defining a dimensional transient contribution parameter Φ as

$$\Phi = q_{CHF,SS}\phi \tag{208}$$

and applying the transients on a one-at-a-time basis, as previously done, Equation 208 takes the form

$$q_{CHF,TR} = q_{CHF,SS} + \Phi_P + \Phi_G + \Phi_Q \tag{209}$$

This form of the equation, with superpositions of individual transient contributions, was reported by the author (Gunnerson 1984). Although it is a valid form for separate effect conditions, it is rather tricky in use for combined-effect transients. To illustrate this fact, the previous example about the one-at-a-time application of individual transients may be used. When the pressure transient is first applied, the transient CHF becomes

$$q_{CHF,TR} = q_{CHF,SS} + \Phi_P \tag{210}$$

Now to apply the flow transient, every $q_{CHF,SS}$ term inherent within Φ_G must be replaced by $q_{CHF,SS} + \Phi_p$. Sometimes this may be impossible, due to the empirical nature of Φ_G which may make the $q_{CHF,SS}$ term unrecognizable. Therefore, a combined CHF transient is more practical in its form given by Equation 205 than by Equation 209. However, at this point, Equation 205 may only be regarded as an improvement to the

quasi-steady approach. It satisfies the fundamental physical limits, but a complete justification requires more experimental data.

CHAPTER XI

SUMMARY AND CONCLUSIONS

In this study, the Critical Heat Flux during transient conditions was investigated. The necessity and the practical significance of such an investigation is introduced in Chapter I. Such a study requires a solid physical understanding of the CHF problem. Therefore, a brief overview of the general aspects of the CHF problem is presented in Chapter II. Chapter III summarizes the theoretical models of steady-state CHF. These models are later used in the analysis of transient CHF. The present study is mostly aimed towards the requirements of the nuclear industry. Hence, the possible accident situations which result in thermal-hydraulic transients in LWRs are summarized in Chapter IV. Since the problem of interest belongs to the general category of conjugate problems, these types of problems are discussed in Chapter IV. The quasi-steady approach, which is a commonly-used solution technique for a conjugate problem, is also introduced in the same chapter.

The application of the quasi-steady approach to predict the transient CHF was discussed in Chapter VI. In this chapter, certain steady-state CHF correlations are compared to transient CHF data compiled from blowdown experiments by Leung (1980). For this purpose, a simple, one-dimensional finite-difference program CODA is used. This program is developed by Gallivan and Leung (Leung 1980).

Chapter VI contains a summary of the studies of Leung (1980) and Lo (1984), and it is supplemented by a previous study conducted at the University of Central Florida (Gunnerson 1984). The results of CODA suggest that the CISE, Biasi and Griffith-Zuber correlations are perhaps best suited to predict the blowdown behavior, and the Bowring and Biasi correlations are successful in predicting the flow transient data. However, a detailed analysis of the results show that they generate more open-ended questions than satisfactory answers. The author's conclusion is that such results cannot be generalized. Between the uncertainties of the empirical correlations and the experimental data and the simplifying assumptions of the CODA program, the results should only be considered as a rough estimate. Special care is required in applying the results of CODA to various other transient conditions. A detailed discussion of these results is also presented in Chapter VI.

The present study is mostly concerned with fast transients where the CHF cannot be predicted through the quasi-steady approach. For such transients, examples from the literature are summarized in Chapter VII. This chapter includes examples of CHF studies during power transients, rapid depressurization, and rapid flow reduction.

In Chapter VIII, a theory is developed to predict the CHF during power transients. The developed theory covers a wide variety of problems, including saturated and subcooled pool boiling over flat surfaces and horizontal wires and forced convective boiling along a vertical cylindrical heater. For such problems, the theory is successfully compared to existing data. All these data are provided from electrical heaters. Unfortunately, no separate effects data from

fuel rods is available. But, the application of the developed theory to nuclear fuel rods is possible, and a discussion of this is presented within the same chapter.

In Chapter IX, the CHF during rapid depressurization and rapid flow reduction is analyzed, based on first principles. The effect of phenomenological time constants on such problems is discussed. Such problems are more complex than the CHF problem associated with power transients. Furthermore, the test data is less abundant. Therefore, no closed-form transient CHF correlations are obtained for hydrodynamic transients in the present study. Although relatively more difficult, it is not impossible to obtain correlations similar to power transient CHF correlations. The author believes that today's state of knowledge of the CHF is strong enough to theoretically handle such problems.

Finally, the important parameters of the transient CHF are identified in Chapter X. These parameters are combined into dimensionless groups, and the physical significance of each group is discussed. The author believes that a general transient CHF correlation may be developed only if the individual effect of various parameters may be identified. Therefore, the first step in such a task must be to develop individual correlations for separate effect tests. Based on the theoretical and experimental observations of the previous chapters, a general form for such correlations is suggested. The suggested form agrees reasonably well with the data from power transients. For the other transients, the quantification of the proposed form requires extensive data. Once the separate effect correlations are obtained, they may be combined through a one-at-

a-time application to obtain a generalized form for a combined effect transient. Extensive test data are required to quantify this correlation and to check its validity. Then again, the suggested form may not be the best. However, the author suggests that, although it may not be the ideal form, the proposed form may bring a noticeable improvement on the quasi-steady approach.

The primary objective of the present study was to investigate the limitations of the quasi-steady approach in determining the CHF during transient conditions. Thus, one must assume that once the requirements are satisfied, the quasi-steady approach can accurately predict the CHF. The inherent conclusion of such an assumption is that the steady-state CHF correlations can accurately predict the steady-state CHF. However, it is a known fact that all the existing correlations, even when applied within the suggested range of parameters, involve a high inaccuracy. Hence, the prediction capability of the quasi-steady approach is restricted by the accuracy of the CHF correlations. The improvement of the steady-state CHF correlations is beyond the scope of the present study. Therefore, the present study assumes that the steady-state CHF can be accurately predicted by the available correlations.

The present study includes the analysis of the effect of power transients, rapid depressurization from the non-boiling state, rapid depressurization from the boiling state, rapid flow reduction, and sudden deceleration of vapor core when the liquid film flow remains constant. For these cases, a qualitative relation between steady-state CHF and transient CHF is shown in Table 14. Power transients for the dryout mechanism and the rapid depressurization dryout mechan-

TABLE 14

QUALITATIVE RELATION BETWEEN $q_{CHF,SS}$ AND $q_{CHF,TR}$ FOR VARIOUS TRANSIENTS

Type of Transient	$\eta = q_{CHF,TR}/q_{CHF,SS}$
POWER TRANSIENTS	$\eta \geq 1$
RAPID DEPRESSURIZATION	
From Boiling State	$\eta \geq 1$
From Non-Boiling State	$\eta \leq 1$
RAPID FLOW REDUCTION	
DNB	$\eta \geq 1$
Sudden Deceleration of Vapor Core, Where the Liquid Film Flow is Constant (Annular Flow)	$\eta < 1$

ism are not included in this table, because no similar data were examined in this study. Further experimental and theoretical research is required to complete Table 14.

With Table 14 and the generalized CHF correlation given by Equation 205, the limitations of the quasi-steady approach may be explicitly obtained. Before this is done, however, a blind application of the quasi-steady approach may lead to erroneous consequences. This is referred to as the "coincidence hypothesis" in an earlier publication (Gunnerson 1984), and it is illustrated in Figure 108.

Figure 108a shows a rapid depressurization with scram. After the initiation of boiling, a rapid depressurization tends to increase the CHF, whereas, a rapid power reduction decreases the CHF. However, the relative effect of individual transients may cancel each other, and the transient CHF may be successfully estimated by the quasi-steady approach. Now, if one wants to draw a conclusion out of this experiment, such that at the given rate of depressurization, for instance, the quasi-steady approach is valid, this would be erroneous. Because, in an experiment with the same rate of depressurization, but this time without scram, the measured CHF would be larger than the value predicted by the quasi-steady approach. This is illustrated in Figure 108b.

Therefore, a successful modeling of transient CHF strongly relies on a complete physical understanding of the CHF mechanism. Once the dynamic nature of the CHF phenomena can be physically modeled in terms of its time constants, the transient CHF problem will cease to be a challenge. The fact that the author is able to analyze the power

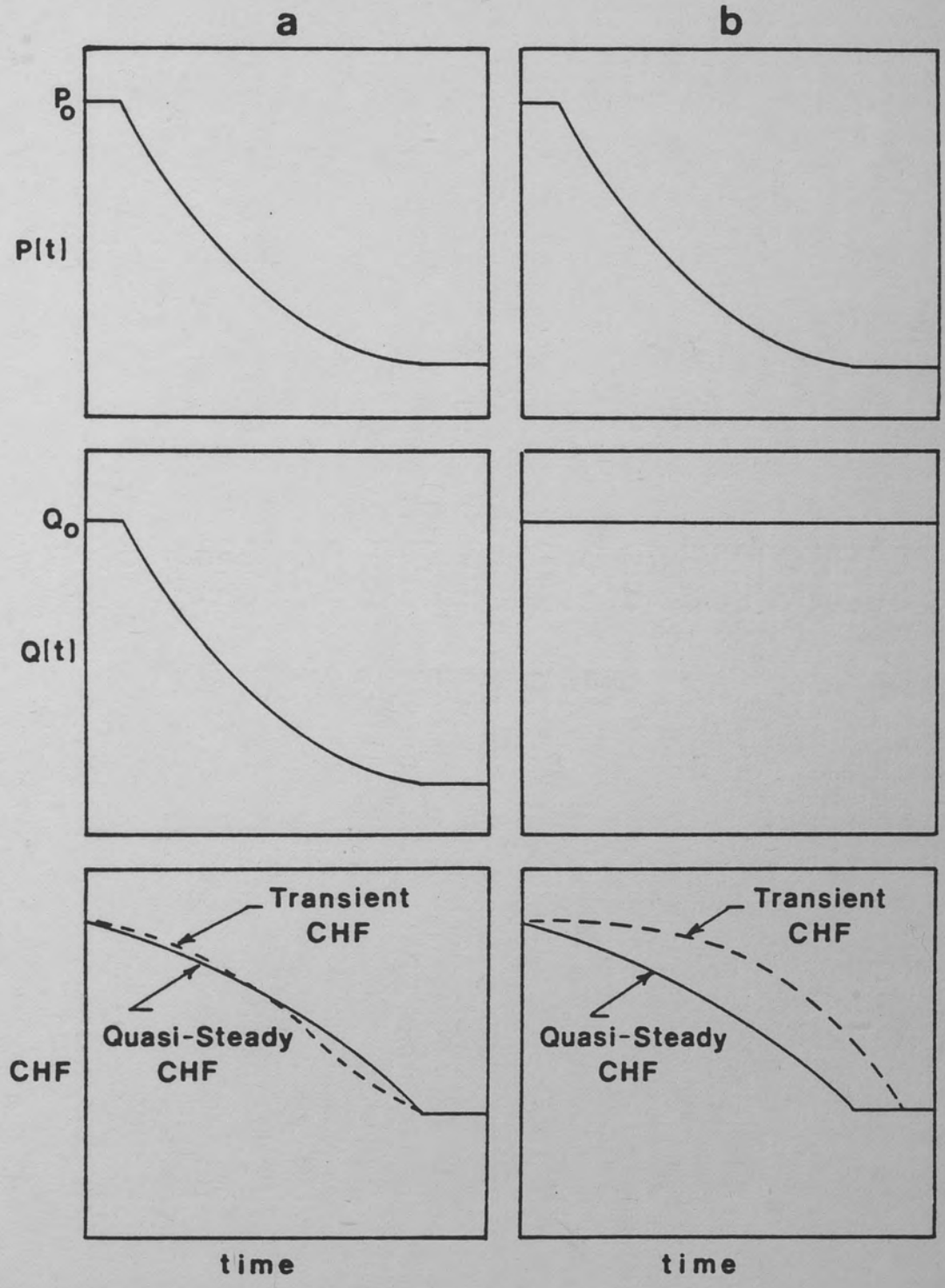

Figure 108. Qualitative Illustration of Coincidence Hypothesis

transients based on first principles, and despite the simplifying assumptions, his success in correlating the various data, encourages further research. A complete understanding of the CHF phenomenon requires a proper definition of its time constants. These time constants, in general, are not as small as the time constants of the single-phase convection and they may have a significant effect on CHF measurements.

The two most important CHF mechanisms are DNB and dryout. For those, the time constants are defined in the present study as the time required for the complete evaporation of the liquid layer and the liquid film, respectively. The time constant of DNB is quantified in Chapter VIII. It is a strong function of pressure, subcooling, heat flux and the heater geometry. For the cases studied in Chapter VIII, the value ranges from a few milliseconds to ~ 50 milliseconds. Such quantification is not done for dryout, since it requires a knowledge of the complex interaction of entrainment and deposition terms. Nevertheless, it is expected to be on the same order as the time constant of DNB.

Identifying the time constants of the CHF and incorporating these time constants into the CHF correlations not only makes the transient CHF analysis possible, but it may also help explain the large uncertainties associated with the CHF correlations. To illustrate this, the saturated pool boiling CHF model of Haramura and Katto (1983) may be examined, since it is a good and possibly a unique example of a CHF model written in terms of its time constant. This is given by Equation 19 in Chapter III. The model (Haramura 1983) basically assumes that the CHF occurs if the liquid layer completely evaporates at the

end of the bubble hovering period τ_d. Therefore, the proposed value of the CHF is a time-averaged value over τ_d, and it is assumed to be constant over the period τ_d. This, on the other hand, means that the rate of change of the liquid layer is constant over the period τ_d as shown by Figure 109.

In reality, however, $d\delta/dt$ may not be constant. One of the postulates employed in the model (Haramura and Katto 1983) is that, as soon as one bubble departs another one is formed almost instantaneously. This obviously requires a large value for $d\delta/dt$ in the beginning of the hovering period τ_d. The exact functional form of $d\delta/dt$ is difficult to obtain, but it is very likely that it is not a constant. As a guess for illustration purposes, the following form may be assumed:

$$d\delta/dt = (2\delta_{c,o}/\tau_d^2)\ (t - \tau_d) \qquad (211)$$

where $0 < t < \tau_d$

Since, in saturated pool boiling, the heat flux is directly proportional to $d\delta/dt$, $q(t)$ may be written as

$$q(t) = (2q_{CHF,SS}/\tau_d)\ (t - \tau_d) \qquad (212)$$

This hypothetical case is illustrated in Figure 110. As shown, although the average heat flux is again $q_{CHF,SS}$, the time-dependent heat flux spans from zero to twice the average value. Thus, the measured value may be anywhere within this range. Obviously, the

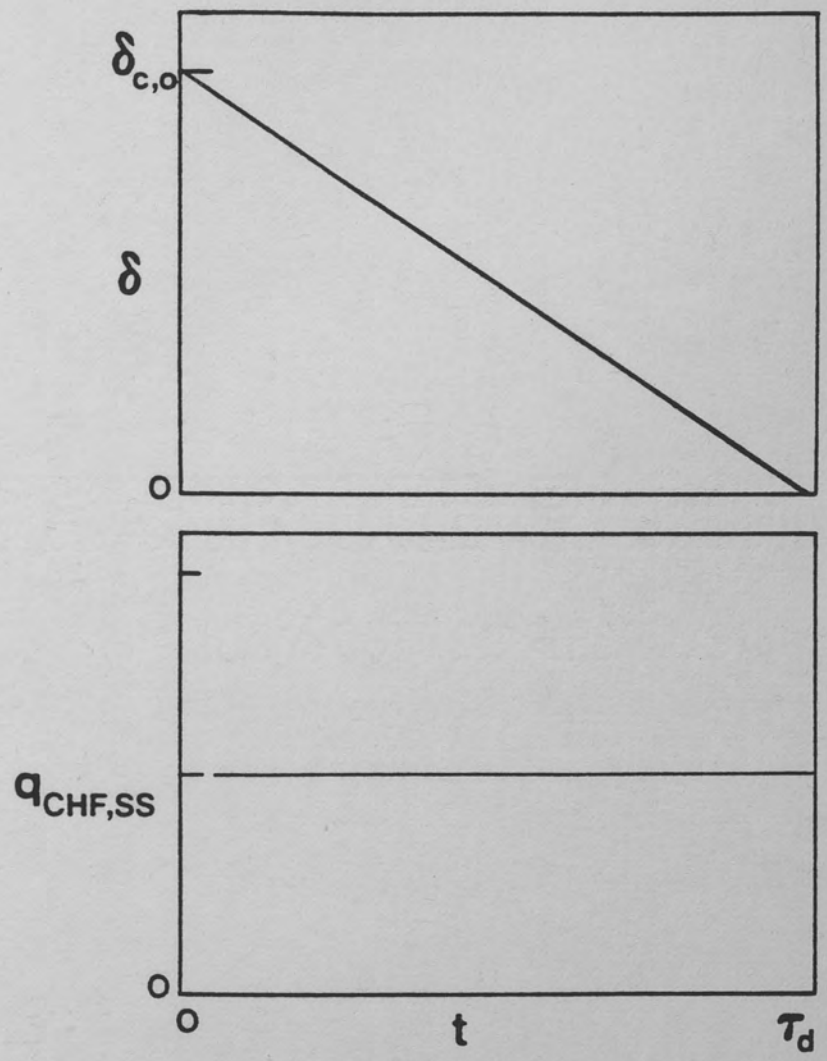

Figure 109. The Liquid Layer Thickness and the Heat Flux as a Function of Time Based on the Model of Haramura and Katto (1983)

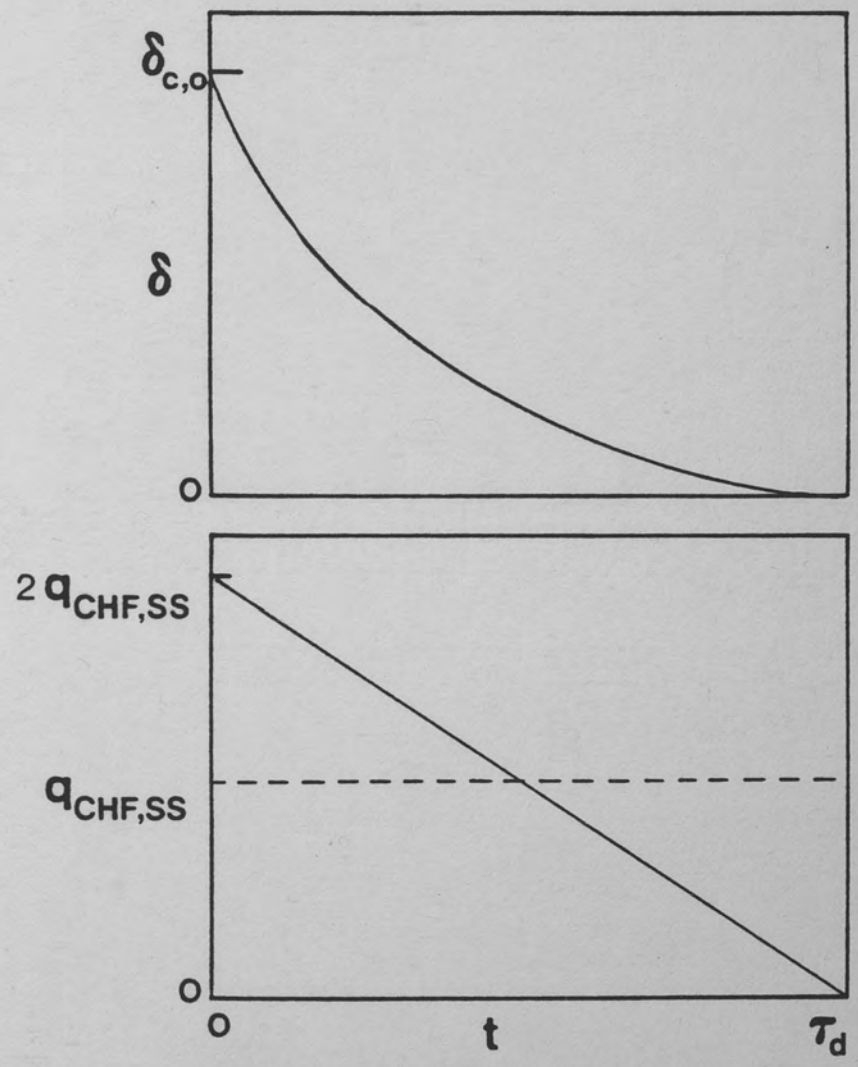

Figure 110. An Hypothetical Variation of Liquid Layer Thickness and Heat Flux With Respect to Time

assumed model is not realistic by any means and it is chosen to illustrate the concept. Nevertheless, it clearly illustrates the effect of the averaging process on the actual value of the CHF.

It is the author's hope that the present study has some degree of contribution in the understanding of the CHF phenomenon. This contribution may be minor or major, and the author believes that this decision may only be made in accordance to its impact on contributing to future research. According to the author, the major conclusion of the present study is neither the developed theory for power transients nor the discussion of the quasi-steady approach, but the fact that it clearly shows the necessity and potential success of further theoretical research in this area. The present study may be valuable in showing that such analytical studies are possible and may generate useful results.

APPENDICES

APPENDIX A

CHF CORRELATIONS

This appendix contains the various empirical CHF correlations referenced within the text. These are:

1. Local Barnett Correlation
2. Babcock-Wilcox Correlation (BWC)
3. Babcock and Wilcox-2 Correlation (B & W-2)
4. Biasi Correlation
5. Bowring Correlation
6. Combustion Engineering-1 Correlation (CE-1)
7. Centro Informazioni Studie d'Experience Correlation (CISE)
8. Condıe Mod-7 Correlation
9. EPRI Correlation
10. General Electric Correlation (GE)
11. Hsu-Beckner Correlation
12. Katto Correlations
13. Loss-of-Fluid Test Correlation (LOFT)
14. Savannah River Correlation
15. Westinghouse-3 Correlation (W3)
16. Griffith-Zuber Correlation (G-Z)
17. Modified Zuber Correlation (MZ)

All the correlations in this listing are in English units, except for the Katto Correlations which are in terms of dimensionless groups.

The following units are used in various parameters:

d:	Rod Diameter (Hydraulic or Equivalent)	inches
L:	Tube Length	inches
P:	Pressure	psia
G:	Mass Flux	lbm/ft^2-hr
h:	Various Enthalpy Terms	Btu/lbm
q_{CHF}:	Critical Heat Flux	$Btu/hr\text{-}ft^2$
T:	Temperature	°F

In this appendix the nomenclature is the same as the main text unless it is otherwise defined. Usually, the empirical constants are copied from the original reference and may be conflicting with the general nomenclature.

Local Barnett Correlation (Barnett 1966)

$$q_{CHF} = 10^6 \frac{A + B\,(h_{fg}x)}{C} \qquad \text{(A1)}$$

where:

$A = 69.40\ d_{HE}^{0.751}\ G'^{0.226}\ [1.0 - 0.672 \exp(-6.09\ d_{HY}G')]$

$B = -0.250\ d_{HE}\ G'$

$C = 165.9\ d_{HY}^{1.246}\ G'^{0.329}$

with $G' = G/10^6$

The parametric ranges are given as:

d_{HE}: 0.0215 to 0.316 in

d_{HY}: 0.01058 to 0.0729167 in

L: 24 to 108 in

P: 1000 psia

G: 0.14×10^6 to 6.20×10^6 lbm/ft^2-hr

$(\Delta h_{SUB})_i$: 0 to 412 Btu/lbm

Babcock-Wilcox Correlation (Lo 1984)

$$q_{CHF} = \frac{A_5\{(A_1G)^{[A_3+A_7(P-2000)]} - A_8 h_{fg} Gx\}}{(A_2G)^{[A_6+A_7(P-2000)]}} \qquad (A2)$$

where:

$A_1 = 0.309191 \times 10^{-6}$

$A_2 = 0.388223 \times 10^{-5}$

$A_3 = 0.964882$

$A_4 = 0.301423 \times 10^{-3}$

$A_5 = 0.554836 \times 10^{-7}$

$A_6 = 0.727729$

$A_7 = 0.189646 \times 10^{-4}$

$A_8 = 0.175233 \times 10^{-8}$

B&W-2 Correlation (Gellerstedt 1969)

$$q_{CHF} = \frac{(a - bd)[A_1(A_2G)^{A_3+A_4(P-2000)} - A_9Gxh_{fg}]}{A_5(A_6G)^{[A_7+A_8(P-2000)]}} \qquad (A3)$$

where:

$a = 1.155$

$b = 0.407$

$A_1 = 0.37 \times 10^{8}$

$A_2 = 0.591 \times 10^{-6}$

$A_3 = 0.830$

$A_4 = 0.685 \times 10^{-3}$

$A_5 = 12.71$

$A_6 = 0.3054 \times 10^{-5}$

$A_7 = 0.712$

$A_8 = 0.2073 \times 10^{-3}$

$A_9 = 0.1521$

The parametric ranges are given as:

P : 2060 to 2440 psia

G : 0.7×10^{6} to 4×10^{6} lbm/hr-ft^2

x : -0.03 to 0.20

d : 0.2 to 0.5 in

Biasi Correlation (Biasi 1967)

This correlation consists of two equations, and the q_{CHF} value is given by the higher of the two values.

For low quality region:

$$q_c = \frac{2.63 \times 10^7}{(2.54d)^n \, G^{0.167}} \left[\frac{4.43 \, F}{G^{0.167}} - x \right] \qquad \text{(A4)}$$

For high quality region:

$$q_c = \frac{2.506 \times 10^9 H}{(2.54d)^n \, G^{0.6}} (1 - x) \qquad \text{(A5)}$$

where $n = 0.4$ for $d \geq 0.394$ in

$n = 0.6$ for $d < 0.394$ in

$F = 0.7249 + 6.83 \times 10^{-3} P \exp(-2.21 \times 10^{-3} P)$

$H = 1.159 + 1.028 \times 10^{-2} P \exp(-1.31 \times 10^{-3} P) + 130 P/(2100 + P^2)$

For $G < 0.2 \times 10^6$ lbm/ft^2-hr, Equation A5 is always used. The parametric ranges are given as:

D: 0.118 to 1.476 in

L: 8 to 236 in

P: 40 to 2000 psia

G: 0.08×10^6 to 4.43×10^6 lbm/ft^2-hr

x: $1/(1 + \rho_f/\rho_g)$ to 1

Bowring Correlation (Bowring 1972)

$$q_{CHF} = \frac{Gdh_{fg}}{4C} (A - x) \qquad (A6)$$

Where:

$A = 2.317\ F_1/(1 + 3.092\ F_2\ d^{0.5}\ G')$

$C = 104.4\ F_3\ dG'/(1 + 0.347\ F_4\ G'^{n})$

with $G' = G/10^6$

for $P \leq 1000$ psia

$F_1 = \{P_R^{18.942} \exp [20.89\ (1 - P_R)] + 0.917\}/1.917$

$F_2 = 1.309\ F_1/\{P_R^{1.316} \exp [2.444\ (1 - P_R)] + 0.309\}$

$F_3 = \{P_R^{17.023} \exp [16.658\ (1 - P_R)] + 0.667\}/1.667$

$F_4 = F_3\ P_R^{1.649}$

for $P > 1000$ psi

$F_1 = P_R^{-0.368} \exp [0.648\ (1 - P_R)]$

$F_2 = F_1\ P_R^{0.448}/\exp [0.245\ (1 - P_R)]$

$F_3 = P_R^{0.219}$

$F_4 = F_3\ P_R^{1.649}$

with $P_R = P/1000$

The parametric ranges are given as:

P: 29.4 to 2793 psia

G: 0.10×10^6 to 13.7×10^6 lb/ft^2-hr

CE-1 Correlation (CENPD 1977)

$$q_{CHF} = 2.8922 \times 10^6[(B_1 + B_2P)(G')^{(B_3+B_4P)} - G' \times h_{fg}]/G'^{(B_5P+B_6G')} \quad (A7)$$

where:

$B_1 = 405.32$

$B_2 = -9.9290 \times 10^{-2}$

$B_3 = -0.67757$

$B_4 = 6.8235 \times 10^{-4}$

$B_5 = 3.1240 \times 10^{-4}$

$B_6 = -8.3245 \times 10^{-2}$

with $G' = G/10^6$

The parametric ranges are given as:

P : 1785 to 2415 psia

x : -0.16 to 0.20

G : 0.87×10^6 to 3.21×10^6 lbm/hr-ft^2

T_i: 382 to 644°F

d_{HE}: 0.4713 to 0.7837 in

L : 84 to 150 in

CISE Correlation (Bertoletti 1965)

The first form of the CISE correlation, CISE1 correlation, is written as:

$$q_{CHF} = \frac{4030 h_{fg}}{d^{0.4}(-1 + 1/P_r)^{0.4}} (a - x) \qquad (A8)$$

where: $a = (1 - P_r)/(1.356 \times 10^{-6} G)^{0.333}$

with $P_r = P/P_{cr}$

P_{cr} being the critical pressure

This correlation is subsequently modified to yield the right limit at low flow.

$$G^* = 2.49 \times 10^6 (1 - P_r)^3$$

if $G > G^*$, $a = (1 - P_r)/(1.356 \times 10^{-6} G)^{0.333}$

if $G < G^*$, $a = \frac{1}{1 + 0.2 \times 10^{-6} G/(1 - P_r)^3}$

This is designated as the CISE4 correlation.

The parametric ranges are given as:

P: 65.5 to 217.5

G: 0.07×10^6 to 3.0×10^6 lbm/ft^2-hr

x: ~0.0 to 1.0

Condie Mod-7 Correlation (Condie 1978)

$$q_c = 8.0793 \times 10^6 \frac{(G')^{[0.17751n(1+x)]}}{(1+x)^{3.3906}\, p^{0.3234}} \qquad \text{(A9)}$$

with $G' = G/10^6$

The parametric ranges are given by:

P: 440 to 2500 psia

G: 0.05×10^6 to 3.5×10^6 lbm/ft^2-hr

x: -0.1 to 1.0

EPRI Correlation (Columbia University 1982 & 1983)

$$q_{CHF} = \frac{A - x_i}{C + [(x_{loc} - x_i)/q_{loc}]} \qquad \text{(A10)}$$

$$A = P_1 P_r^{P_2} G^{(P_5 + P_7 P_r)}$$

$$C = P_3 P_r^{P_4} G^{(P_6 + P_8 P_r)}$$

where q_{loc} and x_{loc} are local heat flux and quality, respectively

$P_1 = 0.5328$

$P_2 = 0.1212$

$P_3 = 1.6151$

$P_4 = 1.4066$

$P_5 = 0.3040$

$P_6 = 0.4843$

$P_7 = -0.3285$

$P_8 = -2.0749$

The parametric range of EPRI Correlation is as follows:

Local Mass Flux, G	0.2 to 4.1 M.lbs/hr-ft^2
Pressure, P	200 to 2450 psia
Local Quality, x_{loc}	-0.25 to 0.75
Inlet Quality, x_i	-1.10 to 0.0
Hydraulic Diameter, d_{HY}	0.35 to 0.55 in.
Heated Diameter, d_{HE}	0.25 to 0.55 in.

EPRI Correlation - continued

Length, L	30 to 168 inc.
Rod diameter	0.38 to 0.68 in.
Number of Rods	9(3x3) to 25(5x5)
Radial Profile	Uniform and Non-Uniform (Radial and Corner Peaking)
Axial Profile	Uniform
Subchannel Type	Matrix Channels only
Rod Bundle Type	PWR and BWR (With and Without Unheated Rods)

If the cold-wall correction factor is required, the correlation is modified as follows:

$$q_{CHF} = \frac{AF_A - x_i}{CF_c + \left[\frac{x_{loc} - x_i}{q_{loc}}\right]} \qquad (A11)$$

where, F_A and F_C are cold cold wall correction factors

$$F_A = G^{0.1}$$

and,

$$F_C = 1.183\ G^{0.1}$$

EPRI Correlation - continued

Parameter Ranges:	
Pressure:	600 to 1500 psia
Local Mass Flux	0.15 to 1.4 M. lbs/hr-ft^2
Local Quality:	0.0 to 0.70
Subchannel Type:	Corner Subchannels Only

If the grid-spacer factor is required, the correlation is modified as follows:

$$q_{CHF} = \frac{A - x_i}{CF_g + \left[\frac{x_{loc} - x_i}{q_{loc}}\right]} \qquad \text{(A12)}$$

The term F_g is the grid spacer correction factor.
Optimization of F_g in terms of grid loss coefficient C_g resulted in the following grid correction factor:

$$F_g = 1.3 - 0.3C_g$$

For standard grids the grid loss coefficient is approximately equal to one. Therefore, for these grids the grid correction factor becomes one.

GE Correlation (Slifer 1971)

$$q_{CHF} = 10^6(0.84 - x) \qquad \text{(A13)}$$

if $G < 0.5 \times 10^6$ lbm/hr=ft^2

$$q_c = 10^6(0.80 - x) \qquad \text{(A14)}$$

if $G \geq 0.5 \times 10^6$ lbm/hr-ft^2

The parametric ranges are given as:

P: 880 to 1323 psia

G: less than 0.5×10^6 lbm/ft^2-hr

x: 0 to 0.84

Hsu-Beckner Correlation (Hsu 1978)

$$\frac{q_{CHF} - q_{steam}}{q_{\substack{W-3 \\ x=0}} - q_{steam}} = [1.76\ (0.96 - \beta_v)]^{\frac{1}{2}} \qquad \text{(A15)}$$

where:

$$q_{steam} = h_{D-B}\ (T_W - T_{SAT})$$

h_{D-B} = Dittus-Boelter heat transfer coefficient for steam

$$q_{\substack{W-3 \\ x=0}} = 0.955 \times 10^{6}\{[1.04 + 0.148 \times 10^{-6}G][2.192 - 0.53 \times 10^{-3}P]$$
$$[0.2664 + 0.9357 \exp(-3.15/d)]\}$$

Since q_{steam} is small compared to q_{CHF} and $q_{\substack{W-3 \\ X=0}}$, it can be dropped. Hence, Equation A15 becomes:

$$q_{CHF} = q_{\substack{W-3 \\ X=0}}\ [1.76\ (0.96 - \beta_v)]^{\frac{1}{2}} \qquad \text{(A16)}$$

The parametric ranges are:

P: 882 to 2205 psia

G: all velocities

x: 0 to 1.0

Katto Correlations [(Katto 1978) through (Katto 1982)]

The Katto Correlations are given in terms of the dimensionless groups $q_{co}/(Gh_{fgY})$, $(\sigma\rho f)/(G^2L)$, ρ_g/ρ_f, L/d in four different CHF regimes (L, N, H, and HP regimes). The term $q_{CHF,O}$ denotes the CHF value with zero inlet subcooling. The relation between q_{CHF} and $q_{CHF,O}$ is given by:

$$q_{CHF} = q_{CHF,O}[1 + K\ (\Delta h_{SUB})_i/h_{fg}] \qquad \text{(A17)}$$

The correlations for $q_{CHF,O}$ and K are given as follows:

L-Regime

$$q_{CHF,O}/(Gh_{fg}) = C[(\sigma\rho_f)/(G^2L)^{0.043}\ (d/L)] \qquad \text{(A18)}$$

where:

C = 0.25 for L/d < 50

C = 0.34 for L/d > 150

C varies linearly with L/d in the range $50 \leq L/d \leq 150$

for L/d > 100

and $(\sigma\rho_f)/(G^2L) > 7.84 \times 10^{-4}$

the correlation is given by:

$$q_{LHF,O}/(Gh_{fg}) = 0.25d/L \qquad \text{(A19)}$$

Katto Correlations - continued

$$K = \frac{1.043}{4C[(\sigma\rho_f)/(G^2L)]^{0.043}} \tag{A20}$$

N-Regime and H-Regime

$$q_{CHF,O}/(Gh_{fg}) = 0.098(\rho_g/\rho_f)^{0.133}\,[(\sigma\rho_f)/(G^2L)]^{0.433}$$

$$(L/d)^{0.27}/(1 + 0.0031L/d) \tag{A21}$$

$$K = 0.416\,\frac{(0.0221 + d/L)(d/L)^{0.27}}{(\rho_g/\rho_f)^{0.133}\,[(\sigma\rho_f)/(G^2L)]^{1/3}} \tag{A21}$$

$$q_{CHF,O}/(Gh_{fg}) = 0.10\,(\rho_g/\rho_f)^{0.133}\,[(\sigma\rho_f)/(G^2L)]^{1/3}\,(1 + 0.0031L/d)^{-1} \tag{A22}$$

$$K = \frac{5(0.0124 + d/L)}{6(\rho_g/\rho_f)^{0.133}\,[(\sigma\rho_f)/(G^2L)]^{1/3}} \tag{A23}$$

HP Regime

$$q_{CHF,O}/(Gh_{fg}) = 0.0384\,(\rho_g/\rho_f)^{0.60}\,[(\sigma\rho_f)/(G^2L)]^{0.173}$$

$$\{1 + 0.280\,[(\sigma\rho_f)/(G^2L)]^{0.233}\,(L/d)\}^{-1} \tag{A24}$$

Katto Correlations - continued

$$K = 1.12 \frac{1.52[(\sigma\rho_f)/(G^2L)]^{0.233} + (d/L)}{(\rho_g/\rho_f)^{0.60}\,[(\sigma\rho_f)/(G^2L)]^{0.173}} \qquad (A25)$$

The range of applicability of these equations is shown in Figure 18 in the text for $\rho_g/\rho_f = 0.0484$. Neglecting the existence of any transition region, the equations for the boundaries of each regime are given as follows:

Boundary Between L and H Regimes

$$L/d = \{(0.10/C)(\rho_g/\rho_f)^{0.133}\,[(\sigma\rho_f)/G^2L)]^{0.29} - 0.0031\}^{-1} \qquad (A26)$$

Boundary Between N and H Regimes

$$L/d = 0.77/[(\sigma\rho_f)/G^2L)]^{0.37} \qquad (A27)$$

Boundary Between H and HP Regimes

$$L/d = \frac{0.384(\rho_g/\rho_f)^{0.467} - [(\sigma\rho_f)/G^2L)]^{0.160}}{0.280[(\sigma\rho_f)/G^2L)]^{0.393} - 0.00119(\rho_g/\rho_f)^{0.467}} \qquad (A28)$$

Boundary Between HP and N Regimes

$$(\rho_g/\rho_f) = \{[89.3(d/L)^{0.432} + 21.2(d/L)^{0.062}]/[0.119(L/d) + 38.4]\}^{2.14} \qquad (A29)$$

LOFT Correlation (Eide 1977)

$$q_{CHF} = 1.31569 \times 10^{6} - 3.79605 \times 10^{2}P + 8.32015 \times 10^{-2}G + 1.08312 \times 10^{2}Px - 1.01982Gx \quad \text{(A30)}$$

Equation A30 is valid for the following parametric ranges:

P: 200 to 2400 psia

G: $.4 \times 10^{6}$ to 2.5×10^{6} lbm/hr-ft^2

x: -0.30 to 0.20

$$q_{CHF} = (1.880919 \times 10^{6}) - (850.58)P - (1.0986)x + (0.13P^{2} - (1.186207 \times 10^{6})x^{2} \quad \text{(A31)}$$

This equation is valid for the following parametric ranges:

P: 1000 to 2000 psia

G: $.4 \times 10^{6}$ to 2×10^{6} lbm/hr-ft^2

x: -0.05 to 0.50

Savannah River Correlation (Knoebel 1973)

$$q_{CHF} = 188000\ (1.0 + 0.0515U)(1.0 + 0.069\Delta T_{SUB}) \qquad \text{(A32)}$$

where:

U = fluid velocity, ft/s

$\Delta T_{SUB} = T_c - T_{SAT}$

W-3 Correlation (Tong 1972)

$$\begin{aligned} q_{CHF} = \quad & 10^6\{(2.022 - 4.302 \times 10^{-4}P) + \\ & (0.1722 - 9.84 \times 10^{-5}P) \exp [(18.177 - 4.129 \times 10^{-3}P)\, x]\} \\ & (1.157 - 0.869x) \\ & [(0.1484 + x\,(-1.596 + 0.1729\,|x|))\, G' + 1.037] \\ & [0.8258 + 7.94 \times 10^{-4}(h_f - h_i)] \\ & [0.2664 + 0.8357 \exp (-3.151\ (d_{HE}))] \end{aligned} \qquad \text{(A33)}$$

where $G' = G/10^6$

The parametric ranges are:

d: 0.2 to 0.7 in

L: 10 to 144 in

P: 1000 to 2400 psia

G: 1×10^6 to 5×10^6 lbm/ft^2-hr

x: -0.15 to 0.15

Griffith-Zuber Correlation (Griffith 1977)

$$q_{CHF} = (1 - \beta_v)\ 0.131\ \rho_g h_{fg}\ [\sigma g(\rho_f - \rho_g)/\rho^2]^{\frac{1}{4}} \qquad \text{(A34)}$$

valid for $G < 2 \times 10^4$ lbm/hr-ft^2

Modified Zuber Correlation (Smith 1976)

$$q_{CHF} = (0.96 - \beta_v)0.130\ h_{fg}[\sigma g(\rho_f - \rho_g)]^{\frac{1}{4}}[\rho_g \rho_f/(\rho_f + \rho_g)]^{\frac{1}{2}} \qquad \text{(A35)}$$

APPENDIX B

CODA CODE DESCRIPTION

This appendix contains a brief description and a listing of the Coolant Dynamic Analysis (CODA) code developed by Leung and Gallivan (Leung 1980). This program is used by Leung (1980), Lo (1984) and the author (1984) to compare commonly used correlations to blowdown data.

The CODA code was preferred for the present study, due to a variety of reasons, such as:

1. Although less complicated, it was shown by Leung (1980) that CODA gives comparative results to component codes such as SCORE-EVET and COBRA-IV.
2. The CODA code requires less computer time as compared to the other system codes and component codes.
3. The CODA code was easily accessible through the EG & G Idaho National Laboratory.

The CODA code is a simple one-dimensional transient coolant dynamic analysis computer program to analyze the core behavior during a transient. A homogeneous equilibrium flow model, with equal velocity and equal temperature for the two phases, is adapted. In general, this is a valid assumption, especially for high-pressure systems such as PWRs. The code is available in two versions: flow-driven and pressure-driven versions. The flow-driven version is shown (Leung 1980) to give superior results to the pressure-driven version. Thus,

the flow-driven version is used by the author (Gunnerson 1984), Lo (1984), and Leung (1980). The mathematical formulation of the thermal-hydraulic analysis used in the flow-driven version of CODA is briefly outlined in the following section.

CODA Code Formulation

For homogeneous, one-dimensional two-phase flow, the following conservation equations may be written:

Continuity:

$$\frac{\partial \rho}{\partial t} + \frac{\partial G}{\partial z} = 0 \qquad \text{(B1)}$$

Momentum:

$$\frac{\partial G}{\partial t} + \frac{\partial}{\partial z}\left(\frac{G^2}{\rho} + P\right) = -\rho g - \frac{2f}{d\rho} G|G| \qquad \text{(B2)}$$

Energy:

$$\frac{\partial E_t}{\partial t} + \frac{\partial}{\partial z}\left[(E_t + P)\frac{G}{\rho}\right] = \frac{qP_H}{A} \qquad \text{(B3)}$$

where E_t is the volumetric total energy defined as

$$E_t = \rho e + \frac{1}{2}\left(\frac{G^2}{\rho}\right) \qquad \text{(B4)}$$

e is the internal energy which can be written as:

$$e = h - \frac{P}{\rho} \qquad \text{(B5)}$$

In addition to these conservation equations, an equation of state is needed.

In the CODA code formulation, the Courant Stability criterion which limits the time step as:

$$\Delta t \leq \frac{\Delta z}{c + |U|} \tag{B6}$$

is modified to allow larger time increments. The modified stability criterion is written as:

$$\Delta t \leq \frac{\Delta z}{|U|} \tag{B7}$$

This criterion does not take the sonic velocity (c) into account, and it does not allow any fluid particle to traverse more than one nodal spacing during the time period. This new criterion forces the assumption that the pressure has no feedback on the density, and the density is a function of the enthalpy only. Therefore, the equation of state becomes

$$\rho = \rho(h) \tag{B8}$$

This later assumption decouples the momentum equation from continuity and energy equations.

In general, for a variable cross-sectional area, the continuity and the energy equations can be written as follows, by neglecting the kinetic energy term:

Continuity:

$$A \frac{\partial \rho}{\partial t} + \frac{\partial}{\partial z} (GA) = 0 \tag{B9}$$

Energy:

$$A \frac{\partial}{\partial t} (\rho h) + \frac{\partial}{\partial z} (GAh) = qP_H + A\frac{\partial P}{\partial t} \qquad (B10)$$

Equation B10 can be written in the form:

$$A\rho \frac{\partial h}{\partial t} + Ah \frac{\partial \rho}{\partial t} + h\frac{\partial}{\partial z} (GA) + GA\frac{\partial h}{\partial z} = qP_H + A\frac{\partial P}{\partial t} \qquad (B11)$$

where $\frac{\partial}{\partial z} (GA) = - A\frac{\partial \rho}{\partial t}$ from the continuity equation.

Thus:

$$\frac{\partial h}{\partial t} + \frac{G}{\rho} \frac{\partial h}{\partial z} = \frac{qP_H}{\rho A} + \frac{1}{\rho} \frac{\partial P}{\partial t} \qquad (B12)$$

Now, by dividing the flow channel into equally-spaced nodes, equations B12 and B9 may be integrated by using the finite-difference technique. The finite-difference procedure employed in the code is not repeated here. Figure 111 shows the flowchart of the CODA code. For more information about the code, the reader is referred to the study of Leung (1980).

For the flow-driven version of the CODA code, the following parameters must be supplied to the code as input:

1. System pressure as a function of time
2. Inlet or exit mass flow rate as a function of time
3. Heat flux as a function of time and axial location
4. Fluid enthalpy at the inlet boundary as a function of time

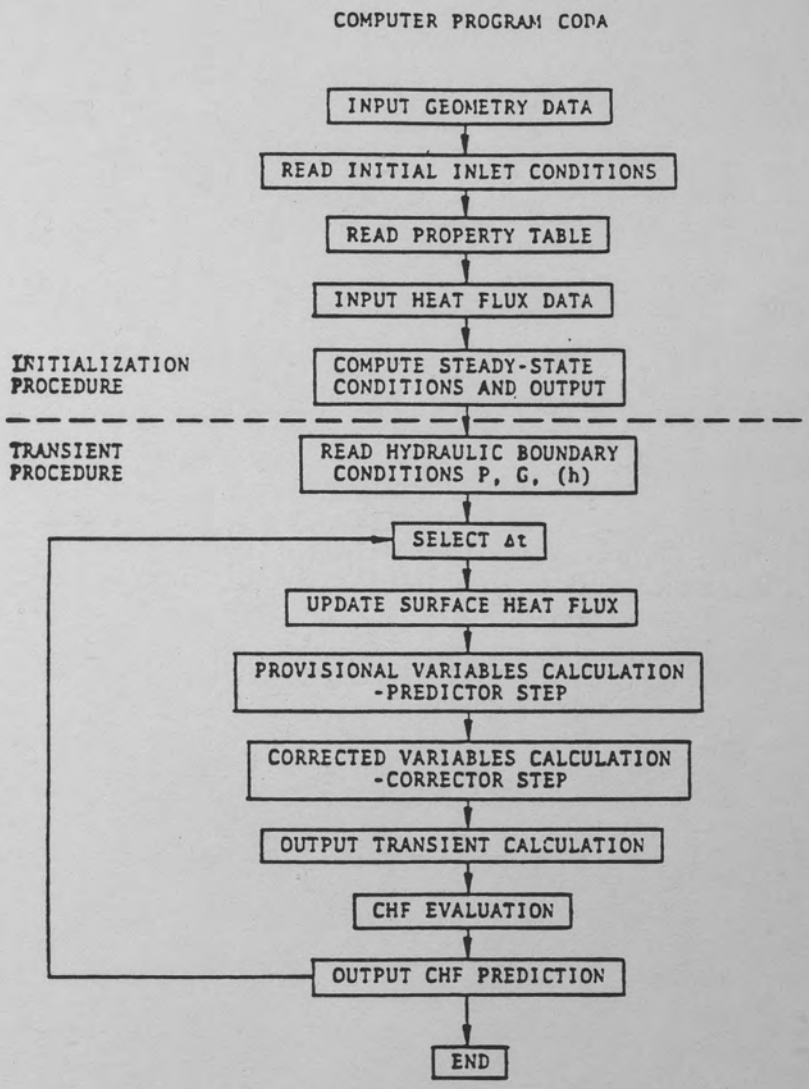

Figure 111. The Flowchart of the Flow Driven Version of CODA Program (Leung 1980)

Given this input, the CODA code calculates the Critical Heat Flux Ratio (CHFR), using the desired correlations, as a function of time and axial location.

In the following section, a listing of the flow-driven version of the CODA code, as adapted to the Digital VAX system of UCF, is given.

Listing of CODA Code

```
      REAL INTERP
      REAL LBNT
      REAL LOFT
      REAL MZUBER
      DIMENSION CHF1(250),CHF2(250),CHF3(250),CHF4(250)
      DIMENSION CHF6(250),RAT6(250)
      DIMENSION CHF7(250),CHF8(250),CHF9(250)
      DIMENSION RAT7(250),RAT8(250),RAT9(250)
      DIMENSION RAT1(250),RAT2(250),RAT3(250),RAT4(250)
      DIMENSION XCHF5(250),RAT5(250)
      DIMENSION CHF10(250),RAT10(250)
       DIMENSION CHF11(250),RAT11(250)
       DIMENSION CHF12(250),RAT12(250)
       DIMENSION CHF13(250),RAT13(250)
       DIMENSION CHF14(250),RAT14(250)
       DIMENSION CHF15(250),RAT15(250)
       DIMENSION CHF16(250),RAT16(250)
       DIMENSION CHF17(250),RAT17(250)
      DIMENSION PHIT(20,30),TPHIT(20,30),BINT(250),
     C AINT(250),NTPHI(250),NCPHI(250)
      DIMENSION GIN(250),TGIN(250)
      DIMENSION PHI(250),HEAT(250),GT1(250),HT1(250),XT1(250)
     C,SPVT1(250),RHOT1(250),VT1(250),PT1(250),TP(50),PR(50),
     CTDP(50),DP(50),HT(250),RHOT(250),SPVT(250),VT(250),
     CXT(250),SIGMA(250),GT(250),
     CXTP(250),GTP(250),VTP(250),SPVTP(250),RHOTP(250),HTP(250)
      DIMENSION PPT(250),TPT(250),VFPT(250),VFGPT(250),
     C HFPT(250),HFGPT(250),VISCPT(250),CONDPT(250),SFTPT(250)
      DIMENSION ALPHA(250),GPR(250),PPR(250)
      DIMENSION AX(250),DIAH(250),DIAE(250)
      DIMENSION CPGPT(250)
      DIMENSION DFBHL(250),TEMPR(250),FLOWM(250)
      DIMENSION SFPT(250),SGPT(250),TDPCR(250),DPCR(250)
C
      OPEN(UNIT=5,FILE='CODA.DAT',STATUS='OLD')
      OPEN(UNIT=6,FILE='CODA.RPT',STATUS='NEW')
C
C
C
       SPRINT=0.0
C
C
C
C
C     PROCEDURE A   INITIALIZATION PROCEDURE
C
C
C     STEP A1         INPUT SECTION
C
C      STEP A1.1      ACCEPT THE INPUT
C
C                      CROSS SECTION AREA (IN.**2)
C                      HEATED PERIMETER (IN.)
C                      WETTED PERIMETER (IN.)
C                      TOTAL LENGTH (IN.)
C                       NUMBER OF NODES
C                     OUTLET PRESSURE(PSI.),
C                     INLET TEMPERATURE(F.)
C                     INLET MASS VELOCITY(LBM/FT**2 S)
      READ(5,1) TL,N
 1     FORMAT(F5.1,1X,I3)
      READ(5,16) NAX
      L2=0
      DO 601 I=1,NAX
```

```
      READ(5,600) AXIN,PH,PW,NNAX
  600  FORMAT(F5.0,1X,F5.2,1X,F5.2,1X,I3)
      L2=L2+NNAX
      L1=(L2-NNAX)+1
      DO 601 J=L1,L2
      AX(J)=AXIN
      DIAH(J)=(4.00*AX(J))/PW
      DIAE(J)=(4.00*AX(J))/PH
  601 CONTINUE
      READ(5,2) PO,TO,GO
  2   FORMAT(F5.0,1X,F5.1,1X,F8.1,1X,F8.1)
C
C     STEP A1.2      OUTPUT THE INPUT
C
      DZ=TL/(N-1)
      WRITE(6,3) TL,DZ
  3   FORMAT('1','TOTAL LENGTH= ',F5.1,' DZ= ',F6.3)
      WRITE(6,602) (I,AX(I),DIAH(I),DIAE(I),I=1,N)
  602 FORMAT(' ',I3,1X,'AX= ',F6.3,' DIAH= ',F6.3,' DIAE= ',F6.3)
      WRITE(6,4) N
  4   FORMAT('0','TOTAL NUMBER OF NODES= ',I4)
      WRITE(6,5) PO,TO,GO
  5   FORMAT('0','PRESS= ',F6.1,2X,'TEMP= ',F5.1,2X,
     C  'MASS VEL= ',F8.1,2X )
C
C
C
C     STEP A1.3      CONVERT INPUT TO PROPER UNITS
C
C
C                    DIA. TO FT.
C                    LENGTH TO FT.
C                    DZ TO FT.
C                    PRESSURE TO PSF.
C                    NOTE: AX IS IN IN.**2 IN THE PROGRAM.
      DO 603 I=1,N
      DIAH(I)=DIAH(I)/12.00
      DIAE(I)=DIAE(I)/12.00
  603 CONTINUE
      TL=TL/12.00
      DZ=DZ/12.00
      PO=PO*144.00
C
C     STEP A1.4    INPUT THE PROPERTY TABLE
C
      READ(5,16) NPROP
      DO 54 I=1,NPROP
      READ(5,55) PPT(I),TPT(I),VFPT(I),VG,HFPT(I),HG,
     C VISCPT(I),CONDPT(I),SFTPT(I)
  55  FORMAT(2F5.0,7F10.0)
      VFGPT(I)=VG-VFPT(I)
      HFGPT(I)=HG-HFPT(I)
  54  CONTINUE
      DO 701 I=1,NPROP
      READ(5,702) CPGPT(I),SFPT(I),SGPT(I)
  702 FORMAT(3(F10..0))
  701  CONTINUE
C
C     STEP A1.5    OUTPUT THE PROPERTY TABLE
C
       GO TO 9020
      WRITE(6,47)
  47  FORMAT(1H1,'PROPERTY TABLE',///)
```

```
      WRITE(6,56)
 56    FORMAT('0',5X,'P',  6X,'T',12X,'VF',11X,'VFG',
     C11X,'HF',11X,'HFG',10X,'VISC',11X,'KF',12X,'ST',7X,'CPG')
      DO 58 I=1,NPROP
      WRITE(6,57) PPT(I),TPT(I),VFPT(I),VFGPT(I),HFPT(I),
     CHFGPT(I),VISCPT(I),CONDPT(I),SFTPT(I),CPGPT(I)
 57    FORMAT(' ',2(3X,F6.1),2(7X,F7.5),2(7X,F6.2),
     C 3(7X,F7.5),2X,F6.3)
 58   CONTINUE
      WRITE(6,902)
 902  FORMAT('0',5X,'SF',7X,'SG')
      DO 900 I=1,NPROP
      WRITE(6,901) SFPT(I),SGPT(I)
 901  FORMAT(' ',3X,F7.4,2X,F7.4)
 900  CONTINUE
 9020 CONTINUE
C
C  STEP A1.6   INPUT PHI(Z,T)
C
C
C  STEP A1.6.1  INPUT NUMBER OF PHI SECTIONS
C
      READ(5,16) NSPHI
C
C  STEP A1.6.2  INPUT PHI AND TIME VALUES
C               FOR EACH SECTION
C
      DO 90 J=1,NSPHI
C
C  STEP A1.6.2.1  INPUT THE NUMBER OF CELLS IN THIS SECTION
C
      READ(5,16) NCPHI(J)
C
C  STEP A1.6.2.2  INPUT THE NUMBER OF TIME POINTS
C                 FOR THIS SECTION
C
      READ(5,16) NTPHI(J)
C
C  STEP A1.6.2.3  INPUT TIME AND PHI VALUES FOR THIS SECTION
C
      NN=NTPHI(J)
      READ(5,17) (TPHIT(J,K),PHIT(J,K),K=1,NN)
 90   CONTINUE
C
C    STEP A2      INITIALIZATION OF VARIABLES
C                  THROUGH STEADY STATE CALCULATIONS
C
C    STEP A2.1     INITIALIZE SYSTEM VARIABLES WHICH
C                  DEPEND UPON OUTLET PRESSURE AND CALCULATE
C                  HEAT FLUX PER NODE
C
C
C  STEP A2.1.1   FUNCTIONS OF PRESSURE
C
      POO=PO/144.00
      SPVFGS=INTERP(PPT,VFGPT,POO,NPROP,1)
      SPVFS=INTERP(PPT,VFPT,POO,NPROP,2)
      HFGS=INTERP(PPT,HFGPT,POO,NPROP,3)
      HFS=INTERP(PPT,HFPT,POO,NPROP,4)
      TSAT=INTERP(PPT,TPT,POO,NPROP,25)
      CPG=INTERP(PPT,CPGPT,POO,NPROP,26)
C
C  STEP A2.1.2  INITIALIZE PHI FOR STEADY STATE
```

```
C
C
C  STEP A2.1.2.1 SET UPPER BOUND TO 0
C
      N2=0
C
C  STEP A2.1.2.2  SET PHI FOR EACH SECTION
C
      DO 81 I=1,NSPHI
C
C  STEP A2.1.2.2.1  MOVE THIS SECTIONS ARRAYS TO
C                   INTERPOLATION ARRAYS
C
      NN=NTPHI(I)
      DO 82 K=1,NN
      AINT(K)=TPHIT(I,K)
 82   BINT(K)=PHIT(I,K)
C
C  STEP A2.1.2.2.2  SET UPPER AND LOWER BOUNDS FOR
C                   THIS SECTION
C
      N2=N2+NCPHI(I)
      N1=(N2-NCPHI(I))+1
C
C  STEP A2.1.2.2.3  SET PHI FOR THIS SECTION
C
      TIME=0.00
      PHIVAL=INTERP(AINT,BINT,TIME,NTPHI(I),5)
      DO 83 K=N1,N2
 83   PHI(K)=PHIVAL
 81   CONTINUE
C
C    STEP A2.2     CALCULATE MASS VELOCITY FOR NODES 1,N
C
      DO 7 I=1,N
 7    GT1(I)=GO*AX(1)/AX(I)
C
C    STEP A2.3     CALCULATE ENTHALPY FOR NODES 1,N
C
      HT1(1)=INTERP(TPT,HFPT,TO,NPROP,6)
      SPVFO=INTERP(HFPT,VFPT,HT1(1),NPROP,7)
      DO 8 I=2,N
 8    HT1(I)=HT1(I-1) +((4.00*PHI(I-1) *DZ)/(DIAE(I-1)*GT1(I-1)))
C
C     STEP A2.4     CALCULATE QUALITY FOR NODES 1,N
C
      DO 9 I=1,N
 9    XT1(I)=(HT1(I)-HFS)/HFGS
C
C    STEP A2.5     CALCULATE SPECIFIC VOLUME AND DENSITY
C                  FOR NODES 1,N
C
      DO 10 I=1,N
      IF(XT1(I).LE.0.00) SPVT1(I)=INTERP(HFPT,VFPT,HT1(I),NPROP,8)
      IF(XT1(I).GT.0.00) SPVT1(I)=SPVFS+(XT1(I)*SPVFGS)
      RHOT1(I)=1.00/SPVT1(I)
      IF(XT1(I).LT.1.00) GO TO 10
      TSH=TSAT+((HT1(I)-(HFGS+HFS))/CPG)
      SPVT1(I)=(SPVFGS+SPVFS)*((460.00+TSH)/(460.00+TSAT))
      RHOT1(I)=1.00/SPVT1(I)
 10    CONTINUE
C
C    STEP A2.6     CALCULATE VELOCITY FOR NODES 1,N
```

```
C
      DO 11 I=1,N
 11   VT1(I)=GT1(I)/RHOT1(I)
C
C     STEP A2.7     CALCULATE PRESSURE FOR NODES 1,N
C
      PT1(N)=P0
      I=N-1
 12   IF(XT1(I).LE.0.00)
     C F=.07900/((ABS(GT1(I))*3600.00*DIAH(I)/INTERP(HFPT,VISCPT,
     C HT1(I),NPROP,9))**.2500)
      IF(XT1(I).GT.0.00) F=.00500
      A=((SPVT1(I+1)*GT1(I+1)**2)-(SPVT1(I)*GT1(I)**2))/DZ
      B=32.200/SPVT1(I)
      C=(2.00*F)/DIAH(I)
      D=((VT1(I)*ABS(VT1(I)))/(SPVT1(I)))*C
      K1=I
      IF(AX(I+1).LT.AX(I)) K1=I+1
      IF(XT1(I).LE.0.00.OR.XT1(I).GE.1.00) COEF=.4500
      IF(XT1(I).GT.0.00.AND.XT1(I).LT.1.00) COEF=.200
      IF (AX(I).LT. AX(I+1))EK=(1.00-(AX(I)/AX(I+1)))**2
      IF(AX(I).GE.AX(I+1))EK=COEF *(1.00-(AX(I+1)/AX(I))**2)
      PT1(I)=PT1(I+1)+(((DZ/32.200)*(A+B+D)))
     C+((EK*((GT1(K1 )**2)/RHOT1(K1 )))/64.400)
      I=I-1
      IF(I.GE.1) GO TO 12
C
C     STEP A2.8     CALCULATE AVERAGE MASS VELOCITY
C
      GT1AV=GT1(1)
C
C  STEP A2.9 CALCULATE VOID FRACTION
C
      DO 71 I=1,N
      ALPHA(I)=XT1(I)*RHOT1(I)*(SPVFGS+SPVFS)
      IF(XT1(I).LE.0.00) ALPHA(I)=0.00
      IF(XT1(I).GE.1.00) ALPHA(I)=1.00
 71   CONTINUE
C
C  STEP A2.10  CALCULATE REMAINING MASS
C
      SUM=.500*DZ*(RHOT1(1)*AX(1)+RHOT1(N)*AX(N))/144.00
      N1=N-1
      DO 110 I=2,N1
 110  SUM=SUM+(RHOT1(I)*DZ*AX(I)/144.00)
      RMASS=SUM
C
C  STEP A2.11 CALCULATE DISTANCE FROM BEGINNING OF
C             HEATED LENGTH FOR EACH NODE
C
      DATA DFBHL /250*0.00/
      IFLAG=0
      PHI(N)=PHI(N-1)
      I=0
 706  I=I+1
      IF(PHI(I).NE.0.00) IFLAG=I
      IF(PHI(I).NE.0.00) I=N
      IF(I.NE.N) GO TO 706
      BHL=((IFLAG-1)*DZ) *12.00
      IF(IFLAG.EQ.0) GO TO 950
      I=IFLAG
 707  I=I+1
      DFBHL(I)=(((I-1)*DZ)*12.00)-BHL
```

```
      IF(PHI(I).EQ.0.00) I=N
      IF(I.NE.N) GO TO 707
  950 CONTINUE
C
C
C     STEP A2.12      OUTPUT STEADY STATE VALUES
C
      WRITE(6,13) HFGS
   13 FORMAT(1H1,'STEADY STATE VALUES',3X,'HFG= ',F9.2,//)
      DO 61 I=1,N
      FLOWM(I)=GT1(I)*AX(I)/144.00
      IF(XT1(I).LT.1.00) TEMPR(I)=TSAT
      IF(XT1(I).LT.0.00) TEMPR(I)=INTERP(HFPT,TPT,HT1(I),NPROP,29)
      IF(XT1(I).GE.1.00) TEMPR(I)=TSAT+((HT1(I)-(HFGS+HFS))/CPG)
      PPR(I)=PT1(I)/144.00
   61 GPR(I)=GT1(I)*3600.00/1.E06
      WRITE(6,14) (I,DFBHL(I),AX(I),HT1(I),TEMPR(I),XT1(I),
     C GPR(I),FLOWM(I),VT1(I),PPR(I),RHOT1(I),ALPHA(I),I=1,N)
   14 FORMAT(' ',I3,1X,'DIS ',F5.1,1X,'AX ',F6.3,1X,'H ',
     C F7.2,1X,'T ',F6.1,1X,'X ',F6.3,1X,'G ', F6.3,
     C '*10**6',1X,
     C 'MF '    ,F7.2,1X,'V ',F7.2,1X,'P ',F7.1,1X,'RHO ',
     C F7.2,1X,'ALPHA ',F6.3)
      WRITE(6,64)
   64 FORMAT(1H1,'STEADY STATE PHI VALUES',/)
      N1=N-1
      WRITE(6,62) (I,PHI(I),I=1,N1)
   62 FORMAT(' ',I4,1X,'PHI= ',F6.2)
      WRITE(6,111)RMASS
  111 FORMAT('0','REMAINING MASS= ',F9.3)
C
C
C
C
C
C     PROCEDURE B     TRANSIENT PROCEDURE
C
C
C     STEP B1    INITIALIZE THE CONTROL VARIABLES
C
C     STEP B1.1    INPUT THE TIME VS. REFERENCE PRESSURE
C                  (PSI.)
C
      READ(5,16) NUMPR
   16 FORMAT(I3)
      READ(5,17) (TP(I),PR(I),I=1,NUMPR)
   17 FORMAT(8(F5.0,F5.0))
C
C     STEP B1.2     WRITE TIME VS.REFERENCE PRESSURE
C
      WRITE(6,18)
   18 FORMAT(1H1,'INPUT VALUES OF TIME AND PRESSURE')
      WRITE(6,19)(TP(I),PR(I),I=1,NUMPR)
   19 FORMAT('0',3(4X,F12.4,1X,F12.4))
C
C     STEP B1.3     CONVERT REFERENCE PRESSURE TO PSF.
C
      DO 20 I=1,NUMPR
   20 PR(I)=PR(I)*144.00
C
C     STEP B1.4     INPUT TIME VS. G (LBM/H FT**2) OR CRITICAL FLOW DATA
C
      READ(5,16) NGID
```

```
      IF(NGIO.NE.0.AND.NGIO.NE.-1) GO TO 905
      READ(5,16) NGIN
      READ(5,65) (TGIN(I),GIN(I),I=1,NGIN)
 65   FORMAT(4(F10.0,F10.0))
      GO TO 5000
 905  READ(5,906) AT,DC1,DC2,DC3,XSTAR
 906  FORMAT(5(F5.0))
      READ(5,16) NDPCR
      IF(NDPCR.NE.0)READ(5,17) (TDPCR(I),DPCR(I),I=1,NDPCR)
 5000 CONTINUE
C
C     STEP B1.5     WRITE TIME VS. G IN OR CRITICAL FLOW DATA
C
      IF(NGIO.NE.0.AND.NGIO.NE.-1) GO TO 907
      WRITE(6,66)
 66    FORMAT(1H1,'INPUT VALUES OF TIME VS. G  '//)
      WRITE(6,67) (TGIN(I),GIN(I),I=1,NGIN)
 67    FORMAT(' ',4(4X,F12.3,1X,F12.3))
      GO TO 908
 907  WRITE(6,909)
 909  FORMAT(1H1,'CRITICAL FLOW DATA',//)
      WRITE(6,910) AT,DC1,DC2,DC3,XSTAR
 910  FORMAT('0','AREA=',F6.3,//,' SINGLE PHASE COEFFICIENT=',
     C F6.3,/,' TWO PHASE COEFFICIENT=',F6.3,/,
     C ' SINGLE PHASE COEFFICIENT=',F6.3,/,
     C ' NON-EQUILIBRIUM QUALITY=',F6.3)
      IF(NDPCR.NE.0)WRITE(6,911)
      IF(NDPCR.NE.0)WRITE(6,912) (TDPCR(I),DPCR(I),I=1,NDPCR)
 911  FORMAT('0','THROAT DELTA P FUNCTION',//)
 912  FORMAT(' ',4(1X,F5.2,2X,F6.2))
      GO TO 915
 908  CONTINUE
C
C     STEP B1.6     CONVERT G TO LBM/S*FT**2
C
      DO 22 I=1,NGIN
 22   GIN(I)=GIN(I)/3600.00
C
C     STEP B1.7     INPUT END TIME AND WRITE STEP
C
 915   CONTINUE
      READ(5,23) ENDT,NPRINT
 23   FORMAT(F5.2,I3)
C
C     STEP B1.8     INITIALIZE BOUNDARY ENTHALPIES AND TIME
C                   TO STEADY STATE VALUES
C
      TIME=0.00
      CTNUM=.500
      HFO=HT1(1)
      HFN=HT1(N)
C
C     STEP B1.9     INITIALIZE WRITE CONTROL VARIABLES
C
      IPRINT=0
C
C     STEP B1.10.   OUTPUT PHI VS. TIME
C
      WRITE(6,59)
 59   FORMAT(1H1,'INPUT VALUES OF PHI VS. TIME')
      DO 92 I=1,NSPHI
      WRITE(6,93) I
 93    FORMAT('0','SECTION= ',I3,//)
```

```
      NN=NTPHI(I)
      WRITE(6,94) (TPHIT(I,K),PHIT(I,K),K=1,NN)
 94    FORMAT(' ',5(3X,F7.4,2X,F7.3))
 92    CONTINUE
C
C     STEP B2     TRANSIENT CALCULATIONS
C                 (PERFORMED UNTIL END OF TRANSIENT CONDITION
C                  CONDITION DETECTED)
C
C     STEP B2.1     UPDATE TIME AND DELTAT
C
C
C      STEP B2.1.1    FIND MAXIMUM VELOCITY
C
 25    CONTINUE
      VMAX=0.00
      DO 15 I=1,N
      IF(ABS(VT1(I)).GT.VMAX) VMAX=ABS(VT1(I))
 15     CONTINUE
C
C     STEP B2.1.2     CALCULATE DELTAT
C
      DELTAT=(DZ/VMAX)*CTNUM
      IF(TIME.LE..500.AND.DELTAT.GT..0100)DELTAT=.0100
C
C
C     STEP B2.1.3    UPDATE TIME
C
      TIME=TIME+DELTAT
C
C     STEP B2.1.4    CHECK FOR END OF TRANSIENT
C
      IF(TIME.GT.ENDT) GO TO 5005
C
C     STEP B2.2 SET REFERENCE PRESSURE, PRESSURE DROP,
C               ENTHALPIES, AND SPECIFIC VOLUMES
C              AND SET PHI FOR THIS TIME
C
C
C   STEP B2.2.1  FUNCTIONS OF PRESSURE
C
      PREF=INTERP(TP,PR,TIME,NUMPR,10)
      PREFF=PREF/144.00
      HF=INTERP(PPT,HFPT,PREFF,NPROP,11)
      HFG=INTERP(PPT,HFGPT,PREFF,NPROP,12)
      VF=INTERP(PPT,VFPT,PREFF,NPROP,13)
      VFG=INTERP(PPT,VFGPT,PREFF,NPROP,14)
      TSAT=INTERP(PPT,TPT,PREFF,NPROP,27)
      CPG=INTERP(PPT,CPGPT,PREFF,NPROP,28)
C
C   STEP B2.2.2  SET PHI FOR THIS TIME
C
C
C   STEP B2.2.2.1  SET UPPER BOUND TO 0
C
      N2=0
C
C   STEP B2.2.2.2  SET PHI FOR EACH SECTION
C
      DO 100 J=1,NSPHI
C
C   STEP B2.2.2.2.1 MOVE THIS SECTIONS ARRAYS TO
C                   INTERPOLATION ARRAYS
```

```
      NN=NTPHI(J)
      DO 101 K=1,NN
      AINT(K)=TPHIT(J,K)
  101  BINT(K)=PHIT(J,K)
C
C  STEP B2.2.2.2.2  SET UPPER AND LOWER BOUNDS FOR
C                    THIS SECTION
C
      N2=N2+NCPHI(J)
      N1=(N2-NCPHI(J))+1
C
C  STEP B2.2.2.2.3  SET PHI FOR THE CELLS IN THIS SECTION
C
      PHIVAL=INTERP(AINT,BINT,TIME,NTPHI(J),15)
      DO 102 K=N1,N2
  102  PHI(K)=PHIVAL
  100  CONTINUE
C
C     STEP B2.3     TRANSIENT VARIABLES CALCULATIONS
C                   (PROVISIONAL VARIABLES)
C
C
C
C     STEP B2.3.1     CALCULATE ENTHALPY FOR PRESENT TIME
C
C
C     STEP B2.3.1.1    CALCULATE ENTHALPY FOR NODES 2,N-1
C
      N1=N-1
      TIMNEW=TIME-DELTAT
      DPDT=(PREF-INTERP(TP,PR,TIMNEW,NUMPR,16))/DELTAT
      DO 24   I=2,N1
      HA=.500*(HT1(I)+HT1(I-1))
      HB=.500*(HT1(I)+HT1(I+1))
      IF(AX(I).NE.AX(I+1).AND.GT1(I).GE.0.00)
     C HB=HT1(I)
      IF(AX(I).NE.AX(I+1).AND.GT1(I).LT.0.00)
     C HB=HT1(I+1)
      IF(AX(I).NE.AX(I-1).AND.GT1(I).GE.0.00)
     C HA=HT1(I-1)
      IF(AX(I).NE.AX(I-1).AND.GT1(I).LT.0.00)
     C HA=HT1(I)
      A=(-GT1(I)*(HB-HA))/(RHOT1(I)*DZ)
      PHIAV=.500*(PHI(I-1)+PHI(I))
      B=((4.00*PHIAV)/(DIAE(I)*RHOT1(I)))+
     C (( SPVT1(I)*DPDT)/777.6500)
      DHDT=(A+B)
      HT(I)=HT1(I)+(DELTAT*DHDT)
   24   CONTINUE
C
C     STEP B2.3.1.2    CALCULATE ENTHALPY AT NODES 1 AND N
C
C     STEP B2.3.1.2.1    NODE 1
C
      IF(GT1(1).GT.0.00) HT(1)=HF0
      IF(GT1(1).EQ.0.00) HT(1)=HT1(1)+
     C ((2.00*PHI(1)*DELTAT)/(RHOT1(1)*DIAE(1)))
      IF(GT1(1).LT.0.00) HT(1)=(2.00*HT(2))-HT(3)
C
C     STEP B2.3.1.2.2     NODE N
C
      IF(GT1(N).GT.0.00) HT(N)=(2.00*HT(N-1))-HT(N-2)
```

```
      IF(GT1(N).EQ.0.00) HT(N)=HT1(N)+
     C ((2.00*PHI(N-1)*DELTAT)/(RHOT1(N)*DIAE(N)))
      IF(GT1(N).LT.0.00) HT(N)=HFN
C
C     STEP B2.3.2  CALCULATE DENSITIES AT PRESENT TIME
C
      DO 52 I=1,N
      IF(HT(I).LT.HF)RHOT(I)=1.00/INTERP(
     CHFPT,VFPT,HT(I),NPROP,17)
      IF(HT(I).LT.HF)  SPVT(I)=1.00/RHOT(I)
      IF (HT(I).LT.HF)GO TO 52
      X=(HT(I)-HF)/HFG
      SPVT(I)=VF+X*VFG
      RHOT(I)=1.00/SPVT(I)
      HG=HFG+HF
      IF(HT(I).LT.HG)GO TO 52
      TSH=TSAT+((HT(I)-HG)/CPG)
      SPVT(I)=(VFG+VF)*((460.00+TSH)/(460.00+TSAT))
      RHOT(I)=1.00/SPVT(I)
 52    CONTINUE
C
C     STEP B2.3.3   CALCULATE  MASS VELOCITY AT NODES 1,N
C
C
C    STEP B2.3.3.1  CALCULATE SIGMA TERMS FOR NODES 1,N-1
C
      N1=N-1
      DO 28 I=1,N1
      SIGMA(I)=(DZ/(2.00*DELTAT))*((RHOT1(I)-RHOT(I))*AX(I)+
     C    (RHOT1(I+1)-RHOT(I+1))*AX(I+1))
 28    CONTINUE
C
C     STEP B2.3.3.2  CALCULATE MASS VELOCITY AT NODE 1
C     (INLET FLOW SPECIFIED)
      IF(NGIO.LT.0) GO TO 68
C
C
      IF(NGIO.EQ.0)GT(1)=INTERP(TGIN,GIN,TIME,NGIN,18)
      RHOINV=1.00/RHOT1(1)
      IF(XT1(1).LT.0.00)
     CPSAT=INTERP(VFPT,PPT,RHOINV,NPROP,111)*144.00
      IF(NGIO.EQ.1)GT(1)=-1.00*CRTFLO(PREF,AX(1),AT,XT1(1),HT1(1),
     C RHOT1(1),PSAT,DC1,DC2,DC3,XSTAR,PPT,SFPT,SGPT,HFPT,
     C HFGPT,VFPT,VFGPT,NPROP,NDPCR,TDPCR,DPCR,TIME)
C
C     STEP B2.3.3.3  CALCULATE MASS VELOCITY AT NODES 2,N
C
      DO 31 I=2,N
     'GT(I)=(GT(I-1)*AX(I-1)+SIGMA(I-1))/AX(I)
 31    CONTINUE
      GO TO 69
C  STEP B2.3.3.4 CALCULATE MASS VELOCITY AT NODE N
C                (OUTLET FLOW SPECIFIED)
C
 68    CONTINUE
      IF(NGIO.EQ.-1)GT(N)=INTERP(TGIN,GIN,TIME,NGIN,19)
      RHOINN=1.00/RHOT1(N)
      IF(XT1(N).LT.0.00)
     CPSAT=INTERP(VFPT,PPT,RHOINN,NPROP,112)*144.00
      IF(NGIO.EQ.-2)GT(N)=CRTFLO(PREF,AX(N),AT,XT1(N),HT1(N),
     C RHOT1(N),PSAT,DC1,DC2,DC3,XSTAR,PPT,SFPT,SGPT,HFPT,
     C HFGPT,VFPT,VFGPT,NPROP,NDPCR,TDPCR,DPCR,TIME)
C
```

```
C  STEP B2.3.3.5 CALCULATE MASS VELOCITY AT NODES N-1,1
C
      I=N-1
 70    GT(I)=(GT(I+1)*AX(I+1)-SIGMA(I))/AX(I)
      I=I-1
      IF(I.GE.1) GO TO 70
 69    CONTINUE
C
C     STEP B2.3.4   CALCULATE VELOCITY AT NODES 1,N
C
      DO 41 I=1,N
      VT(I)=GT(I)/RHOT(I)
 41     CONTINUE
C
C
C     STEP B2.3.5   CALCULATE QUALITY FOR NODES 1,N
C
      DO 42 I=1,N
      XT(I)=(HT(I)-HF)/HFG
 42    CONTINUE
C
C     STEP B2.3.6  MOVE VARIABLES TO PROVISIONAL ARRAYS
C                  FOR NEXT STEP
C
      DO 261 I=1,N
      XTP(I)=XT(I)
      RHOTP(I)=RHOT(I)
      GTP(I)=GT(I)
      VTP(I)=VT(I)
      SPVTP(I)=SPVT(I)
      HTP(I)=HT(I)
 261    CONTINUE
C
C     STEP B2.4     TRANSIENT VARIABLES CALCULATIONS
C                   FROM PROVISIONAL VALUES
C
C
C
C     STEP B2.4.1     CALCULATE ENTHALPY FOR PRESENT TIME
C
C
C     STEP B2.4.1.1   CALCULATE ENTHALPY FOR NODES 2,N-1
C
      N1=N-1
      DPDT=(PREF-INTERP(TP,PR,TIME-DELTAT,NUMPR,20 ))/DELTAT
      DO 240   I=2,N1
      HA=.500*(HTP(I)+HTP(I-1))
      HB=.500*(HTP(I)+HTP(I+1))
      IF(AX(I).NE.AX(I+1).AND.GT1(I).GE.0.00)
     C HB=HTP(I)
      IF(AX(I).NE.AX(I+1).AND.GT1(I).LT.0.00)
     C HB=HTP(I+1)
      IF(AX(I).NE.AX(I-1).AND.GT1(I).GE.0.00)
     C HA=HTP(I-1)
      IF(AX(I).NE.AX(I-1).AND.GT1(I).LT.0.00)
     C HA=HTP(I)
      A=(-GTP(I)*(HB-HA))/(RHOTP(I)*DZ)
      PHIAV=.500*(PHI(I-1)+PHI(I))
      B=((4.00*PHIAV)/(DIAE(I)*RHOTP(I)))+
     C ((SPVTP(I) *DPDT)/777.6500)
      DHDT=(A+B)
      HT(I)=HT1(I)+(DHDT*DELTAT)
 240    CONTINUE
```

```
C
C     STEP B2.4.1.2   CALCULATE ENTHALPY AT NODES 1 AND N
C
C     STEP B2.4.1.2.1   NODE 1
C
      IF(GT1(1).GT.0.00) HT(1)=HF0
      IF(GT1(1).EQ.0.00) HT(1)=HT1(1)+
     C ((2.00*PHI(1)*DELTAT)/(RHOTP(1)*DIAE(1)))
      IF(GT1(1).LT.0.00) HT(1)=(2.00*HT(2))-HT(3)
C
C     STEP B2.4.1.2.2    NODE N
C
      IF(GT1(N).GT.0.00) HT(N)=(2.00*HT(N-1))-HT(N-2)
      IF(GT1(N).EQ.0.00) HT(N)=HT1(N)+
     C ((2.00*PHI(N-1)*DELTAT)/(RHOTP(N)*DIAE(N)))
      IF(GT1(N).LT.0.00) HT(N)=HFN
C
C     STEP B2.4.2  CALCULATE DENSITIES AT PRESENT TIME
C
      DO 520 I=1,N
      IF(HT(I).LT.HF)RHOT(I)=1.00/INTERP(
     CHFPT,VFPT,HT(I),NPROP,21 )
      IF(HT(I).LT.HF) SPVT(I)=1.00/RHOT(I)
      IF(HT(I).LT.HF) GO TO 520
      X=(HT(I)-HF)/HFG
      SPVT(I)=VF+X*VFG
      RHOT(I)=1.00/SPVT(I)
      HG=HFG+HF
      IF(HT(I).LT.HG) GO TO 520
      TSH=TSAT+((HT(I)-HG)/CPG)
      SPVT(I)=(VFG+VF)*((460.00+TSH)/(460.00+TSAT))
      RHOT(I)=1.00/SPVT(I)
  520   CONTINUE
C
C     STEP B2.4.3   CALCULATE  MASS VELOCITY AT NODES 1,N
C
C
C    STEP B2.4.3.1  CALCULATE SIGMA TERMS FOR NODES 1,N-1
C
      N1=N-1
      DO 280 I=1,N1
      SIGMA(I)=(DZ/(2.00*DELTAT))*((RHOT1(I)-RHOT(I))*AX(I)+
     C   (RHOT1(I+1)-RHOT(I+1))*AX(I+1))
  280   CONTINUE
      IF(NGIO.LT.0) GO TO 680
C
C     STEP B2.4.3.2  CALCULATE MASS VELOCITY AT NODE 1
C     (INLET FLOW SPECIFIED)
C      (NOTE:  G ALREADY CALCULATED IN PREDICTOR STEP)
      GT(1)=GT(1)
C
C     STEP B2.4.3.3  CALCULATE MASS VELOCITY AT NODES 2,N
C
      DO 310 I=2,N
      GT(I)=(GT(I-1)*AX(I-1)+SIGMA(I-1))/AX(I)
  310   CONTINUE
      GO TO 690
  680   CONTINUE
C
C   STEP B2.4.3.4  CALCULATE MASS VELOCITY AT NODE N
C                  (OUTLET FLOW SPECIFIED)
C                   (NOTE:  G ALREADY CALCULATED IN PREDICTOR STEP)
      GT(N)=GT(N)
```

```
C  STEP B2.4.3.5 CALCULATE MASS VELOCITY AT NODES N-1,1
C
      I=N-1
  700   GT(I)=(GT(I+1)*AX(I+1)-SIGMA(I))/AX(I)
      I=I-1
      IF(I.GE.1) GO TO 700
  690   CONTINUE
C
C     STEP B2.4.4   CALCULATE VELOCITY AT NODES 1,N
C
      DO 410 I=1,N
      VT(I)=GT(I)/RHOT(I)
  410     CONTINUE
C
C
C     STEP B2.4.5   CALCULATE QUALITY FOR NODES 1,N
C
      DO 420 I=1,N
      XT(I)=(HT(I)-HF)/HFG
  420   CONTINUE
C
C  STEP B2.4.6  CALCULATE REMAINING MASS
C
      SUM=.500*DZ*(RHOT(1)*AX(1)+RHOT(N)*AX(N))/144.00
      N1=N-1
      DO 112 I=2,N1
  112   SUM=SUM+(RHOT(I)*AX(I)*DZ)/144.00
      RMASS=SUM
C
C     STEP B2.5  COMPLETE PROCESSING FOR THIS TIME STEP
C
C
C  STEP B2.5.1 FACILITATE NEXT TIME STEP
C
      IPRINT=IPRINT+1
      DO 43 I=1,N
      HT1(I)=HT(I)
      GT1AV=GTAV
      RHOT1(I)=RHOT(I)
      SPVT1(I)=SPVT(I)
      VT1(I)=VT(I)
      XT1(I)=XT(I)
      GT1(I)=GT(I)
  43    CONTINUE
C
C  STEP B2.5.2 OUTPUT THE VARIABLES
C
      IF(TIME.LT.SPRINT) IPRINT=0
      IF(TIME.LT.SPRINT) GO TO 25
      IF(IPRINT.NE.NPRINT) GO TO 25
C
C     STEP B2.5.2.1   OUTPUT THE TRANSIENT VARIABLES
C
      GINPR=GT(1)*3600.00
      PRP=PREF/144.00
      WRITE(6,44) TIME,PRP,GINPR,HFG,CTNUM
  44    FORMAT(1H1,'PARAMETERS AT TIME= ',E14.5,2X,'PREF= ',F14.5,2X,
     C 'G IN = ',F14.1,2X,'HFG= ',F7.2,2X,'COURANT NUMBER= ',F10.5,//)
      WRITE(6,113)RMASS
  113   FORMAT('0','REMAINING MASS= ',F9.3)
      DO 63 I=1,N
      FLOWM(I)=GT(I)*AX(I)/144.00
```

```
      IF(XT(I).LT.1.00) TEMPR(I)=TSAT
      IF(XT(I).LT.0.00) TEMPR(I)=INTERP(HFPT,TPT,HT(I),NPROP,30)
      IF(XT(I).GE.1.00) TEMPR(I)=TSAT+((HT(I)-(HFG+HF))/CPG)
      GPR(I)=GT(I)*3600.00/1.E06
      ALPHA(I)=XT(I)*RHOT(I)*(VFG+VF)
      IF(XT(I).GE.1.00)ALPHA(I)=1.00
 63    IF(XT(I).LE.0.00) ALPHA(I)=0.00
      DO 5999 I=1,N
      GGPR=GPR(I)
      FFLOWM=FLOWM(I)
      IF(ABS(FFLOWM).GT.9000.) FFLOWM=9999.0
      VV=VT(I)
      IF(ABS(VV).GT.9000.) VV=9999.0
      IF(ABS(GGPR).GT.900.) GGPR=999.0
      IF(ABS(GGPR).LT.0.001) GGPR=0.0
      WRITE(6,45) I,DFBHL(I),AX(I),HT(I),TEMPR(I),RHOT(I),VV,
     CGGPR,FFLOWM,XT(I),ALPHA(I)
 45    FORMAT(' ',I3,1X,'DIST ',F5.1,1X,'AX ',F6.3,1X,'H ',F7.2,1X,
     C 'T ',F7.2,1X,'RHO ',F7.2,1X,     'V ',F8.2,1X,'G ', F6.3
     C ,'*10**6',1X,
     C 'MFLOW ',F8.2,1X,'X ',F9.5,1X,'ALPHA ',F8.5)
 5999 CONTINUE
C
C     STEP B2.5.2.2   CALCULATE PHI CHF DATA
C
      N1=N-1
      DZR=DZ*12.00
      PSR=PREF/144.00
      RHOF=1.00/VF
      RHOG=1.00/(VFG+VF)
      STSR=INTERP(PPT,SFTPT,PREF/144.00,NPROP,24)
      DO 500 I=1,N1
      DSR=DIAH(I)*12.00
      G1=ABS(GT(I))
      G2=ABS(GT(I+1))
      GSR=.500*3600.00*(G1+G2)
      XSR=.500*(XT(I)+XT(I+1))
      ASR=.500*(ALPHA(I)+ALPHA(I+1))
      TSR=TEMPR(I)
      VSR=VT(I)
      DIAHSR=DIAH(I)
      DIAESR=DIAE(I)
      CHF1(I)=BOWRNG(PSR,DSR,GSR,XSR,HFG)
      CHF2(I)=BIASI(PSR,DSR,GSR,XSR)
      CHF3(I)=CISE1(PSR,DSR,GSR,XSR,HFG)
      CHF4(I)=CISE4(PSR,DSR,GSR,XSR,HFG)
      XCHF5(I)=CISEBL(PSR,DSR,GSR,N,XT,I,DZR)
      CHF6(I)=GRIFZU(RHOG,RHOF,ASR,HFG,STSR)
      CHF7(I)=GE(XSR,GSR)
       CHF8(I)=CONDIE(GSR,XSR,PSR)
      CHF9(I)=BW2(PSR,DSR,HFG,XSR,GSR)
      IF(ASR.LT..9600)CHF10(I)=HSU(ASR,GSR,PSR,DSR)
      IF(ASR.GE..9600)CHF10(I)=0.00
       CHF11(I)=W3(XSR,PSR,GSR,HFG,HIN,TO,DIAESR)
       CHF12(I)=SVANAH(VSR,TSR,TSAT)
       CHF13(I)=CE1(PSR,XSR,GSR,HFG)
       CHF14(I)=LBNT(GSR,XSR,DIAHSR,DIAESR,HFG)
       CHF15(I)=LOFT(PSR,XSR,GSR)
       CHF16(I)=BWC(PSR,XSR,GSR,HFG)
       CHF17(I)=MZUBER(RHOG,RHOF,ASR,HFG,STSR)
      RAT1(I)=0.00
      RAT2(I)=0.00
      RAT3(I)=0.00
```

```
      RAT4(I)=0.00
      RAT5(I)=0.00
      RAT6(I)=0.00
      RAT7(I)=0.00
      RAT8(I)=0.00
      RAT9(I)=0.00
      RAT10(I)=0.00
       RAT11(I)=0.00
       RAT12(I)=0.00
       RAT13(I)=0.00
       RAT14(I)=0.00
       RAT15(I)=0.00
       RAT16(I)=0.00
       RAT17(I)=0.00
      IF(PHI(I).EQ.0.00) GO TO 500
      RAT1(I)=CHF1(I)/PHI(I)
      RAT2(I)=CHF2(I)/PHI(I)
      RAT3(I)=CHF3(I)/PHI(I)
      RAT4(I)=CHF4(I)/PHI(I)
      RAT5(I)=XCHF5(I)/XSR
      RAT6(I)=CHF6(I)/PHI(I)
      RAT7(I)=CHF7(I)/PHI(I)
      RAT8(I)=CHF8(I)/PHI(I)
      RAT9(I)=CHF9(I)/PHI(I)
      RAT10(I)=CHF10(I)/PHI(I)
       RAT11(I)=CHF11(I)/PHI(I)
       RAT12(I)=CHF12(I)/PHI(I)
       RAT13(I)=CHF13(I)/PHI(I)
       RAT14(I)=CHF14(I)/PHI(I)
       RAT15(I)=CHF15(I)/PHI(I)
       RAT16(I)=CHF16(I)/PHI(I)
       RAT17(I)=CHF17(I)/PHI(I)
       IF(ABS(RAT1(I)).GT.900.) RAT1(I)=999.0
       IF(ABS(RAT2(I)).GT.900.) RAT2(I)=999.0
       IF(ABS(RAT3(I)).GT.900.) RAT3(I)=999.0
       IF(ABS(RAT4(I)).GT.900.) RAT4(I)=999.0
       IF(ABS(RAT5(I)).GT.900.) RAT5(I)=999.0
       IF(ABS(RAT6(I)).GT.900.) RAT6(I)=999.0
       IF(ABS(RAT7(I)).GT.900.) RAT7(I)=999.0
       IF(ABS(RAT8(I)).GT.900.) RAT8(I)=999.0
       IF(ABS(RAT9(I)).GT.900.) RAT9(I)=999.0
       IF(ABS(RAT10(I)).GT.900.) RAT10(I)=999.0
       IF(ABS(RAT11(I)).GT.900.) RAT11(I)=999.0
       IF(ABS(RAT12(I)).GT.900.) RAT12(I)=999.0
       IF(ABS(RAT13(I)).GT.900.) RAT13(I)=999.0
       IF(ABS(RAT14(I)).GT.900.) RAT14(I)=999.0
       IF(ABS(RAT15(I)).GT.900.) RAT15(I)=999.0
       IF(ABS(RAT16(I)).GT.900.) RAT16(I)=999.0
       IF(ABS(RAT17(I)).GT.900.) RAT17(I)=999.0
 500   CONTINUE
C
C   STEP B2.5.2.3    OUTPUT PHI CHF DATA
C
      WRITE(6,501) TIME
 501   FORMAT(1H1,'PHI DATA' ,5X,'TIME=',E12.5,//)
      WRITE(6,503)
 503   FORMAT('0',4X,'DISTANCE     ',2X,'PHI',5X,'BOWRING',1X,'BIASI',3X,
     C'CISE1',3X,'CISE4',3X,'CISEBL',4X,'GRIFZU',2X,
     C'GE',6X,'CONDIE',2X,'BW2',5X,'HSU',//)
      N1=N-1
      WRITE(6,502)(I,DFBHL(I),DFBHL(I+1),PHI(I),RAT1(I),RAT2(I),RAT3(I)
     C,RAT4(I),RAT5(I),RAT6(I),RAT7(I),RAT8(I),RAT9(I),RAT10(I),I=1,
     C N1)
```

```
 502   FORMAT(' ',I3,1X,F5.1,'-',F5.1,1X,F7.3,1X,F7.3,1X,F7.3,1X,F7.3,1X
     C ,F7.3,
     C1X,F9.4,1X,F7.3,1X,F7.3,1X,F7.3,1X,F7.3,1X,F7.3)
       WRITE(6,504)
 504   FORMAT('1',4X,'DISTANCE',6X,'PHI',6X,'W-3',3X,'SAVANAH',2X,'CE-1
     C  ',1X,'L-BARNETT',1X,'LOFT',4X,'BWC',1X,'M-ZUBER',//)
       DO 6000 I=1,N1
       III=I+1
       WRITE(6,505) I,DFBHL(I),DFBHL(III),PHI(I),RAT11(I),RAT12(I),
     C RAT13(I),RAT14(I),RAT15(I),RAT16(I),RAT17(I)
 505   FORMAT(' ',I3,1X,F5.1,'-',F5.1,1X,F7.3,1X,F7.2,1X,F7.2,1X,F7.2,
     C  1X,F7.2,1X,F7.2,1X,F7.2,1X,F7.2)
 6000 CONTINUE
      IPRINT=0
      GO TO 25
 5005 CONTINUE
C
C
      CLOSE(UNIT=5,STATUS='KEEP')
      CLOSE(UNIT=6,STATUS='KEEP')
C
C
      STOP
      END
      FUNCTION INTERP(A,B,X,N,M)
      REAL INTERP
      DIMENSION A(N),B(N)
C    A IS THE ARRAY WHICH CONTAINS X.
C    X IS THE KNOWN VALUE.
C    B IS THE ARRAY WHICH CONTAINS THE UNKNOWN CORRESPONDING
C    TO X.
C    N IS THE NUMBER OF ELEMENTS IN A AND  B.
      IF(X.LT.A(1).OR.X.GT.A(N)) WRITE(6,1) ,X,N,M
      IF(X.LT.A(1).OR.X.GT.A(N)) GO TO 5005
 1     FORMAT('0','INPUT OUT OF RANGE. EXECUTION TERMINATING'
     C ,E12.5,1X,I5,1X,I5)
      I=1
 11    IF(I.EQ.N) GO TO 12
      IF(X.EQ.A(I)) INTERP=B(I)
      IF(X.EQ.A(I)) GO TO 5000
      IF(X.GT.A(I+1)) GO TO 10
      FRACT=(X-A(I))/(A(I+1)-A(I))
      INTERP=B(I)+(FRACT*(B(I+1)-B(I)))
 5000 CONTINUE
       RETURN
 10    I=I+1
      GO TO 11
 12    WRITE(6,2)
 2     FORMAT('0','ERROR IN INTERP.EXECUTION TERMINATING')
 5005 CONTINUE
      STOP
      END
      FUNCTION BOWRNG(P,D,GI,X,HFG)
C (CORRELATION FOR WATER)
C THIS FUNCTION CALCULATES CHF USING BOWRING'S
C CORRELATION.  INPUT IS P (PSI.),D (IN.),
C G (LBM/H FT**2);X.  PHI IS RETURNED IN
C BTU/S FT**2
C (IF G=0  0 IS RETURNED
C
      G=GI/1.E06
      IF(G.EQ.0.00) BOWRNG=0.00
      IF(G.EQ.0.00) GO TO 10
```

```
      PR=P/1000.00
      IF(PR.GT.1.00) GO TO 10
      F1=((PR**18.94200*EXP(20.8900*(1.00-PR)))
     C+.91700)/1.91700
      F2=((PR**1.31600*EXP(2.44400*(1.00-PR)))+.30900
     C)/1.30900
      F2=F1/F2
      F3=((PR**17.02300*EXP(16.65800*(1.00-PR)))
     C+.66700)/1.66700
      F4=PR**1.64900
      F4=F3*F4
      GO TO 20
 10    F1=PR**(-.36800)*EXP(.64800*(1.00-PR))
      F2=PR**(-.44800)*EXP(.24500*(1.00-PR))
      F2=F1/F2
      F3=PR**.21900
      F4=PR**1.64900
      F4=F3*F4
 20    A=(2.31700*F1)/(1.00+(3.09200*F2*(D**.500)*G))
      E=2.00-(.500*PR)
      C=(104.400*F3*D*G)/(1.00+(.34700*F4*(G**E)))
      BOWRNG=(G*D*HFG)*(A-X)/(4.00*C)
      BOWRNG=(BOWRNG*1.E06)/3600.00
 5000 CONTINUE
      RETURN
      END
      FUNCTION BIASI(P,D,G,X)
C (CORRELATION FOR WATER)
C THIS FUNCTION CALCULATES CHF USING BIASI'S
C CORRELATION.  INPUT IS P (PSI.),
C D (IN.),G (LBM/H FT**2),X.
C IT RETURNS PHI IN BTU/S FT**2.
C (IF G=0  0 IS RETURNED)
C
      IF(G.EQ.0.00) BIASI=0.00
      IF(G.EQ.0.00) GO TO 10
      F=.724900+(6.832E-03*P*EXP(-2.21E-03*P))
      IF(D.LT..39400) E=.600
      IF(D.GE..39400) E=.400
      PHIL=(2.63E07/((2.5400*D)**E*G**.16700))
      PHIL=PHIL*(((4.4300*F)/(G**.16700))-X)
      A=-1.15900+(1.028E-02*P*EXP(-1.31E-03*P))+
     C((130.00*P)/(2100.00+P**2))
      PHIH=(2.506E09*A)*(1.00-X)/(((2.5400*D)**E)*G**.600)
      IF(G.LE..2E06) BIASI=PHIH/3600.00
      IF(G.LE..2E06) GO TO 10
      IF(PHIH.GT.PHIL) BIASI=PHIH/3600.00
      IF(PHIL.GE.PHIH) BIASI=PHIL/3600.00

 10    CONTINUE
      RETURN
      END
      FUNCTION CISE1(P,D,G,X,HFG)
C (CORRELATION FOR WATER)
C  THIS FUNCTION CALCULATES CHF USING CISE-1
C  CORRELATION.  INPUT IS P(PSI.),D(IN.),
C  G (LBM/H FT**2),X,HFG (BTU/LBM)
C  IT RETURNS PHI IN BTU/S FT**2.
C  (IF G=0  0 IS RETURNED)
C
      IF(G.EQ.0.00) CISE1=0.00
      IF(G.EQ.0.00) GO TO 5000
      PC=3208.00
```

```
      PR=P/PC
      A=4030.00*HFG
      B=D**.400*(((1.00/PR)-1.00)**.400)
      A=A/B
      C=1.00-PR
      D1=(G/737300.00)**.33300
      C=(C/D1)-X
      CISE1=(A*C)/3600.00
 5000 CONTINUE
      RETURN
      END
      FUNCTION CISE4(P,D,G,X,HFG)
C (CORRELATION FOR WATER)
C THIS FUNCTION CALCULATES CHF USING CISE-4
C CORRELATION.  INPUT IS P (PSI.),D (IN.),
C G (LBM/H FT**2),X,HFG (BTU/LBM).
C PHI IS RETURNED IN BTU/S FT**2.
C (IF G=0  0 IS RETURNED)
C
      IF(G.EQ.0.00) CISE4=0.00
      IF(G.EQ.0.00) GO TO 5000
      PC=3208.00
      PR=P/PC
      GSTAR=3375.00*737.300*(1.00-PR)**3.00
      IF(G.GT.GSTAR)A=(1.00-PR)/((G/737300.00)**.33300)
      IF(G.LE.GSTAR)A=1.00/(1.00+(1.481E-04*((1.00-PR)
     C**(-3.00))*(G/737.300)))
      CISE4=(4030.00*HFG)/(D**.400*(((1.00/PR)-1.00)**.400))
      CISE4=(CISE4*(A-X))/3600.00
 5000 CONTINUE
      RETURN
      END
      FUNCTION CISEBL(P,D,G,N,XA,I,DZ)
      DIMENSION XA(N)
C (CORRELATION FOR WATER)
C THIS FUNCTION CALCULATES X CHF USING CISE BOILING
C LENGTH CORRELATION.  INPUT IS P (PSI.),D (IN.),
C G (LBM/H FT **2),N=NUMBER OF NODES,XA=NODAL
C QUALITIES ARRAY,I=CELL BEING CALCULATED,DZ (IN.)
C IF G EQUALS 0  0 IS RETURNED.
C
      IF(G.EQ.0.00) CISEBL=0.00
      IF(G.EQ.0.00) GO TO 5000
      X=.500*(XA(I)+XA(I+1))
      IF(X.LT.0.00) CISEBL=0.00
      IF(X.LT.0.00) RETURN
C
C CALCULATE THE AXIAL LENGTH OF THE CELL MIDPOINT.
C
      XL=(I*DZ)-(DZ/2.00)
C
C CALCULATE THE LENGTH OF THE SINGLE PHASE SLUG.
C
      K=0
 10    K=K+1
      IF(XA(K).GE.0.00) GO TO 20
      GO TO 10
 20    IF(K.EQ.1) SPL=0.00
      IF(K.EQ.1) GO TO 30
      F=(0.00-XA(K-1))/(XA(K)-XA(K-1))
      IF(K.EQ.2) SPL=F*DZ
      IF(K.EQ.2) GO TO 30
      SPL=((K-2)*DZ)+(F*DZ)
```

```
 30     BL=XL-SPL
        PR=P/3208.00
        A=(1.00-PR)/((G/737300.00)**.33300)
        T=((1.00/PR)-1.00)**.400
        B=5.171E-06*(D**1.400)*G*T*12.00
        CISEBL=A*(BL/(B+BL))
 5000 CONTINUE
        RETURN
        END
        FUNCTION GRIFZU(RHOG,RHOF,ALPHA,HFG,SIGMA)
C (CORRELATION FOR WATER)
C THIS FUNCTION CALCULATES PHI CHF
C USING GRIFFITH-ZUBER CORRELATION.
C INPUT IS RHOG,RHOF,HFG,VOID FRACTION,AND SURFACE TENSION.
C PHI IS RETURNED IN  BTU/S FT**2.
C
        A=(1.00-ALPHA)*3600.00*.13100*RHOG*HFG
        B=1036.8400*SIGMA*(RHOF-RHOG)
         C=B/(RHOG**2)
        GRIFZU=A*(C**.2500)
        GRIFZU=GRIFZU/3600.00
        RETURN
        END
        FUNCTION GE(X,G)
C (CORRELATION FOR WATER)
C THIS FUNCTION USES GE CORRELATION TO
C CALCULATE PHI CHF.
C INPUT IS QUALITY AN MASS VELOCITY(LBM/H FT**2)
C PHI IS RETURNED IN BTU/S FT**2
C
        GC=ABS(G)
        IF(GC.LT..5E06) GO TO 10
        GE=(1.E06*(.8400-X))/3600.00
        GO TO 20
 10       GE=(1.E06*(.800-X))/3600.00
 20     RETURN
        END
        FUNCTION CONDIE(G,X,P)
C (CORRELATION FOR WATER)
C THIS FUNCTION CALCULATES PHI CHF
C USING CONDIE'S CORRELATION.
C INPUT IS MASS VELOCITY(LBM/H FT**2),
C QUALITY,AND PRESSURE(PSI.).
C PHI IS RETURNED IN BTU/S FT**2
C
        A=G/1.E06
        B=.177500*ALOG(1.00+X)
        A=A**B
        A=8.0793E06*A
        B=(1.00+X)**3.390600
        C=P**.323400
        CONDIE=(A/(B*C))/3600.00
        RETURN
        END
        FUNCTION BW2(P,D,HFG,X,G)
C (CORRELATION FOR WATER)
C THIS FUNCTION CALCULATES PHI CHF USING
C B&W-2 CORRELATION.
C INPUT IS PRESSURE(PSI),DIAMETER(IN.),
C HFG,QUALITY,MASS VELOCITY(LBM/H FT**2).
C PHI IS RETURNED IN BTU/S FT**2.
C O IS RETURNED IF G = 0
C
```

```
      IF(G.EQ.0.00) BW2=0.00
      IF(G.EQ.0.00) GO TO 5000
      A=1.1550900
      B=.4070300
      A1=.3702E08
      A2=.59137E-06
      A3=.830400
      A4=.68479E-03
      A5=12.7100
      A6=.30545E-05
      A7=.7118600
      A8=.20729E-03
      A9=.1520800
      E1=A-(B*D)
      E3=A3+(A4*(P-2000.00))
      E2=A1*((A2*G)**E3)
      E4=A9*G*X*HFG
      TOP=E1*(E2-E4)
      E1=A7+(A8*(P-2000.00))
      BOT=A5*((A6*G)**E1)
      BW2=(TOP/BOT)/3600.00
 5000 CONTINUE
      RETURN
      END
      FUNCTION HSU(A,G,P,D)
C     (CORRELATION FOR WATER)
C    THIS FUNCTION USES HSU'S CORRELATION TO
C    CALCULATE CRITICAL HEAT FLUX
C    INPUT IS VOID FRACTION,G (LBM/H FT**2)
C    P (PSI), D (IN.).
C    PHI IS RETURNED IN BTU/S FT**2.
C
      F=(1.7600*(.9600-A))**.500
      C=-3.1500/D
      T1=.955E06*(1.0400+.148E-06*G)
      T2=2.19200-.53E-03*P
      T3=.266400+(.83500*EXP(C))
      W3=T1*T2*T3
      HSU=F*W3/3600.00
      RETURN
      END
C
C
      FUNCTION W3(X,P,G,HFG,HIN,TO,D)
C
C     ( CORRELATION FOR WATER)
C     THIS FUNCTION USES W-3 CORRELATION TO
C      CALCULATE CRITICAL  HEAT FLUX.
C     INPUT IS VOID FRACTION,P(PSI),D(FT),
C     G(LBM/H FT**2),HFG(BTU/LBM)
C     HIN(BTU/LBM)
C     PHI IS RETURNED IN BTU/S FT**2
C
      HIN=1.000*(TO-70.)
      A1=2.022-4.300E-04*P
      A2=0.1722-9.84E-05*P
      A3=EXP((18.177-4.129E-03*P)*X)
      A4=1.0E+06  *(A1+A2*A3)
      A5=1.157-0.869*X
      A6=(0.1484+X*(-1.569+0.1729*ABS(X)))*G*1.0E-06+1.037
      A7=0.8258+7.94E-04*(HFG-HIN)
      A8=0.266+0.83*EXP(-3.151*(12.0*D))
      W3=A4*A5*A6*A7*A8
```

```
      W3=W3/3600.0
      RETURN
      END
C
      FUNCTION SVANAH(V,T,TSAT)
C
C
C     ( CORRELATION FOR WATER)
C     THIS FUNCTION USES SAVANAH RIVER
C     CORRELATION TO CALCULATE CRITICAL
C     HEAT FLUX.   INPUT IS V(FT/S),TSUB(F)
C     PHI IS RETURNED IN BTU/S FT**2
C
C
      TSUB=TSAT-T
      SVANAH=1.88E+05*(1.0+0.0515*V)*(1.0+0.069*TSUB)
      SVANAH=SVANAH/3600.0
      RETURN
      END
C
      FUNCTION CE1(P,X,G,HFG)
C
C
C      ( CORRELATION FOR WATER)
C      THIS FUNCTION USES CE-1 CORRELATION
C      TO CALCULATE CTITICAL HEAT FLUX.   INPUT IS
C       QUALITY (%),PRESSURE (PSI),G (LBM/S  FT**2)
C      HFG(BTU/LBM)
C      PHI IS RETURNED IN BTU/S FT::2
C
C
      IF(G.LT.100) CE1=0.0
      IF(G.LT.100) GO TO 10
      G1=G*1.0E-06
      A1=4.0532E+02-9.929E-02*P
      A2=-0.67757E+0+6.8236E-04*P
      A3=A1*(G1**A2)-G1*X*HFG
      A4=1.0E+06*2.8922E-03*(1.0E+0**(-0.50749))*A3
      A5=3.124E-04*P-8.3245E-02*G1
      A6=G1**A5
      CE1=A4/A6
      CE1=CE1/3600.0
 10   CONTINUE
      RETURN
      END
C
C
      FUNCTION LBNT(G,X,DIAH,DIAE,HFG)
C
C
C     (CORRELATION FOR WATER)
C     THIS FUNCTION USES LOCAL BARNETT
C     CORRELATION TO CALCULATE CRITICAL
C     HEAT FLUX.   INPUT IS G(LBM/H FT**2),
C     QUALITY (%),HFG(BTU/LBM),DIAE(FT),
C     DIAH(FT).
C     PHI IS RETURNED IN BTU/S FT**2
C
      REAL LBNT
      G1=G*1.0E-06
      A1=69.400*(DIAE**0.75100)*(G1**0.22600)
      A2=1.000-0.67200*EXP(-6.0900*DIAH*G1)
      A=A1*A2
```

```
      B=-0.2500*(DIAE**1.00)*(G1**1.00)
      C=165.900*(DIAH**1.24600)*(G1**0.32900)
      LBNT=1.0E+06*((A+B*HFG*X)/C)
      LBNT=LBNT/3600.0
      RETURN
      END
C
C
      FUNCTION LOFT(P,X,G)
C
C
C     (CORRELATION FOR WATER)
C     THIS FUNCTION USES LOFT
C     CORRELATION TO CALCULATE
C     CRITICAL HEST FLUX.   INPUT
C     IS P(PSIA),QUALITY(%),
C     G(LBM/H FT**2)
C     PHI IS RETURNED IN BTU/S FT**2
C
      REAL LOFT
      LOFT=1.31569E+06-3.79605E+02*P+8.32105E-02*G
     A  +1.08312E+01*P*X-1.0198200*G*X
      LOFT=LOFT/3600.0
      RETURN
      END
C
C
      FUNCTION BWC(P,X,G,HFG)
C
C
C     (CORRELATION FOR WATER)
C     THIS FUNCTION USES BWC CORRELATION
C     TO CALCULATE CRITICAL HEAT FLUX.
C     INPUT IS P(PSIA), QUALITY(%),
C     G(LBM/H FT**2),HFG(BTU/LBM)
C     PHI IS RETURNED IN BTU/S FT**2
C
      IF(P.LE.1600.) GO TO 10
      A1=0.309191E-06
      A2=0.388223E-05
      A3=0.96488200
      A4=0.301423E-03
      A5=5.54836E+06
      A6=0.72772900
      A7=0.189646E-04
      A8=0.175233E-08
      A=A3+A4*(P-2000.)
      B=A1*G
      C=A*B
      D=A8*HFG*G*X
      TOP=A5*(C-D)
      E=A6+A7*(P-2000.)
      F=A2*G
      BOT=F**E
      BWC=TOP/BOT
      BWC=BWC/3600.
   10 RETURN
      END
C
C
      FUNCTION MZUBER(RHOG,RHOF,ALPHA,HFG,SIGMA)
```

```
C      (CORRELATION FOR WATER)
C      THIS FUNCTION USES MODIFIED ZUBER
C      CORRELATION TO CALCULATE CRITICAL
C      HEAT FLUX.  INPUT IS RHOG(LBM/FT**3),
C      RHOF(LBM/FT**3), ALPHA(%),
C      HFG(BTU/LBM), SIGMA(LBF/FT)
C      PHI IS RETURNED IN BTU/S FT**2
C
       REAL MZUBER
       A=(0.9600-ALPHA)*3600.00*0.13000
      C    *HFG*((RHOG*RHOF)**0.500)
       B=1036.8400*SIGMA*(RHOF-RHOG)
       C=B/((RHOG+RHOF)**2.00)
       MZUBER=A*(C**0.2500)
       MZUBER=MZUBER/3600.
       RETURN
       END
C
C
C
C
       FUNCTION CRTFLD(PO, AO, AT, XO, HO, RO, PSAT, C1, C2, C3, XSTAR,
      C PPT, SFT, SGT, HFT, HFGT, VFT, VFGT, NT, NDP, TDP, DPT, TIME)
       REAL INTERP
C
C THIS SUBROUTINE CALCULATES THE BOUNDARY VALUE
C OF MASS VELOCITY USING CRITICAL FLOW CALCULATIONS.
C G IS RETURNED IN LBM/S FT**2.
C
C  INPUT :
C          PO=PRESSURE AT BOUNDARY (PSF.)
C          AO=CROSS SECTIONAL AREA AT BOUNDARY (IN.**2)
C          AT=CROSS SECTIONAL AREA AT THROAT (IN.**2)
C          XO=QUALITY AT BOUNDARY
C          HO=ENTHALPY AT BOUNDARY (BTU/LBM)
C          RO=DENSITY AT BOUNDARY (LBM/FT**3)
C          PSAT=SATURATION PRESSURE AT BOUNDARY DENSITY(PSF.)
C          C1=DISCHARGE COEFFICIENT FOR SINGLE PHASE LIQUID
C          C2=DISCHARGE COEFFICIENT FOR TWO PHASE
C          C3=DISCHARGE COEFFICIENT FOR SINGLE PHASE VAPOR
C          XSTAR=QUALITY FOR NONEQUILIBRIUM COEFFICIENT
C          NT=NUMBER OF ROWS IN THE PROPERTY TABLE
C          PPT=PRESSURE COLUMN OF THE PROPERTY TABLE (PSI)
C          SFT=ENTROPY OF FLUID COLUMN OF THE PROPERTY TABLE
C               (BTU/LBM F)
C          SGT=ENTROPY OF THE GAS COLUMN OF THE PROPERTY TABLE
C               (BTU/LBM F)
C          HFT=ENTHALPY COLUMN OF THE PROPERTY TABLE(BTU/LBM)
C          HFGT=HFG COLUMN OF THE PROPERTY TABLE (BTU/LBM)
C          VFT=SPECIFIC VOLUME COLUMN OF THE PROPERTY TABLE
C               (FT**3/LBM)
C          VFGT=VFG COLUMN OF THE PROPERTY TABLE (FT**3/LBM)
C          NDP=NUMBER OF TIME,DELTA P POINTS
C          TDP=TIME VALUES OF TIME,DELTA P POINTS (SECS.)
C          DPT=DELTA P VALUES OF TIME DELTA P POINTS (PSI.)
C          TIME= VALUE OF PRESENT TIME (SECS)
C
C
       DIMENSION PPT(NT),SFT(NT),SGT(NT),HFT(NT),HFGT(NT)
       DIMENSION VFT(NT),VFGT(NT),TDP(NDP),DPT(NDP)
       IF(XO.GE.0.00) GO TO 10
```

```
C       SINGLE PHASE LIQUID SECTION
C
        IF(NDP.EQ.0)ETA=PSAT/P0
        IF(NDP.NE.0)ETA=INTERP(TDP,DPT,TIME,NDP,100)
        IF(NDP.NE.0)ETA=1.00-(ETA*144.00/P0)
        IF(ETA.GE.1.00.AND.NDP.EQ.0)ETA=.9900
        GT=C1*(64.400*R0*P0*(1.00-ETA))**.500
        CRTFLO=(GT*AT)/A0
        RETURN
C
C       TWO PHASE SECTION
C
 10     CONTINUE
        IF(X0.GE.1.00) GO TO 20
        IF(NDP.NE.0)ETA=INTERP(TDP,DPT,TIME,NDP,101)
        IF(NDP.NE.0)ETA=1.00-(ETA*144.00/P0)
        IF(NDP.EQ.0.AND.X0.LT.1.00)ETA=.6700-.11700*X0
        IF(NDP.EQ.0.AND.X0.LT.400)ETA=.7900-.42700*X0
        IF(NDP.EQ.0.AND.X0.LT..1800)ETA=.8600-.81100*X0
        PT=ETA*P0
        P00=P0/144.00
        SF=INTERP(PPT,SFT,P00,NT,102)
        SFG=INTERP(PPT,SGT,P00,NT,103)-SF
        S0=SF+X0*SFG
        PTT=PT/144.00
        SF=INTERP(PPT,SFT,PTT,NT,104)
        SFG=INTERP(PPT,SGT,PTT,NT,105)-SF
        XT=(S0-SF)/(SFG)
        HT=INTERP(PPT,HFT,PTT,NT,106)+XT*
      C INTERP(PPT,HFGT,PTT,NT,107)
        VT=INTERP(PPT,VFT,PTT,NT,108)+XT*
      C INTERP(PPT,VFGT,PTT,NT,109)
        EQN=XT/XSTAR
        IF(EQN.GT.1.00)EQN=1.00
        G=((50073.00*(H0-HT))**.500)/VT
        GT=(C2*G)/(EQN**.500)
        CRTFLO=(GT*AT)/A0
        RETURN
C
C       SINGLE PHASE VAPOR SECTION
C
 20     CONTINUE
        GAMMA= 1.314400-6.599E-5*P0+2.95E-9*P0**2
        F=GAMMA/(GAMMA-1.00)
        IF(NDP.EQ.0)ETA=(2.00/(1.00+GAMMA))**F
        IF(NDP.NE.0)ETA=INTERP(TPT,DPT,TIME,NDP,110)
        IF(NDP.NE.0)ETA=1.00-(ETA*144.00/P0)
        T1=(64.400*GAMMA)/(GAMMA-1.00)
        T2=R0*P0
        F1=2.00/GAMMA
        F2=(GAMMA+1.00)/GAMMA
        T3=ETA**F1-ETA**F2
        GT=C3*((T1*T2*T3)**.500)
        CRTFLO=(GT*AT)/A0
        RETURN
        END
```

APPENDIX C

PRESSURE AND MASS VELOCITY HISTORIES IN BLOWDOWN EXPERIMENTS

This appendix contains the Figures 112 through 126. These Figures show the pressure and the mass velocity as a function of time for the blowdown experiments studied by the author (1984) and shown in Table 9. The values shown in the figures are the measured values of pressure and mass velocity as input to the CODA code by Leung (1980).

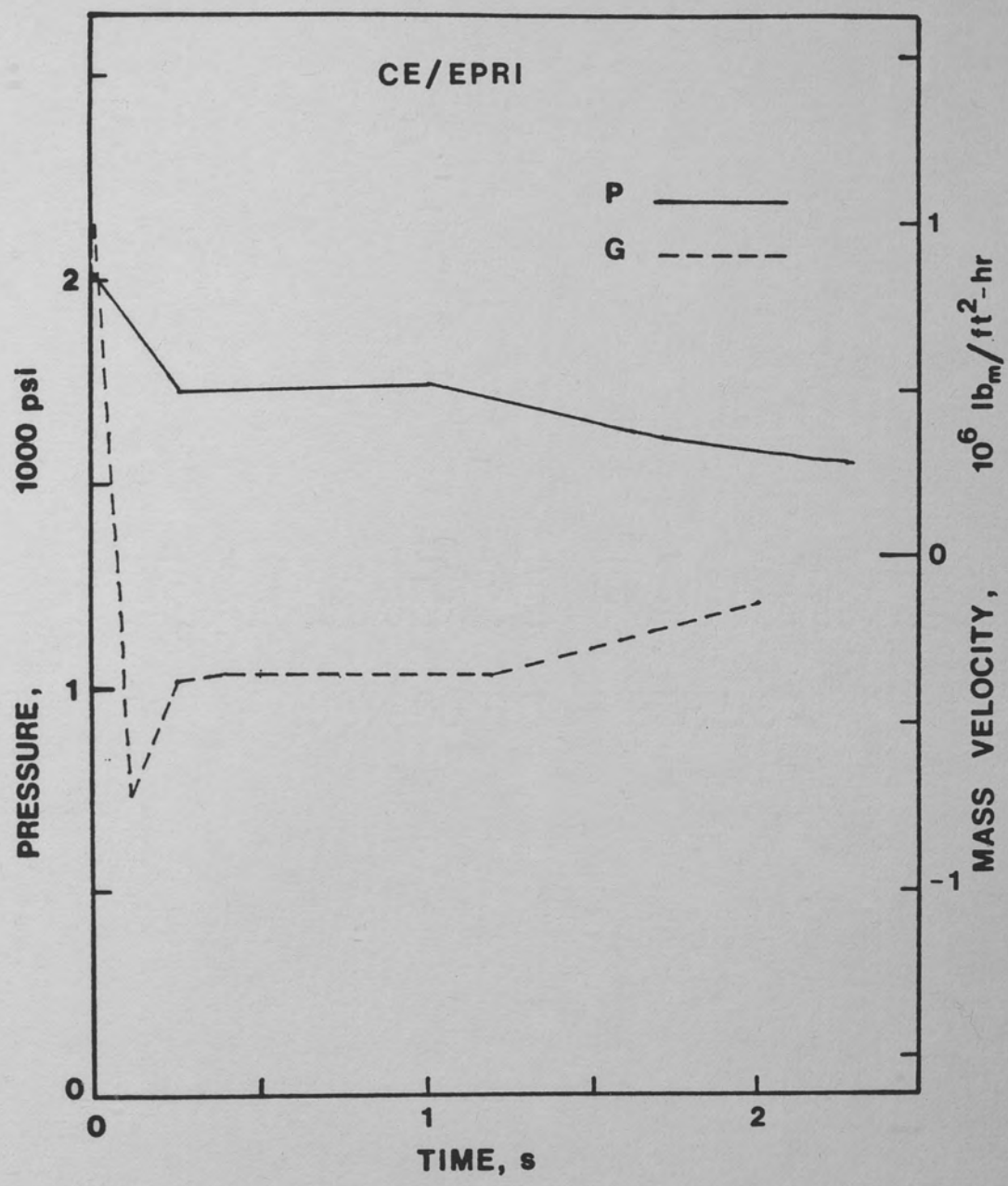

Figure 112. Pressure and Flow History in Test CE/EPRI

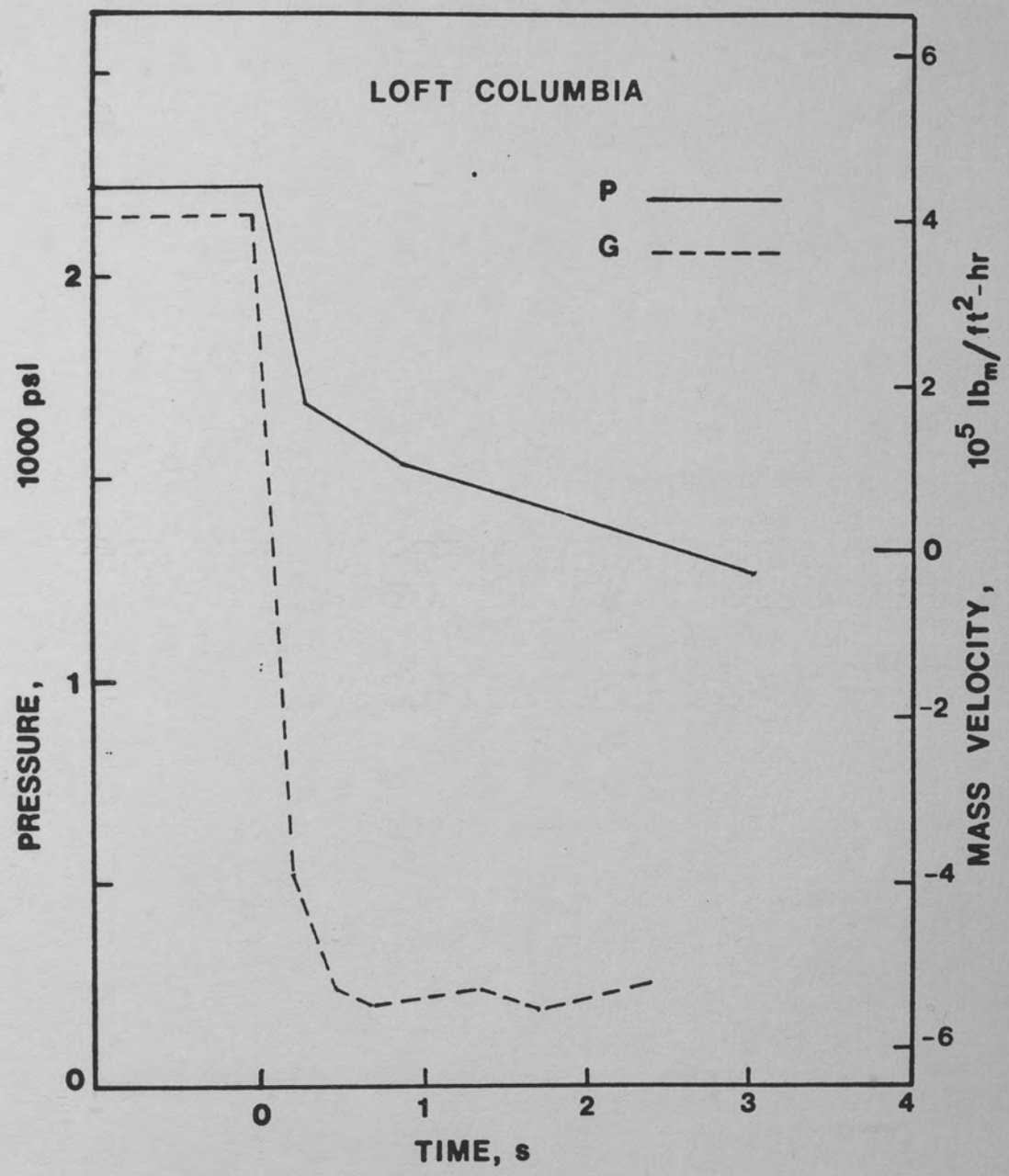

Figure 113. Pressure and Flow History in Test LOFT Columbia

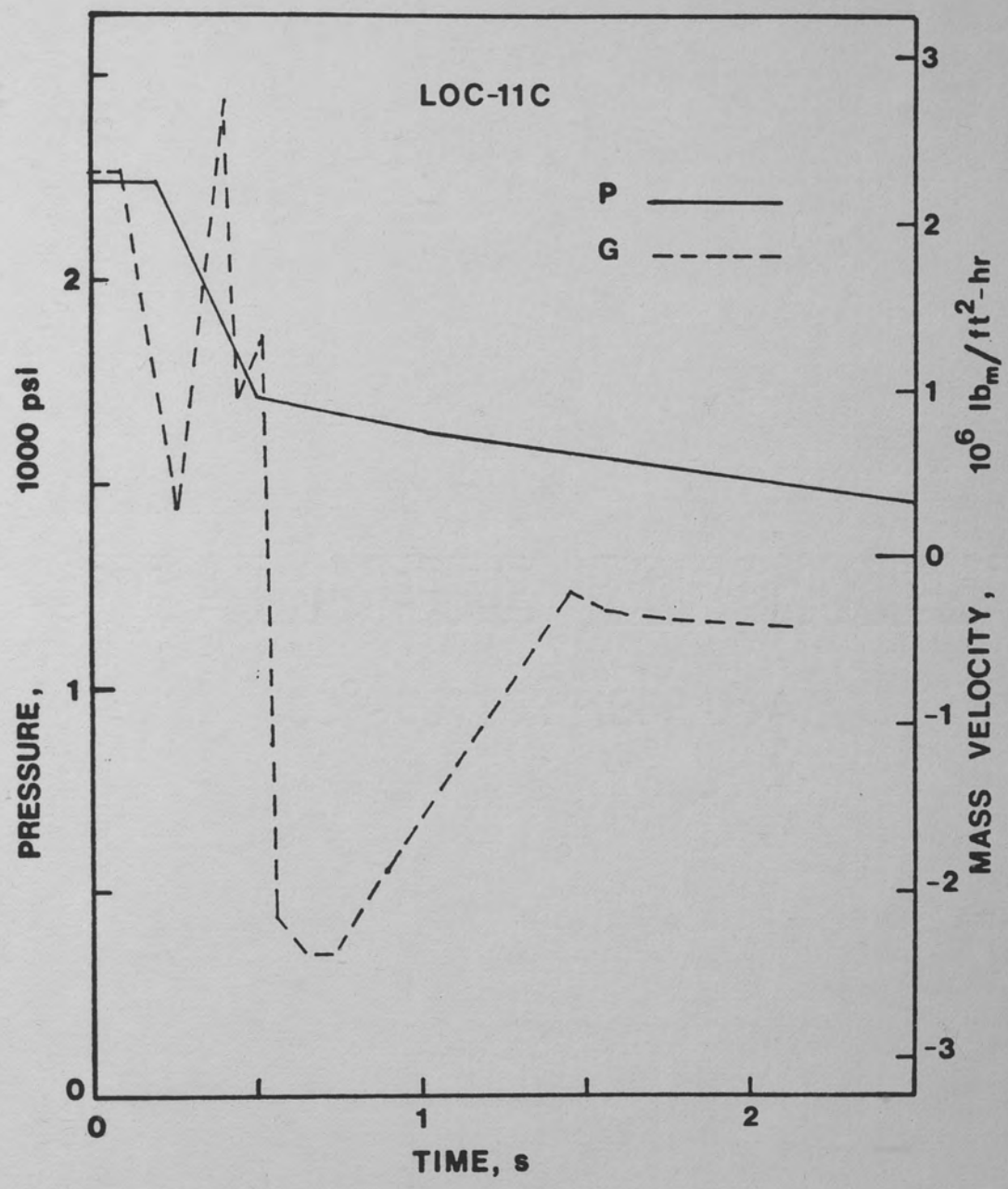

Figure 114. Pressure and Flow History in Test LOC-11C

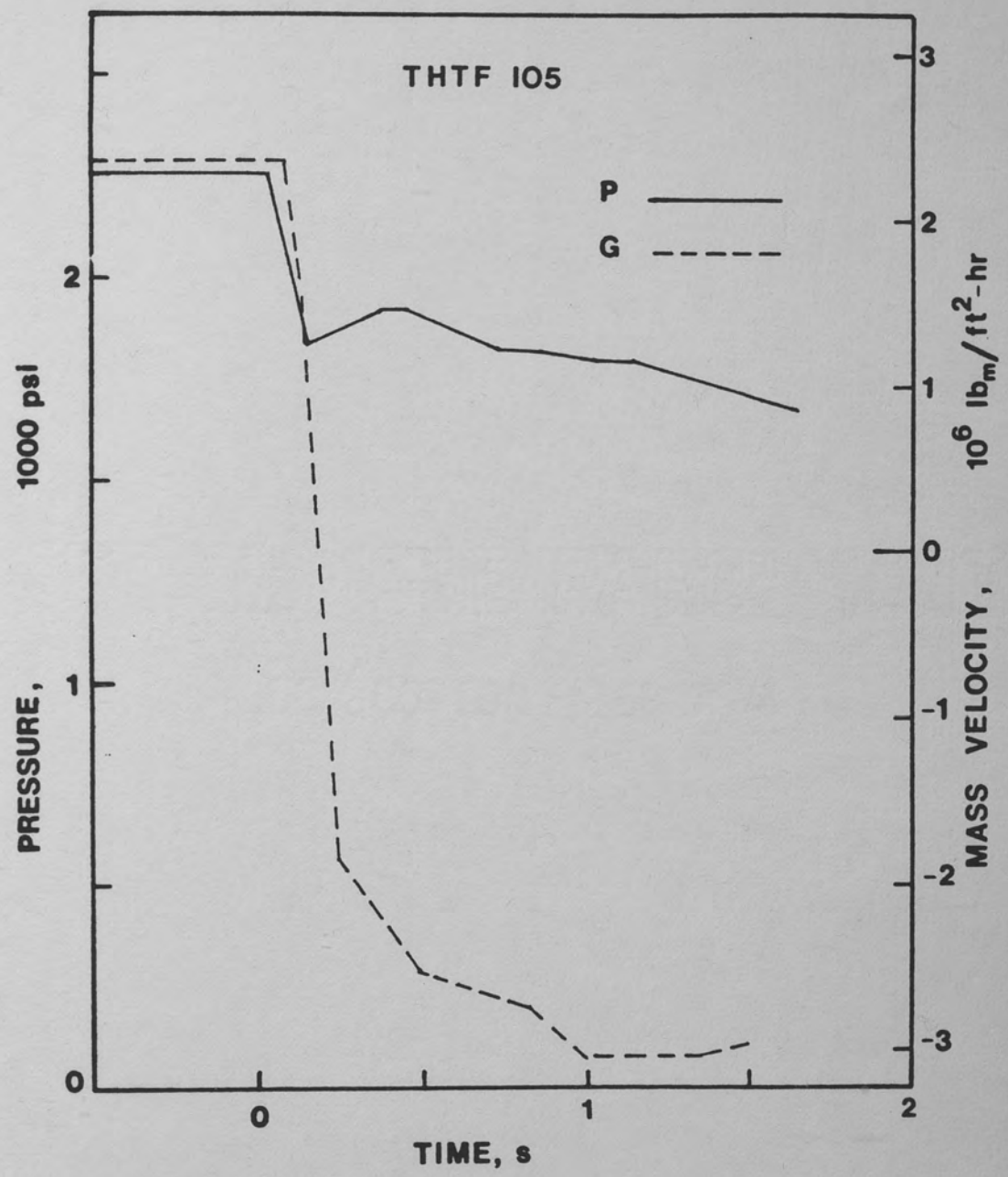

Figure 115. Pressure and Flow History in Test THTF 105

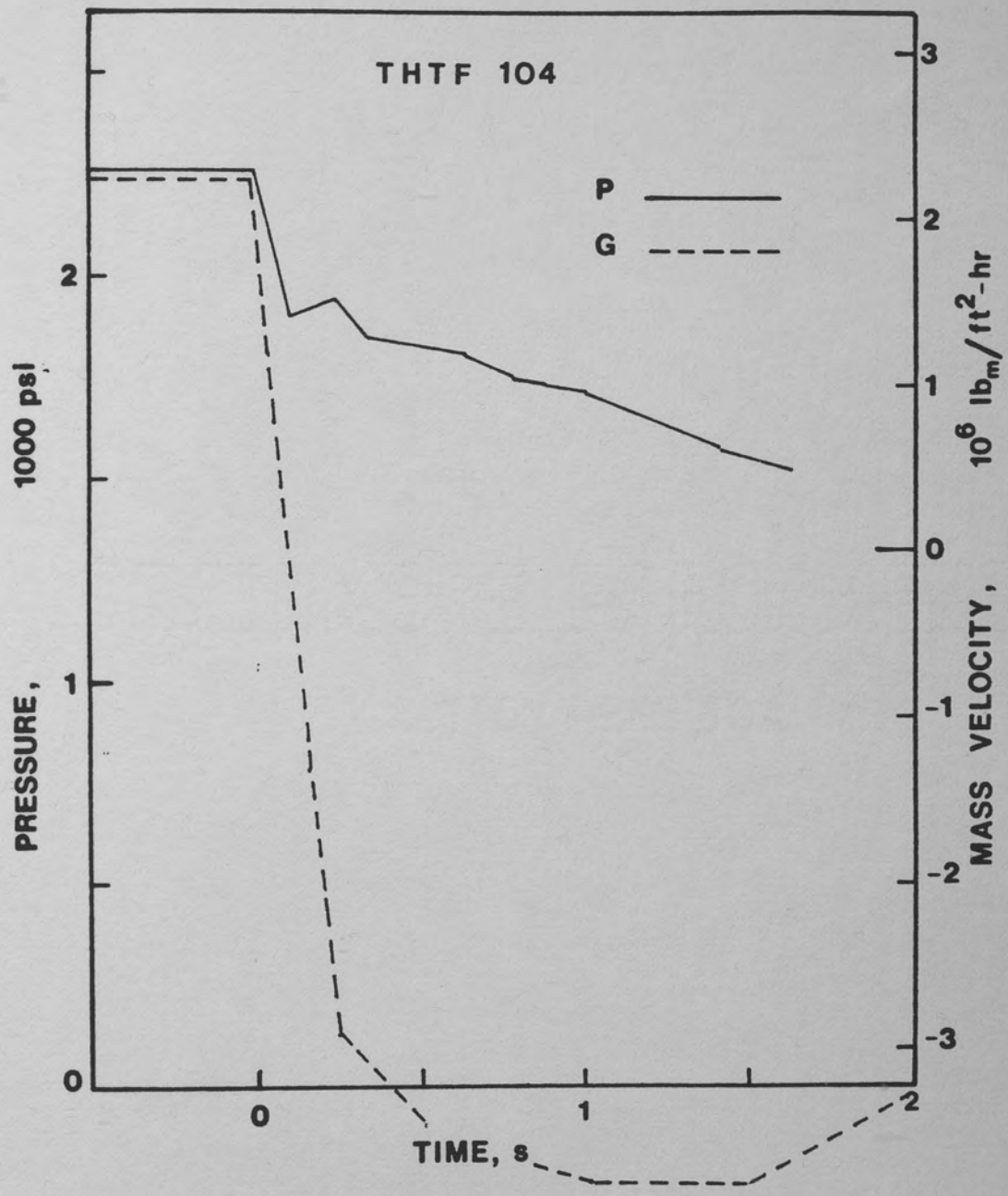

Figure 116. Pressure and Flow History in Test THTF 104

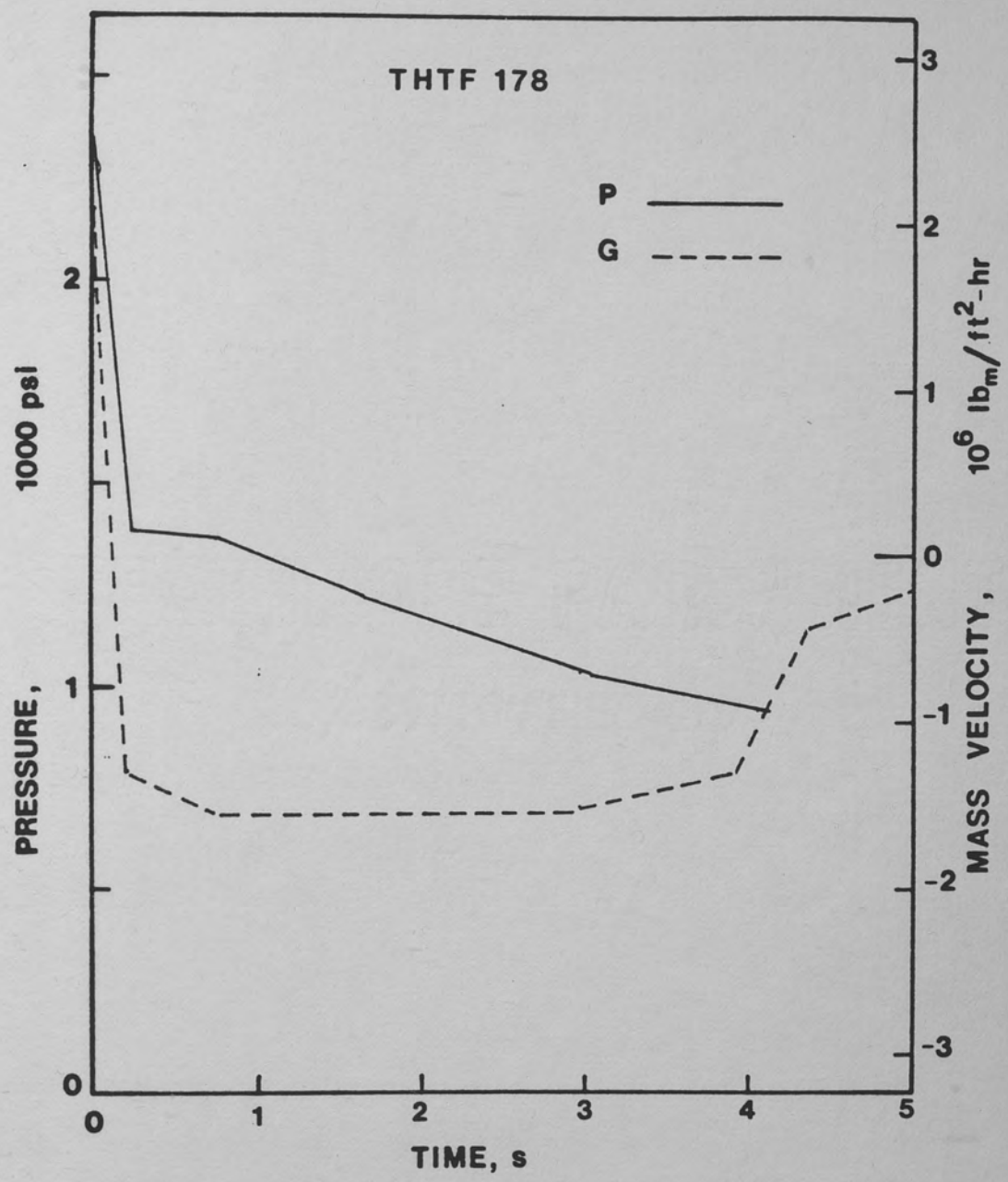

Figure 117. Pressure and Flow History in Test THTF 178

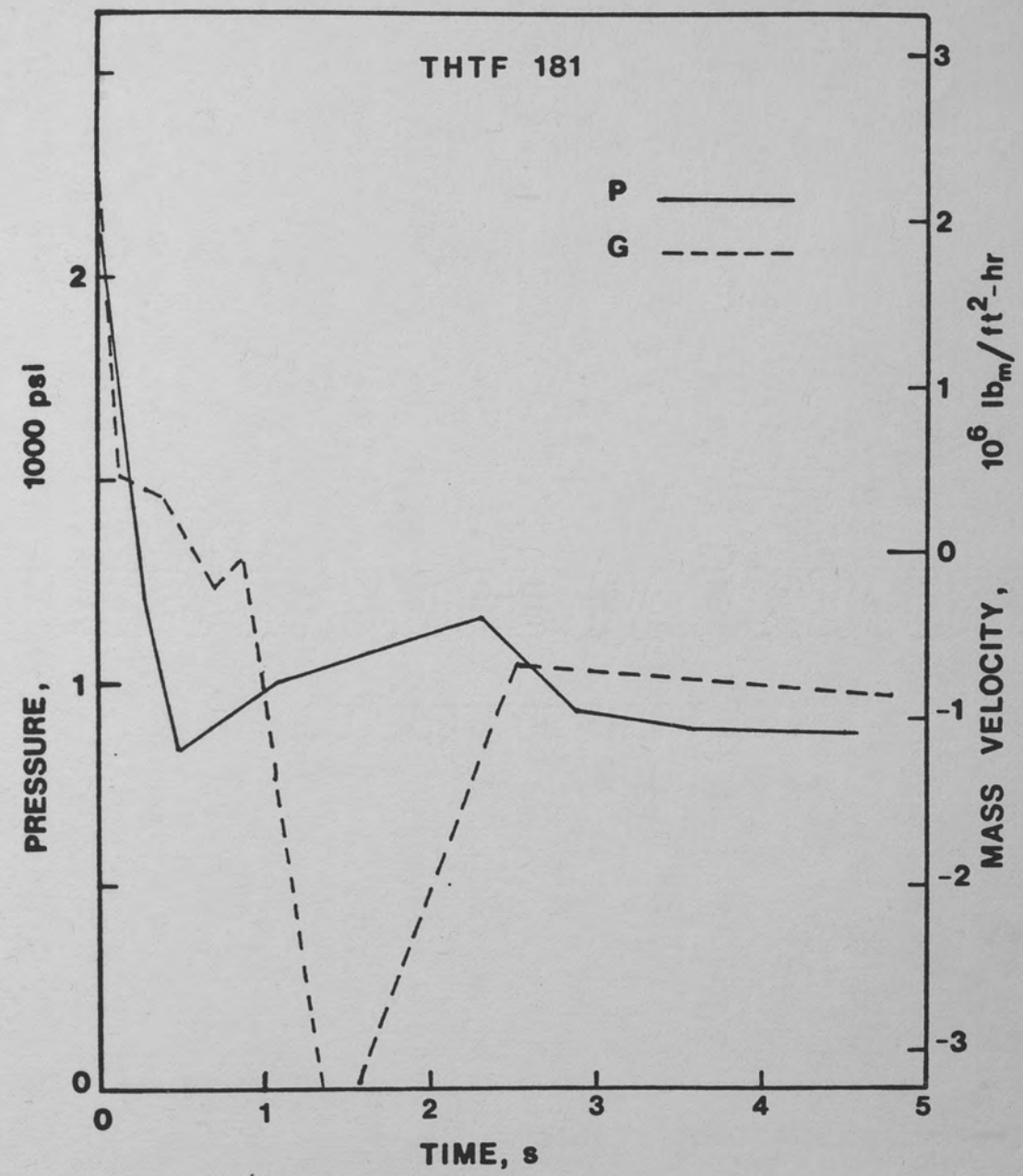

Figure 118. Pressure and Flow History in Test THTF 181

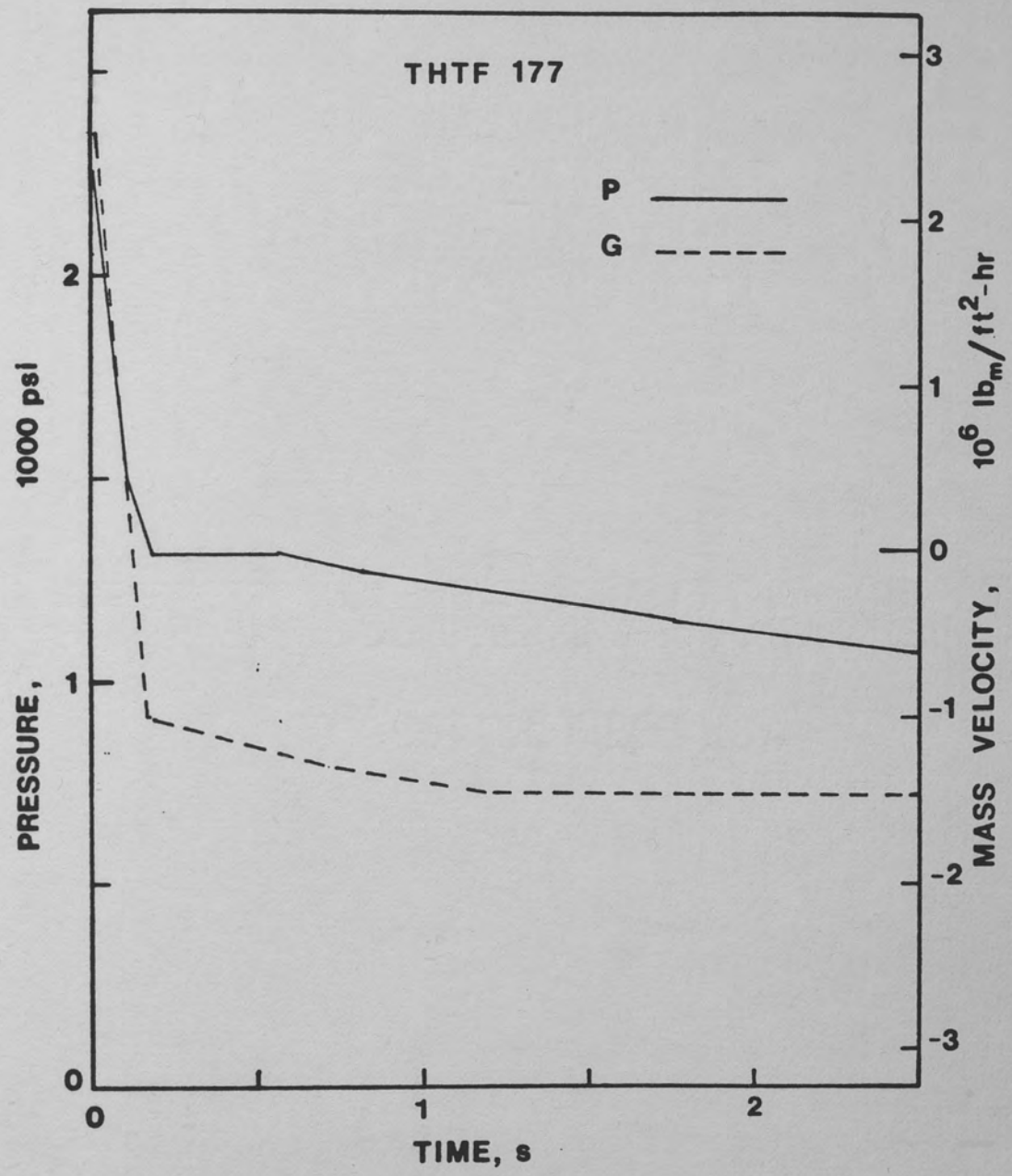

Figure 119. Pressure and Flow History in Test THTF 177

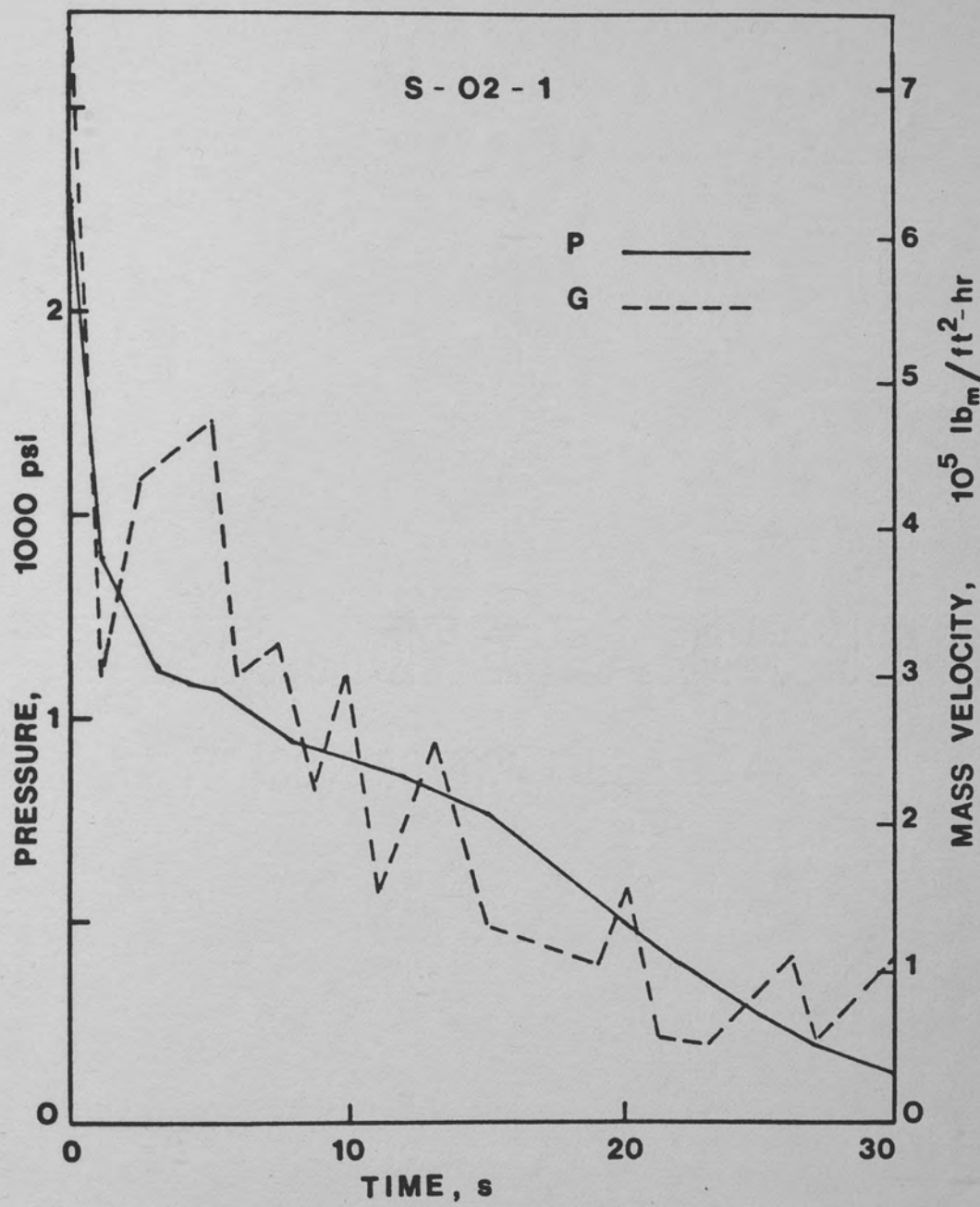

Figure 120. Pressure and Flow History in Test S-02-1

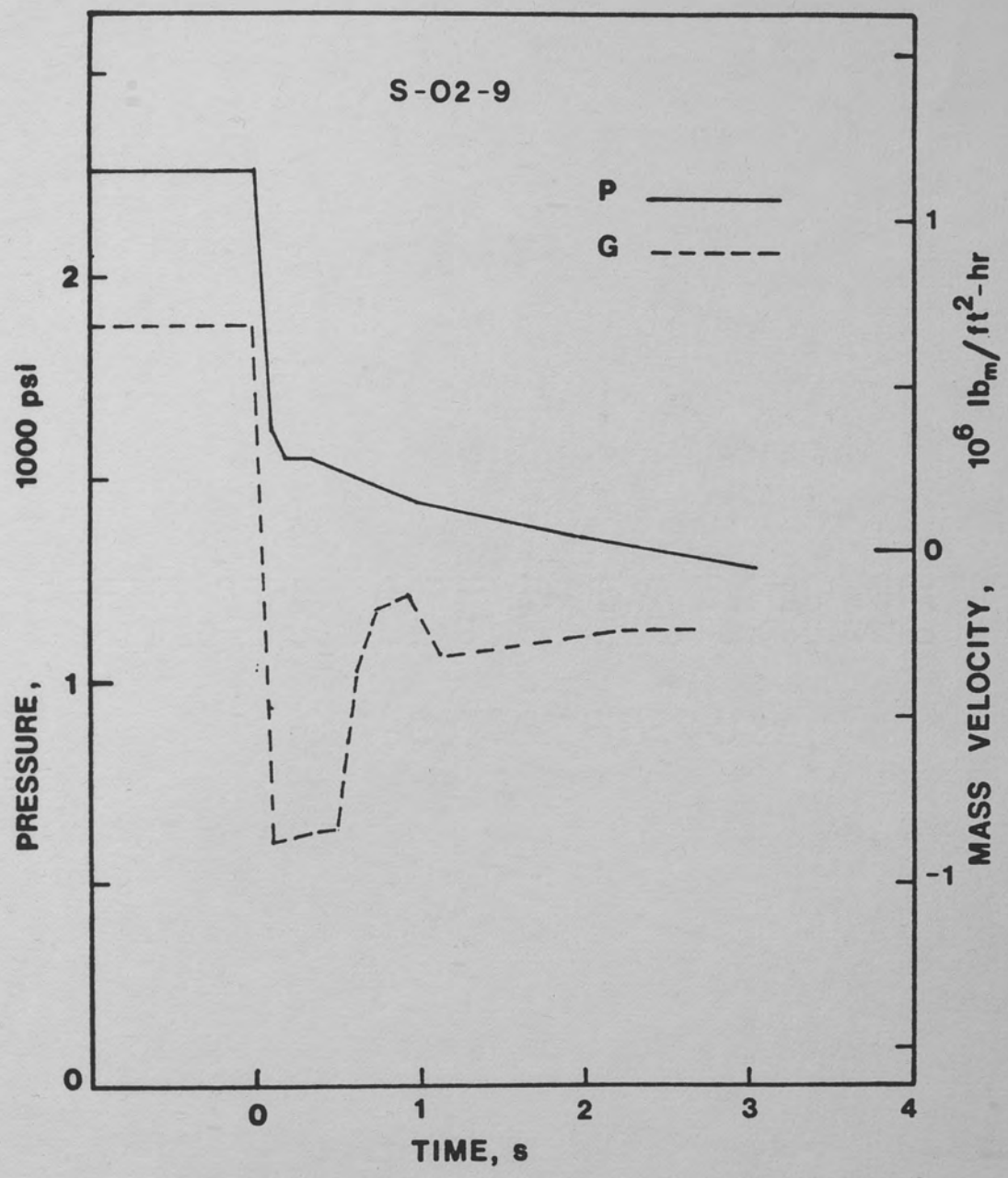

Figure 121. Pressure and Flow History in Test S-02-9

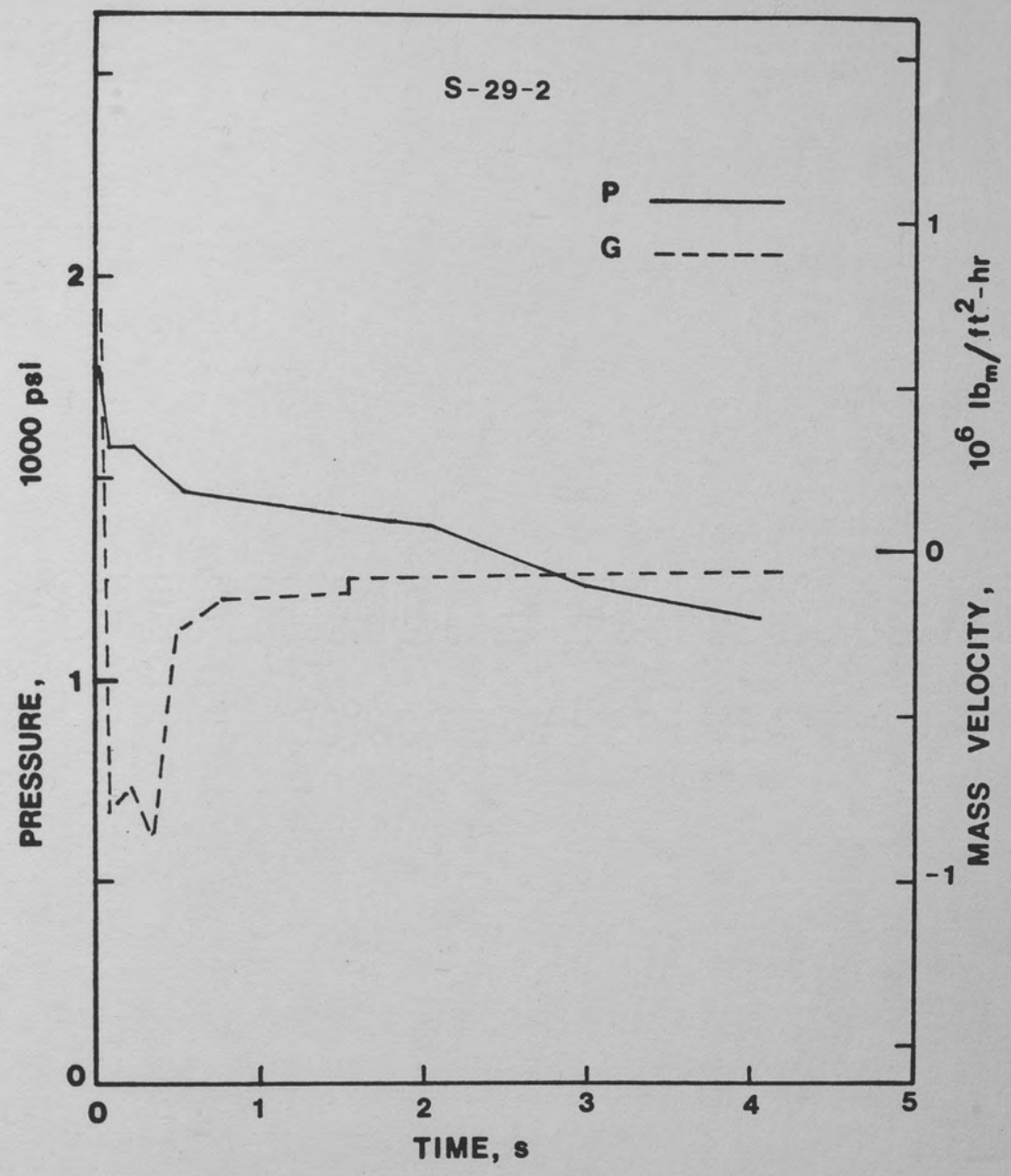

Figure 122. Pressure and Flow History in Test S-29-2

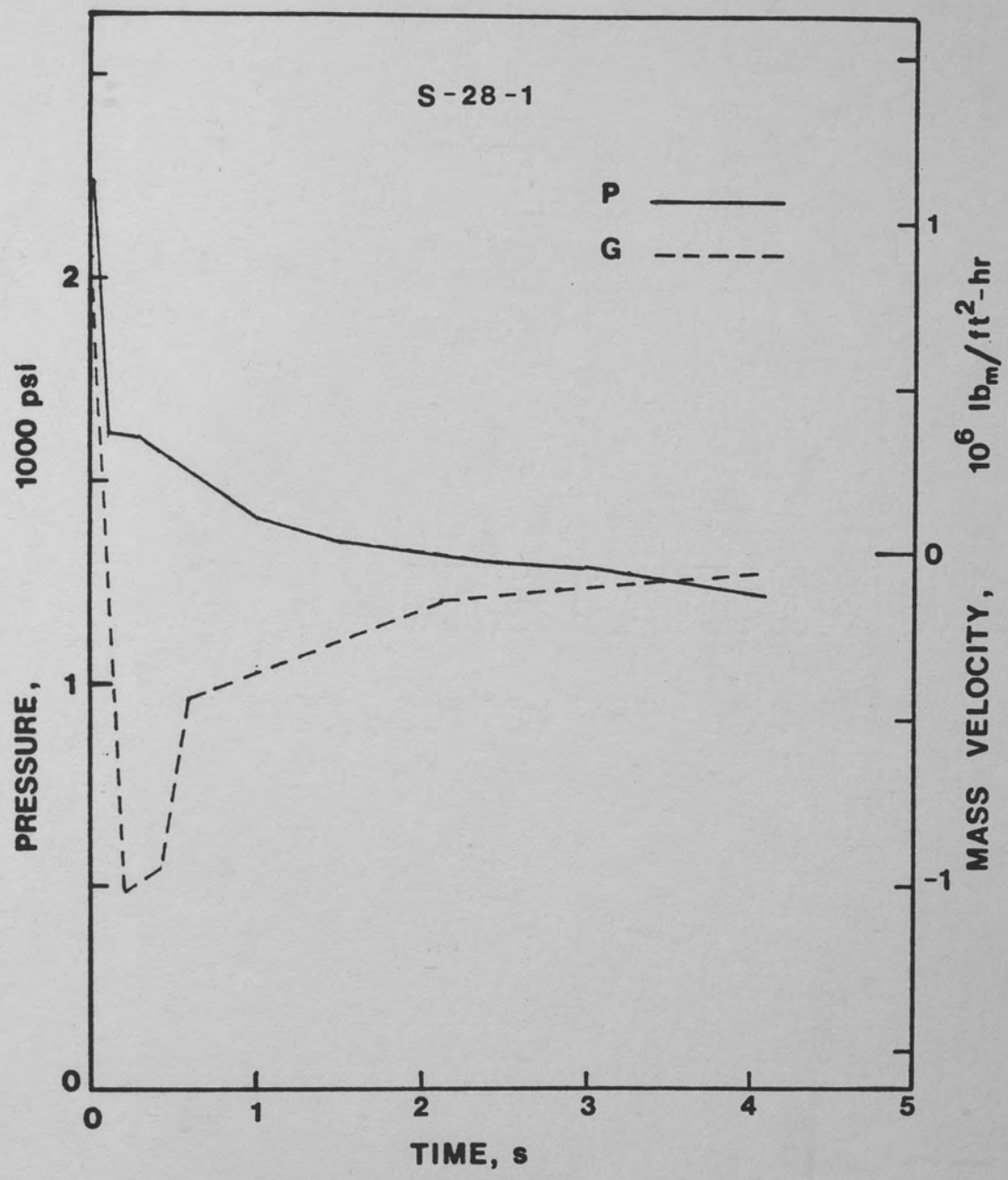

Figure 123. Pressure and Flow History in Test S-28-1

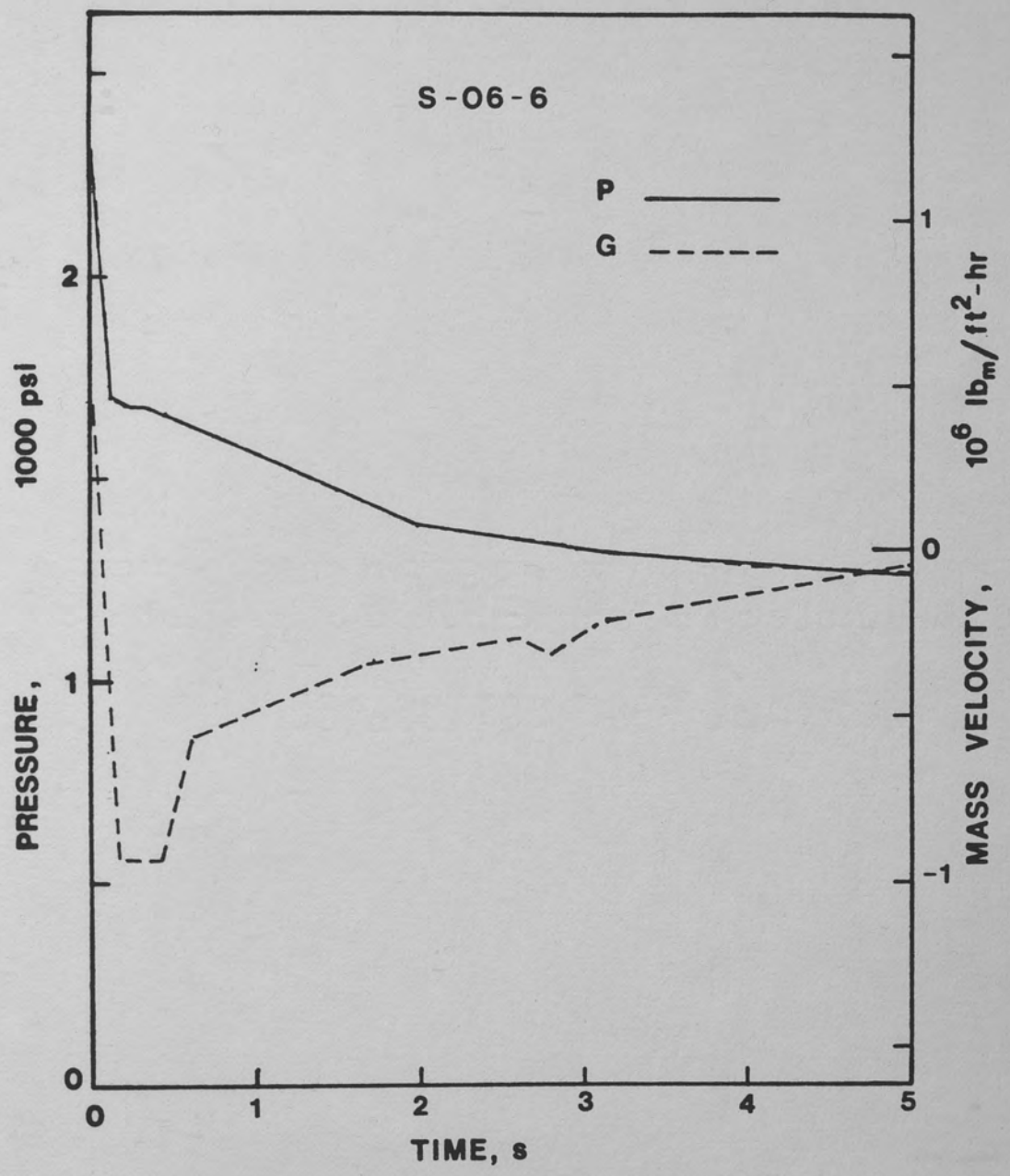

Figure 124. Pressure and Flow Histories in Test S-06-6

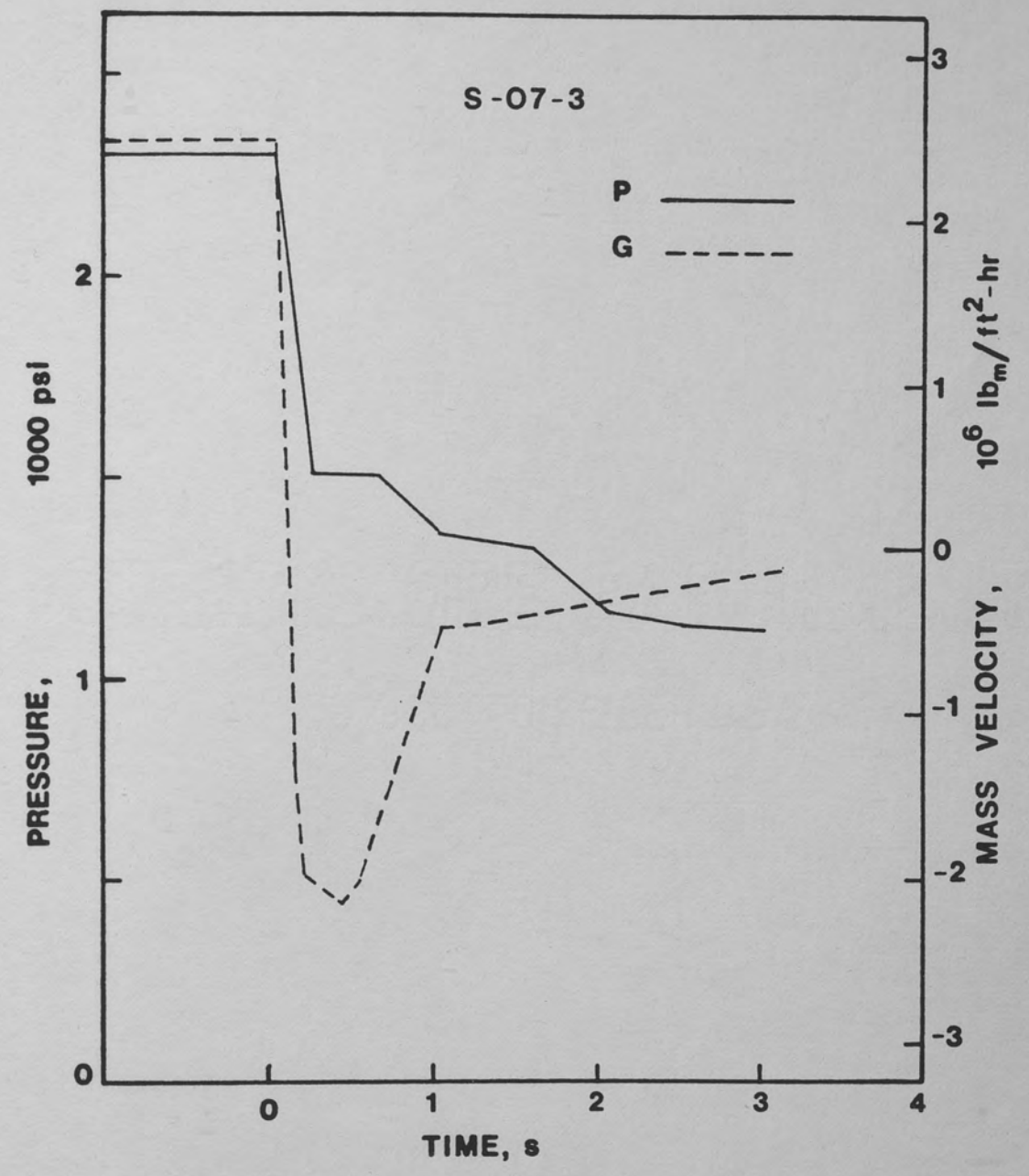

Figure 125. Pressure and Flow Histories in Test S-07-3

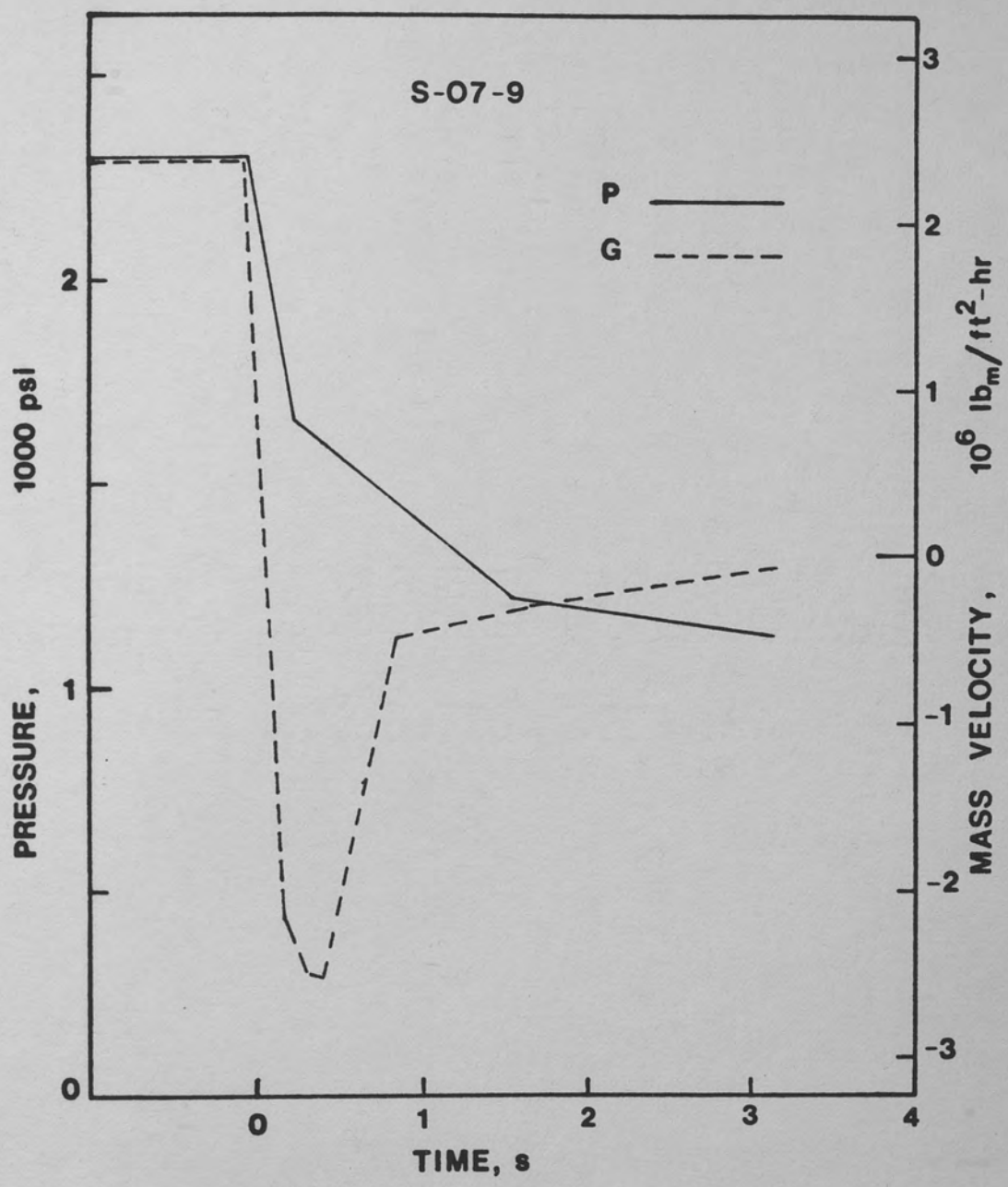

Figure 126. Pressure and Flow Histories in Test S-07-9

LIST OF REFERENCES

Adams, D. E., and Gebhard, B. "Transient Forced Convection from a Flat Plate Subjected to a Step Energy Input." J. Heat Transfer, Trans. ASME 86 (1964): 253-258.

Ahmad, S. Y. "Fluid to Fluid Modelling of Critical Heat Flux: A Compensated Distortion Model." Int. J. Heat Mass Transfer 16 (1973): 641-661.

Aoki, S., Kozawa, Y., and Iwasaki, H. "Critical Heat Flux Under Transient Conditions (Case of Transient Heat Input)." Proceedings of the International Meeting on Reactor Heat Transfer. Karlsruhe, Germany. (October 1973).

Aoki, S., Kozawa, Y., and Iwasaki, H. "Boiling and Burnout Phenomena Under Transient Heat Input." Bulletin of JSME 19 (June 1974): 667-681.

Aoki, S., Inoue, A., and Kozawa, Y. "Transient Boiling Crisis During Rapid Depressurization." Heat Transfer 1974, Proceedings of 5th International Heat Transfer Conference, Tokyo, Japan. 4, Paper: B6.3 (1974).

Barnett, P. G. A Correlation of Burnout Data for Uniformly Heated Annuli and its Use for Predicting Burnout in Uniformly Heated Rod Bundles. AEEW-R463, 1966.

Bejan, A. Convective Heat Transfer. New York:John Wiley & Sons, 1984.

Berenson, P. J. "Experiments on Pool Boiling Heat Transfer." Int. J. Heat Mass Transfer 5 (1962): 351-35.

Bergles, A. E. "Burnout in Boiling Heat Transfer, Part II: High-Quality Forced Convection Systems." Nuclear Safety 20 (1979): 671-68.

Bergles, A. E., Collier, J. G., Delhaye, J. M., Hewitt, G. F., and Mayinger, F. Two-Phase Flow and Heat Transfer in the Power and Process Industries. Washington, DC: Hemisphere, 1981.

Bertoletti, S., Gaspari, G. P., Lombardi, C., Peterlongo, G., Silvestri, F., and Tacconi, F. A. "Heat Transfer Crisis with Steam Water Mixtures." Energia Nucleare 12 (1965): 121-129.

Biasi, L., Clerici, G. C., Garriba, S., Sala, R., and Tozzi, A. "Studies on Burnout, Part 3: A New Correlation for Round Ducts with Uniform Heating and Its Comparison with World Data." Energia Nucleare 14 (1967): 530-536.

Boucher, T. J., and Dimenna, R. A. Semiscale Mod-2A Intermediate Break Test Series/Test Results and Comparison. NUREG/CR-3126, 1983.

Bowring, R. W. A Simple But Accurate Round Tube Uniform Heat Flux Dryout Correlation Over the Pressure Range 0.7-17 MN/m². AEEW-R789, 1972.

Buckland, R. H., White, C. E., and Abott, D. G. Experiment Data Report for PBF LOCA Tests LOC-11B and 11C. NUREG/CR-0516, TREE-1232, 1978.

Buckland, R. H. Experiment Data Report for Test RIA 1-1 (Reactivity Initiated Test Series). NUREG/CR-0516, May 1979.

Cathcart, J. V. Zirconium Metal Water Oxidation Kinetics, IV. Reaction Rate Studies. ORNL/NUREG-17, 1977.

Celata, G. P., Cumo, M., D'Annibale, F., Farello, G. E., and Setaro, T. "Critical Heat Flux in Flow Transients." Paper submitted to 8th International Heat Transfer Conference, San Francisco, California, August 1986.

CENPD-162-P-1. "C-E Critical Heat Flux for CE Fuel Assemblies with Standard Spacer Grids." Supplement 1-A, February 1977.

Clemons, V. D. PWR Blowdown Heat Transfer Separate-Effects Program, Thermal-Hydraulic Test Facility Experimental Data Report for Test 105. ORNL/NUREG/TM-143-1977.

Collier, J. G. Convective Boiling and Condensation. 2nd ed., New York:McGraw-Hill, 1981.

Collins, B. L. "Experimental Data Report for Semiscale Mod-1 S-28-1 (Steam Generator Tube Rupture Test)." ANCR-1231, 1975.

Columbia University. Parametric Study of CHF Data, Volume 1: Compilation of Rod Bundle CHF Data Available at the Columbia University Heat Transfer Research Facility. EPRI-NP-2609, September 1982.

Columbia University. Parametric Study of CHF Data, Volume:2: A Generalized Subchannel CHF Correlation for PWR and BWR Fuel Assemblies EPRI-NP-2609, January 1983.

Condie, K. G., and Bengston, S. J. "Development of the Mod-7 CHF Correlation." EG&G Report PN-181-78, November 1978.

Cook, B. A., Fukuda, S. K., Martinson, Z. R., and Bott-Hembree, P. Reactivity Initiated Accident Test Series, Test RIA 1-2, Fuel Behavior Report. NUREG/CR-1842, January 1981.

Costa, J., and Charlety, P. "Forced Convection Boiling of Sodium in Narrow Channels." Presented at ASME Winter Meeting, New York, New York, November 1970.

Cozzuol, J. M. "Quick Look Report for Semiscale Mod-3 Small Break Tests S-SB-P3 and S-SB-P4." EGG-SEMI-5158, May 1980.

Craddick, W. G. "Quick Look Report on Thermal-Hydraulic Test Facility Test 178." ORNL/BDHT-2250, April 1979.

Craddick, W. G. "Quick Look Report on Thermal-Hydraulic Test Facility Test 181." ORNL/BDHT-2252, April 1979.

Craddick, W. G. PWR Blowdown Heat Transfer Separate Effects Program, Thermal-Hydraulic Test Facility Experimental Data Report for Test 177. ORNL/NUREG/TM-295, 1980.

Crapo, H. S. "Experimental Data Report for Semiscale Mod-1 Test S-02-1 (Blowdown Heat Transfer Test)." ANCR-1231, 1975.

Crapo, H. S., "Experimental Data Report for Semiscale Mod-1 Tests S-02-9 and S-02-9A (Blowdown Heat Transfer Tests)." ANCR-1236, 1976.

Crapo, H. S., and Sackett, K. E. Experimental Data Report for Semiscale Mod-1 Test S-29-3 (Integral Test from Reduced Initial Pressure). ANCR-NUREG-1329, 1976.

Croucher, D. W., and Charyulu, M. K. "Experiment Requirement for the Study of Anticipated Transients With or Without Scram." TFBP-TR-308, January 1979.

Croucher, D. W., and Loyd, R. J. "Experiment Requirement to Determine and Relate Fuel Damage Limits to Core-Wide Conditions in Pressurized Water Reactors." EGG-TFBP-5011, September 1979.

Cumo, M. "Prediction of Burnout Power with Freon up to the Critical Pressure." Presented at European Two-Phase Group Meeting, Rome, Italy, 1972.

Cumo, M., Fabrizi, F., and Palazzi, G. "Transient Critical Heat Flux in Loss-of-Flow Accidents (L.O.F.A.)." Int. J. Multiphase Flow 4 (1978): 497-509.

Dahlquist, J. E., Gunnerson, F. S., and Nelson, R. A. "Considerations for Modeling Critical Heat Flux Behavior." Nuclear Technology 68 (1985): 252-262.

Dingman, S. E., Fauble, T. J., and Hewitt, J. R. "Quick Look Report for Semiscale Mod-3 Small Break Tests S-SB-P1, S-SB-P2 and S-SB-P7." EGG-SEMI-5137, April 1980.

Dorfman, A. A. "Solution of the External Problem of Unsteady-State Convective Heat Transfer with Coupled Boundary Conditions." Int. J. Chemical Engineering 17 (1977): 505-510.

Eide, S. A., and Gotula, R. G. Evaluation and Results of LOFT Steady-State DNB Tests. TREE-NUREG-1043, April 1977.

Esparza, V., and Sackett, K. E. Experiment Data Report for Semiscale Mod-1 Test S-06-6 (LOFT Counterpart Test). TREE-NUREG-1126, 1977.

Fand, R. M., and Keswani, K. K. "Influence of Subcooling on Pool Boiling Heat Transfer from a Horizontal Cylinder to Water." Heat Transfer 1974, Proceedings of the 5th International Heat Transfer Conference, Tokyo, Japan. 4, Paper:B1.3 (1974).

Fauble, T. J. "Quick Look Report for Semiscale Mod-3 Small Break Test S-SB-2A." EGG-SEMI-5113, March 1980.

Gaertner, R. F., and Westwater, J. W. "Population of Active Sites in Nucleate Boiling Heat Transfer." Chemical Engineering Program Symposium Series 56 (1960): 39-48.

Gaertner, R. F. "Photographic Study of Nucleate Pool Boiling on a Horizontal Surface." J. Heat Transfer, Trans. ASME 87: 17-29 (1965).

Gambill, W. R. "Burnout in Boiling Heat Transfer, Part II: Subcooled and Low Quality Forced Convection Systems." Nuclear Safety 18 (1977): 467-480.

Gellerstedt, J. S. "Correlation of Critical Heat Flux in a Bundle Cooled by Pressurized Water." Presented at ASME Winter Meeting. Los Angeles, California, 1969.

Gillins, R. L. Experimental Data Report for Semiscale Mod-3 Blowdown Heat Transfer Test S-07-3 (Baseline Test Series). NUREG/CR-0356, 1978.

Gorlov, I. G., Rzayev, A. I., and Khudyakov, V. F. "Boiling of Potassium in Pipes at High Pressure." Heat Transfer-Soviet Research 7, No. 4, 1975.

Gottula, R. C. LOFT Transient (Blowdown) Critical Heat Flux Test. TREE-NUREG-1240, 1978.

Griffith, P., Pearson, J. F., and Lepkowski, R. J. "Critical Heat Flux During a Loss-of-Coolant Accident." Nuclear Safety 18 (1977): 298-309.

Groeneveld, D. C., Cheng, S. G., Stewart, J. C., Snoek, C. W., Wilson, K. E., and Shaw, P. B. "Chalk River Process in Updating Best Estimate Heat Transfer Correlations." Presented to U.S.N.R.C. Workshop, 1981.

Guerrero, H. N. "Single Tube and Rod Bundle Blowdown Heat Transfer Experiments Simulating Pressurized Water Reactor LOCA Conditions." ASME Paper 76-HT-11 (1976).

Gunnerson, F. S., Pasamehmetoglu, K.O., and Hosler, E.R. "Transient Critical Heat Flux Mapping." Proceedings of 12th Water Reactor Safety Research Information Meeting held at Gaithersburg, Maryland, October 22-26, 1984. NUREG/CP-0058 Vol.1, (January 1985): 307-330.

Haramura, Y., and Katto, Y. "A New Hydrodynamic Model of Critical Heat Flux, Applicable Widely to Both Pool and Forced Convection Boiling on Submerged Bodies in Saturated Liquids." International J. Heat Mass Transfer 26 (1983): 389-399.

Henry, R. W., and Leung, J. C. M. "A Mechanism for Transient Critical Heat Flux." Proceedings of Topical Meeting on Thermal Reactor Safety, Sun Valley, Idaho (August 1977): 692-703.

Hewitt. G. F. "Course on Two-Phase Heat Transfer in Steady and Transient States." Stanford, August 20-24, 1979.

Holman, J. P. Heat Transfer. 5th Edition, New York:McGraw-Hill, 1981.

Hsia, A. H. Rod Bundle Blowdown Heat Transfer Tests Simulating Pressurized Water Reactor Loss of Coolant Accident Conditions. EPRI NP-113, 1977.

Hsu, Y. Y., and Graham, R. W. Transport Processes in Boiling and Two-Phase Systems. Washington:Hemisphere, 1976.

Hsu, Y. Y., and Beckner, W. D. "A Correlation for the Onset of Transient CHF." Unpublished report as cited by Tong, L.S. in "Heat Transfer in Reactor Safety." Presented at 6th Heat Transfer Conference, Toronto, Canada, 1978.

Hutchinson, P. and Walley, P. B. "A Possible Characterization of Entrainment in Annular Flow." Chemical Engineering and Science 28 (1973): 974-982.

Inabe, T., Semken, R. S., and Martinson, Z. R. "Reactivity Initiated Accidents Tests Series/Test RIA 1-1, RIA1-2/Experiment Predictions." TFBP-TR-294, September 1978.

Ishigai, S., Naganishi, S., Yamauchi, S., and Masuda, T. "Effect of Transient Flow on Premature Dryout in Tubes." Heat Transfer 1974, Proceedings of 5th International Heat Transfer Conference, Tokyo, Japan, 4, Paper:B6.13, September 1974.

Ivey, H. J., and Morris, D. J. On the Relevance of the Vapor-Liquid Exchange Mechanism for Sub-Cooled Boiling Heat Transfer at High Pressure. AEEW-R-157, 1962.

Jiji, L. M., and Clark, J. A. "Bubble Boundary Layer and Temperature Profiles for Forced Convection Boiling in Channel Flow." J. Heat Transfer, Trans. ASME 50 (1964): 50-58.

Johnson, H. A. "Transient Boiling Heat Transfer to Water." Int. J. Heat Mass Transfer 14 (1971): 67-82.

Kataoka, I., Serizawa, A., and Sakurai, A. "Transient Boiling Heat Transfer Under Forced Convection." Int. J. Heat Mass Transfer 26 (1983): 583-594.

Katto, Y., Yokoya, S., and Yasunaka, M. "Mechanisms of Boiling Crisis and Transition Boiling in Pool Boiling." Heat Transfer 1970 5, Paper:B3.2, Amsterdam:Elsevier, 1970.

Katto, Y. "A Generalized Correlation of Critical Heat Flux for the Forced Convection Boiling in Vertical Uniformly Heated Round Tubes. Int. J. Heat Mass Transfer 21 (1978): 1527-1542.

Katto, Y. "General Correlations of Critical Heat Flux for the Forced Convection Boiling in Vertical Uniformly Heated Annuli." Int. J. Heat Mass Transfer 22 (1979a): 575-584.

Katto, Y. "A Generalized Correlation of Critical Heat Flux for the Forced Convection Boiling in Vertical Uniformly Heated Round Tubes, A Supplementary Report." Int. J. Heat Mass Transfer 22 (1979b): 783-794.

Katto, Y. "An Analysis of the Effect of Inlet Subcooling On Critical Heat Flux of Forced Convection Boiling in Vertical Uniformly Heated Tubes." Int. J. Heat Mass Transfer 22 (1979c): 1567-1575.

Katto, Y. "General Features of CHF of Forced Convection Boiling in Uniformly Heated Vertical Tubes with Zero Inlet Subcooling." Int. J. Heat Mass Transfer 23 (1980a): 493-504.

Katto, Y. "CHF of Forced Convection Boiling in Uniformly Heated Vertical Tubes (Correlation of CHF in HP Regime and Determination of CHF Regime Map)." Int. J. Heat Mass Transfer 23 (1980b): 1573-1580.

Katto, Y. "General Features of CHF of Forced Convection Boiling in Vertical Concentric Annuli with a Uniformly Heated Rod and Zero Inlet Subcooling." Int. J. Heat Mass Transfer 24 (1981a): 109-116.

Katto, Y. "General Features of CHF of Forced Convection Boiling in Uniformly Heated Rectangular Channels." Int. J. Heat Mass Transfer 24 (1981b): 1413-1419.

Katto, Y. "On the Heat Flux/Exit Quality Type Correlation of CHF of Forced Convection Boiling in Uniformly Heated Vertical Tubes." Int. J. Heat Mass Transfer 24 (1981c): 533-539.

Katto, Y. "On the Relation Between CHF and Outlet Flow Patterns of Forced Convection Boiling in Uniformly Heated Vertical Tubes." Int. J. Heat Mass Transfer 24 (1981c): 541-544.

Katto, Y. "A Study on Limiting Exit Quality of CHF of Forced Convection Boiling in Uniformly Heated Vertical Channels." J. Heat Transfer, Trans, ASME 104 (1982a): 40-47.

Katto, Y. "An Analytical Investigation of CHF of Flow Boiling in Uniformly Heated Vertical Tubes with Special Reference to Dimensionless Groups." Int. J. Heat Mass Transfer 25 (1982b): 1353-1361.

Katto, Y., and Haramura, Y. "Critical Heat Flux on Uniformly Heated Horizontal Cylinder in an Upward Cross-Flow of Saturated Liquid." Int. J. Heat Mass Transfer 26 (1983): 1199-1205.

Katto, Y. "Prediction of Critical Heat Flux for Annular Flow in Tubes Taking Into Account the Critical Liquid Film Thickness Concept." Int. J. Heat Mass Transfer 27 (1984): 883-891.

Katto, Y. "Critical Heat Flux." Advances in Heat Transfer 17, New York:Academic Press (1985): 1-85.

Kawamura, H., Tachibana, F., and Akiyama, M. "Heat Transfer and DNB Heat Flux in Transient Boiling." Heat Transfer 1970, 5, Paper: B3.3, Amsterdam:Elsevier, 1970.

Kawamura, H. "Experimental and Analytical Study of Transient Heat Transfer for Turbulent Flow in a Circular Tube." Int. J. Heat Mass Transfer 20 (1977): 443-449.

Kays, W. M., and Crawford, M. E. Convective Heat and Mass Transfer. 2nd edition, New York:McGraw-Hill, 1980.

Knoebel, D. K. "Forced Convection Subcooled critical Heat Flux, D_2O and H_2O Cooled with Aluminum and Stainless Steel Heaters." Dupont Savannah River Laboratory, DP-1306, 1973.

Koshkin, V. K., Kalinin, E. K., Dreitser, G. A., Galitseisky, B. M., and Isosimov, V. G. "Experimental Study of Nonsteady Convective Heat Transfer in Tubes." Int. J. Heat Mass Tr. 13 (1970): 1271-1281.

Kottowski, H. M., and Savatteri, C. "Fundamentals of Liquid Metal Boiling Thermohydraulics." Nuclear Engineering and Design 82 (1985): 281-304.

Kuroda, Y. "Effects of Liquid Subcooling on Transient Boiling of Water with an Increase in Heat Generation." M.S. Thesis, Kyoto University, 1979 (in Japanese).

Kutadelatze, S. S. Fundamentals of Heat Transfer. New York:Academic Press, 1963.

Kutadelatze, S. S., and Leodnev, A. I. "Some Applications of the Asymptotic Theory of Turbulent Boundary Layer." Proceedings of 3rd International Heat Transfer Conference, Chicago, 1966.

Lee, D. H. An Experimental Investigation of Forced Convection Burnout in High Pressure Water. AEEW-R-479, 1966.

Leidenfrost, G. C. "De Aquaea Communis Nonnulis Qualitatibus Tractatus. (A Track About Some Qualities of Common Water.)" 1756, Translation in Int. J. Heat Mass Transfer 9 (1966): 1154-1166.

Leinhard, J. H. A Heat Transfer Textbook. New York: Prentice Hall, 1981.

Leon, D. M. PWR Blowdown Heat Transfer Separate-Effects Program, Thermal-Hydraulic Test Facility Experimental Data Report for Test 103. ORNL/NUREG/TM-187, 1978.

Leung, J. C. M. Critical Heat Flux Under Transient Conditions, Literature Survey 1978. NUREG/CR-0056, 1978.

Leung, J. C. M. "Transient Critical Heat Flux and Blowdown Heat Transfer Studies." Ph.D. Dissertation, Northwestern University, June 1980.

Levy, S. Prediction of Critical Heat Flux for Annular Flow in Vertical Pipe. EPRI NP-1619 RP 1380-1, Final Report, November 1980.

Lo, R. K., Argonne National Laboratory, Private Communications.

Macbeth, R. V. "The Burnout Phenomenon in Forced Convective Boiling." Advances in Chemical Engineering. New York:Academic Press, 1968.

MacDonald, P. E., Seiffert, S. L., Martinson, Z. R., McCardell, R. K., Owen, D. E. , and Fukuda, S. K. "An Assessment of Light Water Reactor Fuel and Core Damage During a Reactivity Initiated Accident." A preliminary manuscript submitted to International Center for Heat and Mass Transfer for the seminar on Nuclear Reactor Safety Heat Transfer, Dubrovnik, Yugoslavia, 1980.

Martinson, Z. R., Semkin, R. S., Inabe, T., Smith, R. H., Cook, T. F., and Appelhans, A. D. "Reactivity Initiated Accident Test Series/ RIA Scoping Test/Quick Look Report." TFBP-TR-289, September 1978.

Martinson, Z. R., Semken, R. S., Inabe, T. Smith, R. H., White, C. E., Osetek, D. J., and Mehner, A. S. "Reactivity Initiated Accident

Test Series/Test RIA 1-1, Quick Look Report." TFBP-TR-3000, October, 1978.

Martinson, Z. R., Semken, R. S., Smith, R. H., and Osetek, D. J. "Reactivity Initiated Accident Test Series/ Test RIA 1-2/Quick Look Report." TFBP-TR-303, December 1978.

Miyasaki, D. H. Experimental Data Report for Semiscale Mod-3 Blowdown Heat Transfer Test S-07-9 (Baseline Test Series) NUREG/CR-0815, 1979.

Moissis, R., and Berenson, P. J. "On the Hydrodynamic Transition in Nucleate Boiling." J. Heat Transfer, Trans. ASME 85 (1963): 221-229.

Moxon, D., and Edwards, P. A. Dryout During Flow and Power Transients. AEEW-R-553, 1967.

Mudawwar, I. A., El-Masri, M. A., Wu, C. S., and Ausman-Mudawwar, R. J. "Boiling Heat Transfer and Critical Heat Flux in High Speed Rotating Liquid Films." Int. J. Heat Mass Transfer 28 (1985): 295-806.

Nelson, R. A., and Duffey, R. B. "Quenching Phenomena." Presented at International Workshop at Post Dryout Heat Transfer, Salt Lake City, Utah, April 1984.

Nukiyama, S. "The Maximum and Minimum Values of the Heat Q Transmitted from Metal to Boiling Water Under Atmospheric Pressure." Int. J. Heat Mass Transfer 9 (1934): 1419-1433.

Pasamehmetoglu, K. O., and Gunnerson, F. S. "Theoretical Considerations of Transient Critical Heat Flux." Proceedings of 3rd International Topical Meeting on Reactor Thermal-Hydraulics, New Port, Rhode Island, Vol.2 Paper:18-F, October 1985.

Pawel, R. E. "Oxidation Diffusion in Beta Zircaloy During Steam Oxidation." J. Nuclear Materials 50 (1974): 247-258.

Roumy, R. "Burnout in Transient Conditions in Circular Tubes." Presented at European Two-Phase Flow Mtg. Harwell, UK (June 1974)

Sakurai, A., Mizukami, K., and Shiotsu, M. "Experimental Studies on Transient Boiling Heat Transfer and Burnout." Heat Transfer 1970, 5, Paper:B3.4, Amsterdam: Elsevier, 1970.

Sakurai, A., and Shiotsu, M. "Transient Pool Boiling Heat Transfer/Part 1:Incipient Boiling Superheat." J. Heat Transfer, Trans. ASME 99 (1977): 540-553.

Sakurai, A., and Shiotsu, M. "Transient Pool Boiling Heat Transfer/ Part 2:Boiling Heat Transfer and Burnout." J. Heat Transfer, Trans. ASME 99 (1977): 554-560.

Sakurai, A., Shiotsu, M., and Hata, K. "Transient Boiling Caused by Rapid Depressurization from Initial Non-Boiling State." In Multiphase Transport, 2, edited by Veziroglu, N., Washington: Hemisphere, 1980.

Schrock, V. E. "Transient Boiling Phenomena." University of California, Berkeley, Report No. NE-66-2, 1966.

Segev, A., and Bankoff, S. G. "Physical Modeling of Blowdown CHF." Northwestern University Report MU822603.1, February 1976.

Seiffert, S. L., Martinson, Z. R., and Fukuda, S. K. Reactivity Initiated Accident Test Series/Test RIA 1-1 (Radial Average Fuel Enthalpy of 285 cal/g) Fuel Behavior Report. NUREG/CR-1465, September 1980.

Semken, R. S., Eaton, A. M., Smith, R. H., and Resch, S. C. "Reactivity Initiated Accident Test Series/RIA Scoping Test/Experiment Predictions." TFBP-TR-275, June 1978.

Serizawa, A. "Theoretical Prediction of Maximum Heat Flux in Power Transients." Int. J. Heat Mass Transfer 26 (1983): 921-932.

Shah, M. M. "A Generalized Graphical Method for Predicting CHF in Uniformly Heated Vertical Tubes." Int. J. Heat Mass Transfer 22 (1979): 557-568.

Shimeck, D. J. Analysis of Semiscale Mod-2A System UHI/SBLOCA Experiments. NUREG/CR-3195, April 1983.

Siegel, R. "Heat Transfer for Laminar Flow in Ducts for Arbitrary Time Variations in Wall Temperature." J. Applied Mechanics, Trans, ASME 82 (1960): 170-180.

Siegel, R., and Perlmutter, M. "Laminar Heat Transfer in a Channel With Unsteady Flow and Wall Heating Varying With Position and Time." J. Heat Transfer, Trans. ASME 85 (1963): 358-365.

Siegel, R. "Forced Convection in a Channel with Wall Heat Capacity and with Wall Heating Variable with Axial Position and Time." Int. J. Heat Mass Transfer 6 (1963): 607-620.

Slifer, B. C., and Hench, J. E. "Loss-of-Coolant Accidents and Emergency Core Cooling Models for General Electric Boiling Water Reactors." Report NEDO-10329, April 1971.

Smith, O. G., Tong, L. S., and Rohner, W. M. "Burnout in Steam-Water Flows with Axially Non-Uniform Heat Flux." ASME Paper 65-WA/HT-33, 1965.

Smith, R. A., and Griffith, P. "A Simple Model for Estimating Time to Critical Heat Flux in a Pressurized Water Reactor Loss-of-Coolant Accidents." ASME Paper 76-HT-9, 16th Annual Heat Transfer Conference, St. Louis, April 1976.

Soliman, M., and Johnson, H. A. "Transient Heat Transfer for Forced Convection Flow over a Flat Plate of Appreciable Thermal Capacity and Containing an Exponential Time Dependent Heat Source." Int. J. Heat Mass Transfer 11 (1968): 27-38.

Sparrow, E. M., and Siegel, R. "Unsteady Turbulent Heat Transfer in Tubes." J. Heat Transfer, Trans. ASME 82 (1960): 170-180.

Sparrow, E. M., and DeFarias, F. N. "Unsteady Heat Transfer in Ducts with Time Varying Inlet Temperature and Participating Walls." Int. J. Heat Mass Transfer 11 (1968): 837-853.

Sucec, J. "Unsteady Heat Transfer Between a Fluid with Time Varying Temperature and a Plate: an Exact Solution." Int. J. Heat Mass Transfer 18 (1975): 25-36.

Sucec, J. "An Improved Quasi-Steady Approach for Transient Conjugated Forced Convection Problems." Int. J. Heat Mass Transfer 24 (1981): 1711-1722.

Subbotin, V. I., Sorokin, D. N., Ovechkin, D. M., and Kudryavtsev, A. P. Heat Transfer in Boiling Metals by Natural Convection. Moscova:Iztatel'stvo Nauka, translated from Russian by Israel Program for Scientific Translations, 1969.

Subbotin, V. I., Sorokin, D. N., Tzyganok, A. A., and Gribov, A. A. "Investigation of Vapor Bubbles Effect on Temperature of Heat Transferring Surface at Nucleate Boiling." Heat Transfer 1974, Proceedings of 5th International Heat Transfer Conference, Tokyo, Japan, 4, Paper: B2.5, 1974.

Tachibana, F., Akiyama, M., and Kawamura, H. "Heat Transfer and Critical Heat Flux in Transient Boiling (I)." J. Nuclear Science and Technology 5 (1968): 117-126.

Tien, C. L., and Leinhard, J. H. Statistical Thermodynamics. Washington: McGraw-Hill, 1979.

Thorgerson, E. J., Knoebel, D. H., and Gibbons, D. H. "A Model to Predict Convective Subcooled Critical Heat Flux." J. Heat Transfer, Trans. ASME 96 (1974): 79-82.

Tong, L. S. "Influence of Axially Non-Uniform Heat Flux on DNB," Chemical Engineering Program Symposium Series 64 (1966): 35-40.

Tong, L. S. "Prediction of Departure from Nucleate Boiling for an Axially Non-Uniform Heat Flux Distribution." J. Nuclear Energy 21 (1967): 241-248.

Tong, L. S. "An Evaluation of the Departure from Nucleate Boiling in Bundles of Nuclear Fuel Rods." Nuclear Science and Engineering 33 (1968a): 7-15.

Tong, L. S. "Boundary Layer Analysis of the Flow Boiling Crisis." Int. J. Heat Mass Transfer 11 (1968b): 1208-1211.

Tong, L. S. "Boiling Crisis and Critical Heat Flux." U.S. Atomic Energy Commission Office of Information Services, TID-25887, August 1972.

Walley, P. B., Hutchinson, P., and Hewitt, G. F. "The Calculation of Critical Heat Flux in Forced Convective Boiling." Heat Transfer 1974, Proceedings of 5th International Heat Transfer Conference Tokyo, Japan, 4, 1974.

Walley, P. B., Hutchinson, P., and Hewitt, G. F. "Prediction of Annular Flow Parameters for Transient Conditions and for Complex Geometries." Presented at European Two-Phase Flow Group Meeting, Haifa, Israel, 1975.

Walley, P. B. The Calculation of Dryout in Rod Bundle AERE-R-8319, 1976.

Walley, P. B. The Calculation of Dryout in Rod Bundle-A Comparison of Experimental and Calculated Results. AERE-R-8977, 1978a.

Walley, P. B. "The Calculation of Critical Heat Flux in Complex Situations Using an Annular Flow Model." Proceedings of 6th International Heat Transfer Conference, Toronto, Canada, 5, 1978b.

Weisman, J., and Pei, B. S. "Prediction of Critical Heat Flux in Flow Boiling at Low Quality." Int. J. Heat Mass Transfer 26 (1983): 1463-1477.

Weisman, J. "Theoretically Based Predictions of Critical Heat Flux." Proceedings of 3rd International Topical Meeting on Reactor Thermal-Hydraulics held at Newport, Rhode Island, 2, Paper: 18-A, October 1985.

Westinghouse Electric Corp. Full Scale Controlled Transient Heat Transfer Tests-Data Report. EPRI-NP-1810, April 1981.

Westinghouse Electric Corp. Full Scale Controlled Transient Heat Transfer Data Analysis Report. EPRI-NP-2547, August 1982.

Yu, C., and Mesler, R. B. "A Study of Nucleate Boiling Near the Peak Heat Flux Through Measurements of Transient Surface Temperature." J. Heat Transfer, Trans. ASME 20 (1977): 827-840.

Zimmermann, C. L., White, C. E., and Evans, R. P. Experiment Data Report for Test RIA 1-2 (Reactivity Initiated Accident Test Series). NUREG/CR-0765, June 1979.

Zuber, N. "On the Stability of Boiling Heat Transfer." Trans. ASME 80 (1958): 711-720.